Utilization of Marble Waste into Value Added Product- "Hydroxyapatite"

This thesis is submitted as a partial fulfilment of the PhD programme in Engineering by

Dhiraj Mehta

2013RCH9010

Under the supervision of

DR. SUJA GEORGE

Associate Professor

DEPARTMENT OF CHEMICAL ENGINEERING

MALAVIYA NATIONAL INSTITUTE OF TECHNOLOGY JAIPUR

JAIPUR-302017

Dec, 2017

© Malaviya National Institute of Technology Jaipur, 2017. All rights reserved.

CERTIFICATE

This is to certify that the work reported in this thesis entitled

"Utilization of Marble waste into value added Product-Hydroxyapatite"

has been carried out by Mr. Dhiraj Mehta and submitted to Malaviya National Institute of Technology, Jaipur for the award of Doctor of Philosophy. It is a bonafide record of research work carried out by him under my supervision. The thesis work has reached the requisite standard, fulfilling the requirements for the degree of Doctor of Philosophy. The thesis embodies the original work done by him and has not been carried out earlier to the best of my knowledge and belief.

Dr. Suja George
Associate Professor
Department of Chemical Engineering
MNIT, Jaipur

DECLARATION

I hereby certify that the work which is presented in the thesis entitled **"Utilization of Marble waste into value added product-Hydroxyapatite"** in partial fulfilment of the requirements for the award of Doctor of Philosophy, in the Department of Chemical Engineering, Malaviya National Institute of Technology, Jaipur, is an authentic record of my own work unless otherwise referenced or acknowledged. The thesis was completed under the supervision of Dr. Suja George, Associate Professor, Department of Chemical Engineering, Malaviya National Institute of Technology, Jaipur. The results presented in this thesis have not been submitted in part or full, to any other University or Institute for award of any degree. The content of the thesis has been checked using online software "Turnitin".

Dhiraj Mehta

2013RCH9010

Department of Chemical Engineering

MNIT, Jaipur

"...Whatever you do, give your best out of it, because every work done is for the Almighty,..." I dedicate my PhD- thesis to my parents and my fiancé who showed faith in me and motivated me throughout my journey...!!

with love, Dhiraj

ACKNOWLEDGMENT

The journey of completing my PhD thesis would not be truly complete without showing my gratitude to several people who helped to keep my zeal for research lighted.

Firstly, I would like to express my earnest gratitude to my PhD supervisor ***Dr. Suja George***, who not only guided me in the research front but also acted as a spiritual mentor. Her immense knowledge and experience in the research field was huge support for my PhD work.

Besides my supervisor, I would like to thank ***Dr. V.K Saharan*** for always encouraging my research and believing that I could achieve new horizons. His insights in the area of ultrasonication helped to give a new edge to this work. I would like to thank ***Dr. R.K Vyas*** and ***Dr. P. Pandit*** members my DREC (Department Research Evaluation Committee), for their insightful comments. I extend my gratitude to ***Dr. Kailash Singh (HOD)*** and all other faculties of Chemical Engineering Department for their sincere support. The financial support of MNIT is genuinely acknowledged along with the sincere support for research activities from ex-Director ***Prof. I.K. Bhat*** and current ***Director Prof. U.R. Yaragatti.***

Characterization studies & their analysis were an important part of this thesis for which I am grateful to the staff of **Materials Research Center** especially *Mr. Ramesh, Mr. Shubham and Mr. Hitesh*. I also acknowledge the selfless help received ***from Dr. K. S Ramarao, Senior scientist IICT, Hyderabad*** for BET surface area measurements. The help from ***SAIF, Punjab University*** is also appreciated in analysis of XRD of some samples. A special thanks to *Mr. Ramesh and Mr. Reddy, Lab Technicians* who helped in fabricating the experimental setup in stipulated time period.

The impact fluorosis has on rural population can only be understood by going among them. I am thankful to the LINC (Learning in community) programme, a partnership between ***MNIT and University of Illinois, USA*** under which the field visits to fluoride

prone rural areas were arranged. It provided me an opportunity to learn the root causes of fluorosis and what step can be beneficial on a community level to eradicate the issue.

I thank my fellow research mates and lifetime friends ***Mr. Prakash and Mr. Shivendu*** for the exciting discussions, for the sleepless nights in the laboratory when we were working together before deadlines, and for all the fun we have had in the past four years. Also, I thank *Mr. Swapnil, Mr. Jitendra and Mr Sunil* for supporting me whenever needed. My sincere appreciation also goes to my dear friend *Mr. Anurag, Mr. Sushant and Mr. Sachin*.

My earnest gratitude to my fiancé ***Dr. Poonam Mondal*** for her immense patience and encouragement throughout my research. The dedication she had towards her PhD work was contagious and it led me to work harder for my thesis. I would like to convey my warmest appreciation to my sister *Mrs. Diksha* and brother in law *Mr. Amit* for the constant motivation. My heartfelt thanks also go to my extended family *Mr. PP Mondal, Mrs, Kabita and Abhishek* for having faith in me.

Words cannot express the sacrifices my mother ***Mrs. Vandana Mehta*** and father ***Mr. Vinod Mehta*** have made on my behalf, throughout my education. I am forever indebted to them for whatever I am today and whatever I will be tomorrow.

Dhiraj Mehta

LIST OF PUBLICATIONS

Publications in Journals

1. **Dhiraj Mehta**, Poonam Mondal, Suja George, Virendra Saharan. In-vitro synthesis of marble apatite as a novel adsorbent for removal of fluoride ions from ground water: An ultrasonic approach. *Ultrasonics Sonochemistry, 40 (664-674), 2018.*

2. **Dhiraj Mehta**, Poonam Mondal, Suja George, Virendra Saharan. Synthesis of hydroxyapatite nanorods for application in water defluoridation and optimization of process variables: Advantage of ultrasonication with precipitation method over conventional method. *Ultrasonics Sonochemistry*. 37 (56-70), 2017.

3. **Dhiraj Mehta**, Poonam Mondal, Suja George. Utilization of marble waste powder as a novel adsorbent for removal of fluoride ions from aqueous solution, *Journal of Environmental Chemical Engineering.* 4, 932-942, 2016.

4. **Dhiraj Mehta,** Anjuvan Singh, Suja George. Assessment of Different Synthesis Route of Hydroxyapatite and Study of its Biocompatibility in Synthetic Body Fluids. *International Journal of ChemTech Research.* 9, (267-276), 2016.

5. Poonam Mondal, **Dhiraj Mehta,** Suja George. Defluoridation studies with synthesized magnesium-incorporated hydroxyapatite and parameter optimization using response surface methodology. *Desalination and Water Treatment*, 57(27294-27313), 2016.

6. **Dhiraj Mehta,** Suja George, Poonam Mondal. Synthesis of Hydroxyapatite by Chemical Precipitation Technique and Study of Its Biodegradability. *International Journal of Research in Advent Technology*. 2(4), (159-161), 2014.

7. Poonam Mondal, Suja George, **Dhiraj Mehta**. Use of Calcite for Defluoridation of Drinking Water in Acidic medium. *Research Journal of Chemical Sciences*. 4(6), (62-65), 2014.
8. **Dhiraj Mehta**, Virendra Kumar Saharan, Suja George. Synthesis of hydroxyapatite and study of its applications in water defluoridation: A Review. *Reviews in Chemical Engineering*, De Gruyter. *Communicated*

Publications in Conferences

1. **Dhiraj Mehta,** Poonam Mondal, Suja George, Parimala S. Utilization of Marble Waste into a Value Added Product: Hydroxyapatite. *Proceedings of International Conference on Advances in Chemical Engineering and Technology* ***(Elsevier, India)***, Kollam,16-18 October 2014,338–342 [ISBN:9789351072843].

2. **Dhiraj Mehta**, Poonam Mondal, Suja George. Synthesis of Biomaterial Hydroxyapatite and Effect of calcination on its structure. *Proceedings of Exploring Basic & Applied Sciences for Next Generation Frontiers* ***(Elsevier, India)***, *Jalandhar,* 14 -15 November 2014, Pg-207-209[ISBN:978- 93-5107-313-0].

3. Poonam Mondal, Suja George and **Dhiraj Mehta**. Synthesis of Calcia-Magnesia Adsorbent (CMA) and Utilizing it for Defluoridation of Drinking Water. *Proceedings of Exploring Basic & Applied Sciences for Next Generation Frontiers* ***(Elsevier, India)***, Jalandhar, 14 -15 November 2014,Pg-204- 206 [ISBN:978-93-5107-313-0].

4. **Dhiraj Mehta**, Suja George. Hydroxyapatite: Synthesis and Characterization. *3rd International Conference on Materials for the Future- Innovative Materials, Processes, Products and Applications* on 06-08 November 2013 at Govt. Engineering College, Thrissur, Kerala.

5. **Dhiraj Mehta**, Poonam Mondal, Suja George. Hydroxyapatite synthesis by precipitation method and evaluation of its biodegradability. *International Conference on Innovative Advancements in Engineering & Technology*, 7-8 March 2014, Jaipur National University, Jaipur.

6. Poonam Mondal, Suja George, **Dhiraj Mehta.** Removal of fluoride from acid treated water by using Calcite. *International Conference on Innovative Advancements in Engineering & Technology* ,7-8 March 2014 ,Jaipur National University, Jaipur

7. **Dhiraj Mehta,** Anjuvan Singh. Removal of Arsenic from Drinking Water by Hydroxyapatite. *All India Seminar on Pollution Prevention through development of Biobased material & Energy* on Feb 22-23,2013 at MNIT, Jaipur

ABSTRACT

In the current era of worldwide growth and development, marble industry is a rapidly advancing sector however it is gaining attention in many parts of the world because of its huge uncontrolled wastes. These wastes are piling up in the absence of proper disposal systems and raising serious environmental concern and threat for human health. Marble waste powder is available free of cost as a by-product of the marble processing industries and is primarily composed of carbonates of calcium and magnesium, both of which has very good affinity for fluoride ions. In several places, groundwater is unsuitable for drinking due to the high concentration of naturally occurring minerals such as fluoride ions (F^-). Consumption of water with high concentration of fluoride (>1.0 mg/L) may cause dental and skeletal fluorosis. Hence, treatment of drinking water with suitable technique is needed which is simple and cost efficient for the common population and adsorption technology provides an effective solution for the same. Adsorbents based on calcium compounds have gained interest in the past two decades and have good fluoride removal capacity. The presence of calcium and magnesium in marble waste powder have directed new approach for their utilization for synthesis of calcium based adsorbents for water defluoridation.

In this study, an attempt was made to use marble waste powder (MWP) for the synthesis of a biomaterial "hydroxyapatite" for defluoridation of drinking water. Also the capabilities of MWP and Pure hydroxyapatite nanorods prepared synthetically was also studied as an adsorbent for water defluoridation. Two different methods i.e. conventional method (CM) and ultrasonication method (USM) were used for the synthesis of hydroxyapatite based adsorbents for their application in water defluoridation. The adsorbents were characterized using FTIR, XRD, SEM, TEM/EDS, BET, particle size distribution and TGA-DTA techniques. These studies assisted in identifying the characteristics such as bonding patterns, composition, crystallinity and morphology of Hydroxyapatite with which further experiments were carried out.

Hydroxyapatite synthesized synthetically using ultrasonication with precipitation method (USPM) produced pure Hap nanorods of crystalline structure. SEM

and TEM studies confirmed the formation of nanorod-like crystalline structures in the micrographs. The process yield of the pure Hap produced by both routes when compared was found that it improved from 83.24% to 90.2% when USPM was used over CM. Prior to the synthesis of Hap using marble waste powder (MWP), its characterization studies were done and influence of calcination temperature was studied at three different temperatures i.e. 650ºC, 850ºC & 1000ºC along with its potential for water defluoridation. The calcination temperature influenced the properties of marble waste powder in a significant manner by activating the calcium component present in the powder that further affected the defluoridation capacity. Batch experiments showed that MWP650 had higher removal capacity i.e. 1.20 mg/g than MWP, MWP850, and MWP1000. The treated water quality on treating fluoride water with MWP650 was alkaline in nature with high TDS and hardness, therefore, further improvement was required for utilization of marble waste powder as a defluoridating agent using a different approach. Marble apatite (MA) was thereafter synthesized using marble waste powder by conventional (CM) and ultrasonication method (USM) and it was observed that when USM was used for synthesis, product obtained was more crystalline with lesser intermediate phases. SEM and TEM studies further depicted that with ultrasonication, MA-USM of crystalline nature with well-defined spherical morphology was obtained compared to MA-CM with sword like agglomerated structure. Yield of marble apatite also improved from 67.5% to 78.4% when USM method was employed for synthesis. The adsorption capacity of MA-CM and MA-USM was 0.96 mg/g and 1.826 mg/g respectively. However, due to the presence of intermediates in the form of calcium phosphate and magnesium calcium silicates present in synthesized marble apatite, further modification in the synthesis process was carried out that led to the formation of pure form of hydroxyapatite named MA-Hap.

In MA-Hap synthesis, ultrasonication for 60 min produced pure Hap (MA-Hap USM) with no intermediates or impurities and had a crystallite size of 21.93 nm which was lower than that of MA-Hap synthesized using conventional method (MA-Hap CM) (73.1 nm). The SEM morphology of both the adsorbents indicated similar spherical shaped particles however, TEM analysis depicted needle shaped morphology with the average size of 6 nm to 10 nm. The BET surface area of MA-Hap USM was 44.92 m^2/g

which was comparatively higher than other adsorbents synthesized. The process synthesis time was also decreased from 240 min to 60 min and yield was increased from 81.90% to 89.06% using USM approach. Advantages of using USM over conventional method was improved material quality in terms of crystallinity, reduction in particle size and better yield efficiency. The defluoridation capacities of material synthesized using USM process also significantly increased as compared to CM method. The fluoride adsorption capacities for MA-Hap CM and MA-Hap USM were 1.331 mg/g and 1.824 mg/g respectively and their adsorption equilibrium time was only 30 min.

MA-Hap was then synthesized in a pilot scale lab reactor of 100 L capacity (MA-Hap LR) with working volume of 60 L, which was further pelletized using PVA binder through extrusion-spheronization technique. The pellets formed were used for column defluoridation experiments and studied for varying parameters such as adsorbent particle size, bed height, flow rate and initial fluoride concentration. The adsorption capacity of the column system was found to be 1.21 mg/g at feed fluoride concentration of 10 mg/L, flow rate of 1 LPH and bed height of 25 cm. It was noted that for a bed height of 25 cm, 28.5 bed volumes can be processed while the adsorbent exhaustion rate for the same was 7.4 g/L. The treated volume of water was 14 L for 25 cm bed height at 1 LPH flow rate and 10 mg/L of initial fluoride concentration. Regeneration studies using MA-Hap LR were also done upto four cycles with 1.0 M NaOH solution and its capacities for cycles were 1.21 mg/g, 0.925 mg/g, 0.546 mg/g and 0.211 mg/g. Analysis of physicochemical parameters for treated water quality such as hardness, alkalinity, TDS, calcium & magnesium concentration and pH confirmed within permissible limits and affirmed the use of MA-Hap LR as a potential defluoridating agent for drinking water.

Among all the adsorbents used, nano-sized marble hydroxyapatite (MA-Hap USM) was the best adsorbent, found most suitable for its application in water defluoridation as it can be synthesized from marble waste powder, energy efficiently through advanced ultrasonication method with higher yield, high product quality, high defluoridation capacity and regenerability. This will also lead to effective reuse of tons of marble waste powder available, making it very cost effective and thus reducing the environmental threat of waste disposal.

TABLE OF CONTENT

LIST OF FIGURES

LIST OF TABLES

NOMENCLATURE

List of Abbreviations

AER	Adsorbent exhaustion rate
APHA	American Public Health Association
BET	Brunauer, Emmett and Teller
BIS	Bureau of Indian Standards
BV	Bed volume
CCD	Central composite design
CDTA	1, 2-diaminocyclohexane tetra acetic acid
CM	Conventional Method
CTAB	Cetyl Trimethyl Ammonium Bromide
DCPA	Dicalcium phosphate anhydrous
EBCT	Empty bed contact time
EDX	Energy dispersive X-ray analysis
EDTA	Ethylenediaminetetraacetic acid
E-S	Extrusion- Spheronization
Hap	Hydroxyapatite
Hap CM	Hap synthesized using conventional method
Hap USPM	Hap synthesized using ultrasonication with precipitation method
LR	Lab reactor
MA	Marble apatite
MA-CM	MA synthesized using conventional method
MA-USM	MA synthesized using ultrasonication method
MA-Hap	Marble hydroxyapatite

MA-Hap CM	MA-Hap synthesized using conventional method
MA-Hap USM	MA-Hap synthesized using ultrasonication method
MA-Hap LR	Marble hydroxyapatite lab reactor
MWP	Marble waste powder
PEG	Polyethylene glycol
pH_{PZC}	pH at point of zero charge
SDS	Sodium dodecyl sulfate
TCP	Tri-calcium phosphate
FTIR	Fourier transform infrared spectroscopy
JCPDS	Joint Committee on Powder Diffraction Standards
PAZ	Primary adsorption zone
PVA	Poly(vinyl alcohol)
RSM	Response surface methodology
SEM	Scanning electron microscopy
TDS	Total dissolved solids
TEM	Transmission electron microscopy
TGA-DTA	Thermogravimetric analysis-Differential thermal analysis
TISAB	Total ionic strength adjustment buffer
UNICEF	United Nations Children's Emergency Fund
USM	Ultrasonication Method
USPM	Ultrasonication with precipitation method
WHO	World Health Organization
XRD	X-ray powder diffraction

List of Mathematical symbols

ε	Polanyi potential
A_T	Temkin isotherm binding constant
B_T	Temkin constant related to the heat of adsorption
C_0	Initial fluoride concentration
C_b	Fluoride concentration at breakpoint
C_e	Equilibrium fluoride concentration
C_{EX}	Fluoride concentration at exhaustion point
E_d	Mean adsorption energy
H_{UNB}	Height of unused bed
K_1	Pseudo first order rate constant
K_2	Pseudo second order rate constant
K_a	Adsorption rate constant
k_f	Freundlich adsorption capacity
K_i	Intraparticle diffusion rate constant
k_Y	Yoon - Nelson rate constant
K_{th}	Thomas rate constant
N_0	Adsorption potential
Q_0	Langmuir adsorption capacity
q_b	Adsorption capacity at breakthrough
q_d	Dubinin-Radushkevich constant
q_e	Adsorption capacity at equilibrium
q_t	Adsorption capacity at time t
q_{EX}	Adsorption capacity at exhaustion point
t_b	Breakthrough time

t_f	Time for formation of primary adsorption zone
t_x	Time to establish PAZ
t_z	Time for movement of primary adsorption zone down the column
t_{EX}	Exhaustion time
V	Volume of fluoride solution
V_b	Throughput volume at breakpoint
V_{EX}	Throughput volume at exhaustion
W_{ad}	mass of adsorbent
Z_0	Critical bed depth
%S	Percentage saturation in column
δ	Length of the adsorption zone
ΔG°	Standard free energy change
ΔH°	Standard enthalpy change
ΔS°	Standard entropy change
b	Langmuir constant related to energy
F	Flow rate
f	Fractional capacity
M	Adsorbent mass
R	Universal gas constant
T	Temperature
u	Linear flow velocity
V	Volume of solution
Z	Bed height

CHAPTER 1

INTRODUCTION

The problems of marble waste and high fluoride concentration in drinking water is prevalent causing huge environmental and health issues. The effective measures to overcome these problems are introduced in this chapter.

CHAPTER 1
INTRODUCTION

Reutilization of the industrial wastes and its byproducts has a great importance for sustainable industrialization and economic growth of the country (Eliche-Quesada et al., 2012; Pappu et al., 2007). Treatment of waste and it's proper disposal is one of the foremost environmental issues that persist since the industrial revolution (Ngoc and Schnitzer, 2009; Williams, 2005). A few emerging industries such as marble industries are at high alarming distress for their waste disposal, raising huge environmental concern and threat for human health (Eliche-Quesada et al., 2012; Felipe-Sesé et al., 2011). The top five marble exporting countries that are dominating in marble production are Italy, Turkey, Spain, China, and India (Rassin, 2012; Tozsin et al., 2014). It has been estimated that about 20% of the total weight of the marble processed results into marble waste (Akbulut and Gürer, 2007). The amount of the marble waste generated is very substantial being in the range of 5-6 million tons per annum (Amit and Singh, 2013). Most of the marble waste is generated during the cutting and polishing of the marble, resulting in heaps of uncontrolled waste piling up in the absence of proper disposal systems (Aliabdo et al., 2014). The unsystematic dumping practices pose a severe environmental concern in various ways such as pollution of the top fertile soil making it nonporous, polluting rivers and other water bodies and adversely affecting irrigation and drinking water resources (Segadães et al., 2005). In most parts of the world, groundwater is the major source of fresh water widely used for domestic purposes. However, groundwater with high fluoride concentrations occurs in many areas of the world including large parts of Africa, China, the Middle East, Sri Lanka and India (Lapworth et al., 2012; Mondal and George, 2014). Fluoride (F^-) present in its ionic form in groundwater resources have been found to cause significant adverse effects on people through drinking-water. The acceptable limit for fluoride in drinking water is 1.50 mg/L as per WHO and 1.0 mg/L as per Indian standards, which can exceed to 1.50 mg/L in case of no alternative source

(Gorchev and Ozolins, 2011; Standard, 2012). Therefore, defluoridation of water is needed, which can be carried out using calcium based minerals, as calcium has an affinity to adsorb fluoride.

This chapter introduces marble waste, its composition, problems assosciated with generation of marble waste and its effective utilization in various industries. The problem of elevated level of fluoride concentration in drinking water resources and its serious health effects is also highlighted in this chapter. The different ways in which marble waste can be utilized for the application of development and synthesis of novel adsorbents using new as well as conservative techniques and its application for water treatment has been discussed in this chapter.

1.1. OCCURRENCE OF MARBLE

India is known for decades for its wide spectrum of natural stones such as marble, granite, limestone, sandstone and slate which are largely spread across South India and Western India (Rajasthan and Gujarat) (Agrawal and Gaharwar, 2013). This has fascinated large industrial market across the world for their processing and export. Among all other natural stones, Indian marble is highly commended in the international market because of its outlandish quality. A famous example of the magnificence of Indian marble can be seen from the The World famous Taj Mahal in which marble from Makrana region was used (Pradesh et al., 1957). The term "marble" is derived from the Latin word Murmur meaning a shining stone. It is known for its pleasant colors, uniform texture, smooth and glossy elegant surface and mellifluous feel. Marble occupies an inimitable position among other stones because of its appealing significance. Geologically Marble is metamorphosed limestone which is produced by recrystallization under thermal conditions (Molli et al., 2000). Practically there are infinite marble deposits of over 1200 million tons with splendid varieties of white, green, black, gray etc. are present, making India amongst the top 5 countries in marble export (Agrawal and Gaharwar, 2013).

1.2. PRODUCTION

Rajasthan is the main stockpile of marble which accounts for over 95% of total marble production of the country followed by Gujarat and Madhya Pradesh. Out of 32

districts of Rajasthan, 20 districts have marble reservoir in one or other form(Pradesh et al., 1957). Marble Reserve in the state of Rajasthan is shown in figure 1-1.

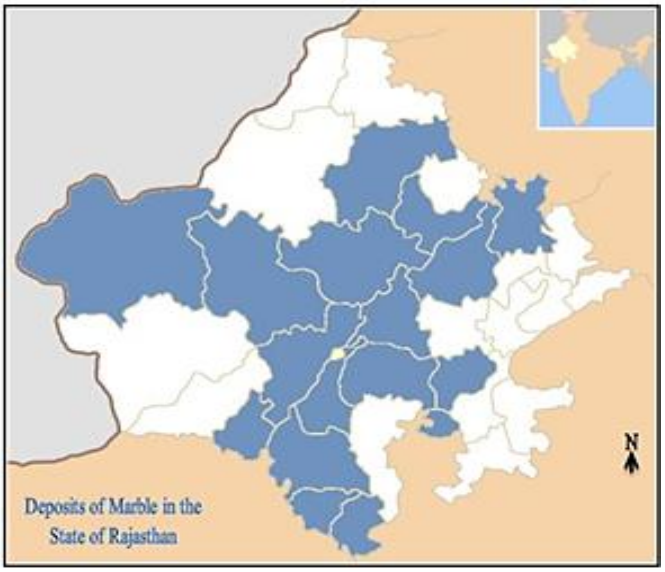

Figure 1-1. Marble reserve in the state of Rajasthan

Makrana area is famous because of its pure white crystalline marble whereas reservoir for green marble is in the district of Udaipur. Other deposits of marble are also found in the state of Gujarat in the districts of Banaskantha, Bharuch, Vadodara, Kachchh and Panchmahal having marble in various shades such as green, white, pink and green. In Haryana, marble deposits are located in the district of Mahendragarh. Marble deposits of Maharashtra are in the form of calcite and dolomite located in the areas of Katta-Hiwara, Kadbikhera, Sakaritola, Pauni, Chorbaoli, Deolapar, Mansar, Kandri, Chargaon, Junewani villages in Nagpur district(Pradesh et al., 1957).

1.3. MARBLE PROCESSING AND WASTE GENERATION

Processing of marble is done in two stages. The first stage of processing involves cutting the blocks into 2 to 3 cm thick slabs by using gang saws, wire saws, and circular saws. Rajasthan has about 95% processing capacity in the country. There are a number of gang saws and many automatic tiling plants that are in operation. Important processing centers in the State are Makrana, Jaipur, Alwar, Ajmer, Udaipur, Nathdwara, Rajsamand, Abu Road and Kishangarh. The conventional quarrying techniques of blasting produce

waste of 60% to 70% whereas processing units generate waste at 30% to 40% of their production (Amit and Singh, 2013; Institute and Govt. of India, Ministry of Micro, 2009).

Marble waste is generated at different phases of mining and processing operations in the form of irregularly shaped pieces if marble with chemical composition same as that of marble, marble waste powder, and marble slurry. Marble waste is not specified as a "Hazardous Waste" under the Hazardous Waste Rules and there is absolutely no method of systematic disposal of waste in the quarrying areas. Marble waste show non-plastic behavior and their major chemical constituent are 28-35% CaO, 10-15%, MgO, 1-2.5% R2O3, 15-20% Acid insoluble and 35-40% Loss on ignition as shown in Table 1.1 (Institute and Govt. of India, Ministry of Micro, 2009).

Table 1.1 Chemical composition of marble waste with respect to their localities

Chemical Composition	Localities			
	Jaipur	Ajmer	Chittorgarh	Udaipur
CaO%	32.80	26.15	38.60	28.55
MgO%	10.80	14.18	6.90	14.75
R_2O_3%	2.65	2.65	0.85	1.05
Acid insolubles%	14.38	23.55	16.80	17.49
Loss on Ingnition %	39.35	33.50	36.75	37.70
Total	99.98	100.3	99.90	99.54

(Institute and Govt. of India, Ministry of Micro, 2009)

1.3.1. MARBLE WASTE DISPOSAL PRACTICES

Heaps of uncontrolled wastes pile up in the absence of proper disposal systems. The unsystematic dumping practices pose a severe environmental concern in various ways such as:

- There are earmarked disposal sites by the government but most of the industries dump the slurry in nearby forest areas or on the road side.
- It was reported that 90% of the industries pump out the waste into the neighboring agricultural lands and is left there to dry.

- In most of the marble processing units there is no proper arrangement made for the collection of waste produced. Even industries in Rajasthan do not employ filter presses.
- Large amount of waste produced is dumped in either vacant land or in surface water source located in the vicinities of the units.
- The main problem faced during disposal of waste marble slurry is that transporters paid a fixed amount to dispose waste at dumping sites. But the drivers dump the slurry at any dumping site so as to reduce the distance and to cover more trips per day.
- Not much attentiveness is there for utilization of this valuable natural resource.
- There is no such law that prevents dumping the waste marble slurry and powder in such a haphazard manner. Marble waste is not even identified as a hazardous waste by the Rajasthan Pollution control Board (Institute and Govt. of India, Ministry of Micro, 2009).

The lack of seriousness towards proper disposal at specified disposal site or without treating the marble waste to save expenditure, time and efforts had created a severe problem in the state of Rajasthan. Indiscriminate quarrying of marble and disposal of the marble dust and slurry in and around the quarry surroundings has led to severe adverse effects on the environment such as reduction in porosity/ permeability of top soil, fertility reduction due to increased soil alkalinity, surface water logging at disposal sites, wet slippery soil surfaces, decrease in ground water levels due to low percolation of recharging rain water, contamination of ground water reservoirs and resources. Moreover, the suspension of the dried slurry in the form of fine marble dust in surrounding environment has led to its settling down on surrounding vegetation, causing respiratory ailments in people of nearby residential areas. The major environmental problems due to marble waste are listed below:

- The slurry when dumped on open land affects adversely the productivity of the land as shown in figure 1-2 as it reduces the porosity and prevents ground water recharge.
- Areas with dumped slurry cannot support vegetation.

- After drying, the finer fraction of slurry becomes airborne and causes serious air pollution which is not only detrimental to human beings but also to vegetation and machinery (Amit and Singh, 2013).
- Even though various Government regulations such as the Water Act, The Air Act, Forest Act, Environment Act etc. have been promulgated and various initiatives taken in order to contain the damages to the environment in the domain of mineral and mineral-based industries, handling of marble slurry waste is still a huge problem in the state and the hazardous dumping practice has become a severe threat to the environment, eco-system and the health of the people and has achieved mammoth proportions.

Figure 1-2 Problems caused by marble wastes, when marble slurry dries and marble waste powder dumped on the road side.

1.3.2. UTILIZATION OF MARBLE WASTE

Taking into account that marble waste is the byproduct of the marble industry and as it is available free of cost presently, it has become necessary to look into its potential considering not as a waste, but as a possible resource that needs to be exploited by developing technically sound and financially viable technologies towards its Total Resource Utilization (TRU). Some of the areas of a utility of marble waste that are being explored include its utilization as filler materials for roads and embankments (Misra et al., 2010), manufacture of cements (Aruntaş et al., 2010), bricks (Hamza et al., 2011),

ceramic tiles (Saboya et al., 2007), sanitary ware products (Anwar et al., 2011), production of concrete (Aliabdo et al., 2014) (Demirel, 2010) etc. Marble waste may also substitute for limestone in various industrial applications such as manufacture of glass, urea, lime, plastics etc. and few of them are also shown in Table 1.2. However an economically viable method of effective and complete utilization of marble slurry is yet to be found as large amounts of the waste is still being generated everyday with the continuous growth of the marble industry.

Table 1.2 Marble waste utilization in various industries

S.No	Industry	Uses	Reference
1	Paper Industry	Improves physical properties	Martin, 1996
2	Civil Industry	Roadwork layers	Singh et al.,2004
3	Marble industry	Reutilization for agglomerate marble	Martin, 1996
4	Ceramic Industry	Fabrication.	Soras , 1997
5	Food Industry	Composed food for animal	Gonclave, 2000

Marble waste principally constitutes of calcium and magnesium compounds which have good fluoride removal capacity. The marble waste consists of recrystallized limestone and its main constituents are calcium carbonate ($CaCO_3$), magnesium Carbonate ($MgCO_3$), lime (CaO) and MgO and some impurities in the form of silicates; hematite and manganese Oxide (Mehta et al., 2016). It has been reported that ground water resources in regions with marble quarries had very low fluoride content which shows that marble is a natural defluoridating agent. Handa stated that there is a negative correlation between fluoride and calcium concentrations in Indian groundwater (Handa, 1975). Many researchers have also reported moderate to the good removal of fluoride by using different forms of calcium and magnesium as adsorbents.

1.4. FLUORIDE

Fluoride is one of the essential element for humans as well as animals, and it plays a crucial role in drinking water. Fluoride in optimum concentration (1.5 mg/L) in water is important for the growth of bones and development of dental enamels. Higher

concentration (>1.5 mg/L) can cause severe health problems such as dental and skeletal fluorosis (Gorchev and Ozolins, 2011; WHO/UNICEF, 2015). Numerous technologies and materials are been used for defluoridation of potable water but many of them have resulted in failure or may not be considered for long-term usage. Therefore, appropriate defluoridation method is needed to be applied for a sustainable solution to the problem (Mondal and George, 2015a).

Groundwater is one of the primary water supply sources for the rural population in developing countries but depending upon the geographical location, groundwater can become unsuitable for drinking due to the high concentration of naturally occurring minerals such as fluoride ions (F^-). The weathering and leaching of F^- bearing minerals in the rocks such as amphiboles, apatite, mica, and fluorite are the main causes of high fluoride ion concentration in groundwater (Frengstad et al., 2001; Rafique et al., 2008). Groundwater may contain up to 44 mg/L of fluoride in the area rich with fluoride-containing minerals. More than 8 mg/L fluoride concentration were reported in some villages of China (Xiang et al., 2003). At least 17 states of India are affected by high level of fluoride in drinking water and are progressively identified since 1937(WHO/UNICEF, 2015). The occurrence of fluorosis in the states of India is also shown in figure 1-3.

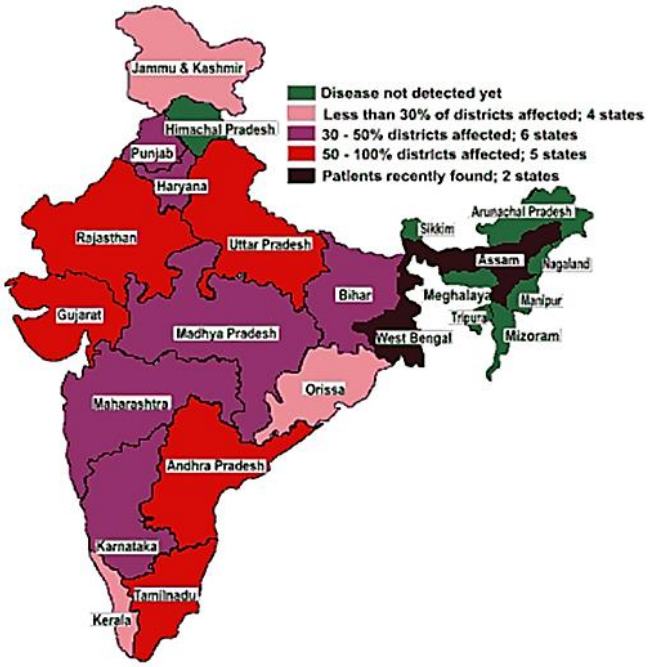

Figure 1-3. Occurrence of fluorosis in the states of India.

In 1987, it was estimated that 25 million people were suffering from fluorosis. In Rajasthan, fluoride concentrations vary between 0.6 mg l^{-1} and 69.7 mg l^{-1} (WHO/UNICEF, 2015). Assam is the recent identified state with high level of fluoride associated with endemic fluorosis.

The high level of fluoride concentration in groundwater is now one of the most crucial problem in India causing an incurable disease fluorosis (skeletal and dental) which causes permanent bone and joint deformations as shown in figure 1-4(Choubisa et al., 2001).

(a) Skeletal Fluorosis (b) Dental Fluorosis

Figure 1-4. The problem of skeletal and dental fluorosis in children.

Fluorine is a highly electronegative element and so have a tendency to get attracted by positively charged ions like calcium and magnesium (Sanderson, 1988). As our bones and teeth are composed mainly of calcium so when fluoride is consumed, the maximum amount of it gets deposited as calcium-fluorapatite crystal. The hydroxyl ion present in hydroxyapatite which is a major constituent of tooth enamel gets replaced by fluoride ion leading to the formation of fluorapatite due to more stability than of hydroxyapatite figure 1-5. Due to this a large amount of fluoride remains bounded in these tissues and only small amount is excreted out of the body which leads to diseases like dental fluorosis (Cury and Tenuta, 2009; McCann, 1952).

Besides skeletal and dental fluorosis, excessive consumption of fluoride may cause severe problems such as muscle fiber degeneration, low hemoglobin levels, deformities in RBCs, excessive thirst, headache, skin rashes, nervousness, and neurological manifestations (C.A, 2015). There are other severe effects of fluoride like the decrease in antioxidant activity leading to stress in the brain, inhibition of thyroid hormone which causes thyroid cancer, etc.(Zhan et al., 2006).

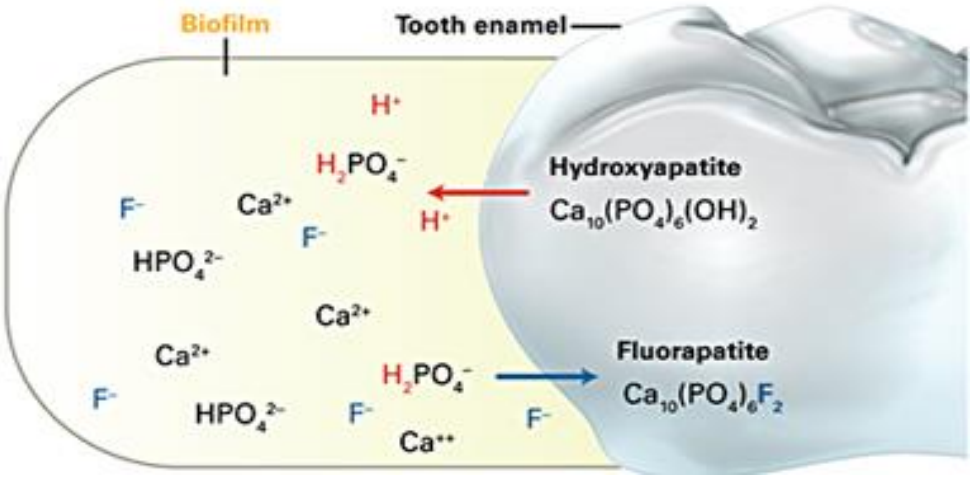

Figure 1-5. The mechanism for the formation of fluorapatite leading to the formation of dental fluorosis (Cury and Tenuta, 2009).

1.4.1. TECHNIQUES FOR FLUORIDE MITIGATION

Removal of fluoride from drinking water is the only option available to overcome the problem of elevated level of fluoride in drinking water. In the course of time, various technologies are developed for water defluoridation such as membrane technology (Arora et al., 2004), ion exchange (Durmaz et al., 2005), electrocoagulation (Zuo et al., 2008) and adsorption (Mehta et al., 2016). Among these, adsorption is the most suitable technique because of its low cost and effective fluoride removal. The comprehensive explanation of each technique is given in the following sections.

1.4.1.1. MEMBRANE SEPARATION PROCESS

The membrane separation process is used widely for industrial application for defluoridation of groundwater, wastewater treatment, and water desalination. Reverse osmosis (RO), dialysis, electrodialysis, and nanofiltration are the common membrane

techniques which are used for the removal of fluoride ions from drinking water. The problem faced during the membrane separation process are that due to the high efficiency it removes all the ions present in water, including essential minerals required for proper growth, and due to this remineralization is required after treatment. The problem of scaling prevails due to chemicals like calcium, magnesium, and silica causing failure of the membrane and allows passage of contaminants in the treated water. The process is expensive as it involves replacement of membranes at regular interval of time (Arora et al., 2004).

1.4.1.2. ION EXCHANGE

Anion-exchange resins containing quaternary ammonium functional group are the common resin used for removal of fluoride from water supplies. The following equation explains the removal of fluoride using ion exchange process:

$$Matrix - NR_3^+Cl^- + F^- \rightarrow Matrix - NR_3^+F^- + Cl^-$$

From the above equation it was observed that the fluoride ions replace the chloride ions of the resin and the process continues until all the sites on the resin are fully occupied by the fluoride ions. Resins failed drastically in the presence of other ions like carbonate, sulfate, phosphate etc. the problem of regeneration of resins leads to fluoride rich waste. The resins and the pretreatment to maintain the pH of the resins, add the extra cost to the process(Durmaz et al., 2005).

1.4.1.3. ELECTROCOAGULATION

Electrocoagulation processes can be useful for a wide range of water and wastewater treatment systems and are effective in removing inorganic contaminants from an aqueous solution by electrolysis. The electrocoagulation is the process that uses external power source which leads to oxidation of the anodes to form active coagulant which is used to remove pollutant by precipitation and flotation. The most common coagulants used for the removal of fluoride are lime and alum. The addition of lime leads to the formation of precipitates of calcium fluoride which raises the pH value of water up to 11–12. The disadvantages of this process are that it removes the small portion of fluoride (18–33%) in the form of precipitates and converts the large portion into soluble

aluminum fluoride complex ion which is itself toxic for example Nalgonda technique. Moreover, regular analysis of treated water is required to calculate the dosage of chemicals to be added for the treatment of fluoride. The cost of the process is also high as it requires regular maintenance and an attendant for the addition of chemicals (Zuo et al., 2008).

1.4.1.4. ADSORPTION

Adsorption is the most suitable procedure for removal of fluoride from water, particularly in the developing and poor regions of the world since it is simple, inexpensive, selective and high removal efficiency compared to other technologies. Adsorption is a surface phenomenon which involves removal of fluoride ions on the active sites of the adsorbent. The drinking water from ground water resources is currently treated using aluminum based adsorbents such as activated alumina, however presence of high fluoride content in raw water and improper maintenance of the defluoridation units may lead to leaching of residual aluminum in treated water. Moreover, studies revealed that aluminum could cause neurotoxicity in humans due to its prolonged consumption through drinking water and other sources. Use of aluminum based adsorbents for defluoridation has, therefore, become a matter of concern. (Rondeau et al., 2009) have demonstrated that presence of aluminum in drinking water may cause Alzheimer's disease, characterized by dementia, sclerosis, and neurological degeneration, making aluminum adsorbents unsuitable for defluoridation (Jagtap et al., 2012; Singh et al., 2016).

It has been observed that fluorosis has mostly affected the rural population who have a calcium deficient diet and mostly the older people who have been consuming high fluoride water over a long period of time. Hence the calcium intake is a very important factor for reducing fluorosis, which gives an added advantage of calcium based adsorbents for their use as a defluoridation agent over other metal based adsorbents. With the increase in interest for alternative adsorbents, many researchers have explored and developed low-cost and effective adsorbents with improved efficiency. Calcium and magnesium both possess a very good affinity to the electronegative fluoride ions and are therefore being used as an adsorbent material for defluoridation. Some of them include

calcite (Mondal et al., 2014), limestone (Nath and Dutta, 2010), eggshell (R. Bhaumik et al., 2012), bone charcoal (Larsen et al., 1993), magnesium amended alumina, magnesium bentonite, nano-magnesium oxide (Maliyekkal et al., 2008; Thakre et al., 2010) magnesium incorporated Hap (Mondal et al., 2016), hydroxyapatite (Chen et al., 2005) etc.

1.5. HYDROXYAPATITE

Hydroxyapatite (Hap) is a biomaterial composed of calcium and phosphorous that has been widely used clinically as it is bioactive, osteoconductive and biocompatible in nature. Hap can be used as a bone integration and have potential to improve cell proliferation and thus improve implant integration and wound healing (Kumar et al., 2010). It is reported that Ca and P ions are not rejected by our body so this property had led to the increased use of Hydroxyapatite for implants in bone fractures and also used as a coating to improve the biocompatibility of biomaterial (Shojai et al., 2013). Hydroxyapatite (Hap) is the primary constituent of bone matrix and tooth enamel with a chemical formula of $Ca_{10}(PO_4)_6(OH)_2$. It has been found that hydroxyl ion present in hydroxyapatite gets replaced by fluoride when consumed through various other sources which lead to the formation of a stable compound fluorapatite causing disease like dental fluorosis (McCann, 1952).

1.5.1. SYNTHESIS OF HYDROXYAPATITE

Various methods like sol-gel approach, multiple emulsion techniques, electrodepositing techniques, precipitation method etc. have been employed for the purpose of synthesis of Hydroxyapatite. From all of the mentioned techniques, precipitation method has gained most popularity due to its simple procedure and synthesis at low cost. For the bulk production of Hap, this method has gained much success (Nayak, 2010).

Precipitation method was employed in the 20^{th} century and it was used for the synthesis of Hap materials. In this method, the use of hydrothermal treatment is employed by which Ca/P ratio was improved. This is the most common method for the process of synthesis and been widely utilized. It is a simple and effective technique. Material which

is obtained by this method is highly porous in nature. Chemicals like calcium hydroxide, ammonium phosphate, calcium hydrogen phosphate are used as a starting material for the purpose of synthesis of Hydroxyapatite. A more elaborate insight of different synthesis methods for Hap is given in chapter 2 i.e. literature review.

1.5.2. APPLICATIONS

Hydroxyapatite is the most widely accepted biomaterial due to its structure similarities to the human hard tissues. It has characteristic features of biomaterials, such as biocompatible, bioactive, osteoconductive, non-toxic, non-inflammatory and faster rate of regeneration with no immunogenic properties. Due to these properties, applications of hydroxyapatite is explored in various fields such as drug delivery and tissue engineering; hydroxyapatite thin film for medical applications; dentistry and bone implants; synthesis of nano-hydroxyapatite crystals; and as an adsorbent for water and waste water treatment (Shojai et al., 2013). Using hydroxyapatite as an implant in dentistry is cost effective and also has biocompatible results. It has been seen that since bacteria attack hydroxyapatite which is the main constituent of enamel, it gets demineralized due to acid secreted by various bacteria (Oliveira and Mansur, 2007). This leads to formation of cavities in the tooth and results to cause disease as shown clearly in figure 1-6 (Aimutis, 2012).

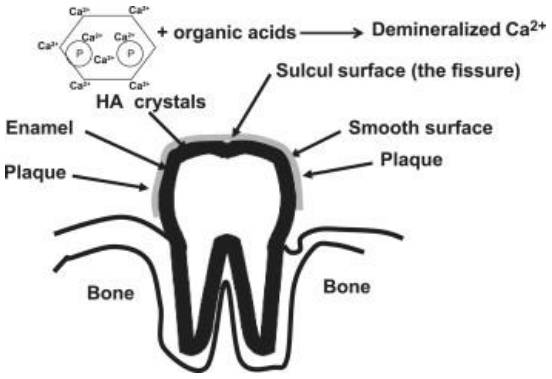

Figure 1-6 Demineralized hap by bacterial attack (Aimutis, 2012).

Synthetic enamel in form of crystals has been designed for growth on enamel surface and it has shown great adhesive properties and will be used with hydroxyapatite. This technique has fulfilled various dentistry applications like filling of cavities, enamel

whitening etc. Hydroxyapatite is directly used in toothpaste for filling of cavities and even for whitening effects. This research had done a great contribution in the field of dentistry and provided a new outlook for the use of hydroxyapatite a biomaterial. Use of hydroxyapatite in toothpaste is inexpensive and in the reach of common man. This application had resulted in interest in the synthesis of hydroxyapatite with improved pore size and with industrial importance (Aimutis, 2012; Oliveira and Mansur, 2007).

1.5.2.1. HYDROXYAPATITE FOR WATER DEFLUORIDATION

Hydroxyapatite is a calcium based compound and has an added advantage of its use as a defluoridating agent over other kinds of fluoride removing agents (Orlovskii et al., 2002). Calcium is an element critical to many body functions. Adequate calcium intake is essential for achieving peak bone mass as inadequate calcium intake is a risk factor for osteoporosis in humans and animals. The recommended calcium intake for maintenance of bone health is at 1000mg/day. A considerable segment of the Indian population, especially in the rural areas, have suboptimal daily calcium intake. Drinking water may contribute significantly to the daily calcium intake for people with calcium-deficient diets. Calcium-rich mineral waters contain higher calcium concentrations, at an average of 200 mg/L of calcium and offer an interesting, effective alternative to calcium supplementation from milk and dairy products because of their comparable or possibly even better bioavailability of calcium. Calcium produces a stimulatory or hyper-excitable effect upon muscle tissue, while magnesium produces a sedative effect (Heaney and Weaver, 2003; Prentice, 2004; Sunyecz, 2008).

A comprehensive literature review on the method for the synthesis of hydroxyapatite and its application on water defluoridation is detailed in the Literature review chapter.

1.6. OBJECTIVE OF RESEARCH

In view of the advantages of calcium, the present research is to focus on the development of an effective process technology for conversion of the marble waste powder into hydroxyapatite (Hap) that can be used for making biomaterials for bone substitutes as well as an effective defluoridation media for bringing down fluoride concentrations in drinking water within permissible range. Moreover, it helps in the conversion of an abundantly generated waste marble powder into a value added product Hydroxyapatite. It is interesting to note that researchers have reported that ground water resources in regions with marble quarries had very low fluoride content which indicates that marble powder is a natural defluoridating agent.

Several methods have been used to prepare hydroxyapatite with specific microstructure such as solid state synthesis, conventional chemical precipitation method, sol-gel method, hydrothermal method, sonochemical method, combustion method, etc. Among them, conventional chemical precipitation method is the simplest low-cost route for the synthesis of Hap. However, process parameters such as temperature, agitation method, the rate of addition of the reagents, aging time and pH maintenance during the synthesis, affect the quality of material synthesized.

With the increase in demand of the material, it is desired to optimize the synthesis process with high reaction rate along with low-cost of production and one such method which had gained much attention in recent years is the sonochemical method. It has been well recognized that ultrasonic irradiations cause cavitation in a liquid medium where the formation, growth and implosive collapse of microbubbles occur. Due to this strong agitation, the reactivity of chemicals is increased for the heterogeneous reactions between liquid and solid reactants along with the reduction of particle size and surface activation of solid materials. Ultrasonic irradiation is a powerful tool for intensification of the synthesis of nanoparticles. With this contextual approach, the synthesis of hydroxyapatite using marble waste powder was investigated in the presence of ultrasound, which is likely to assist in the proper dissolution of reactants and generate product of nano-sized particles.

The major objectives of this research work are as follows:

- Synthesis of hydroxyapatite from marble waste powder using conventional precipitation method and ultrasonication method and characterization of material synthesized via different analytical techniques (FTIR, XRD, FESEM, TEM/EDX, TGA &BET surface area).
- Batch defluoridation studies varying different parameters for optimization and in order to study equilibrium adsorption isotherms and adsorption kinetics.
- Synthesis of hydroxyapatite at a pilot plant scale using marble waste powder and optimization of process parameters.
- Column studies with most suitable adsorbent in order to determine its actual potential for water defluoridation for field applications, to obtain breakthrough performances and number of usable cycles for optimizing defluoridation unit design parameters.
- Regeneration studies for estimating recycle/reuse capacity of adsorbent.

1.7. OUTLINE OF THE WORK CONDUCTED

An outline of the research work conducted is presented in figure 1-7. The first part of the study was the procurement of marble waste powder from the marble processing industry located in the region of Kishangarh, Rajasthan, India. It was processed and used an adsorbent for fluoride removal capability. Also, synthetic hydroxyapatite and hydroxyapatite using marble waste powder was synthesized using conventional precipitation method and ultrasonication method for their application in water defluoridation. Synthesized adsorbent was characterized using FTIR, XRD, SEM, TEM/EDS, BET surface area and TGA-DTA techniques. The characterization studies helped in identifying the promising adsorbent with which further experiments were conducted.

The second part of the study was batch defluoridation studies which were performed by varying crucial process parameters such as pH, contact time, dosage and interfering ions. To get an insight of the mechanism of the process adsorption isotherms and kinetic models were studied. A regeneration method was also developed to check the reusability of the adsorbent.

The third part of the study comprised synthesis of marble hydroxyapatite in a pilot scale reactor which built with the capacity of 100 L in order to scale up the synthesis of marble hydroxyapatite and the material synthesized was used for pelletization via the extrusion-spheronization method. The column adsorption studies with the pelletized adsorbent, varying the operational parameters for evaluating the practical feasibility of the process was also conducted. In the fourth part of the study, field water samples were collected from fluoride prone areas and physicochemical parameters were examined before and after treatment adsorption.

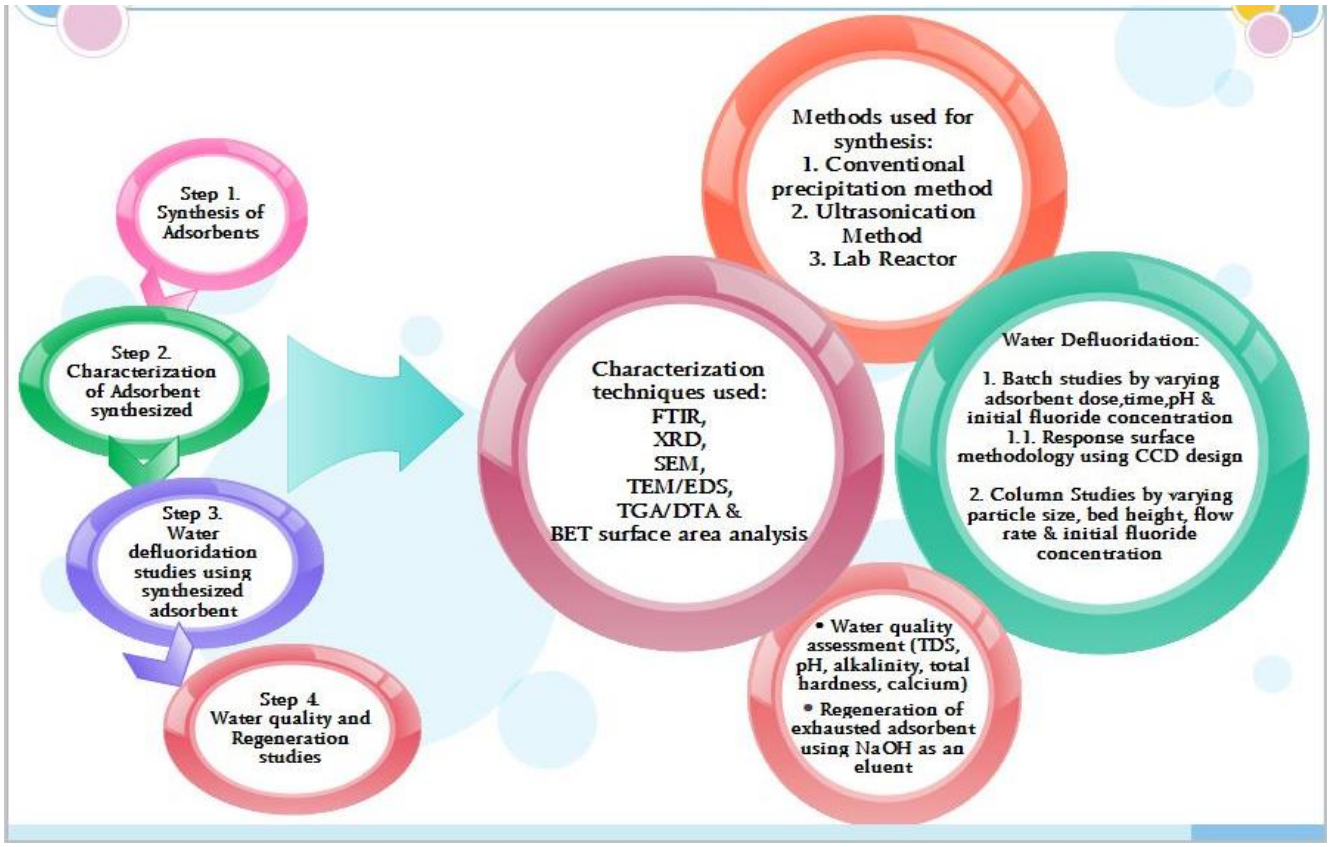

Figure 1-7 Outline of the research work

1.8. ORGANIZATION OF THE THESIS

The present doctoral thesis constitutes of seven chapters. Highlights of the chapters have been summarized below:

Chapter 1. Introduction: The introduction chapter provides an overview of the problem statement, origin of problem and an outline of the work carried out for the present research.

Chapter 2. Literature review: This chapter includes the summary of the literature involving the issues of interest. The literature review is divided into two sections, first section gives the glimpse of methods for synthesis and characterization of hydroxyapatite and its derivatives. Second section gives the detail insight into the fundamentals of hydroxyapatite and its derivatives for defluoridation, comparison with other adsorbent performance.

Chapter 3. Materials and methods: The description of methodology used for the research is presented in this chapter.

Chapter 4. Adsorbents used in the study: Introduction of each adsorbents which have been used in the study is comprised n this chapter. Details of all the adsorbents followed by their applications in water defluoridation are presented in each individual subchapters.

Part I. Pure Hydroxyapatite (synthesized) as an adsorbent: Synthesis and characterization of pure hydroxyapatite as well as batch defluoridation studies using RSM approach is presented in this chapter

Part II. Marble waste powder (MWP) as an adsorbent: Studies on utilization of marble waste as an adsorbent for water defluoridation is depicted in this chapter.

Part III. Marble apatite (MA) as an adsorbent: Attempt for synthesis of hydroxyapatite using marble waste have been done using precipitation and ultrasonication method and its application in water defluoridation using batch studies is summarized in this chapter.

Part IV. Marble hydroxyapatite (MA-Hap) as an adsorbent: Pure hydroxyapatite was synthesized using marble waste powder which was named Marble hydroxyapatite from

ultrasonication method and precipitation method. Its application for defluoridation of drinking water is also explored and detailed in this chapter.

Chapter 5. Synthesis of MA-Hap in lab reactor: Synthesis of MA-Hap and its characterization is presented in this chapter.

Chapter 6. Pellets preparation and Column Studies: This chapter is focused on preparation of MA-Hap pellets and exploring the practical feasibility of the fluoride adsorption process through column studies.

Chapter 7. Summary of the Adsorbents synthesized: The comparative study of all the adsorbents is summarized in this chapter.

Conclusion. Covers of all the major findings in the study

Recommendation for future work. Contributes into the future possibilities for further research.

1.9. SUMMARY OF THE CHAPTER

The marble waste generated by marble industry is a huge environmental concern and threat to human health. To overcome these problems, marble waste had found its application in the field of road construction, cement industry, brick construction etc. but an economically viable method of effective and complete utilization of marble waste is yet to be found. The major constituents of marble waste are compounds of calcium and magnesium, both of which possess affinity towards fluoride ions in an aqueous system. The presence of an excess of fluoride ions in drinking water resources is a major problem and it becomes essential to lower the fluoride concentration in drinking water within permissible limit of 1.5 mg/L and 1.0 mg/L as per the Indian Drinking Water Standards and World Health Organization (WHO) respectively. Defluoridation using adsorption technology serves best in this case due to its high efficacy, selectivity, and comparatively low cost involved for process and helps to alleviate the problem of high fluoride in drinkable water and thereby fluorosis.

The present research is focused on the development of an effective process technology for conversion of the marble waste powder into hydroxyapatite (Hap) that can be used for making biomaterials for bone substitutes as well as an effective defluoridation media for bringing down fluoride concentrations in drinking water within permissible range. Moreover, it helps in the conversion of an abundantly generated waste marble powder into a value added product Hydroxyapatite. It is interesting to note that researchers have reported that ground water resources in regions with marble quarries had very low fluoride content which indicates that marble powder is a natural defluoridating agent.

The next chapter gives an overview of the different methods which are used for the synthesis of hydroxyapatite along with its applications as an adsorbent for defluoridation of drinking water.

CHAPTER 2

LITERATURE REVIEW

In this Chapter, a review of various methods of synthesis and characterization of hydroxyapatite and its derivatives is presented. It also gives a glimpse of role of hydroxyapatite in defluoridation.

CHAPTER 2
LITERATURE REVIEW

The mineral apatite, with general formula $Ca_5(PO_4)_3(F,OH,Cl)$, is the most abundant naturally occurring phosphate on Earth and it is of great importance because of their physical and chemical properties (Omelon and Grynpas, 2008). The physical and chemical nature of apatite allow numerous substitutions, as Ca in the structure can be substituted by metal cations (i.e., K, Na, Mn, Ni, Cu, Co, Zn, Sr, Ba, Pb, Cd, Sb, Y, REEs, U) whereas, PO_4^{3-} can be replaced by anionic complexes (i.e., AsO_4^{3-}, SO_4^{2-}, CO_3^{2-}, SiO_4^{4-}, etc.), which means apatites can incorporate half of the periodic table in its atomic arrangement (Liu et al., 2013). Among the different apatites, calcium apatites (fluorapatite $Ca_{10}(PO_4)_6F_2$ and hydroxyapatite $Ca_{10}(P0_4)_6(OH)_2$) occurs as the foremost source of inorganic phosphorus in nature (Liu et al., 2013). Hydroxyapatite (Hap), the principal constituent of inorganic part of human and animal hard tissues such as bone and teeth, has been of interest in industry and medical fields (Poinern et al., 2014; Wenk and Heidelbach, 1999). Hydroxyapatite is a most thermodynamically stable crystalline phase of CaP in a body fluid that possesses the highest similarity to the mineral part of bone (figure 2-1) (Malmberg and Nygren, 2008; Materials, 2015). The structure of hydroxyapatite is hexagonal, with space group P63/m: essentially a 6-fold c axis perpendicular to three equivalent a-axes at angles of 120º to each other (Henning et al., 2001).

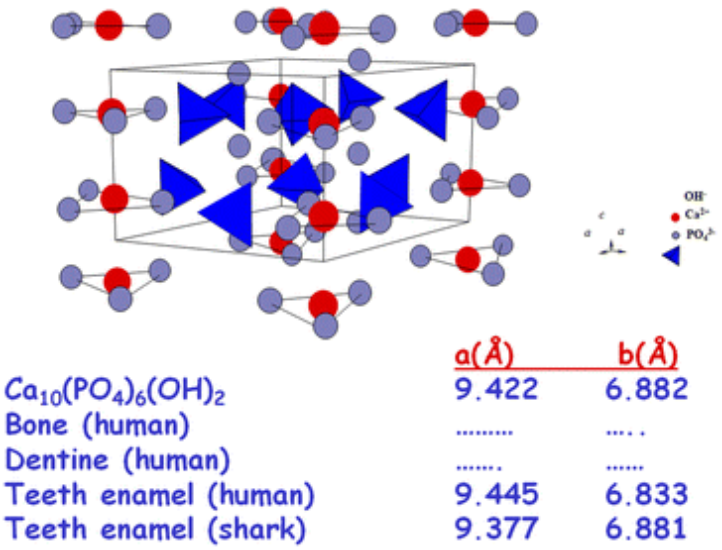

Figure 2-1. Structure of hydroxyapatite and unit cell parameters of different biological hydroxyapatite (Materials, 2015).

Hydroxyapatite was first identified as being the mineral component of bone in 1926 (Rey et al., 2010). It was found that the Hap forms strong chemical bonds with bone in vivo and remains stable under harsh conditions if used as a biomaterial. Due to these properties some researchers from the field of orthopedic, focused on the fabrication and enhancement of bioactive properties of hydroxyapatite and more interest was directed towards the use of Hap, owing to its excellent biocompatibility (Rabiei et al., 2007), affinity to biopolymers (Chen et al., 2007) and high osteogenic potential (Gu et al., 2004). It has been reported that Hap can promote new bone in-growth through osteoconduction mechanism with no immunogenic response (Kokubo and Takadama, 2006; O'Hare et al., 2010). Moreover, numerous studies have revealed that Hap particles successfully inhibit the growth of cancer cells (Li et al., 2008).

Various methods have been developed in the course of time for the synthesis of hydroxyapatite-like sol-gel method (Liu et al., 2001), chemical precipitation method (Singh, 2012), hydrothermal approach (Liu et al., 2003), ultrasonication method (Kim and Saito, 2001) etc. In order to obtain highly pure and improved phase composition of Hap, the main emphasis was given on the stoichiometry of synthesized Hap and also on the development of new methods which can have precise control over the crystallographic and chemical structure of Hap (Shojai et al., 2013).

Presently, Hap has found its application in the field of biomedical and is the material of choice in different areas such as alveolar ridge (Strietzel et al., 2007), dental and bone implants (Nakamura, 1998; Ye et al., 2001), tissue engineering systems (Seol et al., 2009), drug delivery agent (Itokazu et al., 1998) etc. Other than biological applications, hydroxyapatite has also found its importance in numerous nonmedical industrial and technological fields as shown in figure 2-2. It is been used as a chromatographic adsorbent for simple and rapid fractionation of proteins and nucleic acids (Jungbauer et al., 2004), catalysts for dehydration and dehydrogenation of alcohols, methane oxidation etc. Furthermore, studies have demonstrated that Hap is a potential biomaterial for water treatment process (Lin et al., 2009) and remediation of heavy metals (Hashimoto et al., 2009).

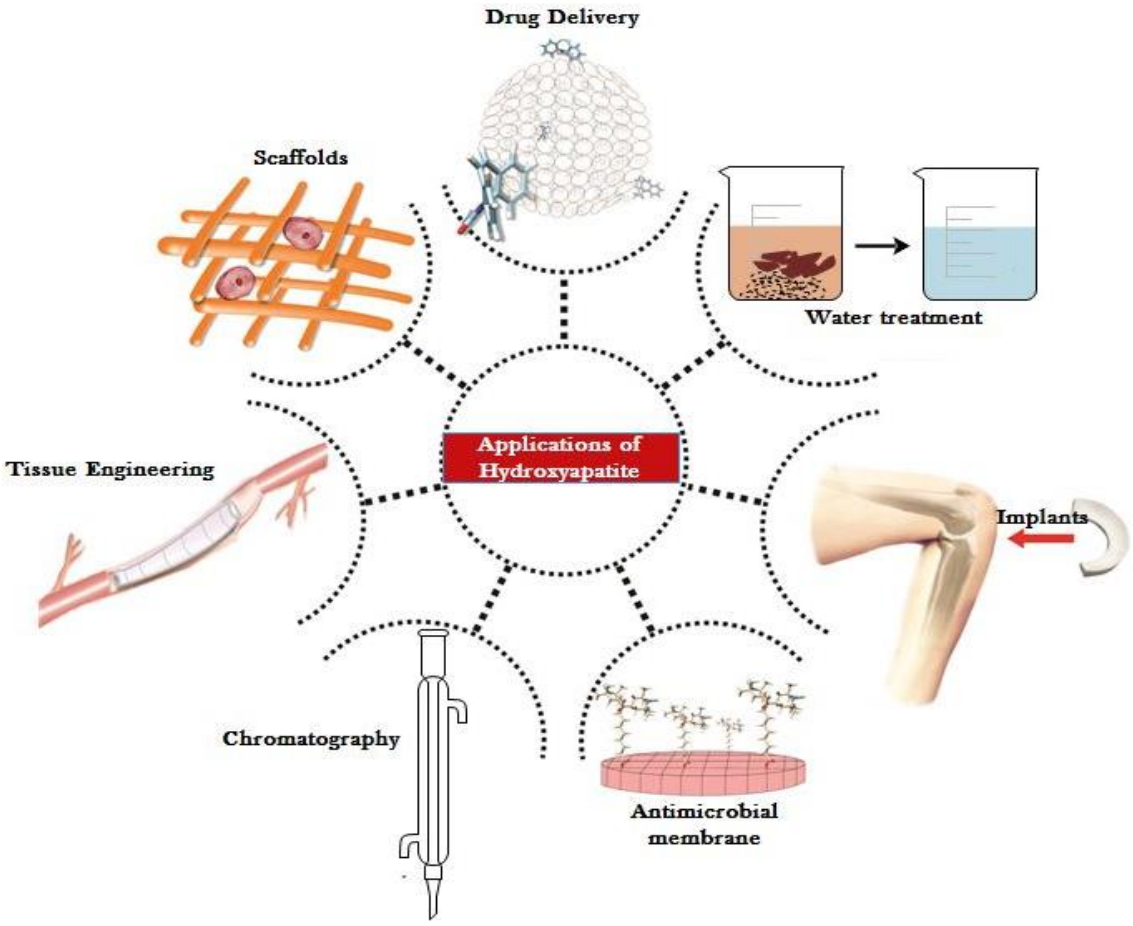

Figure 2-2. Applications of hydroxyapatite (Rojas et al., 2015).

The adsorption capability of hydroxyapatite (Hap) has recently attracted significant attention as an adsorbent for water and wastewater treatment and removal of a variety of heavy metals from aqueous solution. This is owing to the physical and chemical properties of Hap which include high removal capacity, low water solubility, availability, and high stability under oxidizing and reducing conditions (Ghahremani et al., 2017). This influenced the researchers to use different forms of hydroxyapatite (natural or synthetic) to adsorb heavy metals and anions such as fluoride from contaminated water. Natural Hap obtained from fish (Huang et al., 2011) and cow bones (Barakat et al., 2009), bone chars (Jinawath et al., 2002) and food waste (Nayar and Guha, 2009) have been used for the removal of several metallic ions such as lead, zinc, manganese and iron etc (Ma et al., 1994). Whereas some researchers also reported the immobilization of Pb, Zn, and U using natural Hap (Arey et al., 1999; Zhang et al., 2010). A low-crystalline form of hydroxyapatite which is been commercialized under the trade name of Apatite II^{TM} is used to stabilize metal pollution in soils and to remove Zn, Pb, Cd, Cu, Ni, Co, Hg and U from groundwater (Arey et al., 1999). However, the removal efficiency of biogenic (natural) Hap is very less as compared to synthetic Hap as their properties could be tailored during synthesis process.

The adsorption of heavy metals including Ba, Cd, Mg, Ni, Pb, and Zn using synthetic hydroxyapatite has been demonstrated (Thomson et al., 2003). It was found in the studies that the removal mechanisms were different for different metals as lead was involved in a dissolution-precipitation reaction with the formation of two new crystalline phases, whereas, uranium was removed by dissolution-precipitation with the formation of an amorphous-crystalline phase, and Cd was exchanged for Ca. Nano-hydroxyapatite (n-HAp) as synthetic apatite was found to be a suitable sorbent for fluoride because of their low costing, availability and higher adsorption efficiency as previously reported by the authors (Gao et al., 2009a; Sternitzke et al., 2012). Nakahira et al., (2006) reported the removal of arsenic in geothermal water by using hydroxyapatite based materials such as bovine bone and hydroxyapatite modified by a solid solution with SiO2 (Nakahira et al., 2006). It was reported that the surface hydroxyl groups of hydroxyapatite are the active site for adsorbent material and the heavy metals removing by adsorption depends on the surface site (Mobasherpour et al., 2012). Therefore, the removal efficiency should

be greatly enhanced by increasing the number of surface hydroxyl groups. Islam et al., (2011) used cellulose-carbonated hydroxyapatite nanocomposites for the removal of arsenate and reported in the increase in adsorption capacity (Islam et al., 2011). Whereas, while working with Al (III) modified calcium hydroxyapatite Nie et al., (2012) had reported a significant increase in defluoridation capacity of 32.57 mg/g than unmodified hydroxyapatite which showed a capacity of 16.38 mg/g (Nie et al., 2012).

Nano composites are also considered to be interesting functional materials with outstanding features of high mechanical properties and excellent adsorption capacity (Isiklan and Sanli, 2005). Today these composite materials of organic/inorganic origin are extensively studied because of their combined advantages. The mechanical and physical properties of the polymer can help to overcome the low mechanical properties of hydroxyapatite and which would also give better handling properties to hydroxyapatite. In addition, different desirable forms such as beads and membranes could be made using these composite materials (Zhao et al., 2012).

Numerous studies have demonstrated the applications of hydroxyapatite (Hap), which has recently been drawing substantial attention on the development of synthesis methods. This review focuses on providing the information on different methods for the synthesis of hydroxyapatite. Different parameters which plays an important rode during the synthesis of hydroxyapatite such as pH, temperature and time of reaction was focused and their effect on the characteristics of the material obtained is also detailed.

Hydroxyapatite particles are very susceptible to ion substitutions and therefore used as an adsorbent for the purification of wastewater and removal of a variety of heavy metals from aqueous solution. The review is also focused on application of hydroxyapatite for water defluoridation. To the best of our knowledge, it is the first critical review which detailed about the different sources which are used for the synthesis of hydroxyapatite for their application in water defluoridation. The advantage and disadvantages of each methods and different parameters such as adsorption capacity, isotherm and kinetics for each adsorbent is also inherited in the review.

2.1. METHODS FOR SYNTHESIS OF HYDROXYAPATITE

With the span of time, various methods have been used to prepare hydroxyapatite for different applications. Every synthesis method involves different synthesis routes which can have precise control over the microstructure and purity of the hydroxyapatite. In the present review five different synthesis methods such as Hap from natural source, conventional precipitation method, hydrothermal method, sol-gel method and ultrasonication method have been focused. The different processing parameters, characteristics of the hydroxyapatite obtained and their applications with respect to synthesis method are summarized in Table 2.1.

2.1.1. NATURAL (BIOGENIC) SOURCE

Preparation of Hap using natural source such as biogenic materials is a fascinating method because the material obtained through waste recovery will be economically and environmentally sustainable. Hap produced from biogenic sources are widely accepted because of its better immunogenic response due to its physicochemical similarity with natural bone apatite (Sobczak et al., 2009a, 2009b). Different materials have been used which includes biowastes, eggshells, the exoskeleton of marine organisms, etc. as a source for preparation of Hap as shown in figure 2-3 (Barakat et al., 2009; Huang et al., 2011; Ozawa and Suzuki, 2002). The technique of annealing removes the organic materials from the bones in order to obtain pure Hap (Herliansyah et al., 2009; Murugan et al., 2002; Sobczak et al., 2009b). Other than this, extraction methods like hydrothermal treatment, plasma processing, enzymatic and alkaline hydrolysis, etc. were used to prepare Hap using biogenic source (Huang et al., 2011; Yoganand et al., 2011). (Ozawa and Suzuki, 2002) prepared Hap from fish bone waste using a thermal decomposition method. The fish waste was washed using a water jet to remove unwanted fish meat followed by boiling. The bone residue obtained was dried and calcined at 600-1300ºC in air to obtain highly crystalline HAp at temperature varying from 800-1200ºC. Further increasing the temperature to 1300ºC, Hap coexisted with tricalcium phosphate (TCP). Other researchers worked with different methods to decompose, dissolve and hydrolyze the organic compounds using conventional thermal decomposition, subcritical water process, and an underlying hydrothermal method (Barakat et al., 2009). They found that

all three methods had the ability to remove organic maters to produce pure Hap. Thermal treatment resulted in the production of Hap nanorods of about 300 nm in length, whereas other methods produced Hap nanoparticles.

Other than hard tissues, some attempts were made to produce Hap, using eggshell waste (Gergely et al., 2010; Zhao et al., 2008). Eggshells comprise of about 95% calcium carbonate, with a CaCO3 calcite phase and rest is an organic component with protein layer and some salts (Goloshchapov et al., 2013; Kumar et al., 2012). The first treatment step of eggshells is calcination at 900ºC which decomposes the organic matter and convert CaCO3 to CaO as shown in eq. (1) below.

$$CaCO_3 + Heat \rightarrow CaO + CO_2 \quad (1)$$

The obtained CaO on exposure to atmosphere formed Ca(OH)2 that was used for the preparation of Hap by reacting with a suitable phosphorus precursor (Kumar and Girija, 2013). A very simple method was suggested by Chaudhuri et al., (2013) in which calcined eggshells (CaO) were slowly added to the solution of K_2HPO_4 and mixed for 10 min while pH was mainted at 9 using ammonium hydroxide. The resultant solution obtained was subjected to heating at 37ºC which produced the pure form of nano-Hap as observed from XRD analysis. Studies were also conducted on eggshells by treating them with strong acid such as HNO_3 and HCL to produce $Ca(NO_3)_2$ and $CaCl_2$ respectively. Furthermore, preparation of Hap using hydrothermal process were reported by Rivera et al. by using calcined eggshells and treating with tricalcium phosphate (TCP, $Ca_3(PO_4)_2$) at 1050ºC for 3 h. Hap produced by this method also had calcium oxide (CaO) and calcium hydroxide ($Ca(OH_2)$). Boonyang et al., (2010) used the hydrothermal process for the conversion of crocodile eggshells into hydroxyapatite by using three different phosphate sources including diammonium phosphate ($(NH_4)_2HPO_4$), tricalcium phosphate ($Ca_3(PO_4)_2$) and phosphoric acid (H_3PO_4). Monophase of Hap was obtained within 25h and 8 h of heat treatment at 250ºC when $(NH_4)_2HPO_4$ and $Ca_3(PO_4)_2$ was used.

Calcium carbonate sourced from marine species typically showed characteristic porosity and similarity to human bone structure due to which it is considered as another natural raw material of choice for synthesis of Hap (Boonyang et al., 2010; Walsh et al.,

2008). A conventional method for its preparation included ion exchange under hydrothermal conditions, according to the following reaction (2) (Boonyang et al., 2010):

$$10CaCO_3 + 6\,(NH_4)_2HPO_4 + 2H_2O \rightarrow Ca_{10}(PO_4)_6(OH)_2 + 6(NH)_4CO_3 + 4H_2O + 4CO_2 \quad (2)$$

There is a great structural difference between varieties of Hap prepared from different marine species, for example, Hap prepared using corals naturally have a pore size of several hundreds of microns, whereas Hap synthesized using marine algae surpasses a few micrometers (Jinawath et al., 2002). The difference between the structure is similar to that found in the bone naturally, making it more beneficial in bone repair applications. Seashells, oyster shell, snail shell, Conch and giant clam shells are the common marine source for the synthesis of Hap using different phosphorous precursors and synthesis methods. Lamos et al., (2006) synthesized Hap nano-powder using oyster shell using $(NH_4)_2HPO_4$ and additional (KH_2PO_4) by a hydrothermal transformation process at 200ºC (Lemos et al., 2006), whereas, Wu et al., (2011) synthesized Hap from oyster shell powder using a mechanochemical reaction and heat treatment (Wu et al., 2011).

Bio-membranes such as those of eggshell or bamboo, have played a significant role in the synthesis of Hap (Zhang et al., 2011). Biomolecules originating from orange peel, potato peel, egg shell, papaya leaf, and calendula flower have been reported to affect the Hap characteristics during synthesis of Hap powder (Nayar and Guha, 2009). There is the significant role of the extracted biomolecules such as amino acids, carotene, papain, carotenoids, vitamins, etc. over the control on the size of the material synthesized as their small quantities lead to a significant change in both size and morphology of resulting powder. For example, studies from eggshell membranes reported to produce needle-like Hap nanoparticles, whereas, Y. Zhang et al., (2011) reported flower-like structures of Hap using both eggshell membrane and bamboo membrane.

The processing time and temperature for the synthesis of hydroxyapatite from biogenic source was 3 h-4 h and 500ºC-1300ºC which is presented in Table 2.1. Hydroxyapatite had a diverse morphology as there was no control over the shape and size during the preparation. The average size of Hap obtained was in the range from 250µm -

40 nm. It was found that at lower temperature and less processing time, Hap with intermediates were obtained, whereas, with increase in temperature and processing time, purity of Hap was also increased. In order to obtain hydroxyapatite with high purity using biogenic source, temperature in the range of 650ºC to 800ºC with the reaction time 3 h to 5 h is required. The major disadvantage of using biogenic source for the preparation of hydroxyapatite is that morphology of the particles cannot be controlled and higher temperature is required for processing.

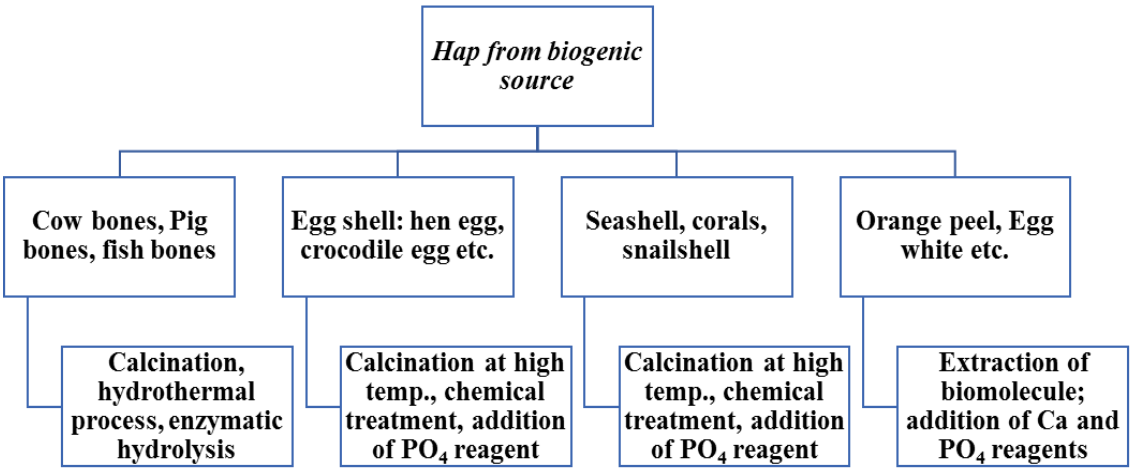

Figure 2-3. Preparation of hydroxyapatite from different biogenic source

2.1.2. CONVENTIONAL PRECIPITATION METHOD

Conventional chemical precipitation method is the most popular and widely used method for synthesis of Hap due to its simple process and reproducibility of results (Santos et al., 2004). Calcium hydroxide or calcium nitrate are used as sources of calcium, whereas; orthophosphoric acid or diammonium hydrogen phosphate are among the common phosphate sources for the synthesis of Hap (Gao et al., 2009b; Sundaram et al., 2008). A simple technique employed in this method is to synthesize Hap by adding phosphate reagent into the solution of calcium reagent with continuous stirring. After complete addition of reactants, suspension solution is kept for aging under atmospheric pressure or in some cases immediately washed, dried and crushed into a fine powder (Nayak, 2010). The schematic representation of synthesis of hydroxyapatite using conventional precipitation method is depicted in figure 2-4.

Process synthesis parameters such as pH, temperature, calcination temperature and aging step are important factors that controls the purity of the hydroxyapatite synthesized using precipitation method. Generally, in precipitation method, the reaction is conducted at high temperature and pH values to obtain a single-crystal hydroxyapatite. Low temperature and low pH during the synthesis process leads to the generation of phase impurities in the form of dicalcium phosphate anhydrous (DCPA), tri-calcium phosphate (TCP) and octacalcium phosphate (OCP) (Catros et al., 2010; Wang and Shaw, 2007; Zhang et al., 2002). Recently, Mehta et al., (2017) reported the use of calcium nitrate and potassium dihydrogen phosphate for synthesis of hydroxyapatite nano-rods via a simple conventional precipitation method. The temperature and pH during the reaction were maintained at 80ºC and 9-10 respectively and material was calcined at 900ºC, and was observed that prominent elongated Hap nanorods were formed (Mehta et al., 2017). Further, Zanotto et al., (2012) observed Hap particle size increased with increase in temperature (Zanotto et al., 2012).

Sung et al., (2007) synthesized Hap nanopowders using a modified chemical precipitation route. The material obtained was observed to be amorphous with, low crystallinity and the particles size were in the range of 50-100 nm. The Ca/P ratio was varied to analyze the amount of Hap and β-TCP phases and observed that Ca/P ratio of 1.70 formation of β-TCP content was least, whereas as the ratio was increased to 1.75, more was the formation of a CaO phase as well as β-TCP (Sung et al., 2007). Highly pure and homogeneous Hap ceramic powder was synthesized and the reagents used for the synthesis, were salts of calcium nitrate tetrahydrate and diammonium hydrogen dissolved in modified simulated body fluid (SBF) solutions at 37°C and pH 7.4. They reported that heating at 1600ºC of the material obtained did not decompose into β-TCP phases (Tas 2000).

Other than temperature, pH, and effect of calcination, the mixing rate and drying method also play a significant role as it determined the rate of reaction. To improve the chemical homogeneity and stoichiometry of the hydroxyapatite, slow titration is being practiced (Ferraz et al., 2004). Wang et al., (2010) reported the effects on the characteristics of the synthesized hydroxyapatite using different solvent systems (pure

water and a water/ethanol mixture) and various types of drying i.e. atmospheric drying, vacuum drying, and freeze-drying. It was reported that with increase in the proportion of ethanol, the size of particles was also increased. TEM analysis of samples provided information that Hap synthesized in water had diameter in the range of 20-30 nm whereas, when ethanol was used, diameter increased significantly to 100-150 nm. The effect of drying was also studied by atmospheric drying, freeze drying and drying under vacuum conditions. When atmospheric drying was used, the particles were smaller than those freeze-dried. When Hap was dried under vacuum, the morphology of the particles was spherical in shape with few rods like structure (Wang et al., 2010).

Various alternative approaches were applied for modifying Hap characteristics such as morphology and crystallinity through the addition of additives such as surfactants (Rhee and Tanaka, 2000; Wang et al., 2010). The most popular surfactant used in the synthesis of Hap is CTAB, whose molecules are ionized to create a tetrahedral structure Hap (Liu et al., 2004; SL Shanthi et al., 2009; Yao et al., 2003). (Liu et al., 2004) reported that Hap nanorods with the diameter of 50–80 nm and 0.5–1.2 nm in length (determined by TEM) were successfully synthesized using CTAB and PEG 400. Hap nano-rods with the diameter of 20 nm and length 100-200 nm were also synthesized (SL Shanthi et al., 2009) by the co-precipitation method using cationic surfactant CTAB as a template, at ambient temperature and pressure. Mesoporous nano-hydroxyapatite (n-HAP) was also synthesized (Wu and Bose, 2005) by low-temperature co-precipitation method in the presence of CTAB. It was analyzed that different ratio of surfactant had a significant role in the structure, surface area, pore volume and pore size of the material synthesized.

Other than CTAB, Tween-80 was also used for synthesis of Hap. (Zhang and Zhu, 2005) synthesized Hap with and without surfactant and observed that there is a significant difference in the morphologies caused due to adsorption of surfactant. Hap was spheroidal in shape with sizes of 80-300 nm (FESEM) when surfactant was not added, whereas, Hap synthesized in the presence of Tween-80 resulted in the form of uniform rods with an average size of 50 nm.

Conventional precipitation method produced pure hydroxyapatite with no intermediates and is the most reliable method to prepare rod-like structured

hydroxyapatite. Table 2.1 shows that the average size of hydroxyapatite synthesized from conventional precipitation method was in the range of 40-200 nm. The synthesis processing time varied from 1 h to 72 h based on the different methodology. pH is the important factor in this conventional method and it varied from 7- 12 whereas, synthesis temperature were different for different applications. Conventional method is best suited for the preparation of hydroxyapatite nano-rods. Table 2.1 represents that, Hap when synthesized at alkaline pH using conventional precipitation method gives pure Hap and Nano-rods were formed. The advantage of using this method for the synthesis of Hap is the simplicity of the procedure and morphology can be controlled based on the synthesis parameters.

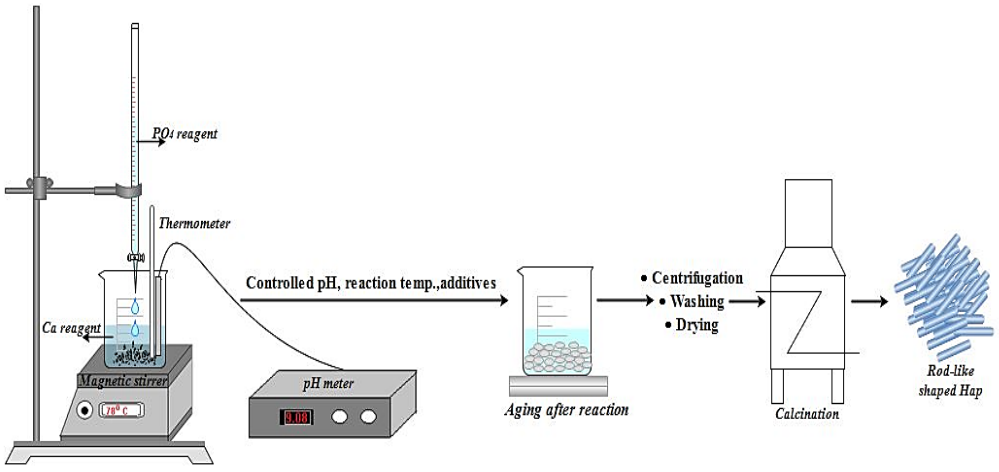

Figure 2-4 Synthesis of hydroxyapatite using conventional precipitation method

2.1.3. HYDROTHERMAL METHOD

Hydrothermal method is one of the most common methods which was used from the 20th century and identified as an important technology for synthesis of hydroxyapatite. In hydrothermal synthesis method, reaction of chemicals utilizing single or heterogeneous phase take place at elevated temperature (T > 25ºC) and pressure (P > 100 kPa)(Jokić et al., 2011; Zhang and Darvell, 2011). It was reported that with increase in temperature and pressure, the Ca/P ratio in the precipitates also improved significantly (Tsiourvas et al., 2011; Zanotto et al., 2012). However, expensive equipment's are required to maintain elevated temperature and pressure, making the hydrothermal process more expensive than

some of the other wet methods. Other problems related to this approach is the longer reaction time and agglomeration of particles that prevent this process from being the most efficient method for synthesis of Hap (Shojai et al., 2013).

The hydrothermal method was mostly explored to prepare single dimensional (1D) nanosized Hap (nano-rods). Usually, the morphology which was obtained by a typical hydrothermal method, is irregular spherical or rod-like with a broad size distribution mostly in the range of 0.7-3.0 μm (Neira et al., 2008), 10-152 nm (Wang et al., 2007) or 10-80 nm (Tsiourvas et al., 2011) determined by TEM and SEM analysis. J. Liu et al., (2003) demonstrated influence of pH and temperature on the morphology of hydroxyapatite synthesized using hydrothermal method by using $Ca(OH)_2$ and $CaHPO_4.2H_2O$ as reagents. The pH during the reaction was maintained between 6-12, whereas temperature was varied from 60ºC-140ºC to investigate the influence on the morphology of hydroxyapatite synthesized. It was observed that at pH 9 and temperature 120ºC, well elongated single crystal particles with diameter of 40 nm and length 600 nm was obtained. Earl et al., (2006) mixed $Ca(NO_3)_2.4H_2O$ and $(NH_4)_2HPO_4$ with distilled water, in a hydrothermal reactor at 200ºC for 24-72 h and determined that longer treatment time resulted in secondary phases (Earl et al., 2006). SEM micrographs of Hap depicted rod-like morphology with size of 100-500 nm in length and 10-60 nm in diameter. Similarly in the previous methods, to improve the morphology and procedure, many modifiers were used, such as calcium chelating agents and various organic surfactants in hydrothermal method (Jiang et al., 2010; Lak et al., 2008; Sun et al., 2009). Using the chelating agents such as EDTA in the process it was found that longer crystal size under low hydrothermal temperature was obtained (Arce et al., 2004; Jiang et al., 2010). This can be attributed to the fact that EDTA acted as a potent chelating agent which chelated the free calcium ions and successively controlled the crystal growth of the hydroxyapatite. R. Zhu et al., (2008) reported use of EDTA with the molar ratio of EDTA/Ca 1, using a hydrothermal process at low pH and temperature (160ºC) which resulted in large Hap prism sized particles. Lak et al., (2008) reported dandelion-like Hap nanostructures using EDTA at the very high pH value of 12.

Other than EDTA, organic modifiers, such as PEG, Tween-20, and sorbitol, at different hydrothermal temperatures were used for synthesis of hydroxyapatite of desired characteristics (Y. Li et al., 2008; Mizutani et al., 2005; Zhou et al., 2007). Yan et al., (2001) used SDS and CTAB in order to regulate the nucleation and crystal growth of hydroxyapatite particle with a hydrothermal method. The Hap obtained at room temperature were fibrous, and after hydrothermal treatment, uniform nanorods were obtained. A. Wang et al., (2007) reported the use of CTAB to control the size and morphology using hydrothermal method and results indicated that particles obtained were in the form of uniform rod-like monocrystals. Different elements such as magnesium and silicon were substituted into the hydroxyapatite to enhance its properties. It was observed that addition of Si during the synthesis of hydroxyapatite leads to an enhancement of its bioactive behavior (Kim et al., 2002; Lee et al., 2004; Patel et al., 2003), whereas, magnesium ions inhibited the growth of the face of Hap crystals which allowed modification of physicochemical properties of hydroxyapatite by controlling the Mg ion substitution (Aminian et al., 2011). Suchanek et al., (2002) prepared magnesium-substituted hydroxyapatite powders by the mechanochemical-hydrothermal method at room temperature via a heterogeneous reaction between $Mg(OH)_2/Ca(OH)_2$ powders and an $(NH_4)_2HPO_4$ solution. From the XRD analysis, it was observed that phase pure Mg-HAp containing 0.8-12 wt% of Mg was obtained. Also, through dynamic light scattering analysis, it was observed that particle size of Mg-Hap was in the range of 102 nm-1.2 µm (Suchanek et al., 2002). Tang et al., (2005) reported synthesis of silicon-substituted hydroxyapatite (Si-HA) by hydrothermal method using $Ca(NO_3)_2.4H_2O$, $(NH_4)_3PO_4$ and $Si(OCH_2CH_3)_4$(TEOS) solutions as reagents. A 0.5 M solution of $Ca(NO_3)_2.4H_2O$ containing 0.2 g Polyethylene Glycol was added to $(NH_4)_3PO_4$ and TEOS solutions, which was stirred for 0.5 h, followed by hydrothermal treatment at 200ºC for 8 h to obtain Si-Hap. It was observed that addition of polyethylene glycol made the better dispersion of Si-Hap nanoparticles. Also, substitution of the silicate groups caused some OH^- loss to maintain the charge balance that changed the lattice parameters of HA (Tang et al., 2005).

Hydrothermal method is best to control the morphology of hydroxyapatite. Table 2.1 demonstrate that Hap produced from this method had diverse morphology with different shapes like needle, prism, flower, plate, dandelion, fiber etc. Although average

size varied from few nanometers to 150µm pure Hap was obtained through this technique. Temperature is the most important parameter in hydrothermal process and for the synthesis of pure hydroxyapatite the optimum temperature is in the range of 110ºC to 200 ºC.

2.1.4. SOL-GEL METHOD

The sol-gel process is a wet chemical method and had gained much attention as it did not require high vacuum and high temperature. It was found to be an efficient method for the synthesis of nano phasic Hap, due to the possibility of having a strict control of process parameters. The schematic representation for the synthesis of Hap using Sol-gel method is depicted in figure 2-5. The molecular-level mixing in the sol-gel process helped in improving the chemical homogeneity to a significant extent (Montero et al., 2009; Padmanabhan et al., 2009; Ramanan and Venkatesh, 2004). Additionally, in-vitro and in-vivo studies revealed that Hap synthesized using sol-gel process was more biocompatible and similar to biological apatite (Fathi et al., 2008). But the major disadvantages is to maintain the monophasic Hap as the generation of secondary phases such as CaO occurred during the sol-gel method. This hampered the biocompatibility of the material and additional efforts were required to remove the secondary phases by washing of the material with dilute acid or modification of the synthesis procedure (Hosseini et al., 2007).

The method for preparation of Hap using sol-gel process includes the mixing of alkoxides (or other suitable precursors) in either an aqueous or an organic phase, which is followed by aging at room temperature. The gelation formed was dried on a hot plate, and organic residues were removed from the resulting dried gel during post-heat treatment i.e. calcination (Chen et al., 2011; Ioiţescu et al., 2009). All the parameters had significant effect on the purity of the material synthesized. For example, inadequate aging, uncontrolled gelation and heat treatment process were some of the reasons for generation of various impurities, mainly CaO, $Ca_2P_2O_7$, $Ca_3(PO_4)_2$ and $CaCO_3$ (Hosseini et al., 2007; Hsieh et al., 2001). (Hwang and Lim, 1999) observed the chemical and structural changes of hydroxyapatite films when calcium nitrate and phosphoric acid were used as reagents. Hydroxyapatite formed at 500ºC whereas, presence of secondary phases

in the form of β-tricalcium phosphate was observed at 700ºC from XRD analysis. (Brendel et al., 1992) synthesized Hap using sol-gel method at low temperature (400° C) using $Ca(NO_3)_2.4H_2O$ and phenyl diclorophosphite ($C_6H_5PCl_2$) as starting reagents and observed that Hap obtained was of low purity and poor crystallinity at low temperature, but as temperature was increased to 900ºC, pure and well-crystallized, Hap was obtained. Similar observations were made by (Kumar and Kalainathan, 2010) when Hap was synthesized using $Ca(NO_3)_2.4H_2O$ and $(NH_4)_2HPO_4$ dissolved in ethanol at 85°C using the sol-gel method. The product was sintered at 400, 750 and 1100ºC and the crystallinity of the material also improved with the increase of temperature to 1100ºC.

Hsieh et al., (2001) studied the effect of gelation rate on the formation of nanocrystalline Hap using $Ca(NO_3)_2$ and $6(C_2H_5O)_3P(O)$ as a precursor. It was observed that slow gelation resulted in few CaO phases which was removed by washing with distilled water, whereas, fast gelation resulted in formation of high CaO phases. While working with triethyl phosphite and calcium nitrate as phosphorus and calcium precursors, Liu et al; reported the stability of the sols formed and observed that no gelling occurred in ambient conditions for up to 5 days. Further XRD analysis depicted that apatitic structure appeared at 350ºC and crystal size and Hap content increased with increase in calcination temperature (Liu et al., 2002). Han et al., (2004) worked on citric acid sol-gel combustion method for the synthesis of nanocrystalline hydroxyapatite (HAP) powder using calcium nitrate, diammonium hydrogen phosphate, and citric acid as precursors. The reaction was carried out at 70-80ºC for 4-6 h for the formation of a gel which was dried at 110-120ºC. Calcination at 750ºC resulted in pure form of Hap as no other phases were observed. Due to agglomeration at 750ºC, material was sintered at 1200ºC which resulted in the formation of secondary phases such as β-$Ca_3(PO_4)_2$, (β-TCP), α-$Ca_3(PO_4)_2$, (α-TCP) and CaO (Han et al., 2004). Kuriakose et al., (2004) reported formation of stable hydroxyapatite at 1200ºC without any by-products using $Ca(NO_3)_24H_2O$ and $(NH_4)_2HPO_4$ dissolved in ethanol. The presence of ethanol attributed to providing a thermally stable Hap. This method produced Hap in the particle size range of 1.3 nm in radius making it suitable for applications in bone replacement material. Natarajan et al., (2008) reported the influence of calcium precursors on morphology and crystallinity of sol-gel-derived hydroxyapatite nanoparticles. They used two calcium

precursors named calcium nitrate tetrahydrate, and calcium acetate and the phosphorous precursor was triethyl phosphate. They also observed that the morphology of nano-Haps synthesized using different calcium precursor were different. The morphology of Hap synthesized from calcium nitrate, and triethyl phosphate was spherically shaped whereas, the morphology of Hap synthesized using calcium acetate was found to be fibrous in structure. Also, both the Hap were stable up to 1200ºC, and their crystallinity also increased with increase in sintering temperature (Natarajan and Rajeswari, 2008).

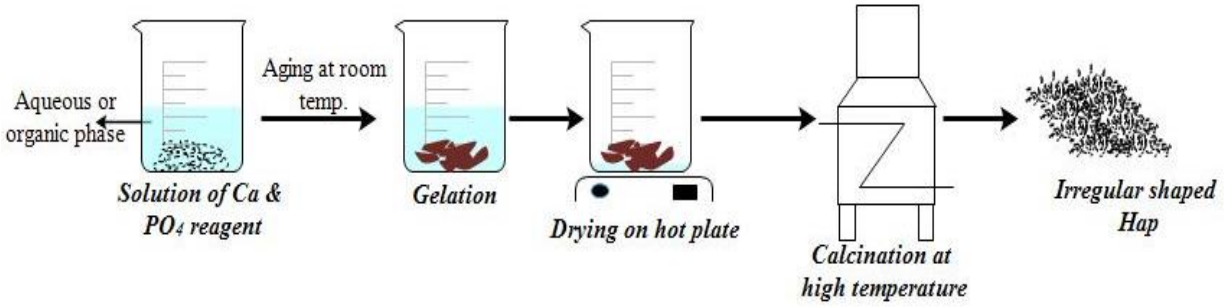

Figure 2-5. Synthesis of hydroxyapatite using the sol-gel method.

It can be summarized from the different studies for the synthesis of hydroxyapatite using sol-gel method that average size obtained were in the range of 25 µm to 30 nm. This is not the best method if morphology is to be maintained as most the studies reported agglomerated structure of hydroxyapatite. The temperature for the synthesis varied from 45ºC- 160ºC which featured that if low temperature is concern then this method maybe suitable for synthesis as observed from Table 2.1.

2.1.5. ULTRASONICATION METHOD

With the increase in demand of nano-hydroxyapatitie material, it is desired to optimize the synthesis process with high reaction rate along with low-cost of production and one such method which had gained much attention in recent years is the sonochemical method. Synthesis of hydroxyapatite using ultrasonication method is presented in figure 2-6. The physical mechanism behind the sonochemical synthesis is acoustic cavitation in a liquid medium where the formation, growth and implosive collapse of microbubbles occur (Jarag et al., 2011; Prasad et al., 2010). These shock waves produced due to cavity

collapse enable the efficient completion of chemical reactions that otherwise require rigorous stirring conditions (Moholkar et al., 2000). (Suslick, 1998) reported about the chemical and physical effects of ultrasound in a fluid medium and identified that chemical effects of ultrasound do not originate through coupling of the acoustic field with chemical species on a molecular level. Instead, it is the sonochemistry, and sonoluminescence derived mainly from acoustic cavitation that causes the formation, growth, and implosive collapse of bubbles/cavities in the liquid medium when irradiated with high-intensity ultrasound waves. Ultrasonic irradiation is a powerful tool for intensification of the synthesis of nanoparticles (Bhanvase et al., 2013). It has been reported that with the help of sonication, crystal growth was increased up to 5.5 times and Hap formed possessed more uniform nanosized and pure crystals with minimum agglomeration (Giardina and Fanovich, 2010; Jarag et al., 2011).

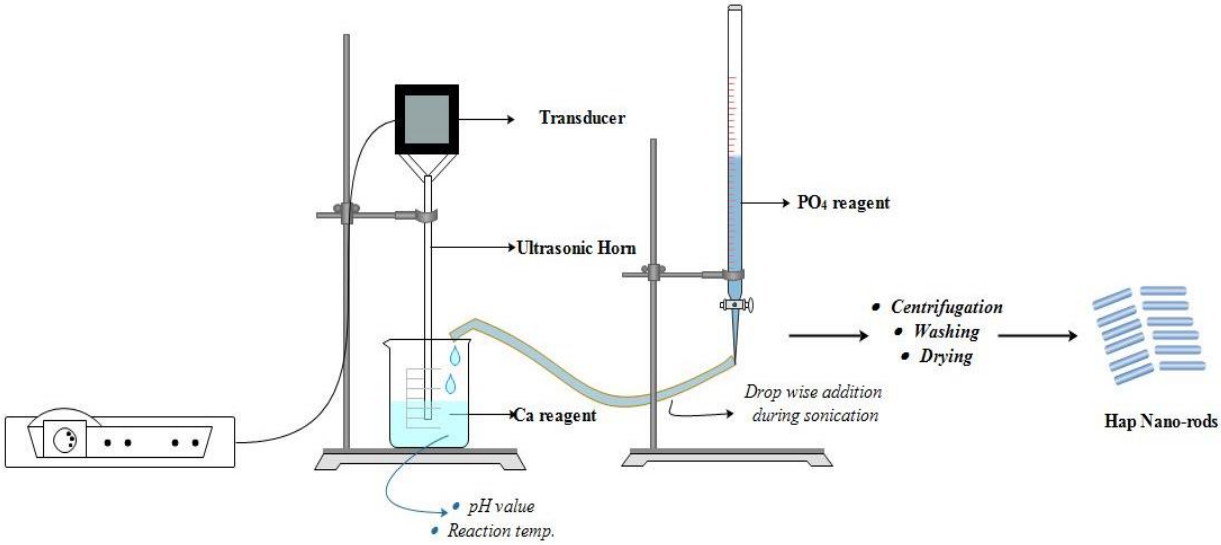

Figure 2-6 Synthesis of hydroxyapatite using ultrasonication method.

Hu et al., (1993) reported the significant decrease in reaction time from 3 h to 15 min from sonication method using mixture of $Ca_4(PO_4)_2O$ and $CaHPO_4(H_2O)$ (brushite) and 38 ± 0.5 °C. Cao et al., (2005) synthesized Hap using ultrasonic precipitation method by using urea as organic modifier in order to prepare needle-like morphology. They calculated the activation energy according to the Arrhenius-derived equation which was found to be 59.9 kJ/mol (Cao et al., 2005). It was reported that with increase in

temperature and synthesis time, Hap content also increased. (Kim and Saito, 2001) investigated the sonochemical effect on preparation of Hap using phosphoric acid and calcium hydroxide as reagents. They observed that pure Hap could be synthesized after 60 min of sonication. Rouhani et al., (2010) proposed a rapid method to prepare ball-like Hap nanoparticles by using pseudo-body solution (PBS) containing inorganic ions. They observed that sonication time is a major factor which affect the formation of crystalline phase as 15 min sonication time (28-34 kHz) produced pure Hap (Rouhani et al., 2010). Moreover, particle size decreased from 30 nm to 18 nm and more spherical sized Hap was produced using ultrasonication method compared to without sonication. Gopi et al., (2012) reported the novel ultrasonic assisted mixed template-directed method for synthesis of hydroxyapatite nanoparticles by using glycine–acrylic acid (GLY–AA) hollow spheres as an organic template. From the FT-IR analysis, they observed that Hap obtained were free from any impurities. Also as the ultrasonic irradiation time was increased, the crystallinity and size of the Hap particles decreased as observed from XRD and SEM analysis.

To enhance the synthesis process efficiency, ultrasonication was assisted with other methods such hydrothermal method and chemical precipitations method. Poinern et al., (2011) developed a method for the synthesis of nanosized Hap using hydrothermal method supported by ultrasonic irradiations. They reported that ultrasonic power of 50 W and temperature in the range of 400ºC was adequate for the formation of Hap, particles in the size range of 30 nm with spherical morphology synthesized using hydrothermal chemical precipitation method incorporating low power sonic irradiation. Recently, a comparison study was made for the synthesis of Hap using conventional precipitation method and ultrasonication with precipitation method. It was observed that by using both methods Hap was formed, but prominent elongated Hap nano-rods of 110-150 nm in length and 18-20 nm diameter was obtained by using ultrasonication with precipitation method. In this technique, potassium dihydrogen phosphate was added dropwise to the solution of calcium nitrate for 60 min at controlled temperature and pH. The obtained solution was sonicated for 30 min in an ultrasonic bath (40 ± 3 kHz) followed by calcination at 500ºC, 700ºC, and 900ºC. It was observed that reaction time for the synthesis of Hap using conventional method was 240 min which was significantly

decreased to 90 min using ultrasonication with precipitation method. Moreover, the yield of the Hap nanorods also improved from 83.24% to 90.2%, with complete phase transformation of Hap, observed using XRD analysis. The average crystallite size estimated using Debye-Scherer formula depicted that ultrasonication was responsible for the reduction of crystallite size as it decreased to 54.83 nm from 70.37 nm (Mehta et al., 2017).

Ultrasonication technique produces material with control over the size of Hap as observed in figure 2-6 and the different parameters are summarized in Table 2.1. The Hap obtained using ultrasonication method was in the range of 1µm-10 nm when pH during the synthesis was carried out in the range of 7-9. This method proved to synthesize hydroxyapatite in very less time as compared to other methods. Most of the studies reported the synthesis time of Hap was 10-90 min.

Table 2.1 Comparison of different methods for synthesis of hydroxyapatite

Method for synthesis	Processing Parameters			Characteristics of Hydroxyapatite			Reagents/Source	References
	Temp. (ºC)	pH	Time of reaction	Morphology	Phase Purity	Size		
Natural (Biogenic) source								
	2980	-	30 s- 120 s	Diverse	Hap with Intermediates	Uneven	Natural bovine bone & NaOH	(Yoganand et al., 2011)
	30-1300	-	1 h	Fibrils	Hap with Intermediates	200-500 nm	Fish-Bone Waste	(Ozawa and Suzuki, 2002)
	900	-	2 h	Agglomerated	Hap with Intermediates	45-150 µm	Bovine Bone	(Herliansyah et al., 2009)
	900	-	3 h	Nano-sized grains	Hap with Intermediates	100 nm	Eggshell	(Gergely et al., 2010)
	250	-	5 h	Nano-rode	Hap with Intermediates	300 nm	Bovine bone	(Barakat et al., 2009)
	550-1000	-	4-5 h	Diverse	Hap with Intermediates	50-250 µm	Bovine bone	(Deydier et al., 2005a)
	1st stage:600 2nd stage: 650-900	-	2 h	-	Pure	-	Bone waste	(Sobczak et al., 2009a)
	650 and 950	-	3 h	Agglomerated	Pure	Diverse	Bone sludge	(Sobczak et al., 2009b)
	1st stage: 300 2nd stage: 850&900	-	1st stage: 1 h 2nd stage: 3 h	Uniform and regular	Pure	41 nm	Eggshell	(Chaudhuri et al., 2013)
	800	-	4 h	Irregular Morphology	Pure	719 nm	Fish scale	(Huang et al., 2011)
	110	-	5 h	Flower-like	-	-	Eggshell	(Kumar and Girija, 2013)

	110	-	5 h	Flower-like	Pure Hap	78 nm	Eggshell	(Kumar et al., 2012)
	700	-	24 h	-	Pure Hap	-	Bovine bone	(Murugan et al., 2002)
	400, 700 & 900	8-9	-	Agglomerated	Pure	30-150 nm	Hen eggshell	(Goloshchapov et al., 2013)
Conventional precipitation Method								
	30	10.4	1 h	Irregular	Hap with intermediates	50-70 nm	Calcium nitrate tetrahydrate, ammonium dihydogenphosphate, yttrium nitrate tetrahydrate & zirconyl nitrate hydrate	(Sung et al., 2007)
	30	7	24 h	Agglomerated	Pure-Hap	60-80 nm	Calcium nitrate, phosphoric acid, & mono-dodecyl phosphate	(Wu and Bose, 2005)
	40	7-11	24 h	Diverse	Pure Hap	-	Calcium hydroxide, orthophosphoric acid & ammonium hydroxide	(Santos et al., 2004)
	37	7.4	24 h	Spherical shaped	Pure-Hap	50 nm	Calcium nitrate, Ammonium Hydrogen Phosphate & ammonia solution	(Tas 2000)
	40	8-11	1.5 h	Sphere, rod, needle, wire & bamboo leaf-Like	Pure Hap	20-150 nm	Calcium nitrate 4-hydrate, & diammonium phosphate	(Wang et al., 2010)
	80	5–6	5 min	Sphere-Like	Pure Hap	40–100 nm	Calcium nitrate, ammonium hydrogen phosphate, & (NH4)2-EDTA	(Gao et al., 2009b)
	40-42	7.5	1 h	-	Pure Hap	-	Calcium monophosphate & calcium dehydrates	(Sundaram et al., 2008)

	30	9.5	30 min	Rod-Like	Pure Hap	100-120 nm	Calcium nitrate & diammonium hydrogen phosphate	(Shanthi et al., 2009)
	36.5	9	3 days	Rod-Like	Pure-Hap	6- 75 nm	Phosphoric acid, & calcium hydroxide	(Rhee 2000)
	40	10	12 h	Rod-like	Pure-Hap	100 nm	Phosphoric acid & calcium hydroxide	(Catros et al., 2010)
	80	11	1 h	Rod-Like	Pure-Hap	50-200 nm	Calcium nitrate, ammonium hydrogen phosphate & ammonia solution	(Zanotto et al., 2012)
	80	9-10	Conventional: 4 h Ultrasonication: 90 min	Rod-Like	Pure-Hap	50-100 nm	Calcium nitrate, potassium dihydrogen phosphate & ammonia solution	(Mehta et al., 2017)
	85	4.5	1 h	Rod-Like	Pure-Hap	Diameter: 50-80 nm	Calcium chloride, ammonium nitrate, Trisodium phosphate, PEG 400 & CTAB	(Liu et al., 2004)
	85-90	-	72 h	Rod-Like	Pure-Hap	50-150 µm	Calcium acetate, di-ammonium hydrogen phosphate & Tween80	(Zhang and Zhu, 2005)
	120	12	24 h	Rod-Like	Pure-Hap	50-100 nm	Calcium chloride, potassium Hydrogen Phosphate & CTAB	(Yao et al., 2003)
Hydrothermal Method								
	25-35	10-11	4 h	Aggregates	CO_3 Hap & $NaCO_3$ Hap	0.35–1.6 µm	Calcium hydroxide, calcium car- Bonate & diammonium hydrogen phosphate	(Suchanek et al., 2002)

	60-140	6-14	24 h	Needle-like	Pure Hap	40-600 nm	Dicalcium phosphate, calcium hydroxide, acetic acid & potassium hydroxide	(Liu et al., 2003)
	80-130	10.6	6 -16 h	Rod-like	Hap with intermediates	5 – 80 nm	Sodium, phosphate, 1,4-diaminobutane poly dotriacontaamine dendrimer, & DAB	(Tsiourvas et al., 2011)
	90	3-3.5	12 h	Prism-like	Pure-Hap	3-9 µm	Calcium nitrate, Diammonium phosphate, & CTAB	(Neira et al., 2008)
	100-200	10	8 h	Fibre-like	Pure Hap	8- 50 nm	Calcium nitrate tetrahydrate, phosphoric acid, ammonia solution, polyethylene glycol (MW 600), Tween 20, trisodium citrate, & D-sorbitol	(Wang et al., 2007)
	100	12	24 h	Needle-like	Pure Hap	1 nm	Potassium Hydrogen Phosphate Trihydrate & CTAB	(Li et al., 2008)
	110	-	1-120 h	Rod-like	Pure-Hap	5-100 nm	Calcium chloride, $ATPNa_2$ & ammonia solution	(Cao et al., 2010)
	120-140	5-9	4 h	Needle-like	Hap with intermediates	12 µm	Calcium chloride hydroxide, Dipotassium phosphate & EDTA	(Arce et al., 2004)
	140	4-6	24 h	Needle-like	Hap with intermediates	30-50 µm	Calcium nitrate, Sodium tripolyphosphate, methanol, ethanol, 1-propanol & 2-propanol	(Mizutani et al., 2005)
	150	3.6	8 h	Flower Like	FHap	~500 nm	Calcium nitra tetetrahydrate (Na_2EDTA), citric acid, & diammonium hydrogen phosphate	(Jiang et al., 2010)
	150	-	10 h	Rod-like	Pure-Hap	150 nmX310 nm	Calcium nitrate, Trisodium phosphate, CTAB, SDS & PVA	(Yan et al., 2001)

	150	10	10 h	Rod-like	Pure Hap	65 X 26 nm	Poly(amidoamine) (PAMAM), carboxylic (–COOH), polyhydroxy (–C(CH2OH)3) group, calcium nitrate & diammonium phosphate	(Zhou et al., 2007)
	160	4.5	10 h	Rod & plate like	Pure Hap	150µmX 10µmX300 nm	Calcium nitrate tetrahydrate, sodium dihydrogen phosphate dehydrate & urea	(Jokić et al., 2011)
	160-200	12.9, 11.4, and 9.7	1-12 h	Prism like	Pure Hap	8-20 µm	Calcium nitrate, potassium dihy-drogen phosphate, EDTA, ammoniumhydroxide & potassium hydroxide	(Zhu et al., 2008)
	180	3	10-15 h	Needle-like	Pure Hap	60–116 µm	Calcium nitrate, acetamide, Diammonium phosphate, & nitric acid	(Zhang and Darvell, 2011)
	200	5.1	24-72 h	Rod-Like	Hap with intermediates	100-500 nm	Calcium nitrate tetrahydrate & di-ammonium hydrogen phosphate	(Earl et al., 2006)
	200	>10	8 h	Needle-like	Si-Hap	<100 nm	Calcium nitrate, diammonium phosphate & Silica aerogel	(Tang et al., 2005)
	200	>11	8 h	Diverse	Si-substituted Hap	50 nm	Calcium nitrate, diammonium phosphate & Silica aerogel	(Aminian et al., 2011)
	200	12	15 h	Dandelion-like	Pure Hap	200 nm	Calcium chloride, Dipotassium phosphate, Potassium hydroxide & EDTA	(Lak et al., 2008)
	1000	-	3 h	-	Si-Hap	-	Calcium hydroxide, Phosphoric acid & TEOS	(Kim et al., 2002)
	1200	-	3 h	Diverse	-	70 µm	Calcium hydroxide & tetraethyl orthosilicate	(Lee et al., 2004)

Sol-Gel Method								
	45-100	-	1 h	Spherical shaped	Pure-Hap	1-25 µm	Phenyldichlorophosphine, acetone, calcium nitrate & alumina substrates	(Brendel et al., 1992)
	60	-	8 h	Fibre-like	-	500 nm	Phosphorous solution, 2-butanol, calcium acetate & acetic acid	(Ramanan and Venkatesh, 2004)
	60	-	6 days	Agglomerated	Pure Hap	90-150 nm	Trimethyl phosphite & calcium nitrate tetrahydrate	(Chen et al., 2011)
	60	9	24 h	nano-hexagonal rods	Pure Hap	70-500 nm	Calcium nitrate tetrahydrate, potassium dihydrogenphosphate & ammonia solution	(Padmanabhan et al., 2009)
	60	-	24 h	-	-	-	Calcium chloride, diethylphosphyte, dibutylphosphyte, Tris-(2-chloroethyl)phosphite & di-isopropylphosphite	(Ioiţescu et al., 2009)
	70-80	2-3	4-6 h	Irregular shaped	Pure Hap	1-5 µm	Calcium nitrate, citric acid & diammonium phosphate	(Han et al., 2004)
	80	-	16 h	Agglomerated	Hap with intermediates	50 nm	Calcium nitrate, triethyl phosphite & hydrolyzed phosphite sol	(Liu et al., 2002)
	80-90	-	16 h	-	Hap with intermediates	-	Calcium nitrate &triethyl phosphate	(Hsieh et al., 2001)
	80	-	24 h	-	Hap with intermediates	40-100 nm	Calcium nitrate, triethyl phosphate & ethanol	(Hosseini et al., 2007)
	80	-	24 h	Spherical	Pure Hap	20-30 nm	Calcium nitrate, phosphorus pentoxide & ethanol	(Fathi et al., 2008)
	85	-	4 h	Agglomerated	Pure Hap	50–-0 nm	Calcium nitrate, diammonium phosphate & polyethylene glycol	(Kumar and Kalainathan, 2010)

	85	-	4 h	Agglomerated	Pure Hap	0.9 µm	Calcium nitrate, diammonium phosphate & ethanol	(Kuriakose et al., 2004)
	110	-	24 h	Fibre like	Pure Hap	100-200 nm	Calcium nitrate tetrahydrate/calcium acetate & triethyl phosphate	(Natarajan and Rajeswari, 2008)
	160	6 & 9	4 h	Needle-like	Pure Hap	0.1-1 µm	Calcium chloride, EDTA & dipotassium phosphate	(Montero et al., 2009)
Ultrasonication Method								
	25	12	7-10 min	Diverse	Hap with intermediates	31-71 nm	Calcium hydroxide & phosphoric acid	(Giardina and Fanovich, 2010)
	37	7.5	6-40 min	Spherical shaped	Pure Hap @ 15 min	30 nm to 18 nm.	Sodium chloride, potassium chloride, disodium phosphate, Monopotassium phosphate, calcium chloride & magnesium chloride	(Rouhani et al., 2010)
	42-65	-	5-120 min	-	Pure Hap @ 60 min	18 µm	Calcium hydroxide & phosphoric acid	(Kim and Saito, 2001)
	25	9	1 h	Rod-like	Hap with intermediates	10-100 nm	Calcium nitrate tetrahydrate, potassium dihydrogen phosphate & ammonia solution	(Poinern et al., 2011)
	37-90	7.4	1-4 h	Needle-like	Pure Hap	20 nm	Calcium nitrate, NH_2CONH_2 & ammonium dihydrogen phosphate	(Cao et al., 2005)
	37	9	90 min	Rod-like	Pure Hap	17- 150 nm	Calcium nitrate & potassium phosphate	(Mehta et al., 2017)
	70		5-7 h	Diverse	Pure Hap	1-5 µm	Calcium nitrate & phosphoric acid	(Hu et al., 1993)
	28	9	17 h	Hollow sphere	Pure Hap	-	Calcium nitrate tetra hydrate, diammonium hydrogen orthophosphate, glycine, acrylic acid & sodium hydroxide	(Gopi et al., 2012)

2.2. HYDROXYAPATITE FOR DEFLUORIDATION

Treatment of water is an uppermost priority in the field of water pollution. Various toxic metals and ions such as chromium (Cr), lead (Pb), copper (Cu), cadmium (Cd), zinc (Zn), cobalt (Co), Selenite (SeO_2^{3-}), nickel (Ni), arsenate (As (V)) and fluoride (F^-) are known to be significantly toxic and hazardous for health. Extensive studies have been carried out during the past decades to find low cost, high capacity adsorbents for the removal of metal ions. Adsorption using materials of biological origin is recognized as an emerging technique for the treatment of water containing heavy metals and toxic ions such as fluoride and arsenate. Hydroxyapatite (Hap) which is a biomaterial have found its application as an efficient adsorbent, having high stability, biocompatibility and biodegradability which would make the material desirable for practical applications. The mechanism behind the remediation of heavy metals by using Hap is that there are three types of substitutions that can occur in the structure of hydroxyapatite. The Ca^{2+} can be substituted by cations such as (Pb^{2+}, Ba^{2+}, Zn^{2+}, Fe^{3+}, and Mg^{2+}), whereas, PO_4^{3-} can be replaced by oxyanions such as (ASO_4^{3-}, VO_4^{3-} and CO_3^{2-}) and OH^- can be exchanged by anions such as F^- and Cl^- as shown in figure 2-7 (Materials, 2015).

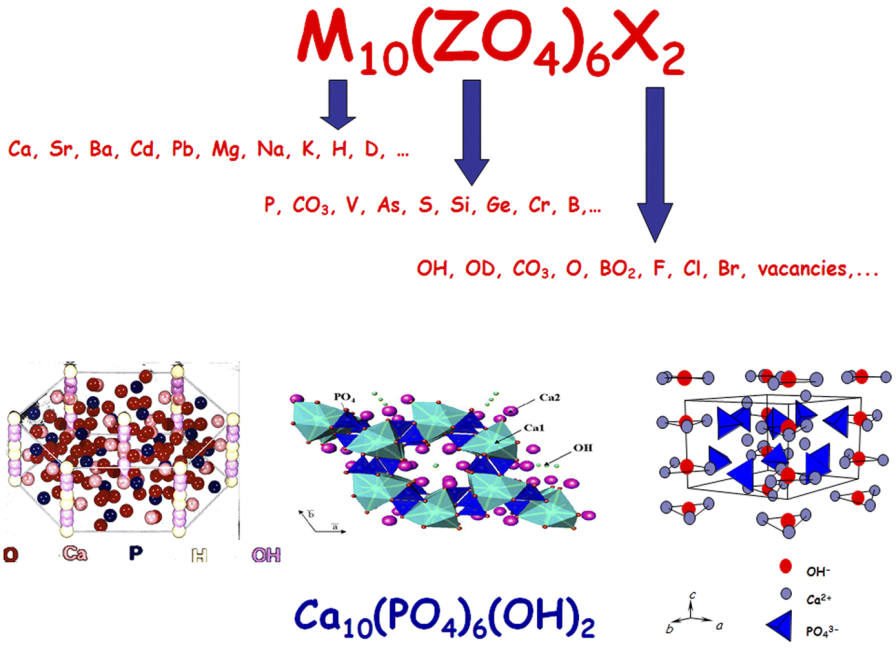

Figure 2-7. Substitution that can occur in the structure of hydroxyapatite (Materials, 2015).

As discussed in section 2.1 that various methods and reagents are used for the synthesis of hydroxyapatite for different applications. This section will detailed about the application of hydroxyapatite as an adsorbent for water defluoridation. Different forms of Hap are used to check their defluoridation potential. Hydroxyapatite prepared using biogenic sources such as eggshell, fish bones and bone char was preferred adsorbent by researchers due to its low-cost but their adsorption capacities was not high and using these adsorbents also has ethical and religious issues. Synthetic Hap was synthesized using different reagents such as calcium hydroxide and orthophosphoric acid in order to overcome the problems related to biogenic hydroxyapatite but there were no significant increase in adsorption capacities. Later researchers modified the hydroxyapatite using different materials such as graphene oxide, CTAB, chitosan etc. to increase the stability and reactivity of hydroxyapatite. Table 2.2 also summarizes the adsorption capacity, reagents/sources used for the synthesis of Hap and experimental conditions required for the removal of fluoride using different forms of hydroxyapatite.

2.2.1. HYDROXYAPATITE-BIOGENIC

In the past decade, tremendous efforts have been made for using low-cost natural materials which are otherwise considered as waste because of certain advantages such as cheap raw material, availability in abundance and economic sustainability (Villaescusa et al., 2004). Biogenic Hap of different origins, such as bone chars, cow bones, fish bones, and eggshell, have found its application for the removal of Zn, Cu, Pb, Cd, U, Se and F from groundwater (Conca and Wright, 2006).

Meat and bone meal or bone char, a waste is a rich and potentially cost-effective source of hydroxyapatite $Ca_{10}(PO_4)_6(OH)_2$ (Deydier et al., 2005b). Bone char is composed approximately of 75% hydroxyapatite, 9–11% of calcite and carbon is being used for the removal of fluoride and heavy metals. Bone char is used widely in many developing areas due to its availability and inexpensive source is required to work as an adsorbent for fluoride removal (Castillo et al., 2007). It is derived by carbonizing the crushed animal bones by heating at 500–700ºC in an airtight iron retort for 4 to 6 h. Bone charcoal was used as a defluoridating agent at the Britton, South Dakota, plant, from 1948 to 1971(Bhargava, 2014). But due to problems related to the bad taste of treated water

and cost of raw materials, bone char did not gain wider acceptance (Bhargava, 2014; Mwaniki, 1992). The optimized condition for synthesis of bone char for fluoride removal from water was studied by (Mayorga et al., 2013). It was found that optimum fluoride uptake capacity of 7.32 mg/g was obtained if pyrolysis temperature of 700ºC is used for bone char synthesis which is 63% more as compared to commercial bone chars. While working with different apatites (Gao et al., 2009a) reported that the maximum defluoridation capacity of bone char and treated bone char was 2.267 mg/g and 2.247 mg/g respectively which is comparable to the defluoridation capacity of synthetic n-Hap (2.311 mg/g). Optimum fluoride adsorption on bone char was obtained in the pH range of 5 to 6 which followed pseudo-second-order kinetics and Langmuir and Freundlich adsorption isotherms. Castillo et al., (2007) reported that the adsorption capacity of bone char made from cattle bone was 2.8 mg/g which was 36 times greater than the commercial available activated alumina and commercial activated carbon (F-400). Among other materials of biogenic Hap, cow bone was used in waste water treatment and removal of fluoride. (Mlilo et al., 2010) reported use of charred cow bones for the effective removal of fluoride and arsenic. But the use of cow or pig bones for the use of water treatment may not be accepted in some Asian Countries due to various religious and cultural beliefs. Therefore, studies were focused on other bone sources, such as fish bones.

The Hap derived from fish scales inherit the same chemical properties as of teeth and bones and can be processed by simple and inexpensive methods (Liu et al., 2008; Metz et al., 2012). They are also important sources of natural Hap, which can be utilized for various applications such as drug delivery systems, biomaterials, and biomedical products (Chen et al., 2002). Hap derived from fish scales has been used as a potential sorbent for fluoride removal from drinking water. (Mlilo et al., 2010), evaluated fish bone char as an appropriate fluoride and arsenic removal agent and found that the best charring temperature is 500ºC for preparing bone char for effective removal of fluoride. They also observed that fish bone char removed fluoride and arsenic simultaneously with insignificant competition.

Hydroxyapatite produced from food resources i.e. eggshell (hydroxyapatite), was also used for the removal of fluoride. Bhaumik et al., (2012) studied use of eggshell

powder as an adsorbent for removal of fluoride conducting batch studies. They found that adsorption process followed pseudo-second-order model. They reported that eggshell powders may effectively be used as a low-cost adsorbent for removal of fluoride from aqueous solution and groundwater. Recently Lunge et al., (2012) reported a new composite material called Eggshell Composite (EC) synthesized using eggshell waste as calcium source for selective fluoride adsorption from water. They studied the effect of various process synthesis parameters such as eggshell (ES): eggshell membrane (ESM) ratio, aluminum loading, mixing time and calcination temperature in order to optimize the synthesis conditions. The adsorption capacity of EC reported to be 37 mg/g and Langmuir model fitted best signifying monolayer adsorption.

Natural Hap was proven to be a good source for defluoridation of drinking water and also economical in nature. Table 2.2 present that the maximum fluoride adsorption capacity was 37 mg/g when alumina eggshell composite were used for the application of defluoridation. Most of the studies were done at room temperature whereas, not much emphasis were given to estimate the rate of reaction.

2.2.2. HYDROXYAPATITE-SYNTHETIC (PURE)

Synthetic hydroxyapatite gained much attention due to its outstanding biocompatibility, affinity to biopolymers and high osteogenic potential (Chen et al., 2011; Shojai et al., 2013). But due to its low strength and brittle nature, sometimes Hap decomposes into calcium phosphate phases such as tricalcium phosphate (TCP) and even tetra-calcium phosphate (TTCP). To overcome these limitations different reagents and methods were used for synthesis and their applications have been explored in various fields such as water treatment processes (Lin et al., 2009) and remediation of heavy metals etc. (Hashimoto et al., 2009). Few of the common reagents which were generally used for synthesis of Hap and later used in the treatment of water are $Ca(OH)_2$, di-ammonium hydrogen phosphate $(NH_4)_2HPO_4$, $Ca(NO_3)_2$, H_3PO_4, whereas being commercially synthesized by Alfa Aesar and Bio-Rad Laboratories etc. In the literature, synthetic hydroxyapatite was used in the adsorption of various heavy metals such as Pb^{2+}, Zn^{2+}, Cd^{2+}, Cu^{2+}, Co^{2+}, Cr^{2+}, Ni^{2+}, Sb^{2+} , AsO_4^{3-} and NO^{3-} but our study is limited to removal of fluoride (F^-) using hydroxyapatite.

Fan et al., (2003) used low-cost adsorbent such as hydroxyapatite, fluorspar, calcite, quartz and quartz activated by ferric ions to study the fluoride adsorption kinetics. They reported that the uptake of fluoride on hydroxyapatite is an ion-exchange mechanism that follows pseudo-first and second order rate equations. Badillo et al., (2007) carried out the studies on fluoride removal using synthetic hydroxyapatite commercially provided by BIO-RAD (Bio-Gel HTP) (Almaraz et al., 2007) and reported that the maximum adsorption on hydroxyapatite occurred at a pH range of 7.0-7.5 with the adsorption capacity of 100 mmol/100 g.

Gao et al., (2009b) synthesized hydroxyapatite using the thermal decomposition of precursors to obtain a different particle size of nHap and investigated the size-dependent defluoridation properties (Gao et al., 2009c). The precursors used for synthesis of nHaps with different particle size prepared by thermal decomposition method include $Ca(NO_3)_2.4H_2O$ and $NH_4H_2PO_4$, ammonia solution for pH adjustment and $(NH_4)_2$-EDTA as the complexing reagent. The bulk Hap was synthesized by the solid-state reaction using $CaCO_3$ and $CaHPO_4.2H_2O$ at 1100ºC for 4 h and reported that Hap with smaller particle sizes had higher adsorption efficiency but Hap with large particle sizes had the low percentage of fluoride removal. The Langmuir adsorption capacity ranged between 0.295 to 0.489 mg/g and the kinetic data fitted to pseudo-second order kinetics and Freundlich isotherms model. Sundaram et al., (2008) described the advantages of nano-hydroxyapatite (n-Hap), as an adsorbent for fluoride removal. They synthesized Hap using calcium hydroxide and orthophosphoric acid as calcium and phosphate precursors. The maximum defluoridation capacity was found to be 1.845 mg/g and adsorption process followed pseudo-second-order and pore diffusion models. Field trials were conducted which indicates the efficiency of the adsorbent, and effects of various parameters such as pH, contact time, fluoride ion concentration, and the dose of sorbent on the adsorption of fluoride ions by hydroxyapatite was reported by (Reyes and Ríos, 2010). Equilibrium was attained in 16 h of contact time with maximum adsorption of 4.7 mg/g at pH_{eq} of 7.5 ± 1 and kinetics followed pseudo-second order model, and adsorption isotherm followed Freundlich isotherm model. Nanostructured hydroxyapatite was synthesized through an ultrasonic and microwave combined technique and studied for the defluoridation behavior (Poinern et al., 2011). It was reported that ultrasonic and

microwave-assisted technique produced highly crystalline and ultrafine particles of hydroxyapatite of uniform size. The equilibrium adsorption data fitted with both the Langmuir and Freundlich isotherms, with a maximum capacity of 5.5 mg/g at 298 K and, the kinetic rate data followed pseudo-second-order model and that of the intra-particle diffusion model.

Mourabet et al., (2015) used Response Surface Methodology (RSM) approach over conventional method for optimization of process parameters such as temperature, initial solution pH, adsorbent dose and initial fluoride concentration on fluoride uptake from aqueous solution. The three-level, four-factor, Box–Behnken design was employed and a second order mathematical model developed by regression analysis of the experimental data. The optimum parameters found by desirability functions were pH (4.16), temperature (39.02ºC), adsorbent dose (0.28g) and initial concentration (20 mg/L) with maximum fluoride removal of 86.34%. Equilibrium data correlated best with Langmuir and Freundlich models whereas, rate fitted well to pseudo-second order kinetic model.

Treatment of waste and its proper disposal is one of the primary environmental issues. Therefore, reutilizing and reducing the harmful effects of the waste produced gained much attention of researchers all over the world (Mehta et al., 2016). Recently Zhang et al., (2012) attempted to utilize waste phosphogypsum for the preparation of hydroxyapatite nanoparticles using microwave irradiation technology. The potential application of synthesized nHap was further investigated as an adsorbent for the defluoridation of water. The morphology of Hap exhibited a hexagonal structure with particle size about 20 nm×60 nm with high purity. The hydroxyapatite also showed a good efficiency in fluoride removal from aqueous solution with the maximum adsorption capacities of 19.742, 26.108, 36.914 and 40.818 mg F^-/g at 298, 308, 318 and 328 K and pH 7 estimated thermodynamically from Langmuir-Freundlich isotherm models.

The different studies carried out on hydroxyapatite as an adsorbent for water defluoridation indicate that the adsorption capacity can be increased with change in reagents as detailed in Table 2.2. Zhang et al., (2012) reported 40.818 mg/g of adsorption capacity when Hap was synthesized using phosphogypsum, diammonium phosphate and

sodium hydroxide as starting the material. Whereas, Gao et al., (2009b) reported 0.489 mg/g adsorption capacity using Hap as an adsorbent when the reagents used for synthesis were calcium nitrate, ammonium dihydrogen phosphate and $(NH_4)_2$-EDTA complex.

2.2.3. HYDROXYAPATITE-COMPOSITE

The pursuit for novel adsorbents for removal of toxic ions from water and wastewater gained much attention for the composite materials, such as polymeric composites of ultrafine phase dimensions. Due to the exceptional properties of natural polymers such as biocompatibility, non-toxicity, biodegradability and adsorption properties they had gained much attention than that of synthetic polymers (Viswanathan and Meenakshi, 2010). Various studies were carried out for preparation of new organic-inorganic hybrid polymeric composites having improved properties for various applications such as drug delivery in tissue engineering, water treatment, defluoridation etc. (Habraken et al., 2007; Viswanathan and Meenakshi, 2010). The natural biopolymers can be effectively used as an adsorbent for removal of toxic ions such as fluoride. It was found that composite materials as adsorbents containing natural polymers had added advantages. For example, the applications of hydroxyapatite was limited due to its fragility moreover, powdered Hap cannot be directly used in fixed bed columns, due to operational difficulties such as excessive pressure drop during field applications. To overcome these limitations, polymeric composites of organic and inorganic origin was studied extensively due to their unique structure and properties. Also, polymeric composites were made into various forms such as beads, membranes, candles, etc. (Pandi and Viswanathan, 2015; Sundaram et al., 2009a). Materials such as Cellulose, Chitin, chitosan, alginate, and gelatin, etc., were utilized along with hydroxyapatite to synthesize composite materials for the removal of fluoride from drinking water.

Cellulose is considered as an abundant renewable biopolymer on earth, which is a favorable raw material obtainable at low cost for the synthesis of adsorbents for defluoridation. Yu et al., (2013) prepared cellulose@hydroxyapatite (HA) nanocomposites in NaOH/thiourea/urea/H_2O solution using in-situ hybridization method for effective removal of fluoride from drinking water. They reported that due to agglomeration of nano-sized Hap particle, it lead to low adsorption capacity, and which

can be overcome by using cellulose as the template. The maximum adsorption capacity observed from Langmuir model was 4.2 mg/g and adsorption equilibrium was attained in 360 min for cellulose@hydroxyapatite adsorbent. Adsorption kinetics followed rapid adsorption rates and pseudo-second-order kinetics. Sundaram et al., (2009) studied the fluoride adsorption potential of novel nano-hydroxyapatite/chitin (n-HApCh) composite (Sundaram et al., 2009b). Chitin is a biopolymer which comprise of β-(1,4)-2-acetamido-2-deoxy-d-glucose units and is the second most abundant polysaccharide occurring in nature, after cellulose (Davila et al., 1990). They synthesized n-HApCh composite by precipitation method using ammonium dihydrogen phosphate, $Ca(NO_3)_2$ and chitin in the ratio 3:2 and nano-hydroxyapatite (n-Hap). The defluoridation capacity of the n-HApCh composite was reported to be 2.840 mg/g, higher than n-Hap which had a capacity of 1.296 mg/g. The adsorption isotherms followed Freundlich isotherm model whereas, the reaction rates followed pseudo-second-order and pore diffusion patterns.

Other than cellulose and chitin, chitosan was also used to synthesize hydroxyapatite composite. Chitosan is considered as the only positively charged and naturally occurring polysaccharide which can interact strongly with negatively charged bodies. Sundaram et al., (2008) prepared a bioinorganic composite, which was named nano-hydroxyapatite/chitosan (n-HApC) composite and studied for its defluoridation efficiency. They observed that the defluoridation capacity of n-HApC composite was 1.560 mg/g which was higher than that of nano-hydroxyapatite (n-Hap) which had a capacity of 1.296 mg/g with contact time of 30 min at 3 pH. Adsorption kinetics was also studied and observed that the rate of adsorption followed pseudo-second-order kinetics model and occurred through pore diffusion (Sundaram et al., 2008).

In recent times, synthesis of magnetic polymeric nanomaterials is being studied due to its many process advantages, such as control over the nucleation and growth of polymer particles and other features such as, cost-effectiveness, environmentally friendliness, and possibility of easy separation of the composite from the aqueous medium. (Pandi and Viswanathan, 2015) prepared eco-magnetic biosorbent through uniform deposition of magnetic Fe_3O_4 particles on the surface of nano-hydroxyapatite (n-Hap)/chitosan nanocomposite which was named Fe_3O_4@n-HApCS composite for its

application in water defluoridation. They prepared n-HApCS composite using precipitation method using (Sairam Sundaram et al., 2008) mixture of $FeCl_2.4H_2O$ (1.85 mmol) and $FeCl_3.6H_2O$ (3.7 mmol) solution added slowly into an n-HApCS medium at pH 10 for 10 min. The formed magnetic Fe_3O_4@n-HApCS composite was aged for 24 h followed by filtration, washing and drying at 80ºC for 24 h to obtain composite powder and studied for fluoride adsorption capacity. The adsorption capacity of Fe_3O_4@n-HApCS was reported to be 4.77 mg/g with a contact time of 20 min, at 3 pH. (Pandi and Viswanathan, 2016) have also worked on fabrication of magnetic iron oxide over Nano-hydroxyapatite using gelatin for defluoridation studies. Gelatin is also a biocompatible, biodegradable, and inexpensive biomaterial which comprises of numerous chemical groups such as amine, and carboxyl groups which have the strong bonding toward toxic ions. They found that the developed hybrid Fe_3O_4@n-HApGel composite had high defluoridation capacity of 5.009 mg/g and the equilibrium isotherm fitted best with Langmuir isotherm model. The enhanced capacity of the magnetic composite was attributed due to electrostatic adsorption and complexation between fluoride ion and composite in addition to ion-exchange. The performance of Fe_3O_4@n-HApGel nanocomposite was also studied for field conditions with the water sample collected from a nearby fluoride prevalent area.

Another study was conducted by (Pandi and Viswanathan, 2014) in which they used alginate for the development of eco-friendly adsorbent for water defluoridation which is bioencapsulating nano-hydroxyapatite (n-HAp) and named n-HApAlg composite. They prepared n-HApAlg composite by using in situ co-precipitation method. $(NH_4)_2PO_4$ solution was added dropwise into the solution of sodium alginate for 15 min and stirred for 1 h at 40ºC. and 1.67 M $Ca(NO_3)_2$ was added to the resultant mixture for 20 min at the same temperature, at 10 pH using ammonia solution. The dried n-HApAlg composite was crushed to a fine powder and used as an adsorbent for water defluoridation with its defluoridation capacity was reported to be 3.870 mg/g. The sorption of fluoride on n-HApAlg composite follows Langmuir isotherm and kinetic studies revealed that fluoride adsorption was controlled by pseudo-second-order and intraparticle diffusion model.

Synthesis of hydroxyapatite composite and their application for removal of fluoride from water provided a new era of application. As seen from the Table 2.2 that adsorption capacity varied from 1.56 mg/g to 5.01 mg/g using Hap-composites. The maximum removal was achieved in neutral pH and at room temperature which is again an advantage for the adsorbent. The rate kinetics of all compared material followed pseudo-second order and adsorption isotherm were Langmuir isotherms which depicted monolayer adsorption and homogeneous phenomena.

2.2.4. HYDROXYAPATITE-MODIFIED

Studies based on natural and synthesized hydroxyapatite as adsorbents showed a lower defluoridation capacity for the removal of fluoride from water/wastewater. Therefore the need to extend the modification of these adsorbents with an affinity towards fluoride ions from the aqueous solution (Prabhu and Meenakshi, 2014). Surface modification technology gained much attention due to its efficient and effective technology. Many researchers tried to utilize the surface modification technology to enhance the chromium removal Choi et al., (2009), nitrate removal (Zhan et al., 2011) and perchlorate removal S. Y. Lin et al., (2013) using various materials like surfactants (CTAB, HDPC, DTAB) that help in providing more positive sites. (Prabhu and Meenakshi, 2014) prepared cationic surfactant modified Hap using CTAB, HDPC, and DTAB for fluoride removal from aqueous solution. They compared the defluoridation capacity of pure Hap with cationic surfactant modified Hap and established the mechanism for fluoride removal. It was reported that the maximum defluoridation capacity onto modified forms of HAp powder was 9.369 mg/g which was almost 3-4 times higher than pure Hap whose capacity was found to be 2.63 mg/g with a contact time of 30 min at room temperature. Adsorption data fitted best with Freundlich isotherm model whereas the adsorption rates followed pseudo-second-order and intraparticle diffusion kinetic models. The mechanism behind the enhanced capacity indicates that the fluoride adsorption on modified forms of Hap powder was fundamentally by an electrostatic attraction and ion-exchange mechanism which depend on the solution pH. Additionally, other materials such as activated alumina, magnesium, sulfate, sodium

calcium borate glass etc. were also been used for the modification of hydroxyapatite and to studied for defluoridation capacity.

Different aluminum based adsorbents were studied for defluoridation as they had a high removal capacity due to high affinity of fluoride ions with aluminum ions (Ghorai and Pant, 2005; Sujana and Anand, 2010). However, studies also revealed that aluminum could cause neurotoxicity in humans due to its prolonged consumption through drinking water and other sources. When aluminum based adsorbents were used, the presence of residual aluminum was found in treated water in the form of colloidal and dissolved aluminum which is a matter of concern (George et al., 2010). Moreover, commercially available activated alumina had a slow rate of adsorption which limits its use for treating large quantities Y. Tang et al., (2009). To overcome these limitations, Tomar et al., (2015) synthesized hydroxyapatite modified activated alumina (HMAA), a hybrid adsorbent by dispersing nanoparticles of hydroxyapatite inside activated alumina granules. The hybrid adsorbent had a maximum defluoridation capacity of 14.4 mg/g which is at least five times higher than virgin activated alumina at pH 7. Equilibrium data fitted both Langmuir and Freundlich isotherms which confirmed surface heterogeneity as well as validated monolayer adsorption on the surface of both the adsorbents (Tomar et al., 2015). Nie et al., (2012) prepared and characterized aluminum-modified hydroxyapatite (Al-HAP) for enhanced fluoride adsorption. The Al-HAP was prepared by co-precipitation method using $Ca(NO_3)_2$, $Al(NO_3)_3$ and H_3PO_4 solution. It was reported that Al-HAP showed higher defluoridation capacity of 32.57 mg/g than that of unmodified hydroxyapatite (HAP) which possessed a capacity of 16.38 mg/g. Adsorption data was well described by the Langmuir isotherm model and the adsorption kinetics followed the pseudo-second-order model. Higher fluoride removal efficiency was attributed to the fact that synthesized Al modified HAP had more adsorption sites, which resulted in abundant surface hydroxyl groups, resulting in higher defluoridation capacity (Nie et al., 2012).

Magnesium ions also found its application for fluoride removal due to its high affinity towards fluoride ions (Maliyekkal et al., 2008). Magnesium was found to influence both matrix and mineral metabolism in the human body, and their depletion may affect skeletal metabolism adversely (Percival, 1999). Due to such advantages,

(Mondal and George, 2015b) prepared a new adsorbent named magnesia-hydroxyapatite (Mg-HAP) which was used as a defluoridating agent. The defluoridation capacity of Mg-Hap was reported to be 1.4 mg/g and equilibrium was attained in 180 min. Adsorption pattern fitted best with Langmuir isotherm and the rate of reaction follows pseudo-second-order kinetics. The water quality parameters of the treated water such as dissolved solids (TDS), turbidity, residual calcium, residual phosphorus content, electrical conductivity, hardness, and total alkalinity were also within the permissible range. Further, (Mondal et al., 2016) also worked on the synthesis of magnesium-incorporated hydroxyapatite (M-i-HAP) for evaluation of its defluoridation potential. The surface area of the adsorbent was found to be 46.62 m^2/g. Optimization of process parameters by response surface methodology method using central composite design produced predictive model and optimum conditions, for treating of 10 mg/L of fluoride was reported to be 303 K temperature, pH 7, 180 min contact time, and 10 g/L of M-i-HAP, to remove 95% of fluoride under these conditions. The process followed the pseudo-second-order kinetic model and the adsorption mechanism was described by Langmuir isotherm with an adsorption capacity of 1.16 mg/g. The regeneration of the spent adsorbent was carried out by using 0.1 M NaOH solution and was able to achieve 91% regeneration.

Recently, sulfate anions were used extensively in the ion-exchange process and used for modification of various adsorbents such as 2-line ferrihydrite/bayerite composites (Jia et al., 2015), Fe-Mg-La metal composite(Jia et al., 2015), and natroalunite microtubes (Zhu et al., 2015), to improve the fluoride removal performance. Chen et al., (2016) synthesized a sulfate-doped hydroxyapatite (HAP) hierarchical hollow microspheres a novel adsorbent to enhance the fluoride removal which was characterized using SEM, TEM, XRD, FTIR, XPS and BET analysis. They reported that the defluoridation capacity of sulfate-doped hydroxyapatite (HAP) was 28.3 mg/g for treating initial fluoride concentration of 100 mg/L at 25ºC and pH 7. The adsorption isotherm followed Freundlich model whereas, adsorption kinetics followed the pseudo-second-order model. The study of adsorption mechanism recommended that the active sites corresponded to hydroxyl groups and the sulfate groups on the surface of the adsorbent which were responsible for the enhanced fluoride removal.

Researchers at the University of Missouri-Rolla converted sodium calcium borate glasses to hydroxyapatite in K_2HPO_4 solutions and the particles obtained were nanometer in range with fine pores (Liang et al., 2008). These special fine pores improved the adsorption ability of HAP effectively. (Liang et al., 2011) synthesized a novel sodium calcium borate glass derived hydroxyapatite (G-HAP) with particle of different size ranges. G-Hap was prepared by immersion sodium calcium borate glass in 0.1 M K_2HPO_4 solution for 7 days. The maximum defluoridation capacity of G-Hap (<100 μm) was found to be 17.34 mg/g at pH 6.72 with the adsorption time of 12 h. The adsorption kinetics and adsorption isotherms were fitted best by a second order kinetic model and Freundlich isotherm model respectively.

The synthesis of hydroxyapatite along with different reagents for the application of fluoride removal resulted into a new domain of study. Various materials were used such as CTAB, grapheme, aluminium nitrate, magnesium hydroxide along with hydroxyapatite in order to enhance the defluoridation capacity as observed from the Table 2.2. The modification of Hap was successful as the Hap-modified had the maximum defluoridation capacity of 44.068 mg/g at neutral pH and room temperature.

Table 2.2 Adsorption capacity and experimental conditions of different forms of hydroxyapatite for removal of heavy metals and anions from aqueous solution

Hap forms	Source/Reagents	Adsorption capacity (mg/g)	pH	Temp (ºC)	Kinetic model	Isotherms	Authors
1. Hap-Natural							
	Eggshell	1.09 mg/g	6	30	Pseudo-second order	Langmuir	(Bhaumik et al., 2012)
	Alumina Eggshell composite	37 mg/g	3-9	30	-	Langmuir	(Lunge et al., 2012)
	Fish Bone	2.53 mg/g	8	20	-	-	(Bhargava, 2014)
	Fish Bone	4.41 mg/g	6.7-8.3	-	-	Langmuir	(Brunson and Sabatini, 2009)
	Bone meal	2.247 mg/g	5-6	25	Pseudo-second order	Langmuir and Freundlich	(Gao et al., 2009a)
	Bone char	2.71 mg/g	3	25	-	Freundlich	(Castillo et al., 2007)
	Bone char	2.8 mg/g	3	25	-	Freundlich	(Castillo et al. 2007)
	Bone char	5.92 mg/g	7	30	-	-	(Mayorga et al. 2014)
	Bone char	7.32 mg/g	7	30	Pseudo-second order	Langmuir	(Mayorga et al. 2013)
	Bone char	11.4 mg/g	-	30	-	-	(Mwaniki, 1992)
2.Hap-Synthetic							
	$Ca(NO_3)_2 4H_2O$ & $NH_4H_2PO_4$, $(NH_4)_2$-EDTA as complex reagent	0.489 mg/g	5	25	Pseudo-second-order	Langmuir and Freundlich isotherms	(Gao et al. 2009)
	Calcium hydroxide & orthophosphoric acid	1.845 mg/g	7.88	-	Pseudo-second-order and pore diffusion models	Langmuir isotherm	(Sundaram et al. 2008)

	$(NH_4)_2$ HPO_4 & $Ca(NO_3)_2.4H_2O$	3.12 mg/g	4.16	39.02	Pseudo second order	Langmuir & Freundlich isotherms	(Mourabet et al., 2015)
	$Ca(NO_3)_2$-$4H_2O$ & $NH_4H_2PO_4$	3.44 mg/g	7	25	Pseudo-second-order	Freundlich isotherms.	(Wang et al. 2011)
	Hydroxyapatite	4.54 mg/g	6	-	Pseudo-second-order	Freundlich isotherm	(Fan et al. 2005)
	Calcium hydroxide & dilute phosphoric acid	4.7 mg/g	5-7.3	-	Pseudo-second-order and pore diffusion models	Freundlich	(Reyes and Ríos, 2010)
	$[Ca(NO_3)_2 \cdot 4H_2O]$ & $[KH_2PO_4]$	5.5 mg/g	6	25	Pseudo-second order	Freundlich	(Poinern et al., 2011)
	Phosphogypsum, diammonium phosphate solution & sodium hydroxide	40.818 mg/g		54.85	Pseudo-second order	Langmuir & Freundlich	(Zhang et al., 2012)
3. Hap-Composite							
	Chitosan, calcium nitrate & ammonium dihydrogen phosphate	1.560 mg/g	7	25	Pseudo-second-order	Langmuir isotherm	(Sundaram et al., 2008)
	Chitin ammonium dihydrogen phosphate & $Ca(NO_3)_2$	2.840 mg/g	7	25	Pseudo-second-order and pore diffusion patterns	Langmuir isotherm	(Sundaram et al., 2009a)
	Sodium alginate, $Ca(NO_3)_2$ & $(NH_4)_2PO_4$	3.870 mg/g	7.88	25	Pseudo-second-order and intraparticle diffusion model	Langmuir isotherm	(Pandi and Viswanathan, 2014)
	Cotton Cellulose & Solution of NaOH/thiourea/urea/H_2O	4.2 mg/g	6.5	-	Pseudo-second-order	Langmuir isotherm	(Yu et al., 2013)
	(nHAp)/Chitosan (CS) nanocomposite & magnetic Fe3O4 particle	4.768 mg/g	3	30	-	Langmuir isotherm	(Pandi and Viswanathan, 2015)
	Gelatin, (Fe_3O_4), $(NH_4)_2PO_4$, $Ca(NO_3)_2$, $FeCl_2 \cdot 4H2O$ & $FeCl_3 \cdot 6H_2O$	5.01mg/g	7	30	-	Langmuir	(Pandi and Viswanathan, 2016)

4. Hap-Modified							
	Potassium phosphate dibasic (K_2HPO_4), calcium nitrate tetrahydrate ($Ca(NO_3)_2 \cdot 4H_2O$), & magnesium nitrate hexahydrate ($Mg(NO)_3 \cdot 6H_2O$)	1.16 mg/g	7	30	Pseudo-second-order	Langmuir isotherm	(Mondal et al. 2016)
	Magnesium hydroxide [$Mg(OH)_2$] & HAP	1.4 mg/g	7.5	25	Pseudo-second-order	Langmuir isotherm	(Mondal and George 2015)
	Calcium nitrate, ammonium dihydrogen phosphate, CTAB, DTAB & HDPC	9.39 mg/g	3	25	Pseudo-second-order & intra-particle diffusion model	Freundlich model	(Prabhu and Meenakshi 2014)
	Activated Alumina granules, ammonium dihydrogen phosphate &calcium chloride	14.4 mg/g	7	-	-	Langmuir & Freundlich isotherms	(Tomar et al., 2015)
	$Na_2O–CaO–B_2O_3$ glass & K_2HPO_4	17.34 mg/g	6.72	25	Pseudo-second order	Freundlich isotherm	(Liang et al., 2011)
	$CaCl_2.2H_2O$, $(NH_4)2HPO_4$ & Na_2SO_4	28.3 mg/g	7	25	Pseudo-second-order	Freundlich model	(Chen et al., 2016)
	$Ca(NO_3)_2$ and $Al(NO_3)_3$, H_3PO_4 & NH_4OH	32.57 mg/g	5	25	Pseudo-second-order	Langmuir isotherm	(Nie et al., 2012)
	Graphene oxide, ammonium dihydrogen phosphate solution & calcium nitrate	44.068 mg/g	7	30	Pseudo-second-order	Freundlich model	(Prabhu and Meenakshi, 2014)

2.3. SUMMARY AND OUTLOOK

Novel strategies have been developed to synthesize a wide range of hydroxyapatite using different materials for specific application. In the present review the following methods were discussed for the synthesis of hydroxyapatite:

a) Natural (Biogenic) source. Hydroxyapatite was produced from natural occurring biowaste materials such as bone waste, eggshells, fishscales, biomembranes etc. This method produce hydroxyapatite with large particle size with less control over the morphology. One of the other problem with this method is the less phase purity of material obtained. However, more emphasis can be given on this method in the near future because of the improved physiochemical properties of hydroxyapatite.
b) Conventional precipitation method. This method is the most common and widely researched method for the synthesis of hydroxyapatite. The morphology of Hap is generally rod-like and the average particle size varied from 40-200 nm. Moreover conventional precipitation method can be used to scale up the process because of its simple procedure and better control over the morphology of hydroxyapatite.
c) Hydrothermal Method. Hydrothermal method utilizes single or heterogeneous phase reactions in aqueous at elevated temperature and pressure. This method produces diverse morphology with different shapes like needle, prism, flower, plate, dandelion, fiber etc. However the problem related to phase purity and time-consuming process are few of the disadvantages of this method.
d) Sol-gel Method. Sol-gel is the simple yet efficient process. Hydroxyapatite of high purity can be obtained using sol-gel method but precise control over the morphology is not achievable.
e) Ultrasonication method: Synthesis of nano-size hydroxyapatite can be achieved using ultrasonication method. Processing time can be significantly reduced and monophasic Hap can be obtained when ultrasonication method is used for the synthesis of hydroxyapatite.

In addition to different synthesis method, the application of hydroxyapatite for water defluoridation was also explored.

Biogenic Hap of different origins, such as bone chars, cow bones, fish bones, and eggshell, has found its application for the removal of F from groundwater. Whereas, Hap synthesized from different methods using various reagents were used as an adsorbent for water defluoridation. The maximum adsorption capacity of 40.818 mg/g was reported by (Zhang et al., 2012) when Phosphogypsum, diammonium phosphate solution and sodium hydroxide was used for the synthesis of hydroxyapatite. Moreover Hap was synthesized along with different composites such as sodium alginate, Chitosan, gelatin, chitin, Cotton Cellulose etc. in order to enhance its properties for water defluoridation. However no significant high defluoridation capacity was observed using Hap-composites and cost of the product is also been increased due to addition of extra-chemicals for the synthesis of hydroxyapatite-composites. To overcome the limitation of high defluoridation capacity using hydroxyapatite, modification of Hap was done by the addition of different materials during the synthesis which had affinity towards fluoride ions. The adsorption capacity of 44.068 mg/g, 32.57 mg/g, 28.3 mg/g was reported by (Chen et al., 2016; Muthu Prabhu and Meenakshi, 2014; Nie et al., 2012) which is significantly high as compared to hydroxyapatite prepared from different methods.

There were different materials which were used to enhance the capacity such as phosphogypsum, activated alumina granules, Alumina etc. which can be toxic if leaching of ions occurs during water treatment as discussed in section 2.2.4. Moreover, commercially available activated alumina had the limitation of slow rate of adsorption which limits its use for treating large quantities.

More efforts are required for the synthesis of modified hydroxyapatite because of its higher defluoridation capacity. Moreover cost effectiveness of an adsorbent is also an important concern in the selection of suitable adsorbent. Even though the literature reports numerous studies on a wide variety of adsorbents both natural, synthetic and composite materials for defluoridation of water, the cost of synthesis has not been reported by most of the authors. Therefore in order to develop a suitable defluoridation unit for rural areas as well as for communities, it is necessary to find an effective adsorbent with high defluoridation capacity, less expensive and simple for the long term usage.

CHAPTER 3

MATERIALS AND METHODS

The brief description of materials and analytical methods employed are summarized in this chapter. Particularly details for each experiment are given in this chapter.

CHAPTER 3
MATERIALS AND METHODS

This chapter introduces the preparation of reagents and standard solution, characterization, defluoridation studies, regeneration studies and analysis of treated water samples. The characterization of adsorbents synthesized was done in Materials Research Center, MNIT, Jaipur and the BET surface area analysis were done at The Indian Institute of Chemical Technology, Hyderabad. Defluoridation studies were carried out via batch defluoridation, and column defluoridation experiments and most suitable adsorbent was analyzed. The pellets of hydroxyapatite synthesized in lab reactor were used for column defluoridation experiments, and the experimental results were verified. The regeneration studies of spent adsorbents play an important role to evaluate the adsorbent performance and reusability which was done using different concentrations of NaOH eluent. Water quality of treated water with all the adsorbents was also evaluated.

3.1. PREPARATION OF REAGENTS AND STANDARD SOLUTION

Analytical grade chemicals were used for the synthesis of hydroxyapatite, preparation of fluoride standard solutions and TISAB buffer. All the solutions were prepared using deionized water (Ultrapure water system, Millipore). Calcium nitrate ($Ca(NO_3)_2$), Potassium dihydrogen phosphate (KH_2PO_4) and ammonia solution (NH_4OH) (LobaChemie) were used for the synthesis of pure hydroxyapatite nano-rods. Whereas calcium nitrate ($Ca(NO_3)_2$) prepared from marble waste powder (MWP) which was procured from marble processing industry located in the region of Kishangarh, Rajasthan, India was used for the synthesis of marble apatite and marble hydroxyapatite. To obtain

calcium nitrate ($Ca(NO_3)_2$) from MWP, nitric acid (HNO_3) and ammonia solution (NH_4OH) was used. For defluoridation experiments, a fluoride stock solution of 1000 mg/L was prepared using sodium fluoride diluted appropriately for batch experiments. Total ionic strength adjustment buffer (TISAB) was prepared using sodium chloride, CDTA and glacial acetic acid (AR grade). pH of the buffer was maintained using 5 M NaOH solution. The defluoridation experiments were carried out in polypropylene flasks to avoid leaching of any impurities into the solutions. The point of zero charge (pH_{PZC}) was determined by the solid addition method. 150 mg of adsorbent was added in 100 ml solution with 0.01 M NaCl as a background electrolyte, whose initial pH values (2–12) were adjusted by small additions of diluted (0.01 M) HCl or NaOH. pH adjustments were done using 0.01 M of NaOH and HCl with a pH meter (Orion 2 Star).

3.2. CHARACTERIZATION

The detailed characterization involves specifying the phase composition, crystallography and morphology of the material synthesized. Phase composition comprises of identification of chemical constituents present in the material synthesized whereas crystallographic analysis provides the identification of different phases. Characterization of shape, size and spatial distribution of the particles corresponds to the morphology of the materials synthesized.

The synthesized adsorbents were characterized using FTIR, XRD, SEM, TEM/EDS, TGA/DTA and BET surface area techniques for its various properties such as composition, surface properties and crystallography analysis.

3.2.1. FTIR

Infrared spectroscopy is a method used for chemical identification, based on the fact that the selective absorption of material occurred in the infrared region. The absorbed intensities are helpful for the identification of the samples, chemical make up as functional group present in the sample are responsible for absorption of radiation at different frequencies. The molecule of chemical substance vibrates in many modes after absorption of IR, giving FTIR absorption spectrum, over wide wavelength range. The

spectrum obtained is a two-dimensional plot which comprises of intensity and frequency of the sample analyzed.

FTIR spectroscopy was used to evaluate bonding patterns of compounds present in the adsorbent synthesized. Samples were analyzed with a FT-IR spectrum 2 (Perkin Elmer) in the range of 450 to 4000 cm^{-1} with a resolution of 4 cm^{-1}. Attenuated total reflected (ATR) mode was used for FTIR analysis by placing the small amount of powdered sample on the quartz crystal mounted on the instrument. The pressure was applied so that sample will be placed parallel to the crystal. Before analysis, an air background scan was collected to avoid background noise. The graphical spectra obtained was taken using the software provided with the instrument.

3.2.2. XRD

X-rays are used to analyze the structural properties of matter. Characteristics of individual crystal structure included diffraction angle and diffracted beam intensity. The intensity of diffracted beam for every material will be inimitable because of the different physical characteristics of each atom. This inimitability helps to identify the structure and determine the structural parameters of the material.

XRD was used to analyze the phase purity and crystallographic information of the material synthesized. XRD was also helpful for providing the information of the mean crystallite size of the material.

Phase analysis of materials, effects of ultrasonication and effect of increased calcination temperature on the properties of the material were analyzed by X-ray diffraction analysis (X'Pert Powder PANalytical, CuKα =1.5406 Å radiations).The X-ray source was operated at 40 kV and 30 mA. Powdered samples were employed on the flat plate which was mounted on an automatic sample chamber. XRD patterns were then recorded at 2θ angle between 10º to 80º with scan step time of 0.600 per sec and step size of 0.15º. The PANalytical X'Pert HighScore software was used for phase identification of the synthesized material by comparing with the standards Joint Committee on Powder Diffraction Standards (JCPDS) card number inbuilt in the software. The crystal size of the materials was later determined using the Debye-Scherrer equation given below (3):

$$D_P = \frac{0.94\lambda}{\beta_{1/2} cos\theta} \quad (3)$$

where Dp is Average Crystallite size, β *is* Line broadening in radians, θ is Bragg angle and λ is X-ray wavelength.

3.2.3. SEM

Scanning electron microscopy (SEM) use a fine electron beam, focused towards the sample under examination. When the electron beam is incident on the sample surface, it emits X-rays and electrons. The backscattered electrons and secondary electrons are detected by the recorder to produce a high resolution spectra of a sample. The three-dimensional appearance of the sample is very effective to examine the surface properties.

The samples to be analyzed were prepared by coating a thin film of platinum using auto fine coater (JEOL/JFC1600) to increase the conductivity. The coated samples were subjected for analysis by scanning electron microscope (Nova Nano SEM 450) for evaluation of the morphology, surface characteristics as well as crystallographic information at various magnifications.

3.2.4. TEM/EDS

Transmission electron microscopy uses a high voltage beam of the electron emitted by a cathode. The interaction between the partially transmitted electrons and the atoms carries information of the samples. The information is then magnified by a series of magnetic lenses which is recorded by CCD camera and displayed in a real time. Energy Dispersive X-ray Spectroscopy (EDS or EDX) is a powerful technique which gives information about elemental and chemical compounds present in the sample. X-ray mapping process was used to gather the information about the elemental composition of the materials. When a beam of electron hits the sample, the amount of X-ray emitted by each element has a direct relationship with the concentration of that element.

Transmission electron microscopy (TEM) was used for microstructural analysis of the samples whereas EDS was used to identify the elemental composition of the materials synthesized.

Transmission electron microscopy (TEM) was performed with a Technai G2T20 coupled with Energy-dispersive X-ray spectroscopy, (X-flash 6TI30 Bruker). The samples were prepared by dispersing a very small amount of sample in a solution of ethanol followed by sonication (Buehler Ultramet) until a homogeneous dispersion was obtained. The dispersed sample was dropped on the copper grid which was mounted on the microscope and samples were analyzed.

3.2.5. TGA/DTA

The effect of temperature on the properties of material was studied by Thermal analysis. TGA measures the change in mass with an increase in temperature which provides information of sample composition, thermal stability and kinetics parameters of chemical reactions in the sample. The weight loss and weight gain of material are also measured by TGA. The difference in temperature between a sample and a reference is measured by Differential thermal analysis (DTA). DTA determine the decomposition temperature of the material and chemical change of inorganic materials.

Thermogravimetric analysis (TGA) and Differential thermal analysis (DTA) were performed in a simultaneous TG-DTA (PerkinElmer STA6000) in the presence of nitrogen atmosphere from room temperature to 900ºC with heating rate of 20ºC/min to study the weight loss and thermal behavior. The simultaneous DTA/TGA uses a pan balance, and the sample was placed in the furnace which was heated and cooled according to the programmed thermal cycle. The TGA and DTA output were stored on the PC for analysis of the data.

3.2.6. BET SURFACE AREA ANALYSIS

Specific surface area of the materials synthesized was estimated by using BET analysis. It is based on the physical adsorption of gas on the surface of powdered material which results from van der waals forces. Specific surface area is determined by calculating the amount of gas adsorbed on the surface which can be measured by a volumetric or continuous flow procedure.

BET surface area of the material synthesized was determined using nitrogen adsorption/desorption isotherm at -196ºC using gas sorption analyzer (Quantachrome, Autosorb-1).

3.3. DEFLUORIDATION STUDIES

3.3.1. BATCH EXPERIMENTS

Multi-ion analyzer (Thermo Scientific Versa Star Orion M93) with ion selective fluoride electrode BN 9609 (Orion, USA) was used for the quantitative analysis of residual fluoride whereas; pH was measured with Orion Versa Star pH meter. A 250 ml PVC containers with 100 ml working volume were used in the batch adsorption studies which were shaken at 200 ± 10 rpm at 303 ± 1 K with the known weight of adsorbent into the desired concentration of fluoridated water. Effect of various parameters like adsorbent dose, contact time, initial fluoride concentration, pH and effect of other ions on the defluoridation capacity of the adsorbents synthesized were studied. The treated samples were filtrated with Whatman filter paper No. 42 after the attainment of equilibrium. TISAB-II buffer was added in the ratio of 1:1 for analysis of residual fluoride to eliminate the polyvalent cations which form the complexes with fluoride ions present in the solution. The adsorption capacity (mg/g) and % fluoride removal were calculated using eq.(4) and eq. (5) respectively:

$$q_e = \frac{C_0 - C_e}{W_{ad}} \times V \tag{4}$$

$$Fluoride\ removal\ (\%) = \frac{C_0 - C_e}{W_{ad}} \times 100 \tag{5}$$

where q_e is the equilibrium adsorption capacity (mg/g); C_0 and C_e are the initial and final equilibrium fluoride concentrations (mg/L) respectively, V is the volume (L) of fluoride solution, and W_{ad} is the mass (g) of the adsorbent. All the batch experiments were repeated two times to confirm the reproducibility of the obtained results. Solid addition method was used to determine the point of zero charge (pH_{PZC}) by adding 150 mg of the

adsorbent with 0.01 M NaCl as a background electrolyte, whose initial pH values (2–12) were adjusted by small additions of dilute (0.01 M) HCl or NaOH.

3.3.1.1. Effect of Dosage

Experiments were carried out with the adsorbents synthesized in the known concentration to fix the optimum dosage of adsorbent that will be required to bring fluoride concentration under the permissible limit (<1.0 mg/L). The solutions were kept for shaking in an orbital shaker at 200±10 rpm for a definite time intervals by keeping the pH, initial fluoride concentration and temperature constant.

3.3.1.2. Effect of Contact time

The effect of contact time on defluoridation efficiency of the adsorbents synthesized was determined by varying the contact time and keeping other parameters such as adsorbent dose, pH and temperature constant.

3.3.1.3. Effect of pH

The pH of the water depends on various geological factors, and it is one of the important parameters to understand the efficiency of removal of fluoride ions in aqueous solution. The different pH range can influence the defluoridation capacity of adsorbent. Hence, to understand the effect of pH, experiments were carried out in the pH range of 3 to 11 keeping the contact time, initial fluoride concentration, temperature and adsorbent dosage constant.

3.3.1.4. Effect of Initial Fluoride concentration

Different fluoride concentrations (0–45 mg/L) were used to study the effect of initial fluoride concentration by keeping other parameters such as dosage (8 g/L) and time (3h) constant. To evaluate the effect of initial fluoride concentration on fluoride removal capacity.

3.3.1.5. Effect of interference ions

Groundwater being the major drinking water source contains several other anions that may compete with fluoride ion for adsorption sites. Therefore, the defluoridation capacity of the adsorbents synthesized in the presence of competing ions like chloride, nitrate, sulfate and bicarbonate was experimentally verified. Studies were

done by varying the concentration of co-existing ions whereas; fluoride concentration was fixed at 10 mg/L. Other parameters such as adsorbent dosage, initial fluoride concentration, temperature, contact time and pH were kept constant. The concentration of interfering ion solutions was obtained by appropriate dilution from the stock solutions prepared.

3.3.2. ADSORPTION ISOTHERMS

Estimation of adsorption capacity is an important factor for designing the adsorption systems which can be achieved by analysis of different fluoride adsorption isotherms. Adsorption isotherms were studied to describe the specific relationship of adsorbed fluoride on the surface of adsorbent and the equilibrium concentration of fluoride in the medium. There are various theoretical models that are used to determine the mechanism of adsorption and maximum capacity of adsorbent. Experimental data were analyzed using four isotherms viz. Langmuir, Freundlich, Temkin, Dubinin–Raduschkevich.

3.3.2.1. LANGMUIR ISOTHERM MODEL

Irving Langmuir in 1916 derived the equation for adsorption under an active equilibrium condition. It is based on the assumption of monolayer adsorption and a homogeneous phenomenon.

The basic assumptions underlying Langmuir isotherm model are:

- The adsorbent surface is flat.
- Only monomolecular adsorption takes place,
- Adsorption is localized.
- Adsorbate molecules do not interact.
- The heat of adsorption is independent of surface coverage.

The linearized form of Langmuir isotherms can be written as given in eq. (6)

$$\frac{C_e}{q_e} = \frac{1}{q_{max}k} + \frac{C_e}{q_{max}} \qquad (6)$$

where C_e is the equilibrium concentration (mg/L); q_e is the experimental data on the equilibrium capacity (mg/g), k is the equilibrium constant (L/g); q_{max} is the maximum amount of adsorbate adsorbed per unit weight of adsorbent to form a monolayer. The values of q_{max} and k can be calculated from the slope and intercept of linear plot of C_e/q_e vs. C_e.

Separation factor (r) in Langmuir isotherm is a dimensionless constant that indicates the efficiency of adsorption process and is expressed as in eq. (7)

$$r = \frac{1}{1 + K'C_0} \tag{7}$$

where C_0 and K' are the initial fluoride concentration (mg/L) and Langmuir isotherm constant. The r <1 indicate favorable adsorption and r >1 indicate unfavorable adsorption.

In particular, the limitations of Langmuir model is that it does not follow when multilayer adsorption is possible. To overcome this Freundlich isotherm model is considered for multilayer adsorption.

3.3.2.2. FREUNDLICH ISOTHERM MODEL

Unlike Langmuir isotherm model, Freundlich isotherms model state the multilayer adsorption and heterogeneity of adsorbent surface. The model assumes that the adsorption occurs on heterogeneous surfaces with diverse adsorption energies. The Freundlich adsorption equation is perhaps the most widely used mathematical description of adsorption in aqueous systems.

The linearized form of Freundlich isotherm model is given by the following eq.(8):

$$logq_e = logk_f + \frac{1}{n}\log(C_e) \tag{8}$$

where k_f (mg/g) and 1/n are temperature dependent Freundlich constants that can be calculated from the slope and intercept of linear plot of log q_e vs. log C_e. The slope 1/n, is a measure of adsorption intensity or surface heterogeneity and its value lies between 0.1 and 1.0.

3.3.2.3. TEMKIN ISOTHERM MODEL

The Temkin isotherm considers the adsorbent and adsorbate interactions. Thus, by ignoring the extremely low and high value of concentrations, it contemplates that heat of adsorption of all molecules in the layer would decrease linearly rather than logarithmic. The following equation (9) expresses this model:

$$q_e = B_T \ln A_T + B_T \ln C_b \quad (9)$$

where B_T is Temkin isotherm constant; A_T is Temkin isotherm equilibrium binding constant (L/g).

3.3.2.4. THE DUBININ-RADUSCHKEVICH ISOTHERM MODEL

The Dubbin–Raduschkevich isotherm is pragmatic in expressing the mechanism of adsorption with a Gaussian energy distribution onto a heterogeneous surface. The distinctive feature of the isotherm is that it is temperature-dependent and its equations (10, (11) is given as follows:

$$\ln q_e = \ln q_d - B\varepsilon^2 \quad (10)$$

$$\varepsilon = RT \ln[1 + \frac{1}{C_e}] \quad (11)$$

where, B is Dubibin–Raduschkevich isotherm constant; q_d (mg/g) is theoretical isotherm saturation capacity and ε is Polanyi potential.

3.3.3. ADSORPTION KINETICS

The rate of reaction and rate limiting step, both play an important role in the adsorption phenomenon. Mechanism of adsorption depends on the physical and chemical characteristics of adsorbent used, which influence the kinetics of reaction taking place in an adsorption process. The study of adsorption kinetics is significant in determining the optimum operating conditions such as residence time required in the design of suitable defluoridation equipment. For comprehending the kinetics of fluoride adsorption process in this study, two mass transfer models (pseudo-first and pseudo-second order) and one intraparticle diffusion model were used.

3.3.3.1. PSEUDO FIRST ORDER KINETIC MODEL (LAGRGREN'S RATE EQUATION)

This model is used to study the non-reversible reaction between the liquid and the solid phase and is based on the following assumptions:

- Adsorption occurs only on limited sites, and there is no interaction between the adsorbed ions.
- The energy of adsorption is independent of surface coverage.
- Maximum adsorption is based on monolayer of adsorbate on the adsorbent surface
- The fluoride ion uptake on the adsorbents is governed by a first-order rate equation.

The logarithmic form of pseudo first order is generally expressed as in eq. (12):

$$\log(q_e - q_t) = log q_e - \frac{K_1}{2.303}\mathrm{t} \qquad (12)$$

where q_e and q_t (mg/g) are the amounts of fluoride adsorbed per unit mass of adsorbent at equilibrium and time t, respectively, and K_1 is pseudo first-order adsorption rate constant (min^{-1}). The value of K_1 can be calculated from the slope of the linear plot of log $(q_e - q_t)$ vs. time (t).

3.3.3.2. PSEUDO SECOND ORDER KINETIC MODEL

Pseudo-second order model is followed when rate-limiting step is surface adsorption i.e. the process involves chemisorption, where adsorbent removal is due to physiochemical interactions between the two phases. The linear form of pseudo second order model can be written as in eq.(13):

$$\frac{t}{q_t} = \frac{1}{K_2\, q_e^2} + \frac{t}{q_e} \qquad (13)$$

where q_t is the amount of fluoride adsorbed at time *t* (mg/g), q_e is the amount of fluoride adsorbed at equilibrium (mg/g), K_2 (mg/g/min) is the rate constant for pseudo second order adsorption. The value of K_2 can be determined by plotting a graph between t/q_t and *t*.

3.3.3.3. INTRAPARTICLE DIFFUSION

The rate of adsorption in the intraparticle diffusion model is described by the speed at which adsorbate diffuses towards adsorbent (i.e., the process is diffusion-

controlled). Intraparticle diffusion mechanism in the process was examined by applying the Weber and Morris equation (14)

$$q_t = K_i t^{1/2} \quad (14)$$

where K_i (mg/g/min$^{-1/2}$) is intraparticle diffusion rate constant and its value can be estimated by plotting a graph between q_t and $t^{1/2}$.

3.3.4. Mathematical Modeling in Batch Studies

Limitation of the classical experimental method for defluoridation was eradicated by optimizing all the factors affecting together by statistical experimental design such as response surface methodology (RSM). Response Surface Methodology (RSM) is a collection of mathematical and statistical techniques useful for the modelling, developing and optimization of experimental data and can be used to evaluate the interaction of multiple variables (Hameed et al., 2008).

3.3.4.1. Response Surface Methodology (RSM)

Experimental design for model preparation in batch defluoridation studies is generated by RSM which comprises of specific set of experiments defined by a matrix.

RSM consists of 3 major steps:

- Execution of statistically designed experiments,
- Estimation of the coefficients in a mathematical model and
- Predicting and checking the response and adequacy of the model.

The purpose of this study was application of RSM coupled with Central composite design (CCD) as a statistic tool for optimization of fluoride adsorption on hydroxyapatite-nanorods synthesized using ultrasonication method.

3.3.4.2. Design of Experiments

RSM design called Central Composite Design (CCD) was applied to optimize three independent variables, i.e., adsorbent dose, pH and contact time for evaluating fluoride removal efficiency (response) using Hap nanorods. This design is extensively being used for fitting a quadratic surface and for optimization of parameters with a

minimum number of experiments to be performed. The Central Composite Design consists of 2^n factorial runs with 2n axial runs and C_n center runs (six replicates). In this study, three independent variables which consist of 8 factorial points, 6 axial points and 6 replicates at the center points were used, which indicate that 20 experiments were required as per the calculations using the following equation (15):

$$N = 2^n + 2n + C_n \tag{15}$$

where N is total number of experiments, n is number of variables, 2^n is the number of factorial runs, $2n$ is axial runs and C_n is center runs.

3.3.4.3. MODEL FITTING AND ANALYSIS OF RESPONSE

The graphical and regression analysis of the data were examined using Design Expert 9.0.4.1 (Stat-Ease, USA; Trial version) software. A second order polynomial equation (16) was fitted for estimating the fluoride removal efficiency using RSM-CCD.

$$Y = b_0 + \sum_{i=1}^{n} b_i X_i + \sum_{i=1}^{n} b_{ii} X_i^2 + \sum_{i=1}^{n} \sum_{j>1}^{n} b_{ij} X_i X_j \tag{16}$$

where Y is the predicted response, b_0 is the constant coefficient, b_i is the linear coefficient b_{ij} is the interaction coefficient, b_{ii} is the quadratic coefficient, and X_i, X_j are the coded values (independent variables). ANOVA polynomial model analyzed the statistical implication of the model, and accuracy of model fit was examined using residual plots. The fit of the polynomial model was expressed by coefficient of determination (R^2). Various other descriptive statistics were used to reflect the statistical significance of this quadratic model including t-ratio, p-value, F-value, degrees of freedom (df), adjusted correlation coefficient (R^2adj), sum of squares (SS), mean sum of squares (MSS), and chi-square (χ^2) test.

3.4. ADSORBENTS SYNTHESIZED

The adsorbents used for defluoridation of water include, pure Hap, marble waste powder, marble apatite synthesized from marble waste and pure Hap synthesized from marble waste powder. The conventional precipitation method (CM) and ultrasonication method (USM) was used for the synthesis of hydroxyapatite (Hap). Conventional precipitation method is the simplest low-cost route for the synthesis of Hap. However, process parameters such as synthesis temperature, calcination temperature, the rate of addition of the reagents, aging time and pH during the synthesis, affect the quality of material synthesized. Therefore during synthesis of Hap using CM, different parameters such as process temperature, calcination temperature and aging time were studied and optimized to prepare pure form of hydroxyapatite.

Use of ultrasonic irradiations has been proved to be a useful tool for process intensification during the synthesis of nanoparticles. Ultrasonic irradiations cause cavitation in a liquid medium where the formation, growth and implosive collapse of micro bubbles occur and their subsequent collapse results in a local temperature of ~5000 K and pressure of ~1000 bar. Due to this, the energy is dispersed and the reactivity of chemicals increases. Therefore, the rapid kinetics of these ultrasound assisted reactions will lead to the completion of the reaction due to improved mass transfer at molecular level. With this approach, synthesis of hydroxyapatite was studied in the presence of ultrasound, which will assist in the proper dissolution of reactants and generate nanosized particles of improved product quality. The role of sonication in process synthesis and its effect on minimizing the synthesis time and energy requirements for completion of the reaction as well as to produce a higher quality product has been studied during the synthesis of adsorbents.

Following adsorbents were synthesized using five different methods from calcium sources including marble waste powder which were utilized for water defluoridation. The various parameters such as calcination temperature, synthesis temperature and time for ultrasonication irradiation were explored for process optimization in the synthesis of the various adsorbents which are listed in the following Table 3.1.

i) Pure hydroxyapatite was synthesized using conventional precipitation method and ultrasonication with precipitation method which was named as Hap CM and Hap

USPM respectively. Effect of calcination on Hap synthesized using USPM method was also analyzed to improve the crystallinity and surface morphology of the adsorbent and product obtained was named according to their calcination temperature viz. Hap USPM 500, Hap USPM 700 and Hap USPM 900.

ii) The second adsorbent which was studied for water defluoridation was marble waste powder (MWP). MWP was calcined at 650ºC, 850ºC and 1000ºC and named according to their respective calcination temperatures i.e. MWP 650, MWP 850 and MWP 1000 respectively. Calcination of MWP results into the dissociation of calcium magnesium carbonate into calcium carbonate, calcium oxide and magnesium oxide, which has good adsorption capacity according to the literature reports published. Calcination also activates the adsorbent which will facilitate higher defluoridation capacity compared to uncalcined marble waste powder.

iii) Third adsorbent studied was marble apatite synthesized from marble waste powder. As it was observed that MWP calcined at 650ºC had better defluoridation capacity, it was calcined at 650ºC before utilizing for the synthesis of hydroxyapatite using both conventional precipitation method and ultrasonication method (named as MA-CM and MA-USM respectively). However the product marble apatite had intermediates such as calcium phosphates and calcium magnesium silicates along with the hydroxyapatite formed. The presence of impurities was mainly due to the presence of silicates in the calcium nitrate derived from marble waste powder.

iv) Further improvisation was done for the synthesis of pure hydroxyapatite using marble waste powder without any impurities and intermediates. Calcium nitrate was derived in its pure form from the marble waste powder. Conventional precipitation method and ultrasonication method was used for the synthesis and different parameters were explored and the product was named as marble hydroxyapatite MA-Hap CM and MA-Hap USM respectively. In the previous studies it was found that MWP on calcination at 650ºC and 850ºC dissociate into $CaCO_3$+MgO and CaO+MgO respectively. In order to optimize the calcination temperature, two different products were synthesized utilizing MWP calcined at 650ºC and 850ºC using conventional precipitation method and named as MA-Hap

650 CM and MA-Hap 850 CM. In ultrasonication method, synthesis time was optimized by varying the ultrasonic irradiation time from 45 min to 75 min during the synthesis of MA-Hap and product obtained was named according to their sonication time i.e. MA-Hap 650 USM 45 min, MA-Hap 650 USM 60 min and MA-Hap 650 USM 75 min.

v) The process scale up of MA-Hap from batch to lab reactor was carried and synthesis temperature was optimized. This results into the three different product which were named as MA-Hap LR 62, MA-Hap LR 72 and MA-Hap LR 82 according to their synthesis temperature i.e. 62ºC, 72ºC and 82ºC respectively. During scale up of MA-Hap LR, temperature required in the synthesis of MA-Hap in lab reactor was optimized based on the purity of the material obtained. The hydroxyapatite synthesized in lab reactor (MA-Hap LR) was further used for the preparation of pellets and column study experiments.

Table 3.1 Different adsorbent synthesized using CM and USM

1. Pure Hap (Hap)	**2. Marble waste powder (MWP)**
1.1.Hap CM 900, 1.2.Hap USPM, 1.3.Hap USPM 500, 1.4.Hap USPM 700 & 1.5.Hap USPM 900	2.1.MWP650, 2.2.MWP850 & 2.3.MWP1000
3. Marble Apatite (MA)	**4. Marble Hydroxyapatite (MA-Hap)**
3.1.MA-CM & 3.2.MA-USM	4.1.MA- Hap 650 CM, 4.2.MA-Hap 850 CM, 4.3.MA-Hap 650 USM 45 min, 4.4.MA-Hap 650 USM 60 min, 4.5.MA-Hap 650 USM 75 min & 4.6.MA-Hap 650 USM 60 min @ 80º C
5. Marble Hydroxyapatite- Lab reactor (MA-Hap LR)	
5.1.MA-Hap LR 62, 5.2.MA-Hap LR 72 & 5.3.MA-Hap LR 82	

The detailed method of synthesis of all the adsorbents listed in above table are elaborated in the results and discussion chapter 4, parts I-IV and chapter 5 which has been described separately with respect to each adsorbent.

3.5. PELLETS PREPARATION & COLUMN EXPERIMENTS

It is essential to formulate powdered adsorbent into pellets form of suitable shape and size for column studies. The Extrusion- Spheronization (E-S) process was used for the preparation of pellets as detailed in the following section.

3.5.1. PELLETS PREPARATION FOR COLUMN STUDIES

Preparation of pellets from adsorbent for utilizing in industrial processes is a major challenge. For lab scale experiments, fine powder are repeatedly shaped into granules, pellets or extrudates using appropriate binder to increase the mechanical strength and handling of the adsorbents. The common method for granulation includes coating and impregnating binder on the surface of solid core material which results in low adsorption capacity due to low availability of the material on the surface. Equally, Extrusion- Spheronization (E-S) technique has long been used to pelletize the material for various industries like pharmaceuticals and fertilizers by extruding and spheronization of a wet mass with a proper binder. The Extrusion- Spheronization (E-S) process involves four steps, explained as follows and also shown in figure 3-1.

i. Combination: The prepared binder was mixed with the adsorbent to form a wet mass. The consistency of binder to powder ratio was kept on an account as it is responsible for the formation of proper extrudes. The wet mass obtained was subjected to second step i.e. extrusion.
ii. Extrusion: The wet mass was compressed by forcing it through a multi-holes screen which forms cylindrical extrudates.
iii. Spheronization: The extrudates obtained were broken up manually into smaller rods and then subjected to spheronizer which comprises of a horizontal rotating friction plate, operating at a speed of 500-1000 rpm which results into rounded spherical shaped pellets.
iv. Drying: The spherical pellets are then dried at 60-70ºC for four hours in a hot air oven.

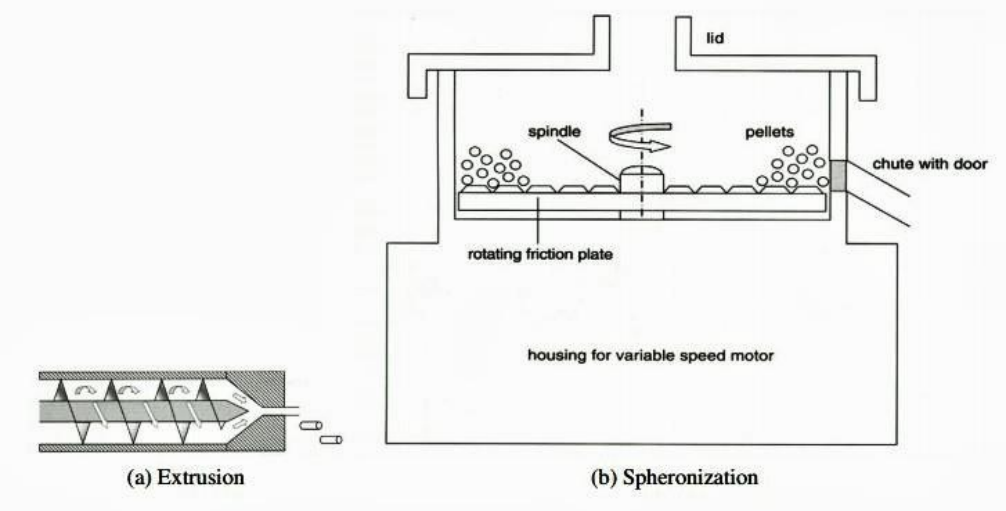

Figure 3-1 Extrusion and spheronization process

There are an extensive variety of organic and inorganic binders which includes cellulose, clays, polyvinyl alcohol (PVA) and sodium silicate and bentonite respectively. Polyvinyl alcohol (PVA) was selected as a model binder due to its wide application in ceramic industries and pressure driven membranes designed for water treatment.

In the present study, pellets of MA-Hap LR 72 synthesized in lab reactor was prepared by using cross-linked PVA as the binder. The PVA was dissolved in deionized water at 10 wt% concentration (intrinsic viscosity 0.85-0.89 dl/g) and kept at 90ºC for 1h in a water bath. For cross-linking, propanedioic acid (5 wt% of PVA) was added to a solution of PVA and kept at 95ºC for 5 h. The cross-linked PVA solution was then added to the powdered adsorbent (MA-Hap LR 72) and mixed thoroughly to obtain a wet mass required for extrusion which was then subjected to extruder (Prism make) comprises of multi-holes screen with a size of 2 mm. The speed of the extruder was kept constant at 60 rpm. The extruded material was then fed into a spheronizer (PRISM make) for making spherical shaped pellets by the action of a horizontal rotating friction plate. The spheronizer was operated at a speed of 750 to 850 rpm fitted with a plate of 2.25 mm. While rotation compressed air was provided at the rate of 2 kg/cm^2 for purging the pellets during the spheronization. The spherical pellets obtained was later dried at 70 ± 5ºC for 4 h before being used in continuous column studies. The step wise process for the preparation of pellets using MA-Hap LR 72 have also been explained in figure 3-2.

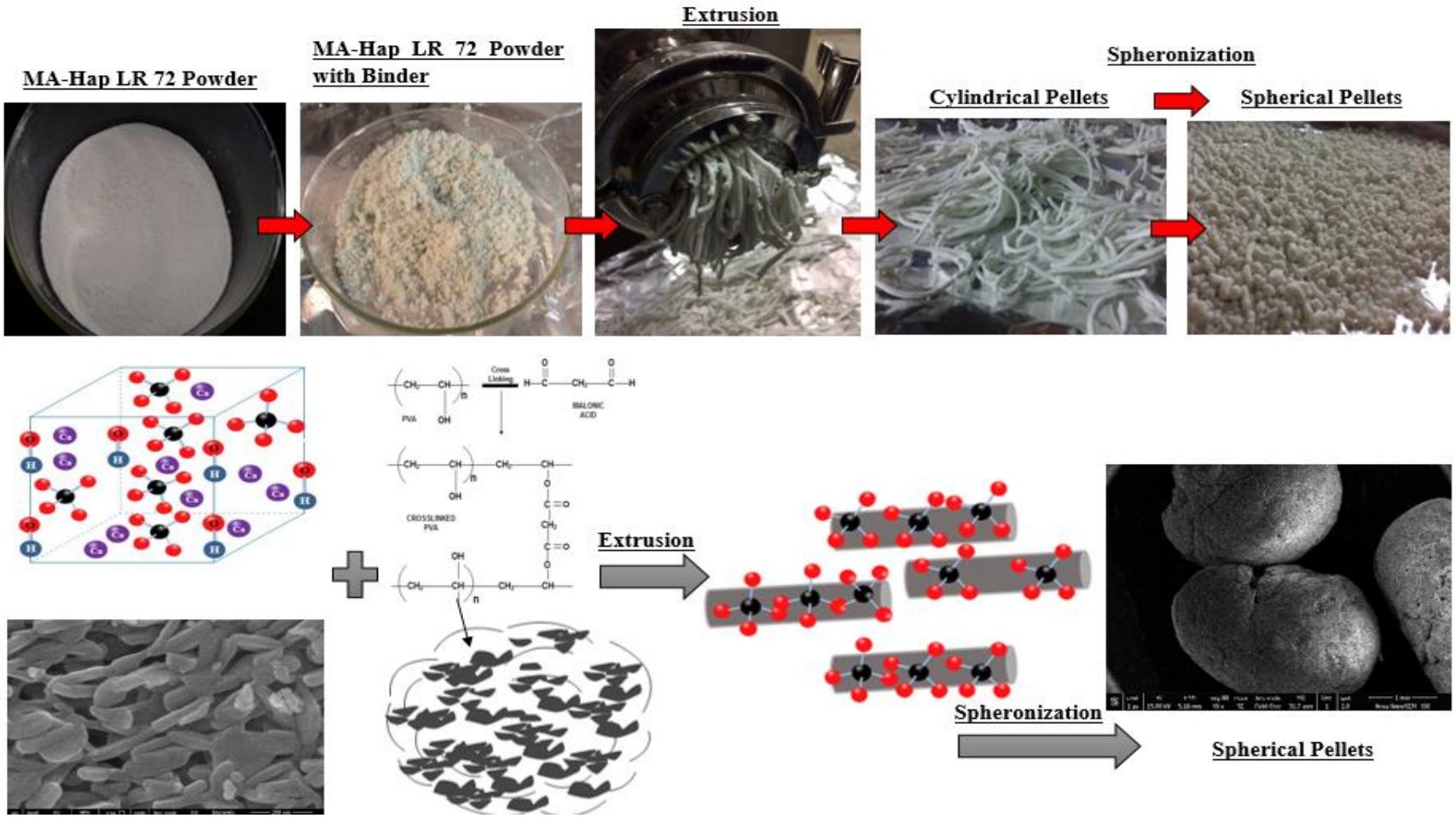

Figure 3-2 Step followed for the preparation of MA-Hap LR 72 pellets using E-S technique**.**

3.5.2. COLUMN EXPERIMENTS

Column studies were conducted at room temperature in a glass column of 50 cm length and 5.0 cm in diameter. A stainless steel tank was used with a feed reservoir of 20 L capacity to pump a feed solution across the packed bed with a magnetic drive pump (Promivac make). The inlet flow rate was controlled by a flow controller (Eureka make). For the uniform distribution of solution from the tank, the mesh was placed above the column. The schematic representation of column setup is shown in figure 3-3.

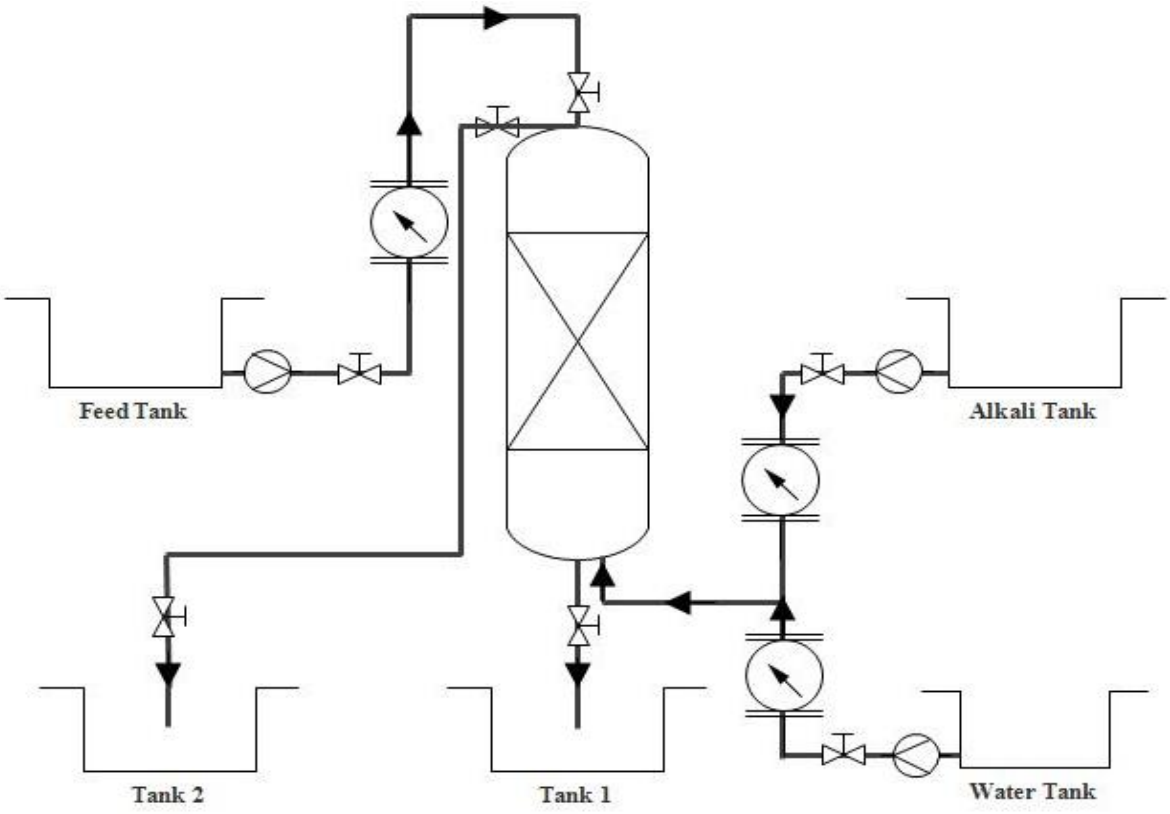

Figure 3-3 Adsorption regeneration column setup.

The Tank 1 in figure 3-3 was employed for storing the overflow solution. For regeneration experiments, the reagent solution was pumped from alkali tank in up flow mode, and Tank 2 was used for collecting the treated water.

The column was packed with MA-Hap LR 72 pellets with different bed heights to check its effect on adsorption capacity using downward flow. The distilled water was run through the columns using water tank with 20 L capacity for 2 h before starting the

experiments to establish equilibrium between the MA-Hap LR 72 pellets and the water. The feed solution of desired fluoride concentration was pumped through the packed bed column with the predetermined flow rates of 1 LPH, 1.5 LPH and 2 LPH to study the effect of the flow rate of fluoride removal. Samples from the outlet were collected at regular intervals of time and examined for fluoride concentration. After exhaustion of the column, when inlet fluoride concentration is approximate equals to outlet fluoride concentration, i.e., C_e/C_0 is approximately equal to one. To obtain the breakthrough curve, the results acquired were plotted in terms of C_e/C0 vs. time. The capacity at the breakthrough point (q_b) is defined as the total quantity of fluoride ions adsorbed by MA-Hap LR 72 pellets when the concentration of fluoride in the effluent reaches ≈5% of the initial concentration. It is determined by the area under the breakthrough curve for a known fluoride concentration from the following equation (17):

$$q_b = \int_0^{t_b} \frac{C_o - C_t}{M} dt \tag{17}$$

where q_b is the capacity at the breakthrough point (mg/g), C_0 and C_t are the inlet and outlet fluoride concentrations respectively (mg/L); M is the mass of adsorbent (g), and tb is the time (L) at the breakthrough point. The breakthrough point was considered at a residual fluoride concentration of 1.0 mg/L (the permissible limit for fluoride in water).

The capacity at the exhaustion point (q_{EX}) corresponds to the quantity of fluoride ions bound by MA-Hap LR 72 pellets when the fluoride outlet concentration reaches approximately equals to 95% of the initial value was calculated from the following equation (18):

$$q_{EX} = \int_0^{t_{EX}} \frac{C_o - C_t}{M} dt \tag{18}$$

where q_{EX} is the capacity at the exhaustion point (mg/g), t_{EX} is the exhaustion time when the column is saturated (h), and C_0, C_t and M, are same as above.

The bed height of the adsorbent and volumetric flow rate was used to determine the empty bed contact time (EBCT) using the following equation (19):

$$EBCT = \frac{Z}{F} \quad (19)$$

where Z is bed height in cm and F is the volumetric flow rate is L/h.

The effect of various process parameters such as bed height, inlet flow rate, initial fluoride concentration and particle size of pellets were studied via column experiments.

3.5.2.1. EFFECT OF PARTICLE SIZE

It is necessary to fabricate powdered adsorption materials into pellets form of a proper size. Extrusion-spheronization (E-S) technique was used to manufacture the pellets by extruding a semi-solid wet powder mass through a screen featuring many holes, followed by spheronization on a rotating plate. The pellets formed were passed through a sieve of the size of 3 mm, 2.5 mm and 2 mm and classified into two groups i.e. 3 to 2.5 mm and 2.5 mm to 2 mm. The pellets obtained were used in the column studies to check the defluoridation capacity at the different flow rate, fixed bed height and fluoride concentration.

3.5.2.2. EFFECT OF BED HEIGHT

In order to study the effect of bed height on fluoride removal in continuous studies, the column was packed with three different bed heights by loading 21 gm. of adsorbent for 5 cm bed height, 63 gm. for 15 cm bed height and 104 gm. for 25 cm bed height with the influent fluoride concentration of 10 mg/L at a flow rates of 1 LPH.

3.5.2.3. EFFECT OF FLOW RATE

The effect of flow rate on fluoride removal was studied by taking 104 gm. (25 cm) of adsorbent (MA-Hap LR 72) with a fluoride concentration of 10 mg/L at different flow rates of 1, 1.5 and 2 LPH.

3.5.2.4. EFFECT OF FLUORIDE CONCENTRATION

Initial fluoride concentration has a significant effect on the breakthrough curve. Fluoride concentration of 5, 10, 15 mg/L was passed through a column packed with 104 gm (25 cm) of MA-Hap LR 72 pellets at a constant flow rate of (1 LPH) to study the effect of fluoride concentration.

3.5.3. MODELING OF BREAKTHROUGH PROFILE IN COLUMN STUDIES

The breakthrough curve and adsorption capacity of the adsorbent were used to design a column adsorption process. Various models have been established to predict the adsorption breakthrough behavior with a high degree of accuracy, efficiency and applicability for industrial scale operations according to the data collected during lab scale experiments. The experimental data of the column studies was fitted using three breakthrough models viz, Hutchins Bed Depth Service Time (BDST) model, Thomas model and Yoon-Nelson model to analyze the column performance for the removal of fluoride from aqueous solution using MA-Hap LR 72 pellets.

3.5.3.1. HUTCHINS BED DEPTH SERVICE TIME (BDST) MODEL

The BDST model has been developed from the work of Bohart and Adams (Ma, Barford, and McKay 2014). The BDST model helps in predicting the capacity of an adsorbent material to remove a specific amount of solute from solution before there is a requirement of regeneration. The BDST model was derived based on the assumption that adsorbate is adsorbed onto the adsorbent surface directly and the mass transfer resistance during the adsorption process is negligible. The initial part of the breakthrough curve, i.e., up to the breakpoint or 10–50% of the saturation points is described by this model (Kundu and Gupta 2006). BDST is a simple model which works from relationship between the service time of the column and the depth of packed bed column which was developed by Bohart and Adams. However, Hutchins has proposed a linear relation between the service time (Tb) and the bed depth (hc) of the form as shown in eq.(20) and eq. (21)

$$t_b = \frac{N_O}{uC_O} Z - \frac{1}{K_a C_O} \ln\left(\frac{C_O}{C_b} - 1\right) \tag{20}$$

Critical bed depth equation is expressed in the following form:

$$Z_O = \frac{u}{K_a N_0} \ln\left(\frac{C_0}{C_b} - 1\right) \tag{21}$$

where t_b (h) is the service time to breakthrough, N_0 (mg/L) denotes the adsorption potential, u (cm/h) is the linear flow velocity, Z (cm) is the bed depth, C_0 and C_b are initial and breakpoint fluoride concentration respectively, u (cm/h) is the linear flow velocity, K_a (L/mgh) is the adsorption rate constant and Z_0 is the critical bed depth.

3.5.3.2. THOMAS MODEL

The behavior of adsorption process in fixed-bed columns is generally attributed by most widely used Thomas model. The assumption made in this model is that the process follows Langmuir kinetics of adsorption-desorption with no axial dispersion. Thomas model derivation is based on second order kinetics, and it considers that adsorption is not affected by the chemical reaction but by the mass transfer at the interface (Bharathi and Ramesh 2013). This can lead to some inconsistency when model adsorption processes in specific conditions are used. The expression (22) by Thomas for an adsorption column is as follows:

$$\ln\left(\frac{C_0}{C_b} - 1\right) = K_{th} q_0 \frac{M}{F} - K_{th} C_0 t \qquad (22)$$

where K_{th} (L/mg h) is the Thomas rate constant, q_0(mg/g) is the equilibrium adsorbate uptake and M is the amount of MA-Hap LR 72 pellets in the column.

3.5.3.3. YOON-NELSON MODEL

Yoon and Nelson developed a less complex model since detailed requirement related to characteristics of adsorbate, adsorbent type and the physical properties of adsorption bed is not required. The assumption in Yoon and Nelson Model is that the rate of decrease in the probability of adsorption of adsorbate molecule is proportional to the probability of the adsorbate adsorption and the probability of an adsorbate breakthrough on the adsorbent (Yoon and Nelson, 1984).

The linearized form of Yoon–Nelson equation can be expressed as given in eq.(23):

$$\ln\left(\frac{C_e}{C_0 - C_e}\right) = k_\gamma t - \tau k_\gamma \qquad (23)$$

where k_γ (h^{-1}) is the Yoon-Nelson rate constant and τ (h).is the time required for 50% adsorbate breakthrough time by using Yoon-Nelson model.

3.5.4. REGENERATION STUDIES

The regeneration and reutilizing of a used adsorbent is a most significant aspect of a cost-effective adsorption technology. The exhausted adsorbent was regenerated using the different concentration of eluent (NaOH) ranging from 0.1 M to 1.5 M. The up flow

mode with a flow rate of 1 LPH was used for faster regeneration due to better contact between the exhausted bed and eluent. The adsorbent bed was later restored by washing with deionized water for approximately 4 h with the same flow rate until pH of the outlet was neutral (7.0 ± 0.2). The reactivated MA-Hap LR 72 pellets were again ready for the next defluoridation cycle. Altogether four cycles of regeneration experiments were conducted until the adsorbent become saturated, and no further desorption take place i.e. retained fluoride concentration by MA-Hap LR 72 pellets are more than the amount recovered by desorption solution (NaOH).

3.5.5. Analysis of Treated water samples

Water quality parameters such as TDS, electrical conductivity (EC), and calcium leached in treated water with an adsorbent were analyzed with their respective ion meter electrodes. Turbidity present in the aqueous solution was measured with a turbidity meter (NT4000, Spectra Lab) whereas the total hardness, total alkalinity, concentration of magnesium and phosphorus in solution was evaluated by APHA standard procedures (APHA/AWWA/WEF, 2012).

3.6. SUMMARY OF THE CHAPTER

This chapter briefed about the materials and reagents along with the description of analytical characterization tools used in this study. Various parameters used for defluoridation in batch studies along with details of adsorption isotherm and kinetic models and column adsorption experiments are specified. Preparation of pellets and method of regeneration is also stated. Method for analysis of water quality parameters is also described in this chapter.

The next chapter marks the beginning of Results and Discussions.

CHAPTER 4

RESULTS AND DISCUSSION

This chapter is divided into four subparts which include the detailed experimental results of all the adsorbents synthesized followed by their applications in water defluoridation.

CHAPTER 4
RESULTS AND DISCUSSION

The studies on the development of materials using waste for easing the environmental pollution have gained much interest. Efforts were drawn to develop and analyze the defluoridation performance of various naturally as well as synthetically prepared Hap from calcium sources and marble waste powder, due to their various added advantages such as:

1. Marble waste powder (MWP) primarily composed of calcium and magnesium based compounds which possess affinity towards fluoride ions.

2. Calcium can be used as a source of reagents for synthesis of calcium based products such as hydroxyapatite.

3. MWP is available in abundant which can be availed free of cost and its utilization will yield cheaper products.

4. The cost of these materials is lower than the cost of commercial adsorbents.

5. Low cost adsorbents can be employed efficiently as the competence of non-conventional adsorbent may vary from 50% to 90% and are readily available and require less maintenance.

The basic raw materials studied as calcium was available from waste marble powder which is a huge environmental concern now a days due to the fast growth of marble industry. Marble is a crystalline metamorphic limestone, which majorly consists

of calcium compounds like calcite ($CaCO_3$), dolomite ($CaMg(CO_3)_2$) and silicon oxides (Segadães, Carvalho, and Acchar 2005). Considering, the significant presence of calcium and magnesium compounds in marble waste powder (MWP), it may be either used as a defluoridation agent or additionally can be used for the synthesis of calcium based material such as hydroxyapatite, which also has potential for defluoridation as well as vast applications.

4.1. ADSORBENTS USED IN THE STUDY

In this study, an attempt was made to use marble waste powder (MWP) for the synthesis of a biomaterial "hydroxyapatite" for defluoridation of drinking water. Also the capabilities of MWP and Pure hydroxyapatite nanorods prepared synthetically was studied as an adsorbent for water defluoridation. Different parameters such as calcination temperature, synthesis temperature and ultrasonication irradiation time were explored in order to enhance the quality of the product in terms of purity and defluoridation capacity.

In the conventional Hap synthesis process, the process conditions play an important role in the quality of Hap synthesized. Moreover the adsorption capacity of the Hap produced can be increased by calcination to prepare better porous, crystalline structure of Hap with improved physical properties. During calcination there is a change in state from amorphous to crystalline form. It was observed that the crystallinity of the adsorbents had improved due to calcination at a higher temperature (range- 800-900ºC), and uniformly sized crystals were obtained which was confirmed from XRD analysis. Crystalline materials even have better adsorption capacity due to more surface area rather than amorphous materials. Since calcination had an effect on the adsorption capacity of Hap, marble waste powder was also subjected to calcination in the temperature range of 650-900ºC and optimized temperature i.e. 650º C was identified.

Since MWP calcined at 650ºC had better defluoridation capacity, this temperature was optimized for preparation of Hap using marble waste powder using conventional and ultrasonication method. Ultrasonication irradiation time for synthesis have an impact on the properties of hydroxyapatite. Ultrasonication will provide the

nuclei for crystal formation and crystal growth as well as cause process intensification of the chemical reactions due to improved mass transfer at the molecular level. Therefore marble hydroxyapatite was synthesized at different irradiation time i.e. from 45 min to 75 min in order to obtain purest form of hydroxyapatite with better defluoridation capacity. Temperature optimization was also a vital factor as higher temperature will favor higher reaction rates. Therefore, time and temperature optimization was considered as crucial parameters for synthesis of different adsorbent using ultrasonication method.

Synthesis temperature also play an important role in the purity of Hap synthesized. Therefore in order to obtain pure form of Hap without any intermediates synthesis temperature need to be optimized. MA-Hap synthesized in lab reactor was processed at different temperature i.e. from 62ºC to 82ºC in order to check and optimize the best suited temperature to obtain monophasic Hap.

The process methodology for synthesis hydroxyapatite (Hap) using marble waste powder is summarized in figure 4-1. Whereas different adsorbents synthesized using conventional and ultrasonication method is depicted in figure 4-2.

Chapter 4, Results and Discussion, is divided into four parts that details about the preparation and synthesis methodology, characterization and batch defluoridation studies of the materials synthesized. Part I, brief about the pure hydroxyapatite, whereas, Part II provides the information about utilization of marble waste powder for removal of fluoride from aqueous solution. Part III and Part IV details about the synthesis of marble apatite and marble-hydroxyapatite from marble waste powder using conventional and ultrasonication method and their applicability as an adsorbent for water defluoridation.

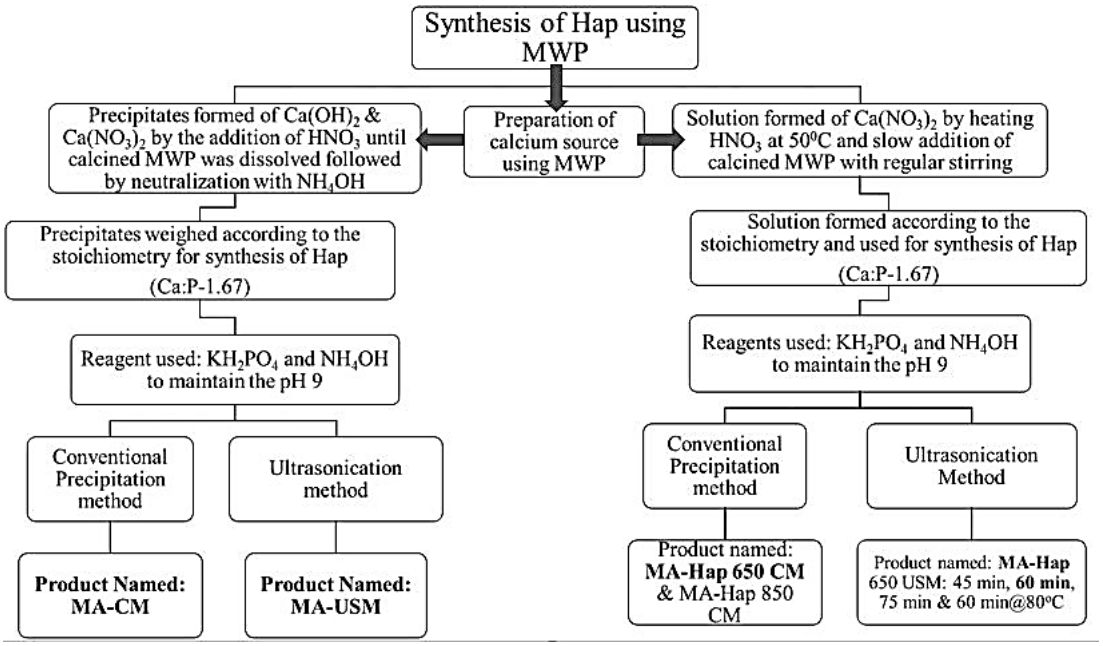

Figure 4-1. Methodology for the synthesis of Marble Apatite & Marble Hydroxyapatite

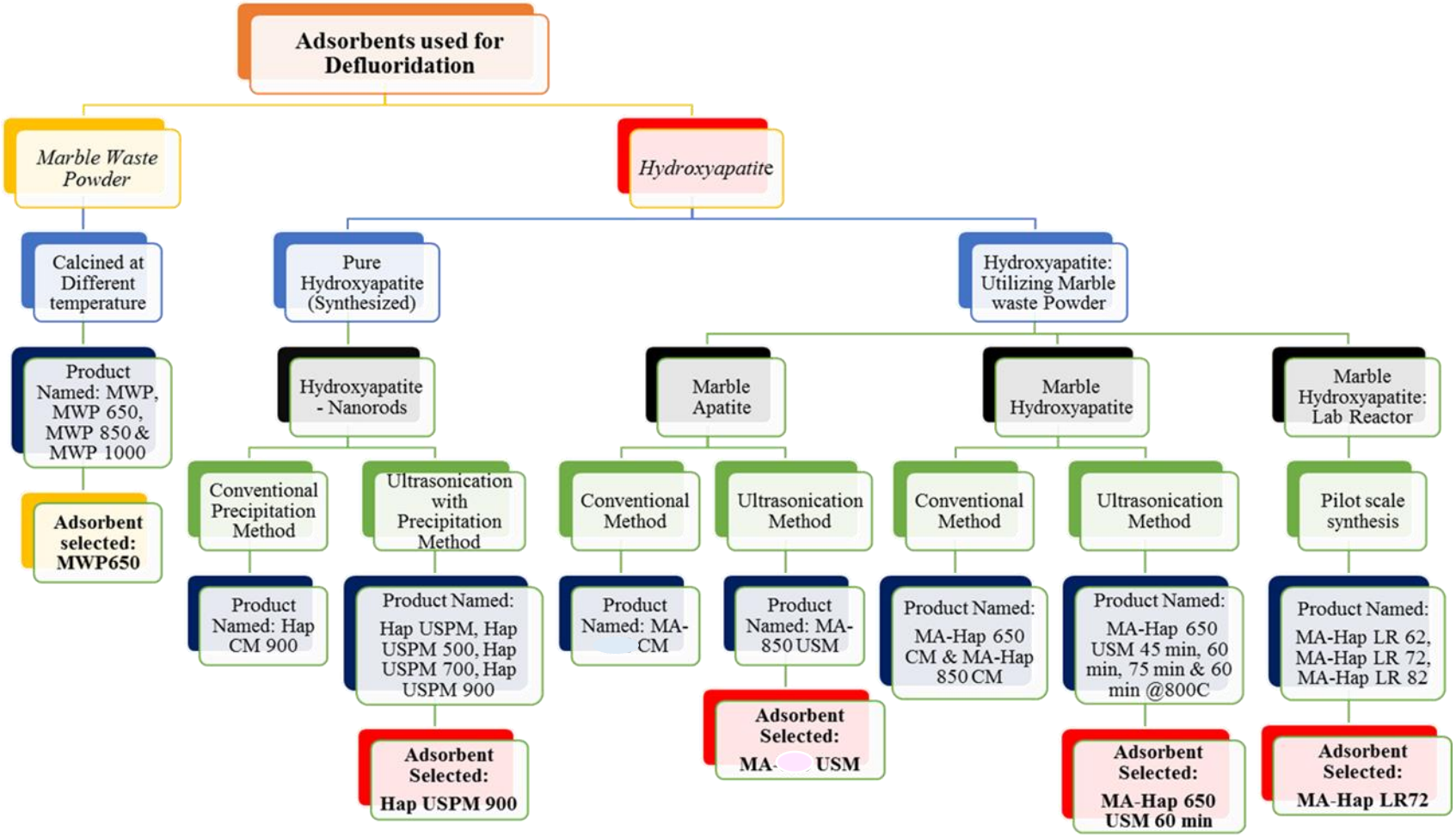

Figure 4-2. Adsorbents used for water defluoridation.

PART I.

PURE HYDROXYAPATITE (HAP) AS AN ADSORBENT

Part I deals with the synthesis of pure hydroxyapatite using conventional precipitation method and ultrasonication with precipitation method. The hydroxyapatite obtained was characterized and best suited material was used as an adsorbent for water defluoridation.

PART 1.
PURE HAP AS AN ADSORBENT

4.2. INTRODUCTION

This work reports the method to synthesize Hydroxyapatite (Hap) nanorods using both methods conventional and ultrasonication with precipitation for its application in water defluoridation. The materials synthesized were compared using different characterization techniques. The limitations of the experimental method for defluoridation were overcome by optimizing all the process parameters by adopting the statistical experimental design technique such as response surface methodology (RSM). RSM is a collection of mathematical and statistical techniques useful for modelling, developing and optimization of experimental data and can be used to evaluate the interaction of multiple variables (Behbahani et al., 2011). The study also presents combined effects of process parameters such as reaction time, pH and adsorbent dose on fluoride removal capacity of hydroxyapatite nanorods using the central composite design (CCD) method in response surface methodology. The mechanism of adsorption was studied through different isotherm models, and kinetic studies were also discussed to determine equilibrium time.

4.3. SYNTHESIS OF PURE HAP

Hydroxyapatite was synthesized using conventional precipitation method and ultrasonication with precipitation method which was later characterized using different analytical technique detailed in following sections.

4.3.1. MATERIALS FOR SYNTHESIS OF PURE HAP

Analytical grade (AR) chemicals, calcium nitrate ($Ca(NO_3)_2$, Lobachemie) and potassium phosphate (KH_2PO_4, Fisher), were weighted according to the required

stoichiometry and used for the synthesis of hydroxyapatite (molar ratio of Ca/P=1:67). The pH of the solution was maintained using ammonia solution (NH_4OH, LobaChemie).

4.3.2. SYNTHESIS OF HYDROXYAPATITE USING CONVENTIONAL METHOD (CM)

Solutions of 0.32 M calcium nitrate and 0.19 M potassium phosphate were prepared using double distilled water. In the conventional method solution of KH_2PO_4 was added drop wise to the solution of $(Ca(NO_3)_2$ with regular stirring using a magnetic stirrer (Model: 5MLH, Remi, India) at a speed of 600 rpm which was gradually increased to 1000 rpm during the process. The clear aqueous solutions turned creamish white initially but as the reaction proceeded, slow precipitation occurred, and got converted into white colored suspension. The process reaction was carried out in 4 h, and pH was maintained at 9 by addition of the NH_4OH solution, and temperature of the reaction mixture was maintained at 80 ± 5ºC. The resultant colloidal solution was further centrifuged at 2200 rpm for 10 min. The precipitate obtained after centrifugation was washed with deionized water, dried at 110ºC for 4 to 5 h in an oven and was ground to powdered form and sieved using 200-250 British Standard Sieves (BSS) for further studies. The Hap powder obtained was calcined at 900ºC in a muffle furnace (Optics Technology) and named as Hap-CM 900. The calcination temperature was increased slowly at the rate of 20ºC/min and Hap was calcined for 3 h.

4.3.3. ULTRASONICATION SET-UP

Ultrasonic experiments were performed in a stainless steel ultrasonic bath, (Labman scientific instruments, India) having internal dimensions of 235 x 135 x 150 mm as shown in figure 4-3. The bath had two transducers located at the bottom, arranged in a fixed position, and the bath was driven at 40 ± 3 kHz frequency at a power rating of 110 W. Glass beaker of 1000 mL capacity containing the sample was placed in the bath at 2 cm above the transducers.

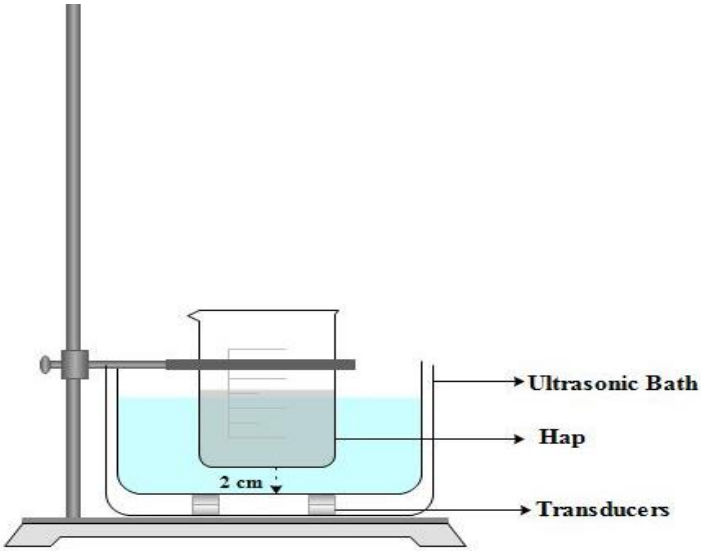

Figure 4-3 Schematic representation of ultrasonication setup.

4.3.4. SYNTHESIS OF HYDROXYAPATITE USING ULTRASONICATION WITH PRECIPITATION METHOD (USPM).

In the USPM method, sonication using ultrasound waves was carried out after the precipitation reaction to obtain hydroxyapatite nanorods as shown in figure 4-4. Potassium phosphate (0.19 M) solution was added dropwise to the solution of calcium nitrate (0.32 M) for 60 min with regular stirring at 600 rpm, and temperature was maintained at 80 ± 5ºC. The pH of the reaction was maintained at 9 using ammonia solution. The obtained solution was sonicated for 30 min in an ultrasonic bath (40 ± 3 kHz). The temperature of the bath was maintained at 50ºC with recirculation of cooling water. The resultant colloidal solution was further centrifuged at 2200 rpm for 10 min. The precipitate obtained was washed with deionized water, dried at 110ºC for 4 to 5 h in an oven and was ground to powdered form and sieved using 200-250 British Standard Sieves (BSS) for further studies. The Hap powder thus obtained was calcined at 500ºC, 700ºC and 900ºC in a muffle furnace (Optics Technology) and named as Hap 500, Hap 700 and Hap 900 respectively. The temperature was increased slowly during calcination at the rate of 20ºC/min and calcined for 3 h.

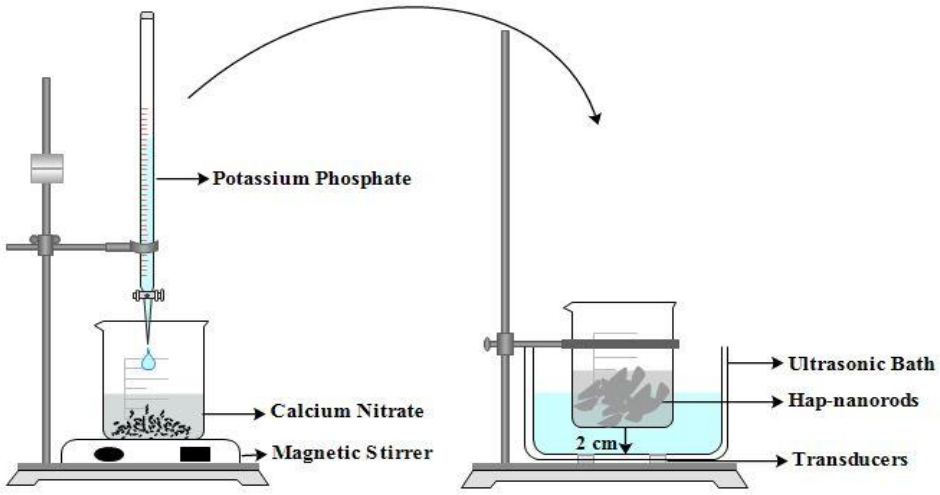

Figure 4-4 Schematic representation of synthesis of hap nanorods using USPM method.

4.3.5. Reaction Mechanism

The reaction mechanism for the formation of Hap from calcium nitrate ($Ca(NO_3)_2$ and potassium phosphate (KH_2PO_4) in water with ammonia solution (NH_4OH) added as a base is as follows:

$$10Ca(NO_3)_2 + 6KH_2PO_4 + 20NH_4OH \rightarrow Ca_{10}(PO_4)_6(OH)_2 + 6KOH + 20NH_4NO_3 + 12H_2O \quad (24)$$

4.3.6. Reaction time and % yield of pure Hap

The reaction time for the conventionally synthesized (CM) Hap nanorods was 240 min while reaction time for Hap nanorods synthesized using ultrasonication with precipitation (USPM) method was 90 min Table 4.1. For the reaction, percentage yield was estimated on the basis of theoretical and the actual weight of the product obtained after complete drying and considering the initial weight of the reagents. It was observed that yield of the reaction when Hap was synthesized using conventional (CM) method was 83.24% whereas when Hap was synthesized using ultrasonication with precipitation (USPM) method % yield was increased to 90.2%. The influence of ultrasonication was evident from the decrease in the processing time as well as an increase in percentage yield. Higher product yield and the reduced reaction time is attributed to ultrasonication

process which caused the enhanced mass transfer due to microjet streaming and interfacial turbulence due to cavity oscillation and collapse.

Table 4.1 Crystallite size and % yield of the Hap nanorods synthesized using conventional method and ultrasonication with precipitation method.

Method	Material	Process reaction Time	Crystallite Size d (nm)	Yield (%)
Conventional	Hap-(CM) 900	240 min	70.37	83.24%
Ultrasonication with precipitation	Hap-900	90 min	54.83	90.20%

4.4. CHARACTERIZATION OF SYNTHESIZED HYDROXYAPATITE

The synthesized hydroxyapatite nanorods were characterized for evaluation of functional group, bonding patterns, surface morphology, crystallographic and elementary analysis, particle size distribution, surface area, thermogravimetric analysis and differential thermal analysis, and the results obtained are detailed as follows:

4.4.1. FTIR OF PURE HAP

The FTIR spectra of synthesized Hap nanorods from USPM & CM methods and calcined at different temperatures are shown in figure 4-5. The peaks observed with FTIR spectra in the range of 3400 to 3500 cm^{-1} are due to the stretching vibrations of O-H bond. The peaks of P-O bond from 1000 to 1100 cm^{-1} with bands at 960 to 965 cm^{-1} and 565 to 601 cm^{-1} correspond to stretching and bending modes respectively (Ramanan and Venkatesh, 2004). Ammonium solution was used to maintain an alkaline condition during synthesis of Hap, and it was removed from the suspension solution by repeated washing with deionized water; still there remains a possibility of the presence of ammonium ion. Hence the broad peak at 1400 cm^{-1} is the characteristic peak of the NH^{4-} group (Dollase, 1986) which disappeared with a gradual increase in temperature in peak above. The effect of calcination on Hap nanorods synthesized using USPM method was also further studied using XRD and SEM analysis. The presence of PO_4^{3-} group and O-H group in FTIR spectra confirmed that Hap was formed using both methods.

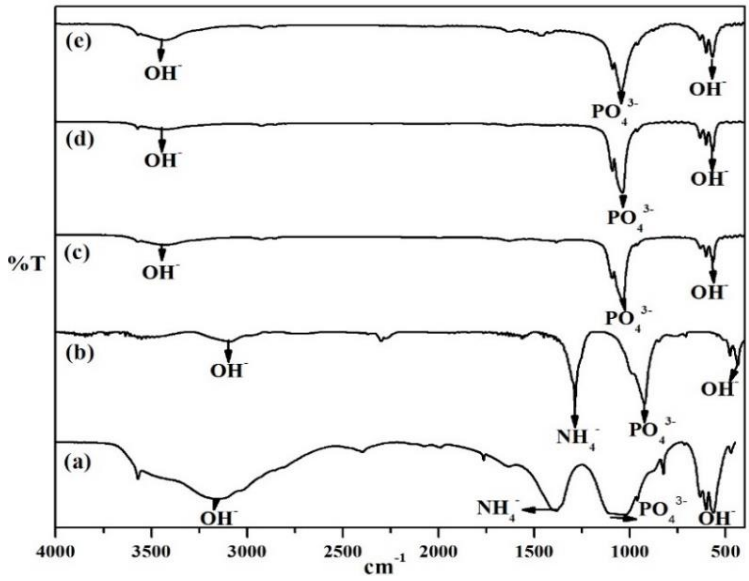

Figure 4-5. FTIR spectra of the Hap nanorods synthesized using (a) CM method, Hap-(CM) 900 and USPM method (b) Hap (USPM), (c) Hap 500, (d) Hap 700 and (e) Hap 900.

4.4.2. XRD OF PURE HAP

It was observed that XRD phase identification of synthesized Hap through both CM and USPM process exactly matched with the XRD patterns of Hap on comparison of the diffraction patterns with JCPDS card no. 01-074-0565. Figure 4-6a depicts that hydroxyapatite synthesized and calcined at 900ºC through conventional method (CM) contain the intermediate phases and peaks were broad indicating presence of small nano crystals in the samples. With Hap synthesized using ultrasonication with precipitation method, intensity of the peaks increased with increase in temperature from ambient to 900ºC and width became narrower. A complete phase transformation with a well-defined crystalline structure occurred at 900ºC as no peaks other than corresponding to Hap was observed indicating formation of pure Hap in the USPM process (figure 4-6e). It can be attributed to the influence of ultrasonication in the process, resulting in intensification of the chemical reaction due to improved mass transfer at the molecular level.

The mean crystallite sizes of Hap synthesized using different methods were also estimated using Debye-Scherer formula as shown in eq. (3) and there values are shown in Table 4.2.

Table 4.2 Mean crystallite size of Hap synthesized using conventional method (CM) and ultrasonication with precipitation method (USPM).

Adsorbent	Wavelength (Å)	Peak Width (Degree)	Peak Position (Degree)	Crystallite Size (nm)
Hap-(CM) 900	1.54056	0.122º	31.7344º	70.37
Hap (USPM)	1.54056	0.2362º	31.5716º	36.51
Hap 500	1.54056	0.1574º	31.9038º	54.85
Hap 700	1.54056	0.1478º	31.9221º	58.42
Hap 900	1.54056	0.1574º	31.7836º	54.83

The impact of ultrasonication was evident not only in the increased yields (83.24% for CM and 90.2% for USPM) but also in the reduction of average crystallite size (Table 4.2). Hap synthesized from CM process had an average crystallite size of 70.37 nm, whereas Hap synthesized using USPM process and calcined at higher temperature had an average crystallite size of 55.6 nm. It was observed that the crystallinity had improved due to calcination at a higher temperature, and uniformly sized crystals were obtained as well as ultrasonication prevents agglomeration of particles during the synthesis and maintained effective size distribution of Hap particles.

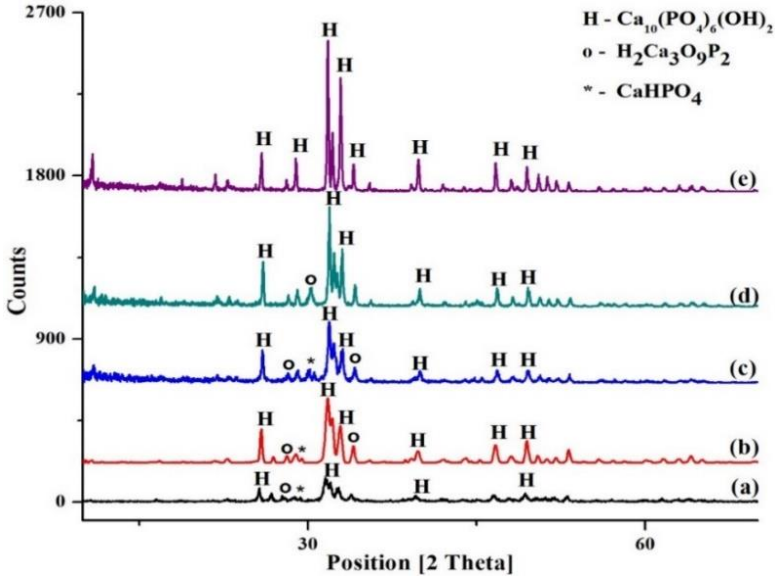

Figure 4-6. XRD spectra of Hap Nanorods synthesized using (a) CM Method Hap-(CM) 900 and USPM method (b) Hap-(USPM), (c) Hap 500, (d) Hap 700 and (e) Hap 900.

4.4.3. SEM ANALYSIS OF PURE HAP

The morphology, surface characteristics as well as crystallographic information of the synthesized Hap was analyzed from the results of SEM. The SEM micrographs of synthesized Hap nanorods with both CM and USPM methods were compared with the same magnification of 100000 X and 200000 X and are shown in figure 4-7 & figure 4-8 respectively. The Hap synthesized using CM methods were in the form of countless agglomerated bundles of nano-rod like structure (figure 4-7a & figure 4-8a) whereas, Hap synthesized using USPM process existed as numerous arrangements of uniform bundles of nano-rod like structure (figure 4-7b & figure 4-8b). Agglomeration of particles was lost in case of USPM synthesized Hap because of the localized high energy dissipation and generation of shock waves by ultrasound. It was observed that structure of CM synthesized Hap consisted of aggregation of smaller particles with larger particles but this was not found for USPM synthesized Hap. From the low and high-magnification SEM images, we can observe that evenly dispersed and uniform nanorods were prepared by using ultrasonication with precipitation approach.

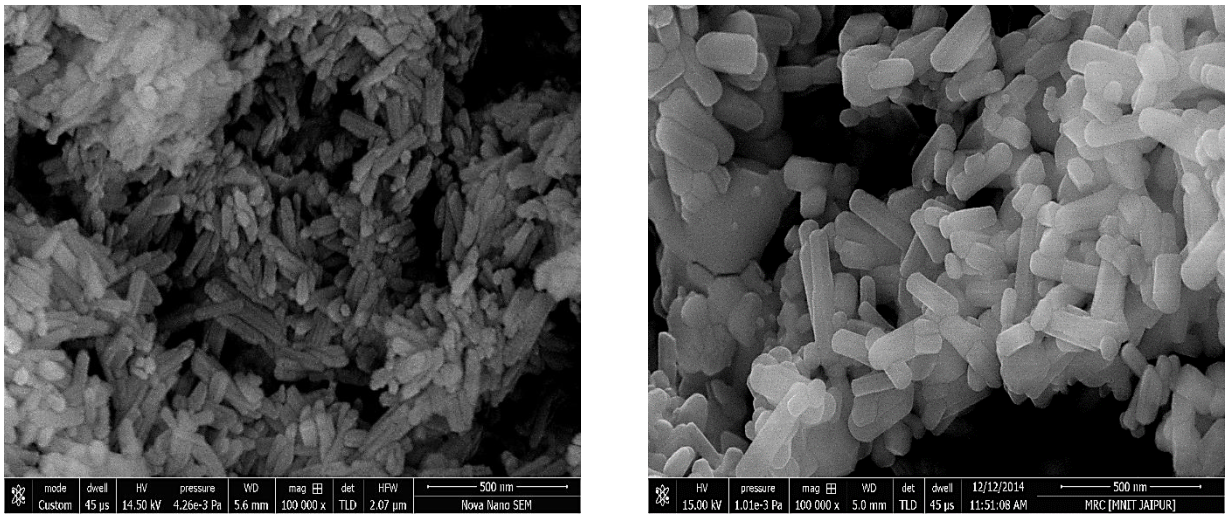

(a) **(b)**

Figure 4-7 SEM micrographs of synthesized Hap nanorods at 100000 X (a) Conventional method (CM) (b) Ultra-sonication with precipitation method (USPM).

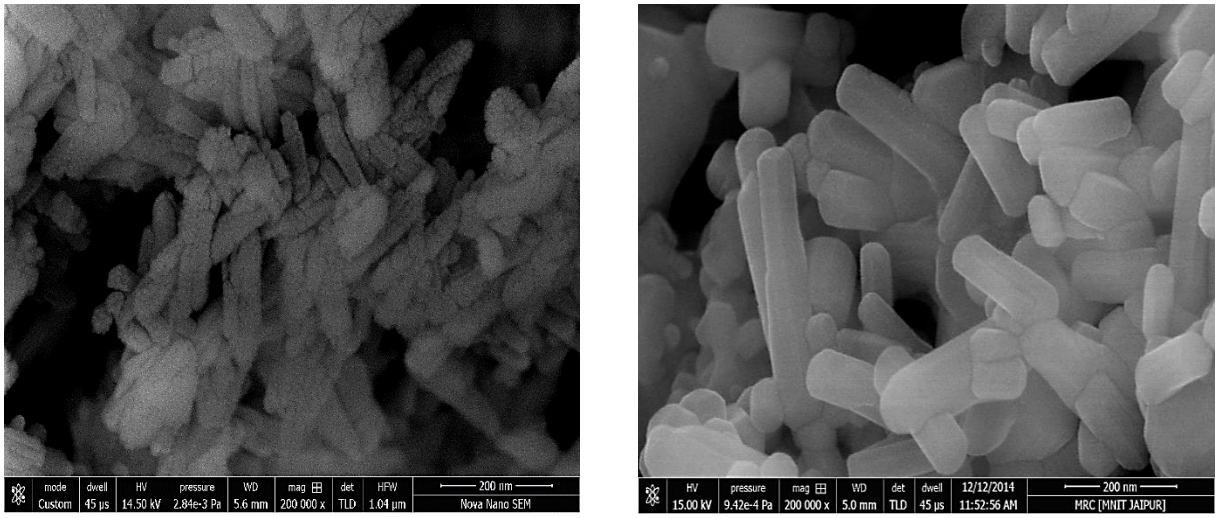

(a) **(b)**

Figure 4-8 SEM micrographs of synthesized Hap nanorods at 200000 X (a) Conventional method (CM) (b) Ultra-sonication with precipitation method (USPM).

Prominent elongated shapes of the nanorods appeared with a gradual increase in temperature from ambient, 500ºC, 700ºC and 900ºC (figure 4-9) which indicated that ultrasonication and higher temperature was helpful to improve the crystallinity of the Hap nanorods synthesized.

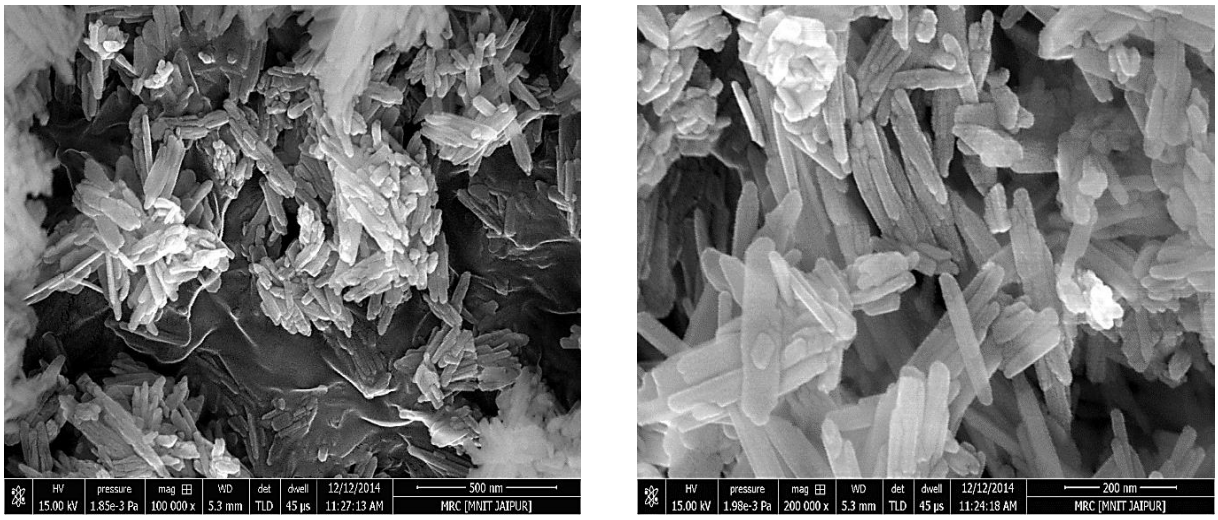

(a) **(b)**

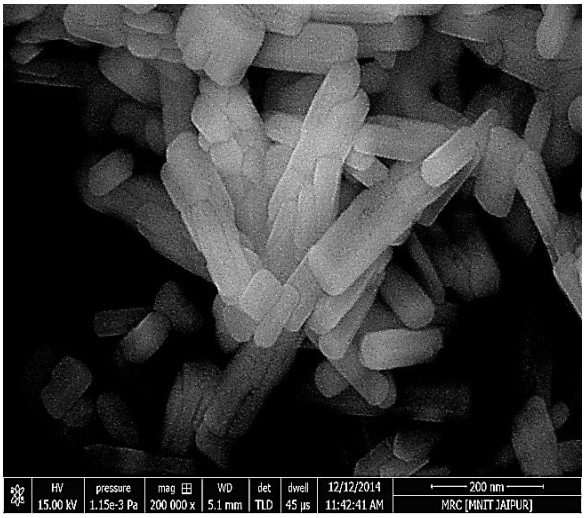

(c)

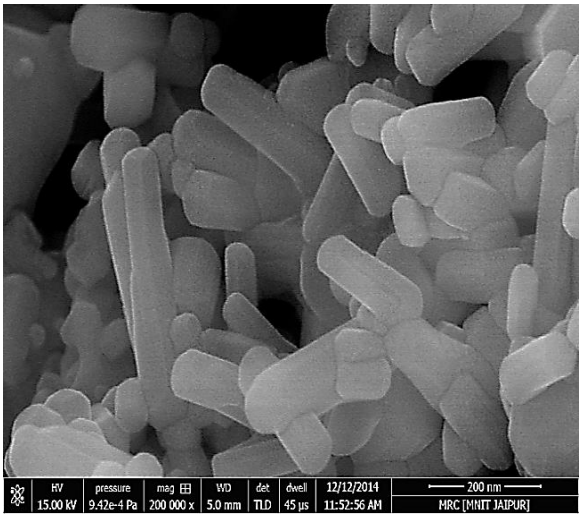

(d)

Figure 4-9 SEM micrographs; (a) Hap-USPM, (b) Hap 500, (c) Hap 700, (d) Hap 900.

4.4.4. TEM Analysis of Pure Hap

The TEM micrograph of Hap 900 synthesized using USPM process (figure 4-10 a) reveal that well-crystallized, elongated nanorods like particles of Hydroxyapatite with an average size range of 166 nm in length and 17.5 nm in width were formed. Whereas, dark field spectra confirmed that the material synthesized was crystalline in nature. The Hap crystals were able to form ordered structures with similar architecture to that of enamel prisms present in the natural form. EDS shows the elemental composition of compounds present in the material. Calcium and phosphorous were primary reagents used for the synthesis of hydroxyapatite, and their presence can be clearly seen with the help of EDS in figure 4-10b. The peak of copper was obtained as the grid used for mounting the sample was made of copper. Other than this no impurities were observed in the spectrum of EDS; hence, pure Hap nanorods was obtained.

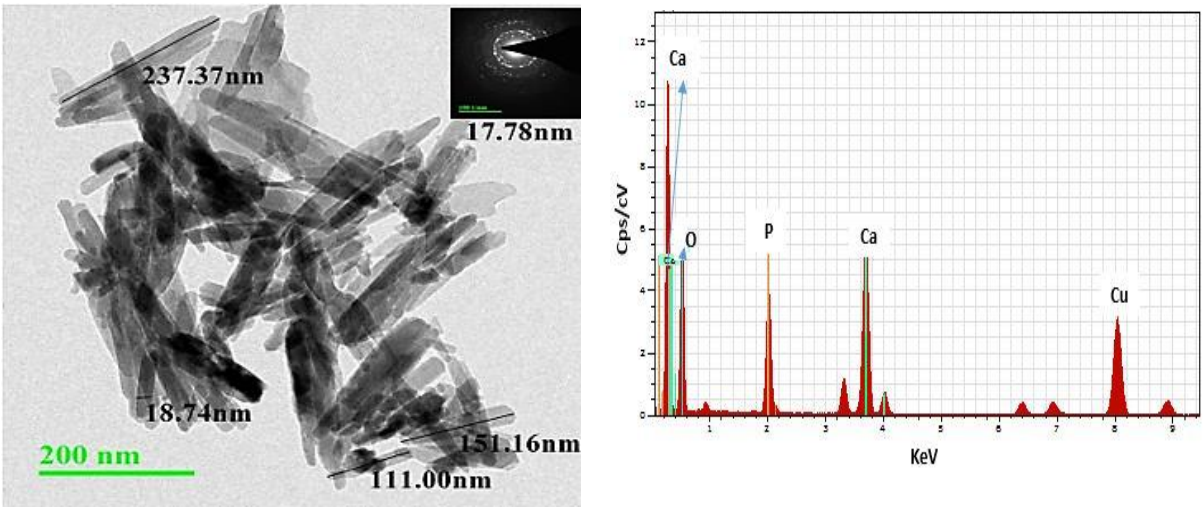

(a) **(b)**

Figure 4-10 (a) TEM micrograph and (b) EDS spectra of Hap 900.

4.4.5. TGA-DTA

Thermogravimetric analysis (TGA) and Differential thermal analysis (DTA) for Hydroxyapatite nanorods synthesized using USPM process were done, from room temperature to 900ºC as illustrated in figure 4-11. The TGA curves demonstrates three main weight losses in the temperature range from 35ºC to 59.5ºC, 97.25ºC to 260.57ºC and 440ºC to 500.5ºC which corresponds to endothermic peak at 38.3ºC (weight loss 2%), 230ºC (weight loss 7.29%) and 442.61ºC (weight loss 1.7%) respectively in the DTA curve. The first stage of decomposition is due to evaporation of physically adsorbed water, and solvent molecules present in the Hap samples, removal of ammonia from the gel formed and degradation of intermediate species during the synthesis process respectively. A peak at around 450ºC is due to crystallization of $Ca_{10}(PO_4)_6(OH)_2$ (Dollase, 1986). The results of thermal decomposition are useful for optimization of conditions to obtain monophasic biomaterial.

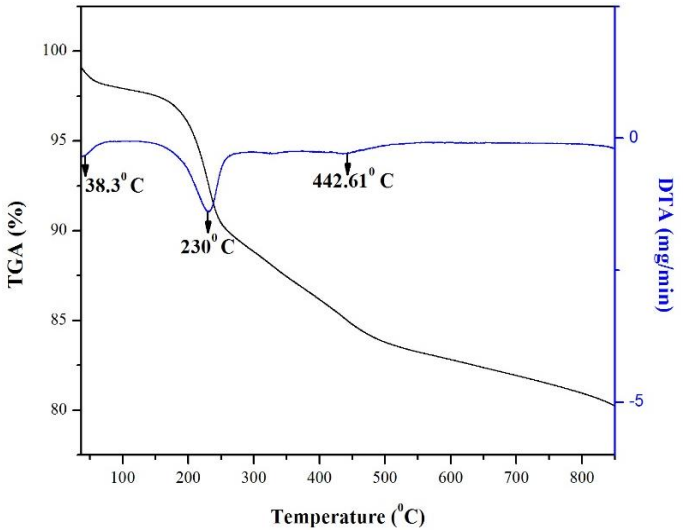

Figure 4-11 DTA-TGA plot of synthesized Hap using USPM process.

4.5. BATCH DEFLUORIDATION STUDIES USING PURE HAP

The batch defluoridation experiments were conducted for optimization of process parameters according to the Central Composite Design matrix developed in Table 4.3.

Table 4.3 Central composite design matrix for three variables with observed and predicted values.

	Factor 1	Factor 2	Factor 3	Response	
Run	**A:pH**	**B:Dose (g/L)**	**C:Time (h)**	**Experimental removal efficiency (%)**	**Predicted removal efficiency (%)**
1	7	7	3	92.86	93.64
2	7	7	2	91.72	93.19
3	3	2	5	70.6	70.74
4	7	10	3	98.21	100
5	7	7	3	92.79	93.64
6	7	7	4	99.33	98.99
7	7	7	3	92.08	93.64
8	7	7	3	92.9	93.64
9	7	5	3	84.91	82.77
10	11	12	1	71	70.78
11	5	7	3	90.72	94.2
12	9	7	3	78	75.65
13	11	2	5	14.4	17.05
14	7	7	3	92.8	93.64
15	3	12	5	98.79	98.07
16	11	2	1	0	0.64

17	11	12	5	85.5	83.73
18	3	12	1	94	91.27
19	3	2	1	58.8	60.49
20	7	7	3	92.82	93.64

4.5.1. SELECTION OF ADSORBENT FOR BATCH DEFLUORIDATION STUDIES

The selection of most suitable Hap adsorbent was an important aspect of this study for further defluoridation experiments to be conducted. The XRD analysis confirmed that among the material synthesized using different approaches, USPM synthesized Hap 900 figure 4-6 had no undesirable components and pure form of Hap was obtained. Moreover prominent elongated shapes of the Hap nanorods appeared in USPM synthesized Hap 900 as observed in SEM micrographs. The average particle size distribution of USPM synthesized Hap 900 was 471.1 nm when dispersed in ethanol as dispersion medium. The results of Brunauer-Emmett-Teller (BET) surface area analysis, volume and pore size of USPM synthesized Hap 900 was 21.2521 m^2/g, 0.090234 cm^3/g and 169.835 Å respectively. Preliminary batch experiments were conducted using five adsorbents namely Hap-CM 900, Hap-USPM, Hap 500, Hap 700, and Hap 900 with initial fluoride concentrations of 10 mg/L, adsorbent dosage of 7 g/L and 3 h of contact time. The results as depicted in

figure 4-12 indicate that the maximum fluoride removal obtained in terms of percentage and uptake capacity was 92.86% and 1.32 mg/g respectively for the adsorbent Hap 900, which was further used for defluoridation experiments.

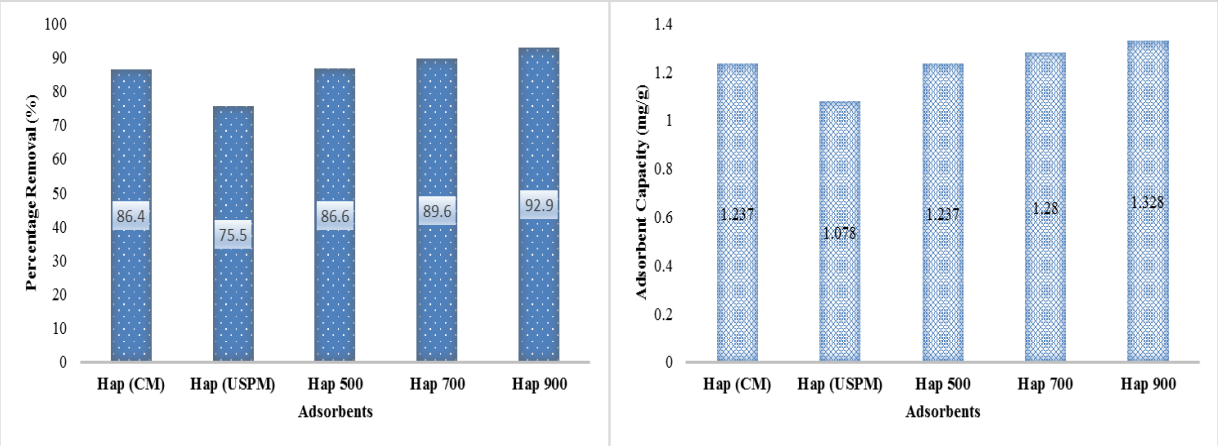

(a) **(b)**

Figure 4-12. Removal of fluoride using Hap synthesized using CM and USPM process (f- concentration: 10 mg/L, dose: 7 g/L, contact time: 3 h, pH: 7±0.1, temperature: 30±0.5ºC)

4.5.2. FLUORIDE ADSORPTION MODEL FITTING USING CCD

The design matrix developed in Table 4.3 present the response regarding fluoride removal efficiency with Hap 900 from an aqueous medium using Central Composite Design. A quadratic regression model equation was developed relating the fluoride removal efficiency with the three chosen process variables pH, dose, and time is as given below:

$$\begin{aligned} Removal\ efficiency \\ &= +92.53 - 18.55 \times A + 25.17 \times B + 5.80 \times C + 9.84 \times AB \\ &+ 1.54 \times AC - 0.86 \times BC - 29.44 \times A^2 - 16.72 \times B^2 + 15.22 \\ &\times C^2 \end{aligned} \quad (25)$$

where A,B and C are the coded variables for pH, dose (g/L), and time (h) respectively.

A positive sign for the terms in equation (25) indicate synergistic effect, whereas a negative sign indicates opposite effect. The model suggests that all three parameters particularly adsorbent dose had a significant impact on fluoride removal. The experimental and predicted removal efficiency of fluoride using Hap 900 is shown in figure 4-13. It is evident from the figure that the developed model is adequate because the residuals are closer to the diagonal line.

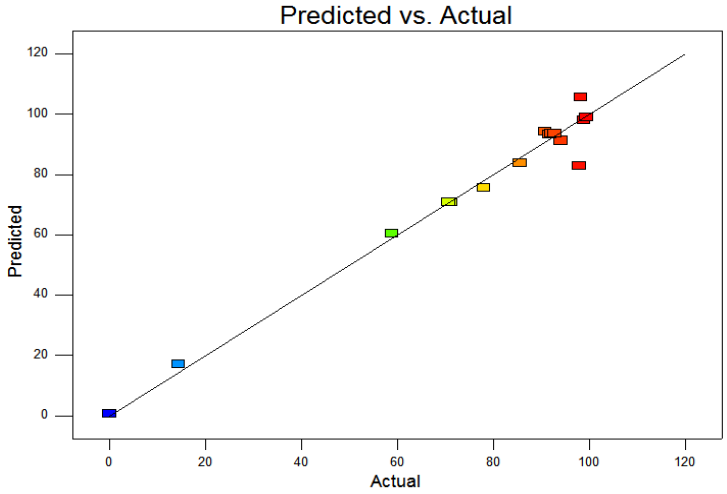

Figure 4-13. Actual and predicted % removal of fluoride using Hap 900.

An ANOVA study for the second-order polynomial was conducted for fluoride removal estimations for Hap 900 as given in Table 4.4. The capability of the model was confirmed and verified by estimation of Fischer variation (F-value), probability values

(p-value) and the correlation coefficient (R^2). The high F-value (220.78) for the quadratic model inferred that the model is significant while the p-value of <0.0001 indicated the high statistical significance of the model. The value of R^2 was observed to be 0.9950 which suggest that 99.50% of the variations in the response could be described by the model.

Table 4.4 ANOVA for response surface quadratic model for fluoride removal

Source	Sum of Squares	df	Mean Square	F-Value	p-value	
Model	13784.21	9	1531.58	220.78	< 0.0001	Significant
A-pH	2923.94	1	2923.94	421.49	< 0.0001	Significant
B-Dose	5331.17	1	5331.17	768.50	< 0.0001	Significant
C-Time	285.88	1	285.88	41.21	< 0.0001	Significant
AB	774.41	1	774.41	111.63	< 0.0001	Significant
AC	18.94	1	18.94	2.73	0.1295	
BC	5.97	1	5.97	0.86	0.3755	
A^2	167.01	1	167.01	24.08	0.0006	
B^2	59.83	1	59.83	8.62	0.0149	
C^2	44.66	1	44.66	6.44	0.0295	

R^2= 0.9950; Adjusted R^2 = 0.9471; Predicted R^2 = 0.9830.

4.5.1. VERIFICATION OF MODEL USING THE DESIRABILITY RAMP

The parameters pH, adsorbent dose and contact time, were set within the studied range, and the response (fluoride removal efficiency) was set for maximum desirability figure 4-14. Finally, for their validation, duplicate confirmatory experiments were conducted using the optimized parameters (pH 7, adsorbent dose 7 g/L, contact time 3 h). The efficiency of fluoride removal was predicted at 93.64% from the model while experimentally it was 92.86%. The obtained value of desirability function was 0.985 which shows that the predicted value may represent the experimental model.

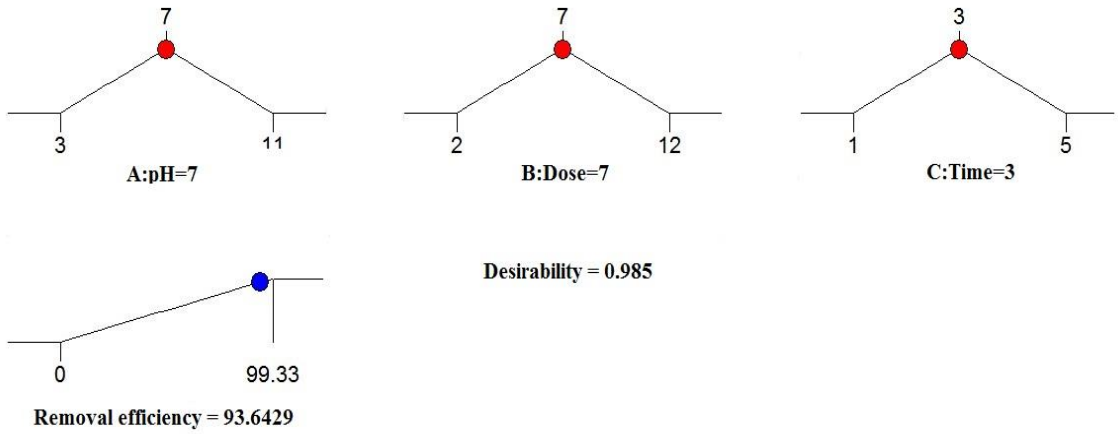

Figure 4-14. Desirability ramp for numerical optimization of three selected parameters.

On the basis of the quadratic model, three-dimensional response surface plots and their corresponding contour plots were plotted for studying the effects of the independent variables and their interactions on fluoride removal efficiency.

4.5.1.1. Effect of Hap 900 dose and pH of solution

The combined effect of adsorbent dose and pH of the solution on fluoride removal is shown in figure 4-15a. It was observed that the percentage removal of fluoride increased with increase in Hap 900 dose due to the availability of a higher number of adsorption sites. At pH of 7, the removal efficiency was maximum while the removal efficiency decreased at alkaline pH (>8) due to competition between F^- and OH^- ions for the active sites. This can also be explained regarding surface zero charge (pH_{PZC}) value for Hap 900, which was found to be 7.5. When pH of the solution is less than the pH_{PZC}, the surface of adsorbent is positively charged and therefore will attract the negatively charged fluoride ions. The contour plot in figure 4-15b showed that fluoride removal efficiency of 93.64% was attained at pH of 7.0 and Hap 900 dose of 7 g/L.

4.5.1.2. Effect of contact time and pH of solution

The effect of contact time and pH of the solution on fluoride removal using Hap 900 can be predicted from the plot as shown in figure 4-15c. It was observed that fluoride removal efficiency increased simultaneously with an increase in contact time, whereas, decreased at high pH values. As depicted in from the contour plots (figure 4-15d), the maximum fluoride removal efficiency (93.64%) was obtained at a contact

time of 3 h and pH value of 7. Decrease in the removal of fluoride with increasing pH value from 6 to 11 was also reported by Gao et al., (2009).

4.5.1.3. Effect of Hap 900 dose and contact time

The three-dimensional response surface plots (figure 4-15e) illustrate the combined effects of adsorbent dose with contact time. With the increase in the Hap 900 dose and contact time, the fluoride removal efficiency was observed to increase. This was due to the increase in active sites ratio to fluoride ions present in the solution. Maximum fluoride removal of 93.64% was seen at an adsorbent dose of 7 g/L and 3 h of contact time from the contour plot in figure 4-15f. Similar results were observed by Mondal and George, 2015; Mehta et al., 2016.

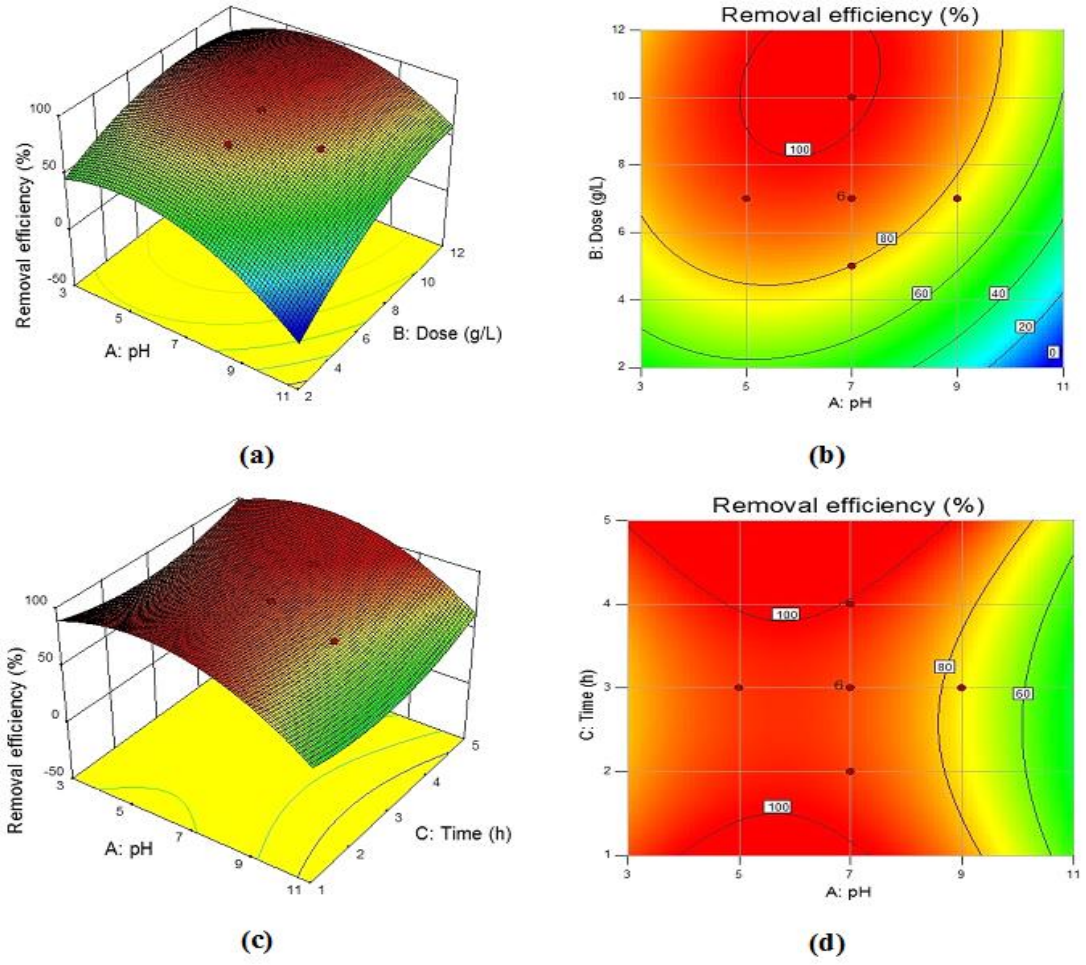

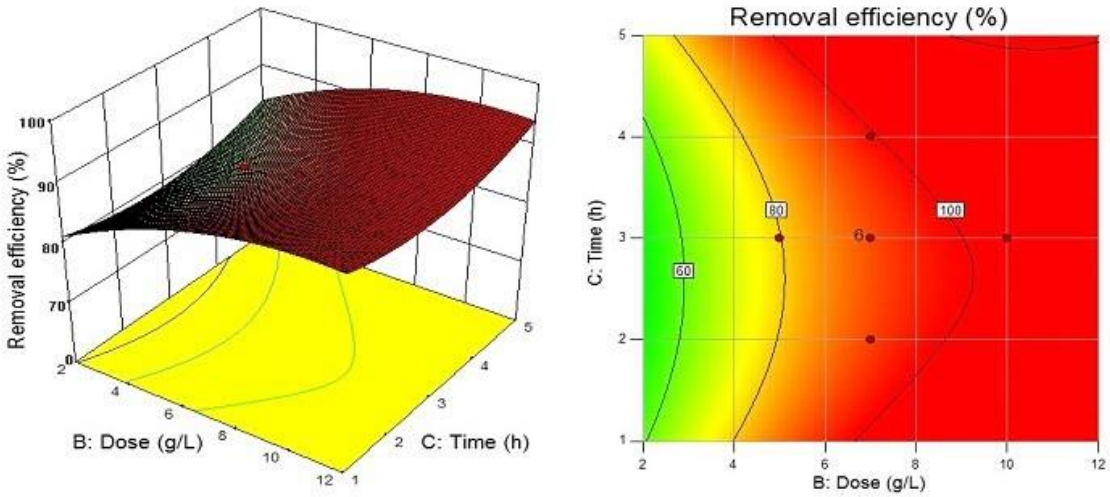

(e) **(f)**

Figure 4-15. Response surface plots and contour plots showing the effect of (a, b) Dose and pH (c, d) Contact time and pH and (e, f) Dose and contact time.

4.5.2. ADSORPTION ISOTHERMS

The equilibrium established between the fluoride adsorbed on the surface of pure Hap and the concentration of fluoride ions in solution was studied by Langmuir, Freundlich and Tempkin isotherms model. The various isotherms parameters were also studied which is shown in Table 4.5.

The best fit model was selected for representing fluoride adsorption based on χ^2 value and R^2 value. Freundlich isotherm model fitted best with correlation coefficient (R^2) close to unity and least χ^2 value observed at 0.139 as given in Table 4.5 . This represents multi-layered adsorption and heterogeneity of Hap 900 surface with an adsorption capacity of 1.49 mg/g. The value of heterogeneity factor '1/n' at 0.53 lies between 0.1 and 1 which depict a favorable adsorption process.

Table 4.5 Adsorption isotherm for defluoridation using Hydroxyapatite

Isotherms	Parameters	Values
Langmuir	q_{exp}	1.33
	q_{max} (mg/g)	4.01
	k(L g^{-1})	0.819
	R^2	0.9577
	χ^2	0.63

Freundlich	1/n	0.5357
	n	1.86
	k_F (mg/g)	1.49
	R^2	0.9849
	χ^2	0.139
Temkin	A_T (L/mg)	5.236
	B_T	1.627
	R^2	0.8407
	χ^2	0.48

4.5.3. ADSORPTION KINETICS

The adsorption kinetics of fluoride on Hap 900 adsorbent was studied with respect to time, and it was observed that during the first 2 h, adsorption occurred very rapidly, after that the rate slowed down and became constant. Adsorption efficiency was obtained at 92.86% in 3 h which was considered as the equilibrium time, beyond which there was no change in the percentage removal of fluoride ions. For comprehending the kinetics of fluoride adsorption process in this study, two mass transfer models (pseudo-first and pseudo-second order) and one intraparticle diffusion model were used.

The correlation coefficient (R^2), rate constants (K_1, K_2, K_i), uptake capacity (q_e), and SSE values on fitting the pseudo first-order, pseudo-second order and intra-particle diffusion model are shown in Table 4.6. The R^2 value for the pseudo-second order was highest (0.9981). Also, the calculated equilibrium capacity from the pseudo-second order is closer to experimental uptake capacity of 1.33 mg/g. Therefore, it can be concluded that adsorption of fluoride on hydroxyapatite nanorods follows pseudo-second order adsorption kinetics.

Table 4.6 Kinetic parameters for Hap 900 adsorbent

q_{exp} **mg/g**	**Pseudo-first-order Kinetics**				**Pseudo-second-order-Kinetics**				**Intraparticle diffusion**		
	K_1	q_e(mg/g)	R^2	SSE	K_2	q_e(mg/g)	R^2	SSE	R^2	K_i	SSE
1.33	1.882	2.26	0.9794	0.94	9.25	0.677	0.9981	0.56	0.9641	29.97	1.31

4.6. WATER QUALITY PARAMETERS (PURE HAP)

The quality of the treated water after using Hap 900 as the defluoridation agent (dose: 7g/L, contact time: 3 h, F^- Conc: 10 mg/L, temp. 303 ± 2 K) determines the suitability of the adsorbent for practical applications. The value of various parameters studied before and after adsorption along with the permissible limit determined by WHO and BIS are given in Table 4.7. Alkalinity and hardness of water in the treated sample was 114 and 236 mg/L respectively. pH of water after adsorption was 7.23 and the TDS was found to be 371 mg/L. Calcium content leached into treated water was 22.24 mg/L while the phosphorous concentration was below detection limit. Results showed that the synthesized adsorbent, Hap 900 can be used for the treatment of fluoride in drinking water as treated water is fit for consumption and all the parameters are within permissible limit.

Table 4.7 Water quality parameters of treated water using Pure Hap

	Before adsorption	**After adsorption**	**Permissible limit (BIS)**
pH	7.47	7.23	6.5-8.5
TDS (ppm)	33	371	500
Alkalinity ($CaCO_3$ eqv; mg/L)	0	114	600
Total Hardness ($CaCO_3$ eqv; mg/L)	0	236	500
Calcium (mg/L)	0	22.24	200
Phosphate	0	Below detection limit	Not mentioned
Fluoride (mg/L)	10	0.714	1.5
Turbidity (NTU)	<0.3	<0.3	10

4.7. ENERGY EFFICACY

The comparison of the energy required for two synthesis methods i.e. conventional precipitation (CM) and ultrasonication with precipitation (USPM) method for obtaining Hap nanorods has been estimated and the sample calculations are reported in Appendix A. The energy utilized for the synthesis of Hap nanorods is the total energy supplied (kJ) per unit weight of the material processed/ obtained (g). The reaction time to synthesize Hap nanorods using CM method was 4 h and for USPM method was 90 min.

Total energy required per unit weight of the material obtained to synthesize Hap nanorods using CM method and USPM method are 15.896 kJ/g and 4.03 kJ/g

respectively. Thus, among the two methods, USPM synthesis method proved to be an energy efficient method which saved 75% more energy than that utilized by conventional synthesis method as well as with added advantage of reduction in the process reaction time for synthesis of Hap.

4.8. NOVELTY OF THE WORK

The following aspects of our work states its novelty:

- Fluoride removal using Hydroxyapatite (Hap) nanorods synthesized via ultrasonication with precipitation and conventional method has been reported in this chapter. This research work is focused on eliminating the problem of fluorosis by utilizing it for defluoridation of drinking water.
- The route used for the synthesis of Hap nanorods and its application for defluoridation has not been attempted anywhere nor have we found any literature report.
- This chapter includes optimization of process parameters for the synthesis of Hap nanorods.
- The comparison of material synthesized using ultrasonication with precipitation method and conventional method have also been discussed using different characterization techniques.
- Economic feasibility of the suggested technique ensures a promising adsorbent for future.

4.9. SUMMARY OF THE CHAPTER (PURE HAP)

- Hap nanorods were successfully synthesized by both conventional precipitation (CM) and ultrasonication with precipitation (USPM) method and followed by calcination at various temperatures from ambient to 900ºC for application in defluoridation of drinking water. The XRD studies revealed that as calcination temperature was increased from ambient to 900ºC, intermediate phases disappeared and pure Hap nanorods of a crystalline structure was obtained when synthesized using USPM

process. SEM and TEM studies confirmed the formation of nanorod-like crystalline structures in the micrographs. The yield of the Hap nanorods improved from 83.24% to 90.2% when ultrasonication was incorporated in the Hap synthesis as in the USPM process.

- RSM method using Central Composite Design was used for optimization of selected process variables viz; pH, adsorbent dose and contact time for estimation of fluoride removal efficiency. A quadratic model representing defluoridation efficiency was developed as a function of these three variables, and statistical analysis (ANOVA) was carried out to evaluate the effects of individual variables as well as their combined effects on the removal process. Numerical optimization helped in determining the optimum process variables estimated at contact time of 3 h, adsorbent dose of 7 g/L and pH of 7 for treating an initial fluoride concentration of 10 mg/L. The percentage fluoride removal was numerically predicted to be at 93.64%, while the experimentally observed value was at 92.86%, which were in good agreement with $R^2 = 0.9950$.

- Study of adsorption isotherms indicated that fluoride adsorption on Hap 900 followed Freundlich isotherm behavior with multi-layered adsorption with an estimated adsorption capacity of 1.49 mg/g. The process followed a pseudo-second order reaction and 3 h of equilibrium time was required to achieve 93% fluoride removal. Analysis of water quality parameters clearly indicate that the treated water is fit for drinking purposes as per World Health Organization (WHO) and Indian drinking water standards.

This study presents a simple, effective technique to synthesize Hap nanorods using ultrasonication with precipitation method for its utilization in defluoridation of drinking water. Production of crystalline hydroxyapatite and its study may also open new dimensions to a better understanding of biomaterials and their efficacy for biomedical applications in bone and dental implants due to its structural similarity to natural bone and teeth material.

PART II.

MARBLE WASTE POWDER (MWP) AS AN ADSORBENT

This chapter details about effect of calcination temperature on marble waste powder which was evaluated via characterization tools and batch studies on water defluoridation using marble waste powder as an adsorbent.

PART II.
MWP AS AN ADSORBENT

4.10. INTRODUCTION

Marble is crystalline metamorphic limestone, which majorly consists of calcium compounds like calcite ($CaCO_3$), dolomite ($CaMg(CO_3)_2$) and silicon oxides (Segadães et al., 2005). Considering, the significant presence of calcium and magnesium compounds in marble waste powder (MWP), it may be used as a defluoridation agent. As per the literature survey, MWP has never been used for fluoride removal studies making it a novel adsorbent. Further, the importance of utilizing marble waste lies in the economic advantage for developing defluoridation cheaper defluoridation systems besides bringing environmental benefit through reducing the quantity of waste accumulated.

4.11. SAMPLE PREPARATION

Marble waste powder (MWP) was obtained from marble processing industry located in the region of Kishangarh, Rajasthan, India. Chemicals used in the present study were of analytical grade (AR) purchased from E-Merck India Ltd., India. Multiple washing of MWP using double distilled water removed the unwanted dust and solid particles present in the powder. Samples were air-dried, crushed using mortar-pestle after which it was sieved to obtain particle sizes corresponding to 200-250 British Standard Sieve (BSS). The oversize particles were repeatedly crushed and sieved so that most of the sample can be utilized. The marble waste powder thus obtained was calcined at 650ºC, 850ºC and 1000ºC in a muffle furnace for 2 h and named as MWP650, MWP850, and MWP1000 respectively. A fluoride stock solution of 1000 mg/L was prepared using sodium fluoride that was appropriately diluted for the batch experiments.

4.12. CHARACTERIZATION OF MARBLE WASTE POWDER

The marble waste powder calcined at different temperature were characterized using various analytical techniques such as FTIR, XRD, SEM, EDS, TEM, TGA/DTA, particle size distribution and BET surface area analysis.

4.12.1. FTIR

The spectra of marble waste powder before and after calcination at different temperatures are shown in figure 4-16. Intense vibrations existed in the band starting from 713 cm^{-1} with an intense peak at 875 cm^{-1} that indicated the presence of MgO bonds (Pei et al., 2010). Peaks obtained beyond 875-2896 cm^{-1} (1452 cm^{-1}, 1798 cm^{-1}, 1819 cm^{-1}, 2517 cm^{-1}, 2526 cm^{-1}, 2896 cm^{-1}) is due to the presence of carbonate (Reig et al., 2002; Vagenas et al., 2003)which was present in all the four forms of MWP. During calcination above 650ºC the $CaCO_3$ turned into CaO and CO_2 due to decomposition, and hence some peaks were missing in the spectra of MWP850 and MWP1000. Bands at 1437 cm^{-1} and 1412 cm^{-1} for MWP850 and MWP1000 respectively indicated stretching vibration of the stable polymorph of carbonate group (Vagenas, 2003). The broad band spectra corresponding to 1412 cm^{-1} is of carbonate group that changed to an intense peak with increase in the calcination temperature from 30 to 1000ºC. Further some small peaks obtained at 3400 cm^{-1} and 3600 cm^{-1} were due to OH stretching and H-OH bending (Sujana and Mohanty, 2011). The effect of calcination was further studied using XRD and TGA-DTA analysis.

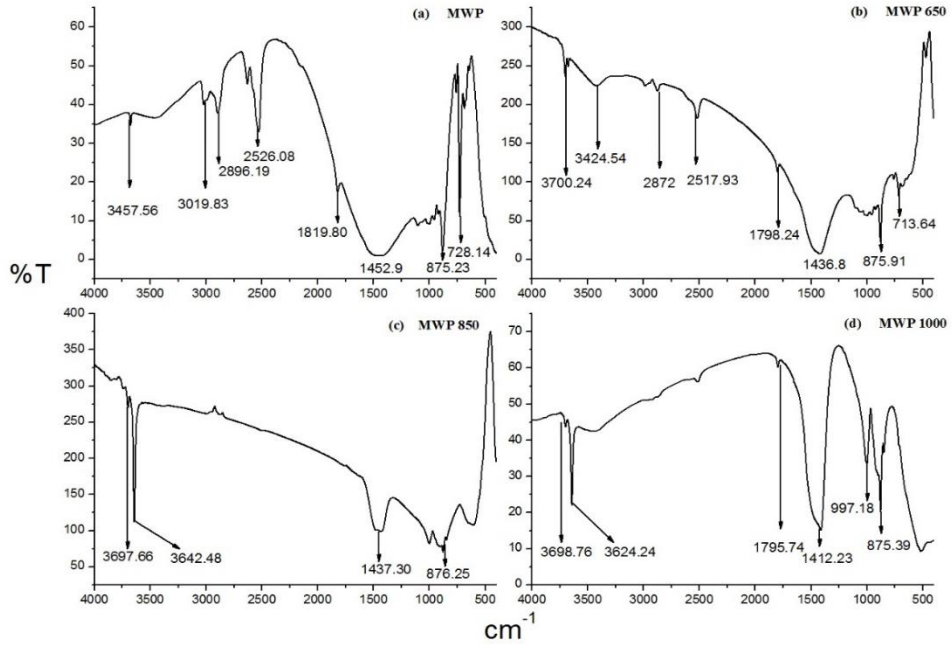

Figure 4-16. FTIR spectra; (a) MWP, (b) MWP650, (c) MWP850 and (d) MWP1000.

4.12.2. XRD

XRD studies were carried out for gaining insight of the composition of marble waste powder. XRD patterns in figure 4-17 showed sharp peaks indicating crystalline nature of the material. The maximum peaks in MWP were of $CaMg(CO_3)_2$ with a small amount of silicon oxide (SiO) (Ramasamy et al., 2009). At 650ºC, silicon oxide in the presence of oxygen got converted to silicon dioxide (SiO_2) while $CaMg(CO_3)_2$ got dissociated thermally and formed calcium carbonate and magnesium oxide. It is well known that all the carbonates undergo thermal decomposition resulting in metal oxides and carbon dioxide. Therefore, when the temperature was further increased to 850ºC, calcium carbonate decomposed to calcium oxide, releasing CO_2 and calcium silicate was formed simultaneously. At 1000ºC, it was observed that the major phase was of magnesium oxide and some smaller peaks of calcium oxide as well as calcium silicate were spotted. The peaks for calcium magnesium carbonate, calcium carbonate, calcium oxide, magnesium oxide, calcium silicate and silicon oxide were matched with JCPDS card no. -074-1687, -083-0577, -070-5490, -079-0612 and -071-6243 respectively.

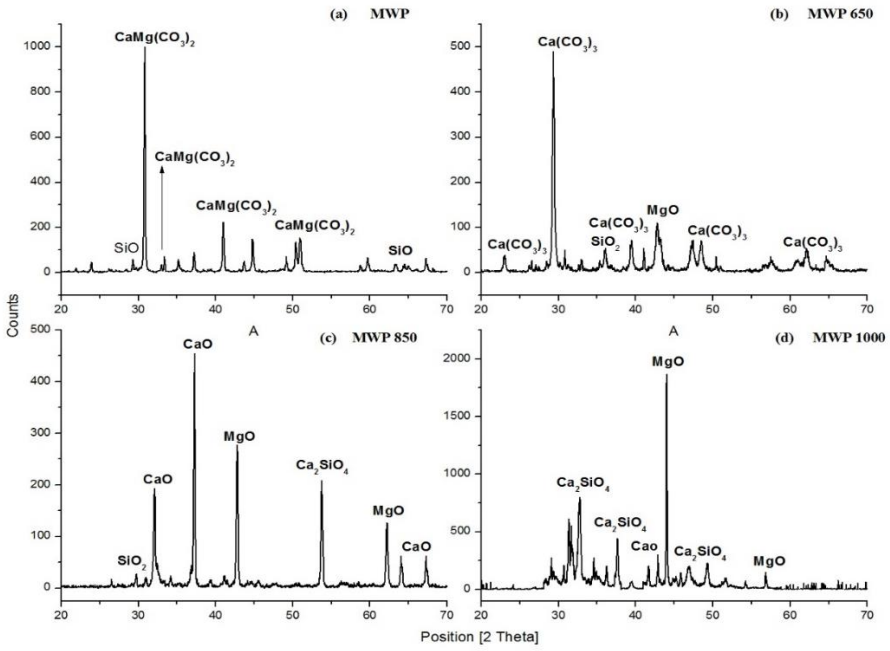

Figure 4-17. XRD Patterns; (a) MWP, (b) MWP650, (c) MWP850 AND (D) MWP1000.

4.12.3. SEM/EDS

A scanning electron microscope (SEM) was used to examine the surface morphology of marble waste powder. SEM micrographs of the calcined and uncalcined samples are shown in figure 4-18, which illustrates that the particles are in the form of separated grains. It was perceived that during calcination process as the temperature was increased from 650ºC to 850ºC, sphere like structures were obtained. This was due to the decomposition of carbonates and formation of new phases (CaO and MgO). Similar results were reported by (Julphunthong, 2015), while working with marble dust waste. The morphology of MWP1000 is almost similar to MWP850.

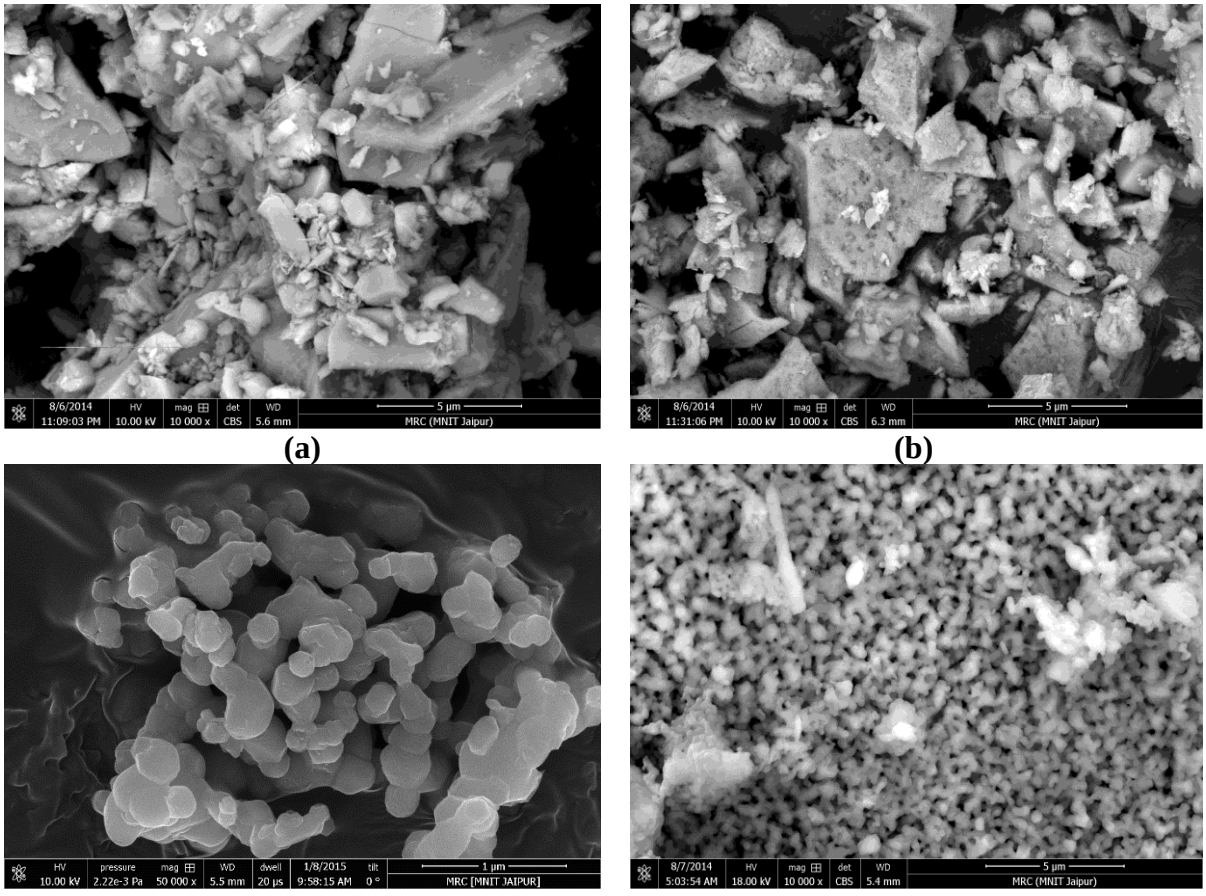

Figure 4-18 SEM micrographs; (a) MWP, (b) MWP650, (c) MWP850 and (d) MWP1000.

The presence of the compositional elements of marble waste powder such as Ca, Mg, Si, and O were detected by EDS (figure 4-19).

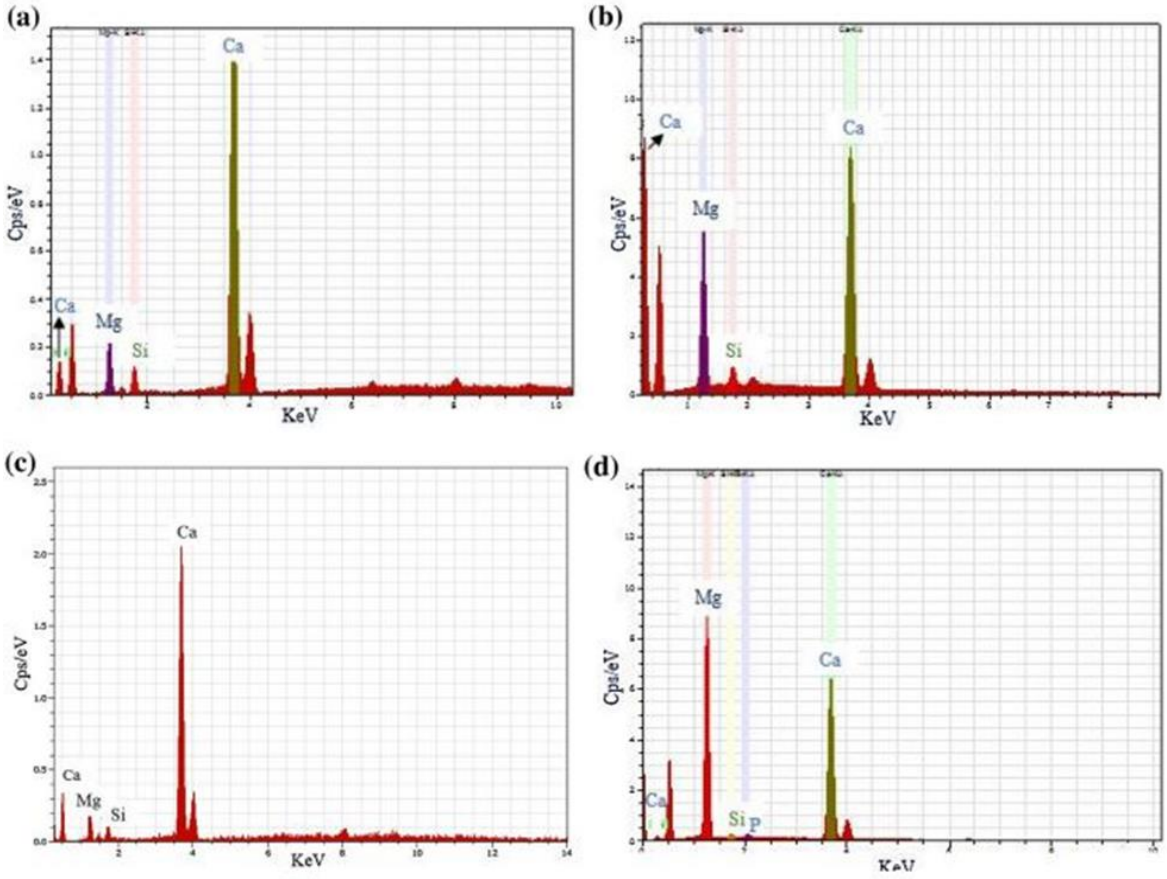

Figure 4-19 EDS patterns; (a) MWP, (b) MWP650, (c) MWP850 and (d) MWP1000.

4.12.4. TEM

TEM images obtained clearly illustrates that uncalcined marble waste powder comprised of coarse and irregular particles. Sphere like particles was observed when MWP was calcined at 850ºC. As the temperature was increased, the structure was changed due to phase transformation that can be observed from figure 4-20.

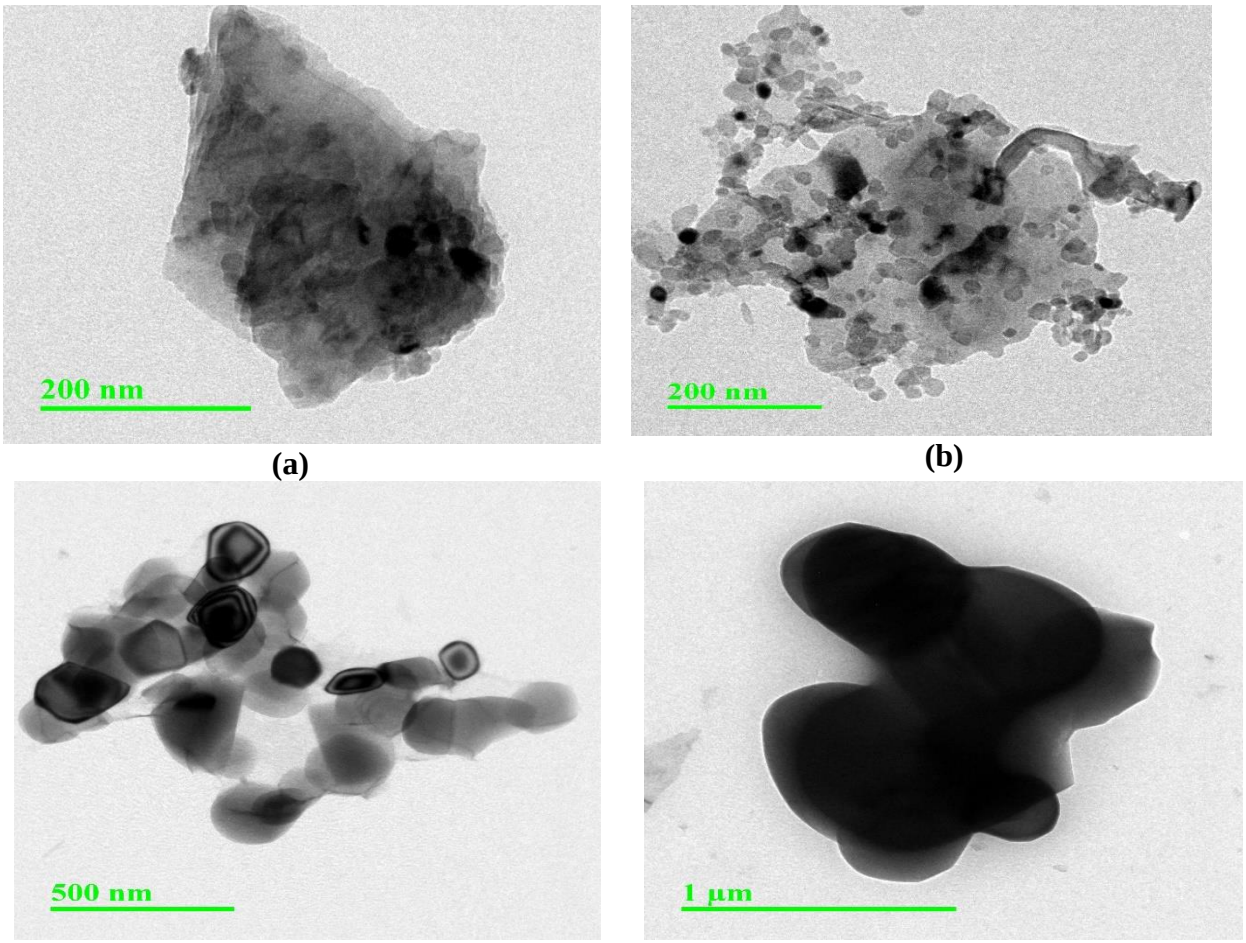

Figure 4-20 TEM micrograph; (a) MWP, (b) MWP650, (c) MWP850 and (d) MWP1000.

4.12.5. TG-DTA

Thermogravimetric analysis (TGA) and Differential thermal analysis (DTA) for studying thermal decomposition of marble waste powder was done from room temperature to 900ºC as shown in figure 4-21. It demonstrates two peaks from 350ºC to 400ºC and 700ºC to 850ºC which corresponds to endothermic peaks at 366.04ºC (weight loss 1.8%) and 838.58ºC (weight loss 28.39%) respectively in the DTA curve. The endothermic peaks are observed due to the evolution of CO_2 with the formation of MgO and CaO respectively. The weight loss observed in marble waste powder is accredited to the decomposition of carbonates in two stages as shown in the equation (Shahraki et al., 2009).

$$CaMg(CO_3)_2 \rightarrow CaCO_3 + MgO + CO_2 \qquad Stage\ 1$$

$$CaCO_3 \rightarrow CaO + CO_2 \qquad Stage\ 2$$

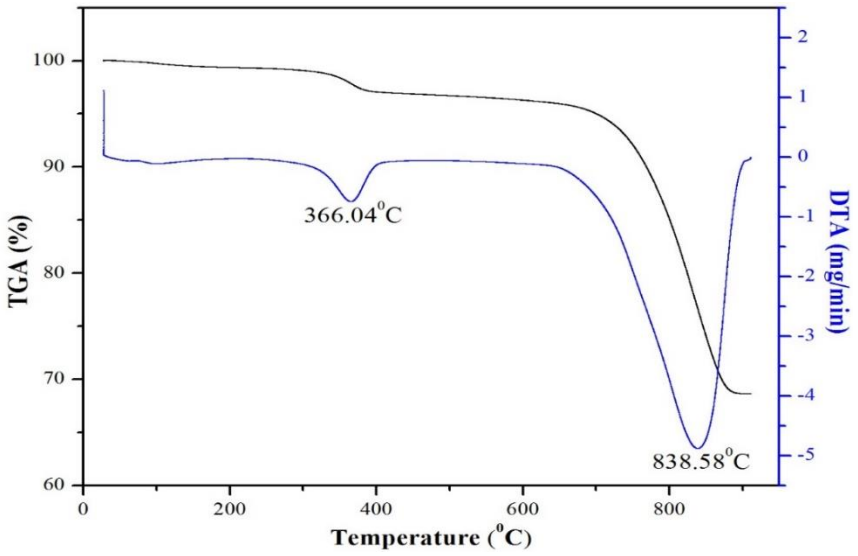

Figure 4-21. DTA-TGA plot of marble waste powder.

4.12.6. PARTICLE SIZE AND SURFACE AREA ANALYSIS

The average particle size distribution of marble waste powder was 572.2 nm. The surface area of uncalcined marble waste powder (MWP) was found to be 4.91 m^2/g. As the marble waste powder was calcined at 650ºC the surface area increased to 7.18 m^2/g. Decomposition of MWP calcined at 650ºC led to changes in the chemical composition of the surface which resulted in the formation of $CaCO_3$ and MgO that caused an increase in specific surface area. The increase in the surface area will facilitate enhanced adsorption of the fluoride ions onto the calcined marble waste powder (MWP650). Similar results were reported by Walker et al. while studying dye adsorption on dolomitic sorbents (Walker et al., 2003). Insignificant difference between the surface areas of MWP850 and MWP1000 was observed viz. 4.4 m^2/g and 5.08 m^2/g.

4.13. BATCH DEFLUORIDATION STUDIES USING MWP

4.13.1. SELECTION OF ADSORBENT FOR BATCH STUDIES

The choice of adsorbent is an important factor in the adsorption process. The XRD analysis confirmed that peaks of $CaCO_3$ were obtained at MWP650. It was reported

that calcium in the form of calcium carbonate (CaCO3) is highly activated when calcined in the range of 600ºC-650ºC (Rao, 1996). Moreover, the surface area of MWP650 (7.18 m2/g) was higher than the other samples due to which higher removal of fluoride from aqueous solution was observed. Thus, from the detailed characterization studies and evaluation of defluoridation capacity of adsorbents as shown in figure 4-22, MWP650 was selected for further studies. This was confirmed after batch experiments were conducted with the four adsorbents. The highest capacity for defluoridation using MWP calcined at 650ºC was due to the formation of calcium carbonate and magnesium oxide, during calcination.

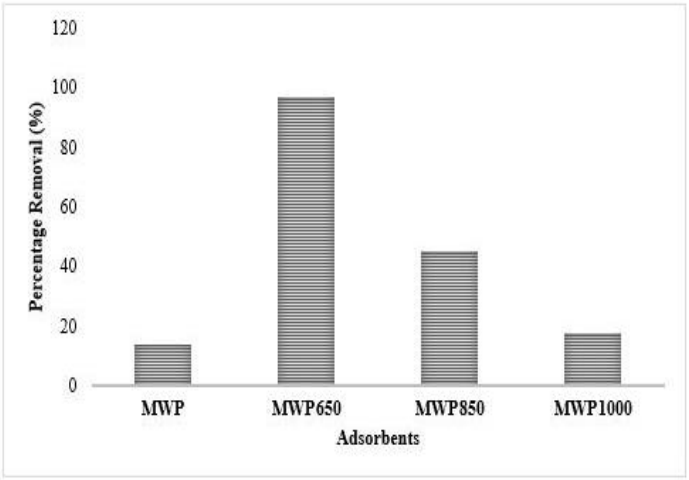

Figure 4-22 Fluoride removal by marble waste powder (F^- concentration: 10 mg/L, dose: 8 g/L, contact time: 3 h, pH: 7±0.1, temperature: 30± 0.5ºC).

4.13.2. EFFECT OF ADSORBENT DOSE

Experiments were carried out with MWP650 in the concentration of 3–15 g/L to fix the optimum dosage of adsorbent that will be required to bring fluoride concentration under the permissible limit (<1.0 mg/L). The effect of adsorbent dose on fluoride removal capacity using marble waste powder is shown in figure 4-23. It was observed from the experiments that percentage removal was increased from 74 to 98% with the increase in adsorbent dose from 3 to 15 g/L. The mechanism behind this observation is that as the dosage increased, the number of the active site for the adsorption of fluoride ions present in the solution also increased and hence removal capacity increases. With the dosage of 8 g/L, the residual fluoride was 0.342 mg/L, thus attaining

the permissible limit as per WHO (1.5 g/L) and BIS (1.0 g/L). Hence, the dosage of 8 g/L was deliberated as the optimum dose for all the batch experiments.

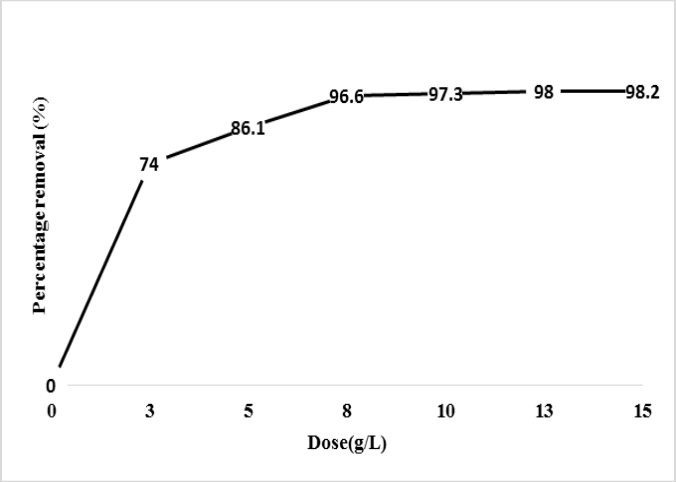

Figure 4-23 Effect of adsorbent dose on fluoride removal (%), (F^- concentration: 10 mg/L, contact time 3 h, dose: 3 to 15 g/L, pH 7±0.1, temperature: 30 ± 0.5ºC).

4.13.3. EFFECT OF CONTACT TIME

The effect of contact time on defluoridation efficiency is shown in figure 4-24. It was observed that fluoride removal progressively increased as the contact time increased. Equilibrium was attained at 3 h with a percentage removal of 96.6%. After 3 h, no significant fluoride removal was observed and hence, it was considered as the optimum time for defluoridation studies. As the contact time increased, the mass transfer rate between the adsorbent and aqueous medium decreased and the adsorption rate eventually lowered.

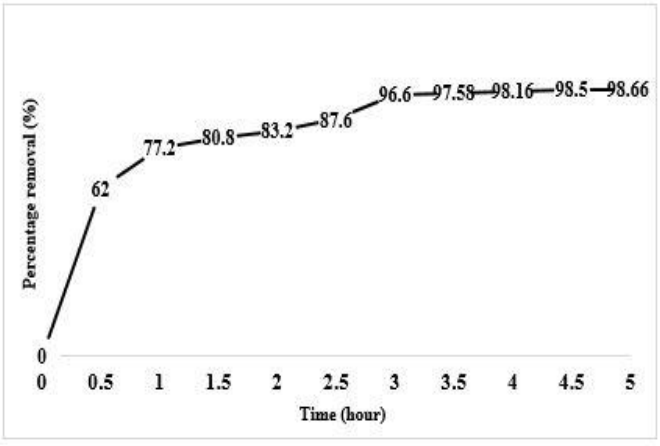

Figure 4-24. Effect of contact time on fluoride removal (F^- concentration: 10 mg/L, contact time 0.5 to 5 h, dose: 8 g/L, pH 7±0.1, temperature: 30 ± 0.5ºC).

4.13.4. EFFECT OF INITIAL FLUORIDE CONCENTRATION

Different fluoride concentrations (0-45 mg/L) were used to study the effect of initial fluoride concentration on marble waste powder by keeping other parameters such as dosage (8 g/L) and time (3 h) constant. It was found from figure 4-25 that with the increase in fluoride concentration, the adsorption capacity also increased rapidly, because initially higher concentration of fluoride ions were available for adsorption, and hence the driving force was high. The saturation reached when there were no active sites left on the surface of MWP650. Similar results were noted by (Mondal and George, 2015a) and (Thakre et al., 2010).

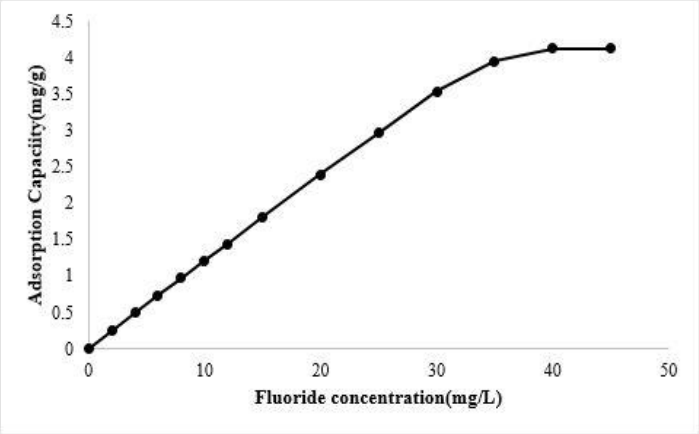

Figure 4-25 Effect of initial fluoride concentration on adsorption capacity (mg/g) (F^- concentration: 0 to 45 mg/L, contact time: 3 h, dose: 8 g/L, pH: 7±0.1, temperature: 30 ± 0.5ºC)

4.13.5. EFFECT OF pH

The pH of the water depends on various geological factors and it is one of the important parameters to understand the efficiency of removal of fluoride ions in aqueous solution. The different pH range can influence the defluoridation capacity of adsorbent. Hence, to understand the effect of pH, experiments were carried out in the pH range of 3-10 as shown in figure 4-26. It was found that at pH 3, fluoride removal was slightly less due to the competition to acquire active site between the fluoride ions which were already present in the solution and weakly ionized hydrofluoric (HF) acid formed at lower pH. However, maximum removal (97.69%) was observed at pH 7. Further increase in pH did not pose any effect on percentage removal of fluoride ions. The surface zero charge

(pH_{PZC}) of MWP650 was found to be 10.5. pH_{PZC} of an adsorbent defines the pH at which net surface charge is neutral. Therefore, when pH <pH_{PZC} (10.5) MWP650 is positively charged and will attract the negative fluoride ions. This surface property of MWP650 contributes to the effective removal of anionic fluoride species. The pH of the water treated with MWP650 was found to be alkaline (~ 9.0).

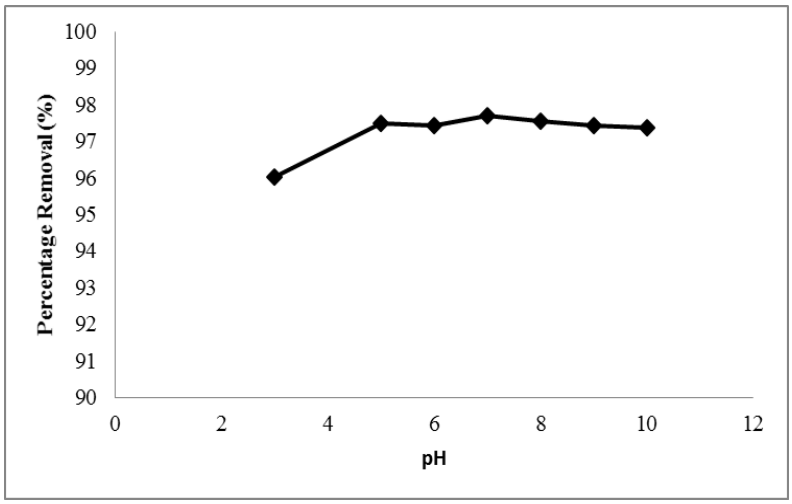

Figure 4-26. Effect of pH on fluoride removal (%), (F^- concentration: 10 mg/L, contact time: 3 h, dose: 8 g/L, pH 7±0.1 to 10±0.1, temperature: 30 ± 0.5ºC).

4.13.6. EFFECT OF CO-EXISTING IONS

Groundwater being the major drinking water source contains several other anions that may compete with fluoride ion for adsorption sites. Therefore, the defluoridation capacity of marble waste powder in the presence of competing ions like chloride, nitrate, sulfate and bicarbonate was experimentally verified. Studies were done by varying the concentration of co-existing ions from 100 to 300 mg/L and fluoride concentration was fixed at 10 mg/L. It is evident from figure 4-27 that the removal capacity slightly decreased from 1.207 mg/L to 1.194 mg/L in the presence of bicarbonate ions with the concentration of 200-300 mg/L. It is noteworthy that there was no effect on the removal capacity in the presence of other ions. It may be inferred that MWP650 emerged as a selective adsorbent for fluoride and interference from other anions did not affect the adsorption capacity extensively. The selective behavior of fluoride by any adsorbent is dependent on size, charge, polarizability and electronegativity difference.

Some other adsorbents such as manganese oxide coated alumina and lanthanum oxide also showed similar results in the presence of interfering anions (Maliyekkal et al., 2006).

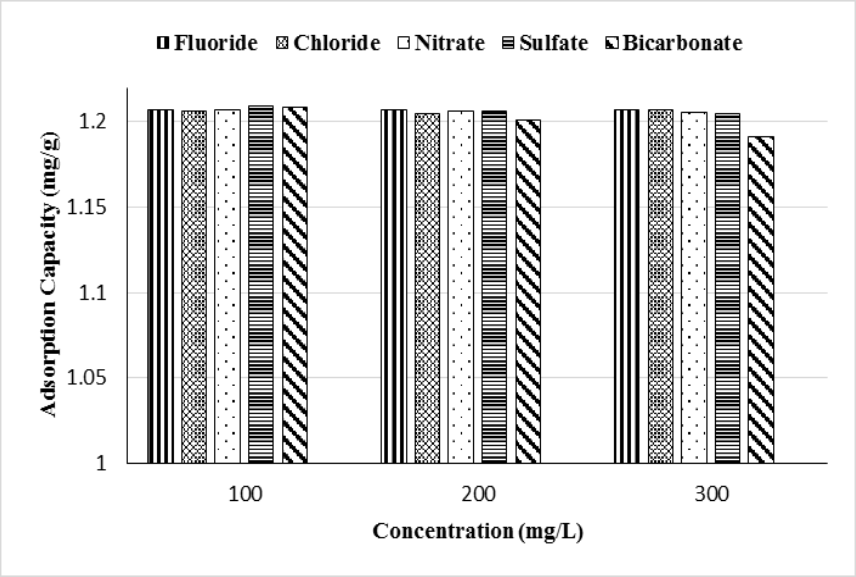

Figure 4-27. Effect of co-existing ions on adsorption capacity (mg/g) (F^- concentration: 10 mg/L, contact time: 3 h, dose: 8 g/L, temperature: 30 ± 0.5ºC)

4.13.7. ADSORPTION ISOTHERMS

Adsorption isotherms were studied to describe the specific relationship of adsorbed fluoride on the surface of marble waste powder and the equilibrium concentration of fluoride in the medium. Experimental data were analyzed using four isotherms viz. Langmuir, Freundlich, Temkin, Dubinin–Raduschkevich.

A smaller value of chi-square depicts a better fit of adsorption isotherm. The value of the separation factor, r is 0.0325 ($r < 1$) which indicated the feasibility of adsorption. It is evident from Table 4.8 that Freundlich isotherm displayed a better fit with smaller χ^2 value and R^2 value close to unity. This represents the multilayered adsorption and heterogeneity of MWP 650 surface. Also the value of heterogeneity factor '1/n' lies between 0.1 and 1 showing favorable adsorption process.

Table 4.8 Adsorption isotherm for defluoridation using marble waste powder

Isotherms	Parameters	Values
Langmuir	q_{exp}	1.207
	q_{max} (mg/g)	5.25
	k(L g^{-1})	0.99
	R^2	0.924
	χ^2	0.46
Freundlich	1/n	0.635
	n	1.57
	k_F (mg/g)	2.51
	R^2	0.993
	χ^2	0.16
Temkin	A_T (L/mg)	13.7
	B_T	1.06
	R^2	0.903
	χ^2	0.87
Dubinin-Raduschkevich	q_d (mg/g)	2.5
	B	4E-08
	R^2	0.924
	χ^2	0.31

4.13.8. ADSORPTION KINETICS

The rate of reaction and rate limiting step, both play an important role in the adsorption phenomenon. Kinetics of fluoride adsorption on the surface of MWP 650 was studied following three different kinetic models: pseudo-first order, pseudo-second order and intraparticle diffusion.

Rate constant, R^2 and SSE values for pseudo-first-order, pseudo-second-order and intraparticle diffusion are shown in Table 4.9. Higher correlation coefficient values and lower SSE values depicted a better fit of the kinetic model. It is clear that R^2 value for the pseudo-second order was highest (0.99) with lowest corresponding SSE value (0.209). Also, the calculated equilibrium capacity from the pseudo-second order (0.691 mg/g) is closer to experimental values (1.207 mg/g). Therefore, it can be concluded that adsorption of fluoride on marble waste powder followed pseudo-second order adsorption

kinetics. It implies that chemisorption process had taken place during the adsorption process.

Table 4.9 Kinetics parameters for MWP as an adsorbent.

q_{exp} mg/g	Pseudo-first-order Kinetics				Pseudo-second-order-Kinetics				Intraparticle diffusion		
	K_1	q_e(mg/g)	R^2	SSE	K_2	q_e(mg/g)	R^2	SSE	R^2	K_i	SSE
1.207	1.579	3.411	0.959	0.223	2.748	0.691	0.994	0.209	0.917	0.552	0.88

A comparative analysis of some adsorbents with respect to their fluoride adsorption capacity around neutral pH, corresponding adsorption isotherms and kinetics is presented in Table 4.10. It can be seen that MWP650 adsorbent has higher defluoridation capacity than many adsorbents. It is worth noting that most of the adsorption mechanisms were following Freundlich isotherm and pseudo-second order reaction in terms of kinetics.

Table 4.10 Comparative analysis of different adsorbents with various parameters

Adsorbent	Adsorption Capacity (mg/g)	Corresponding pH	Equilibrium Isotherm	Kinetics	Reference
Plaster of paris	0.37	3-11	Freundlich isotherm	Intra particle diffusion	(Gao et al., 2009c)
Calcite	0.39	6	Freundlich isotherm	Pseudo 2nd order	(Gopal and Elango, 2007)
Nano sized synthetic Hydroxyapatite	0.489	5-6	Langmuir and Freundlich	Pseudo 2nd order	(X Fan et al., 2003)
Modified immobilized activated alumina	0.76	7	Langmuir	Pseudo 2nd order	Rafique et.,2012
Magnesia Hydroxyapatite	1.40	7.5	Langmuir	Pseudo 2nd order	(Mondal and George, 2015a)
Laterite	0.85	7.5	Langmuir and Freundlich	Pseudo 1st order	(Sarkar et al., 2006)
Marble waste powder (MWP650)	1.20	9	Freundlich	Pseudo 2nd order	Present Work

4.14. MECHANISM OF FLUORIDE MITIGATION BY MWP650

The major chemical composition of MWP is $CaMg(CO_3)_2$ which on thermal treatment dissociated into $CaCO_3$, MgO and released CO_2. Calcium carbonate emerges to be the most prominent material present in MWP 650 as observed through XRD and DTA-TGA analysis figure 4-17 and figure 4-21). Calcium carbonate in the aqueous medium reacts with hydronium ions and releases calcium ions. Two stages governed mechanism of fluoride removal on marble waste powder. The first stage included rapid removal in 1 h while the removal rate was slow in the second stage and equilibrium was reached in 3 h. In the initial stage, the released calcium ions combine with the fluoride ions present in the medium and forms calcium fluoride complex as a precipitate. It is likely that precipitation in the form of CaF_2 may increase the fluoride removal efficiency. Since, the size of calcium fluoride is smaller than calcium carbonate, the replacement reaction may leave additional porosity. The fluoride ions may then diffuse into the material, resulting in diffusing out of carbonate ions from $CaCO_3$. This phenomenon is experimentally proven by (Trautz and Zapanta, 1961). Therefore, the fluoride mitigation by MWP 650 is through both adsorption and precipitation process. Turner et al., (2005) reported similar mechanism of fluoride removal while working with calcite. The magnesium ions also react with the excess of fluoride ions that formed magnesium fluoride. The above stated mechanism is also illustrated in figure 4-28.

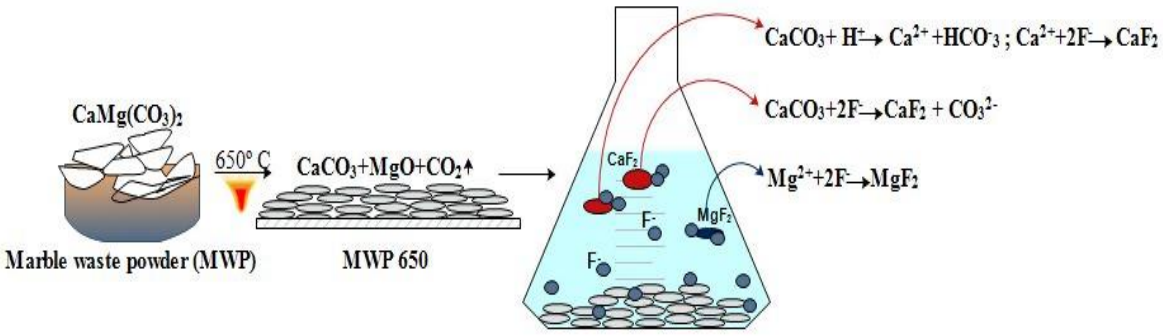

Figure 4-28. Mechanism of fluoride mitigation by marble waste powder (MWP650).

4.15. WATER QUALITY PARAMETERS

The water quality after treating with adsorbent MWP650 was analyzed for total hardness, alkalinity, TDS, conductivity and pH. The pH of water was found to be above 9 which is higher than the permissible limit of drinking water (6.5 to 8.5). The alkalinity TDS, and hardness was also observed to be higher than the corresponding permissible limit as shown in figure 4-29. When the conductivity of treated water was checked the value was noted to be above 2000 µS/cm which is again higher than the permissible limit.

The assessment of water quality parameters indicated that MWP650 cannot be used as such for defluoridation of drinking water.

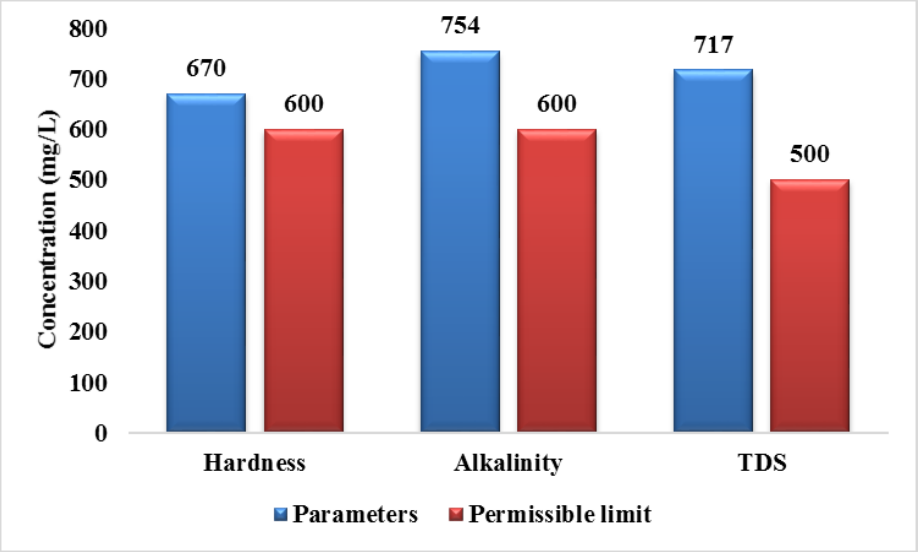

Figure 4-29. Water quality parameters analysis.

4.16. REUSE OF SPENT MARBLE WASTE POWDER

Economic sustainability is the major factor in process designing and optimization. The key cost of developing an adsorption system is governed by the adsorbent material and its synthesis. The marble waste powder used as an adsorbent in the present study being a byproduct of marble processing industry is available in huge quantities at no cost. Moreover the current improper handling of this waste that has caused severe environmental problems can be alleviated by its direct utilization as an adsorbent for fluoride water treatment. The spent adsorbent MWP-Fluoride complex that is rich in

fluoride can become a raw material for making cement, refractory bricks or for direct use in road construction purposes (Al-Zboon et al., 2010). Granite and marble waste content, up to 50 wt.% was combined in clay and used in brick development (Dhanapandian and Gnanavel, 2009). Application of marble waste in concrete and cement mortar mixes was recently reported by Al-Zboon and Al-Zou'by (Al-Zboon and Al-Zou'by, 2015).

4.17. NOVELTY OF THE WORK

The chapter comprises of usage of MWP which is a byproduct of marble processing industry available at almost zero cost and detailed characterization of MWP, technical evaluation of adsorption capacity of MWP for removal of fluoride as well as reuse of spent marble waste powder is suggested. It offers a solution to the disposal problem of marble waste generated and also accounts for the scientific basis on which the fluoride removal is achieved.

The following aspects of our work states its novelty:

- Fluoride removal using marble waste powder (MWP) has been described in this chapter. This research work is focused on eliminating the problem of disposal of marble waste and converting waste to a value added product that can mitigate fluorosis by using it for defluoridation of drinking water.
- This route of converting waste to wealth and for application for defluoridation has not been attempted anywhere nor have we found any literature reported on usage of marble waste powder on fluoride removal.
- Economic feasibility of the suggested technique ensures a promising adsorbent for future.

4.18. SUMMARY OF THE CHAPTER

The summary of this chapter are as follows:

The calcination temperature influenced the properties of marble waste powder in a significant manner by activating the calcium component present in the powder that further affected the defluoridation capacity. Batch experiments showed that MWP650 had higher removal capacity i.e.1.20 mg/g (initial F^-conc. 10mg/L) than MWP, MWP850, and MWP1000. The adsorption was multilayered in nature since the experimental data fitted very well with Freundlich isotherm and the kinetics of the process fitted best in pseudo-second order model. The mechanism of fluoride mitigation was found to be via

both adsorption and precipitation process. Usage of marble waste powder for defluoridation serves a two-way path by mitigating excess fluoride as well as reducing the marble waste produced.

The limitations of using marble waste powder as a defluoridating agent was higher pH, alkalinity and hardness of treated water as per WHO and BIS norms. Therefore, further improvement was required for proper utilization of marble waste powder by using different approach.

PART III.

MARBLE APATITE AS AN ADSORBENT

Marble waste powder was used for the synthesis of apatite primarily composed of hydroxyapatite. Marble apatite was synthesized using conventional precipitation method and ultrasonication method for application in water defluoridation.

PART III.

MARBLE APATITE AS AN ADSORBENT

4.19. INTRODUCTION

The major constituents of marble waste include compounds of calcium and magnesium, both of which possess affinity towards fluoride ions. There are many calcium and magnesium based adsorbents that have been tested for fluoride removal from drinking water such as calcite (Mondal et al., 2014), egg shells (R Bhaumik et al., 2012), magnesium incorporated-Hap (Mondal et al., 2016), marble waste powder (Mehta et al., 2016), Hap-nanorods (Mehta et al., 2014) etc. Considering, the significant presence of calcium and magnesium compounds in marble waste powder (MWP), it was used for the synthesis of calcium based biomaterial such as hydroxyapatite, which is later used as a defluoridation agent.

The current work reports an innovative attempt to prepare apatites using marble waste powder which is otherwise an environmental concern. To the best of our knowledge, the synthesis of apatite primarily consisting of hydroxyapatite derived from marble waste via conventional and sonochemical method and its application for water defluoridation has not yet been reported. The material synthesized using conventional method and ultrasonication assisted method has been compared using various characterization techniques and further batch defluoridation studies were carried out with varying process parameters (pH, dose, contact time, fluoride concentration). The adsorption isotherm were tested on different isotherm models, and kinetic studies were conducted to estimated rate of reaction and its feasibility to be used as an adsorbent for defluoridation was tested. Utilizing marble waste will not only reduce the cost of the product, but also it will be an economic advantage in developing cheaper defluoridation process besides bringing environmental benefit through reducing the quantity of waste accumulated.

4.20. SYNTHESIS OF MARBLE APATITE (MA)

4.20.1. MATERIALS

Marble waste powder (MWP) which is freely available in enormous amounts was obtained from marble processing industry located in the region of Kishangarh, Rajasthan, India and was washed (2 to 3 times) properly using deionized water (Thermo-scientific) and dried at room temperature. The analytical grade (AR) chemicals were used according to the required stoichiometry for the synthesis of adsorbent. For deriving out calcium nitrate ($Ca(NO_3)_2$) from MWP, nitric acid (HNO_3) and ammonia solution (NH_4OH) was required.

4.20.2. SYNTHESIS OF MARBLE APATITE BY CONVENTIONAL PRECIPITATION METHOD (CM)

Marble waste powder (MWP) was washed using double distilled water and dried at room temperature; followed by calcination at 850ºC for 2 hours. As discussed in section 4.12, calcination of marble waste at 850ºC decomposes calcium magnesium carbonate ($CaMg(CO_3)_2$) to calcium oxide (CaO)and magnesium oxide (MgO) as given in eq 26.

$$CaMg(CO_3)_2 \xrightarrow{\Delta} CaO + MgO + 2CO_2 \quad (26)$$

$$CaO + H_2O \rightarrow Ca(OH)_2 \quad (27)$$

$$Ca(OH)_2 + 2HNO_3 \rightarrow Ca(NO_3)_2 + 2H_2O \quad (28)$$

The calcined MWP was further washed with double distilled water and nitric acid was added drop-wise into it, till the powder was fully dissolved followed by neutralization with NH_4OH which led to the formation of gel like precipitates of mixture of calcium hydroxides and calcium nitrate and collected on a Whatman No. 42 filter. The reaction equations as given in eq.27 and eq.28.

These precipitates formed were dried for 4-5 hours at 110º C, and further used for the synthesis of marble apatite. Conventional precipitation method was used for the

synthesis and the schematic representation is depicted in figure 4-30. pH and temperature during the synthesis process was maintained at 9 and 80 ± 5º C respectively. The dried calcium precipitates and KH_2PO_4 were weighed according to Ca/P molar ratio of 1.67 and dissolved in deionised water separately. The pH of both the solutions were maintained to 9 pH using NH_4OH solution. The solution of KH_2PO_4 was then added drop wise (controlled addition at the rate of 5 ml/min) into the calcium solution (calcium hydroxide and calcium nitrate) under constant stirring using magnetic stirrer (Model: 5MLH, Remi, India). The resultant aqueous clear solution turned milky white as the precipitates of hydroxyapatite were being formed after 4-5 h of reaction. After the completion of reaction, white and gelatinous precipitates formed were aged for 24 h and centrifuged at 2000- 2500 rpm for 10 minutes. The precipitate obtained was washed with ultrapure water and filtered with Whatman No. 42 filter paper. Cake obtained after filtration was air dried in oven at 110º C followed by crushing using mortar and pestle. Powder thus obtained was sieved for uniform particle size corresponding to 200-250 British Standard Sieve (BSS) and used as adsorbent named MA-CM for fluoride removal.

The reaction mechanism of formation of marble apatite which was primarily hydroxyapatite is as follows:

$$10Ca(NO_3)_2 + 6KH_2PO_4 + 20NH_4OH \rightarrow Ca_{10}(PO_4)_6(OH)_2 + 6KOH + 20NH_4NO_3 + 12H_2O \quad (29)$$

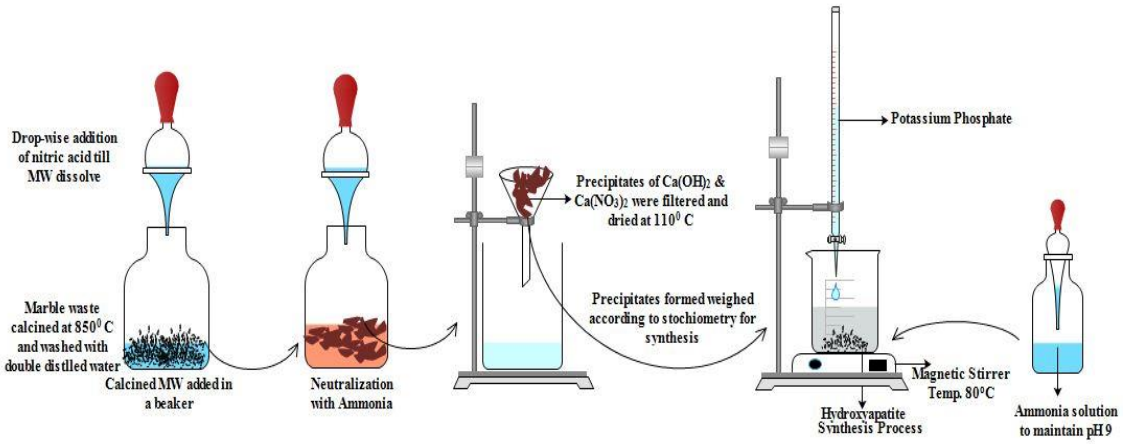

Figure 4-30. Synthesis process of marble apatite using conventional method (MA-CM)

4.20.3. SYNTHESIS OF MARBLE APATITE BY ULTRASONICATION METHOD (USM)

Ultrasonic instrument (horn type) was used to generate ultrasound waves for synthesis of marble apatite using Ultrasonication method. The schematic representation of ultrasonic (Make: Sonics, USA) setup with an operating frequency of 20 kHz and rated output power 750 W is shown in figure 4-31. The tip of horn was dipped 20 mm below solution surface.

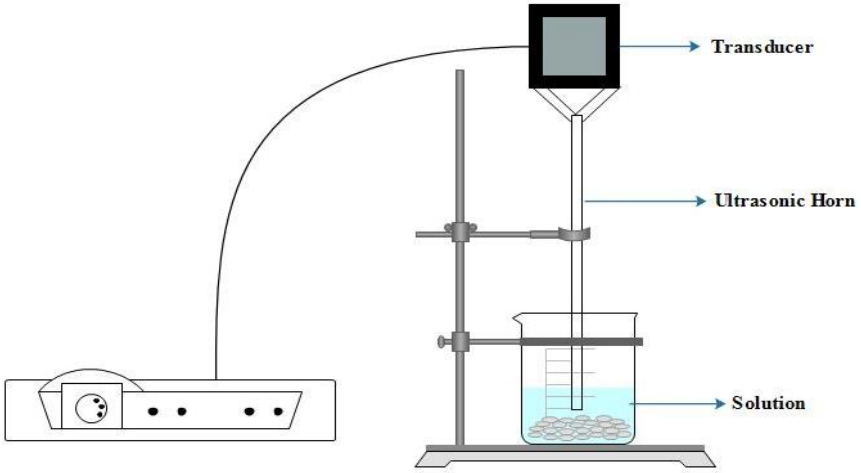

Figure 4-31. Schematic representation of ultrasonication setup.

In the USM method, synthesis of marble apatite was based on sonication using ultrasonic horn as shown in figure 4-32. During the addition of KH_2PO_4 into the solution of $Ca(NO_3)_2$ sonication was set at 40% amplitude for 30 min with a 30 sec pulse and 5 sec relaxation cycle. After the complete addition of KH_2PO_4, sonication was continued for another 15 min so as to obtain the proper crystalline phase of the apatite. The temperature during the reaction was maintained at 45ºC. After the completion of reaction of 45 min, white and gelatinous precipitates were formed which was centrifuged at 2000-2500 rpm for 10 min. Material obtained was washed with ultrapure water and filtered with Whatman No. 42 filter paper. Cake obtained after filtration was dried at 110ºC was crushed and sieved for uniform particle size corresponding to 200-250 BSS and named MA-USM.

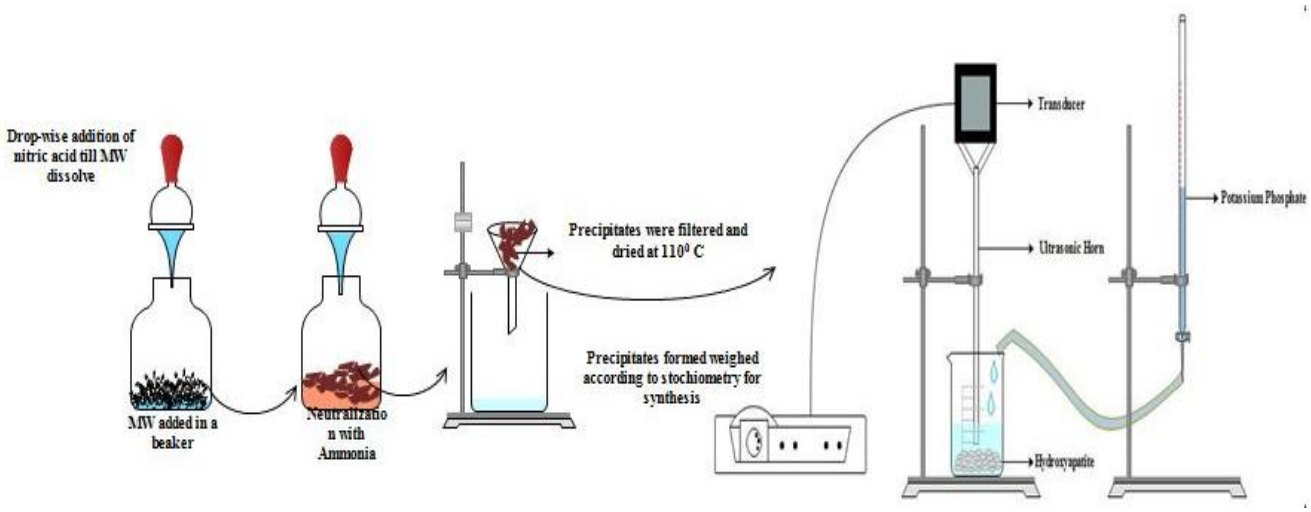

Figure 4-32. Schematic representation of synthesis of marble apatite using USM method.

4.20.4. REACTION TIME AND % YIELD

The process time for synthesis of the conventionally synthesized (CM) marble apatite was 240 min while process time for marble apatite synthesized using ultrasonication method (USM) method was 45 min (Table 4.11). This variation is attributed to extreme pressure (>1000 atm) and temperature (>5000 K) conditions achieved in ultrasonication method which lead to powerful micromixing, improved solute transfer and nucleation rate in aqueous suspension that helped in the improvement of reaction rate and reduction in process reaction time. The product yield with the use of ultrasonication method was 78.4 % which is significantly higher compared to conventional method with 67.5 % yield for the synthesis of marble apatite. The percentage yield was estimated on the basis of theoretical and the actual weight of the product obtained after complete drying and considering the initial weight of the reagents. Improved % yield is attributed to the enhanced mass transfer caused due to microjet streaming and interfacial turbulence created in the ultrasonic irradiation process which resulted in faster reaction rates.

Table 4.11 Reaction time and % yield of the conventionally and ultrasonochemically synthesized marble apatite.

Method	Material	Reaction time (min)	Yield (%)
Conventional	MA-CM	240	67.5%
Ultrasonication	MA-USM	45	78.4%

4.21. CHARACTERIZATION OF MARBLE APATITE (MA)

4.21.1. FTIR

FTIR is a technique to identify the presence of functional groups. FTIR spectra of marble apatite prepared by conventional and ultrasonication method is shown figure 4-33. In case of MA-CM, the characteristic peak at 3433 cm^{-1} and 3218 cm^{-1} are due to the stretching vibrations of O-H bond. The vibrations at 1654 cm^{-1} corresponds to H-OH bending mode. The band at 1050 cm^{-1} is the characteristic band of phosphate stretching vibrations while the bands at 759 $cm^{-1}$and 564 cm^{-1} are due to phosphate bending vibrations. Since ammonia was used in the process its characteristic peak was observed at 1384 cm^{-1}. Similar characteristic peaks are observed in the case of MA-USM. The presence of PO_4^{3-} group and O-H group in FTIR spectra confirmed that marble apatite primarily in the form of hydroxyapatite (Hap) was formed using both methods.

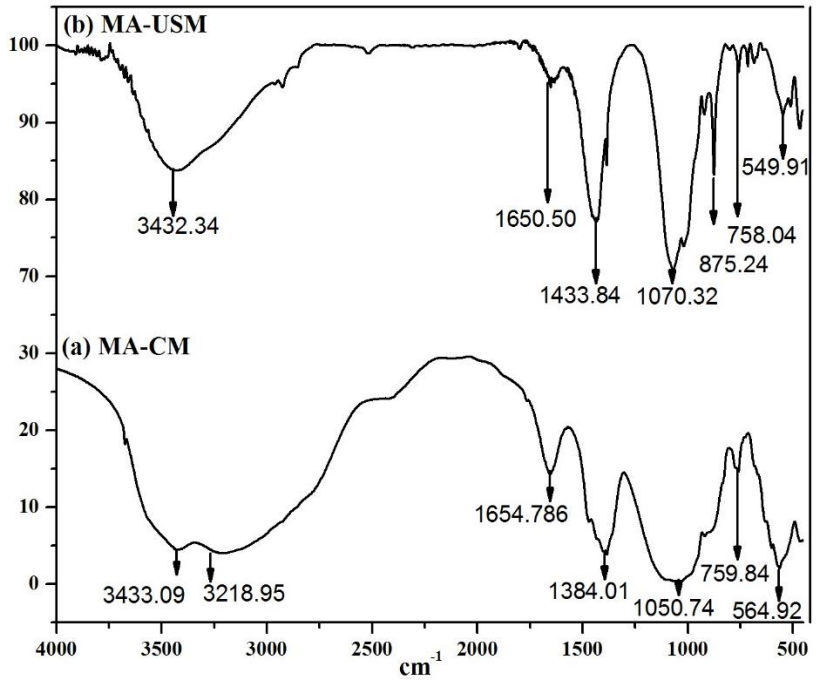

Figure 4-33. FTIR spectra of marble apatite synthesized using (a) CM method (MA-CM) and (b) USM method (MA-USM).

4.21.2. XRD

The XRD patterns for MA-CM and MA-USM are shown in figure 4-34 Major peaks observed in both the spectra were of hydroxyapatite (JCPDS card no. 00-001-1008). In both apatites, other phases like of tri-calcium phosphate (JCPDS card no. 00-044-0763) and magnesium calcium silicates (JCPDS card no.01-074-0990) were also observed which indicated the formation of intermediates and well as presence of impurities (silicates) which were originally present in the reactant marble waste powder as observed in figure 4-34a and figure 4-34b. More pure form of hydroxyapatite, with lesser amount of intermediates and silicates was obtained, when ultrasonic method was used for the synthesis process. Ultrasonication helped in process intensification and completion of the chemical reaction to a greater extent than the conventional technique due to improved mass transfer at the molecular level. The mean crystallite size of marble apatite synthesized using different methods was also estimated using Debye-Scherer formula as shown in eq. (3) and values are given in Table 4.12.

The impact of ultrasonication was evident not only in the increased yields (67.5% for CM and 78.4% for USPM) but also in the reduction of average crystallite size (Table 4.12). Marble apatite synthesized from CM process had an average crystallite size of 87.45 nm, whereas marble apatite synthesized using USM process had an average crystallite size of 58.46 nm. Reduction in average particle size is attributed to the rapid kinetics of the ultrasound assisted reaction which does not provide sufficient time for particle nucleation and growth, therefore, the average particle size gets reduced as well as ultrasonication prevents agglomeration of particles during the synthesis and maintained effective size distribution. The reduction is crystallite size is found to be advantageous, as it produces an adsorbent with higher surface area for its application in adsorption.

Table 4.12 Mean crystallite size of marble apatite synthesized using conventional method (CM) and ultrasonication method (USM).

Adsorbent	Wavelength (Å)	Peak Width (Degree)	Peak Position (Degree)	Crystallite Size (nm)
MA-CM	1.54056	0.0984º	30.547º	87.45
MA-USM	1.54056	0.1476º	31.6837º	58.46

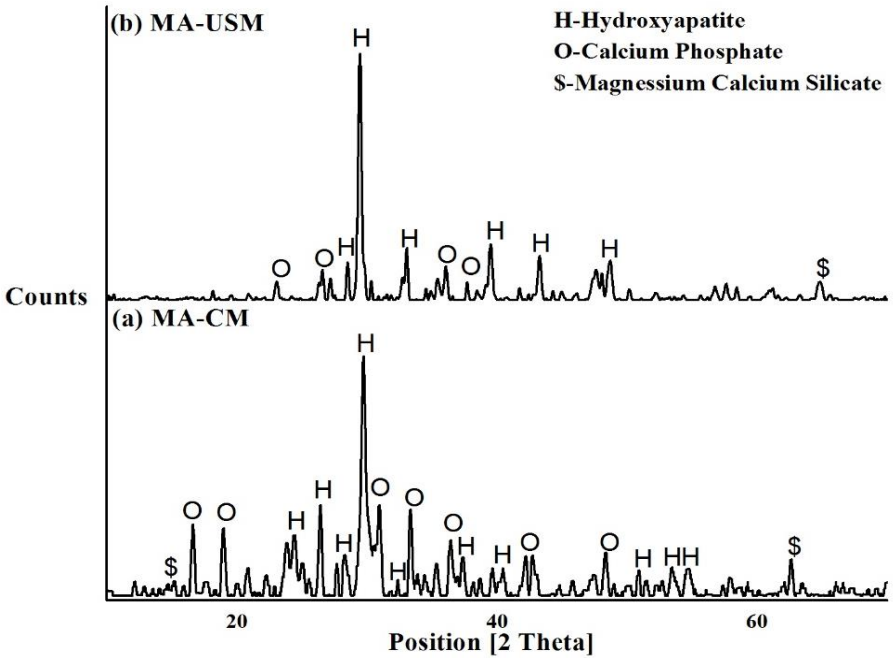

Figure 4-34. XRD spectra of marble apatite synthesized using (a) CM method (MA-CM) and (b) USM method (MA-USM)

4.21.3. SEM

The SEM micrographs of synthesized marble apatite with both CM and USM methods were compared and shown in figure 4-35. MA CM was found to be in the form of countless agglomerated bundles of plate like structure (figure 4-35a and figure 4-355b) whereas, MA-USM (figure 4-35c and figure 4-35d), was found to be with lesser agglomeration and well defined spherical morphology at nanoscale sizes. MA-USM had smaller particle size but also had considerably less agglomeration. Use of cavitation within the process had its influence as process intensification in the reaction step by reducing the particle size in the synthesis process itself. This helped in improving the material properties by increasing the surface area, reducing reaction time and maintaining the particle shapes and uniformity.

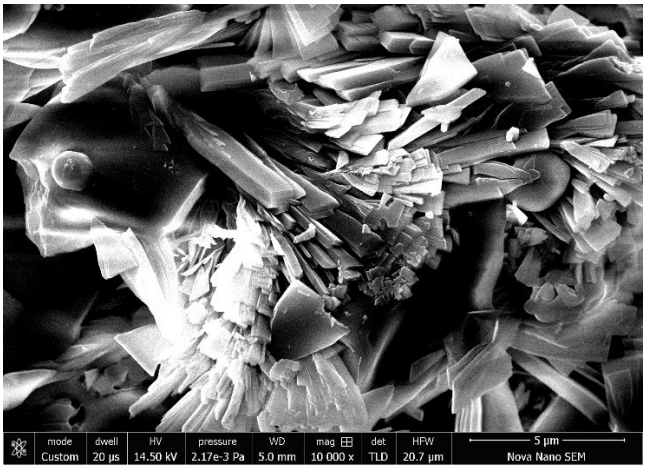

(a)

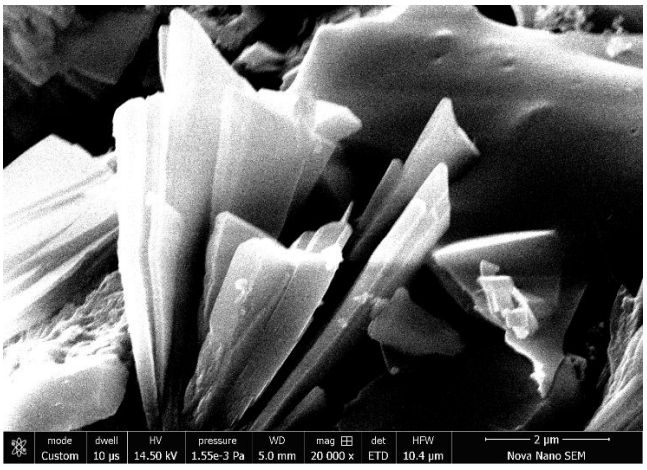

(b)

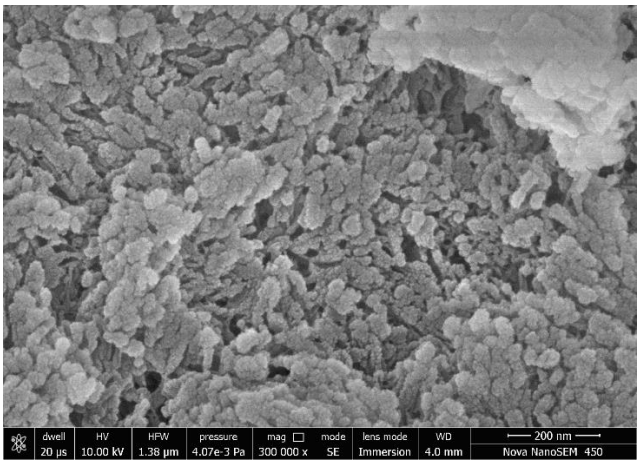

(c)

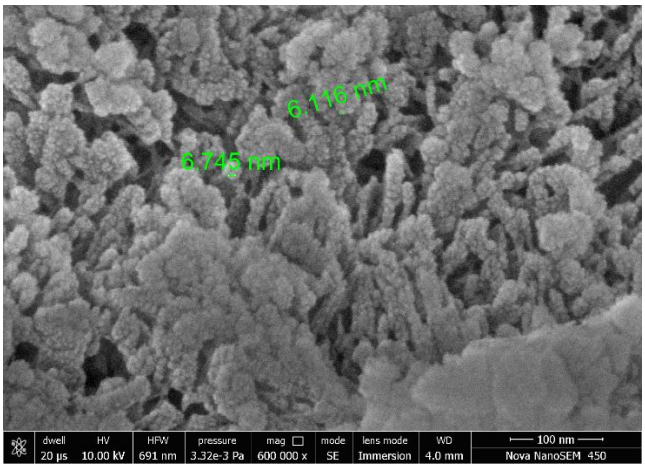

(d)

Figure 4-35. SEM micrographs; (a & b) Marble apatite synthesized using CM method, (c & d) Marble apatite synthesized using USM method.

4.21.4. TEM/EDS

The investigation of the morphology, structure, and chemistry of material synthesized is an important aspect in material science. Transmission electron microscope (TEM) is used to examine the structure, composition, and properties of specimens in submicron detail. TEM analysis was carried out to visualize the size and shape as well as to confirm the nanocrystalline nature of the synthesized marble apatite which is depicted in figure 4-36. The agglomerated needle like morphology was observed in case of MA-CM which resulted into an increase in the particles size as seen in figure 4-36a and figure 4-36b. Shojai et.al 2013 had also reported that conventional precipitation method produced apatite in the form of needle like structure. Agglomeration of marble apatite may be due to the presence of

magnesium phosphate and silicon oxide which was present in reactant marble waste powder, whereas in case of MA-USM, significant reduction in the particles size of sonochemically prepared marble apatite nanoparticles without agglomeration was observed (figure 4-36c and figure 4-36d), which can be attributed to the cavitation effect resulting out of ultrasonic irradiation.

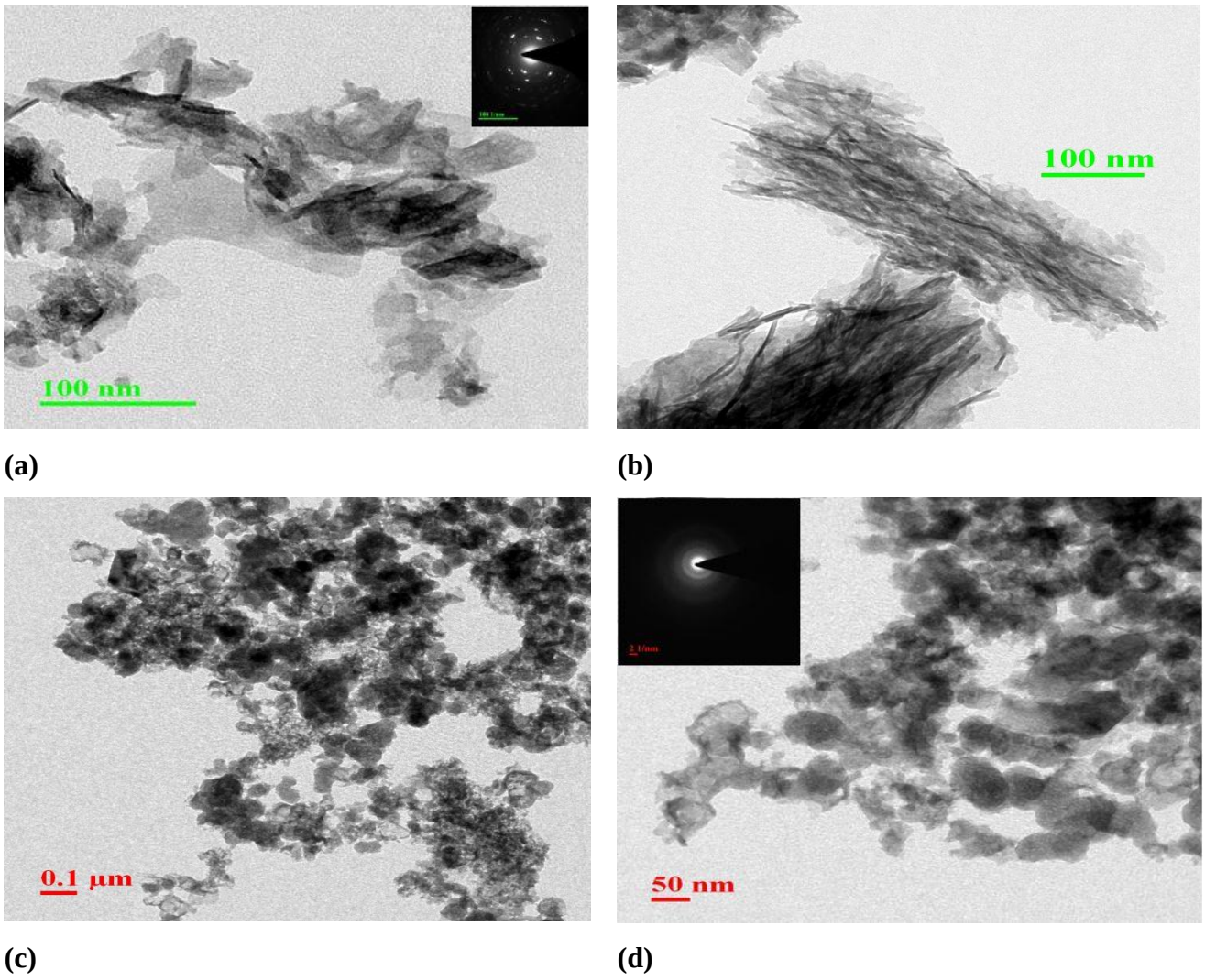

(a) **(b)**

(c) **(d)**

Figure 4-36. TEM micrographs; (a and b) Marble apatite synthesized using CM method, (c and d) Marble apatite synthesized using USM method.

EDS shows the elemental composition of compounds present in the material. Since calcium was derived from marble waste powder, few other compounds such as magnesium, silica and phosphorous which were present along with calcium can also be seen in EDS spectra. However, MA-USM was found superior in quality to MA-CM as

the quantity of magnesium and silica were comparatively lower in MA-USM compared to that of MA-CM as observed in figure 4-37a and figure 4-37b. The peak of copper was obtained as the grid used for mounting the sample was made of copper.

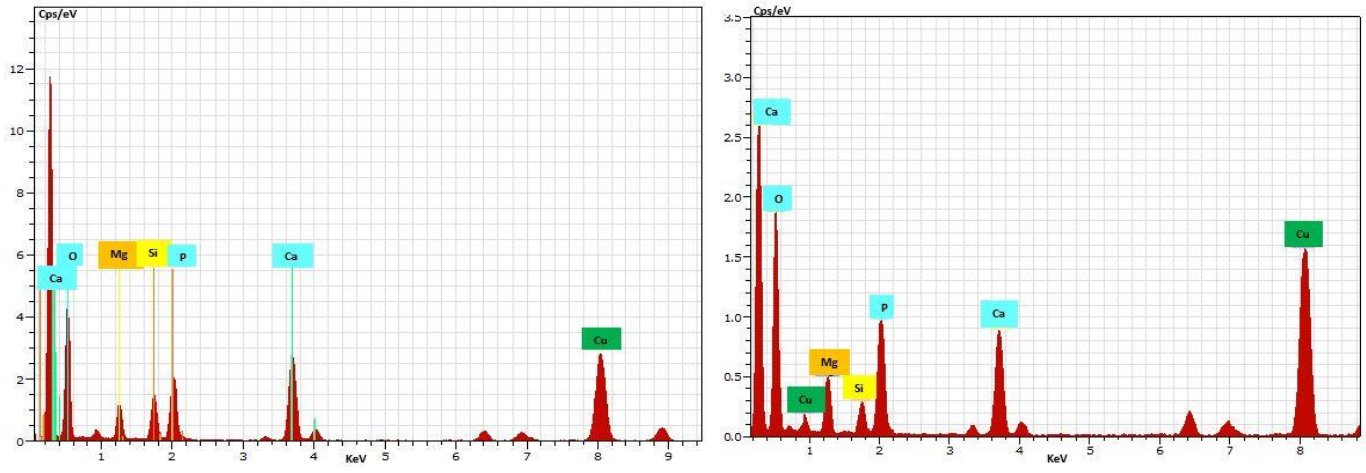

(a) **(b)**

Figure 4-37. EDS spectra of marble apatite synthesized using (a) CM method (MA-CM) and (b) USM method (MA-USM).

4.22. BATCH DEFLUORIDATION STUDIES USING MA AS AN ADSORBENT

The adsorption capacity of the synthesized adsorbents MA-CM and MA-USM for removal of fluoride from aqueous samples were studied to obtain adsorption equilibrium and kinetics rate data. The optimum value for process parameters such as dosage, equilibrium time, initial fluoride concentration and pH etc. were identified through studies on batch defluoridation experiments by varying these parameters.

4.22.1. EFFECT OF ADSORBENT DOSE

The effect of adsorbent (MA-CM, MA-USM) dose varying from 1-15 g/L on fluoride removal capacity for fixed initial fluoride concentration (10 mg/L) and in order to bring down the residual fluoride concentration in permissible limit (1 mg/L) is as shown in figure 4-38. It was observed that percentage removal for MA-USM increased linearly upto 91.3% with increase in adsorbent dose upto 5 g/L and thereafter remained constant with no significant change. In case of MA-CM the percentage removal increased linearly upto 89.2% with dosage upto 8 g/L and thereafter remain constant. The increase

in the available active sites with increase in the adsorbent dose had caused increase in removal capacity. It was observed that the fluoride removal capacity by MA-USM was higher as compared to MA-CM. For 5 g/L of MA-USM, the percentage removal was 91.35% with capacity of 1.83 mg/g and for MA-CM it was 77.2 % with the capacity of 1.54 mg/g. In order to make a comparative study for both the adsorbents, 5 g/L was fixed as an optimum dosage for treating 100 ml of 10 ppm fluoride solution as with this amount of adsorbent the residual fluoride concentration obtained was below the permissible limit of 1.0 mg/L

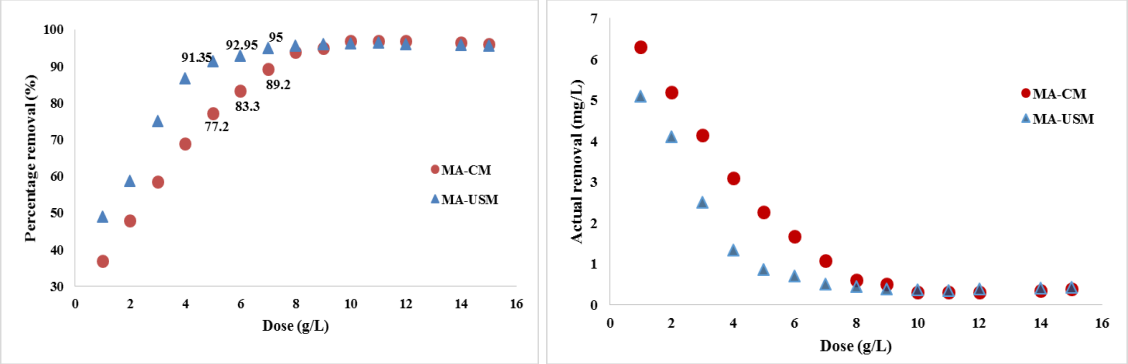

Figure 4-38. Effect of adsorbent dose on percentage removal (%) and actual removal (mg/L) (F^- concentration: 10 mg/L, dose: 1-15 g/L, pH 7, temperature: 30 ± 0.5ºC).

4.22.2. Effect of Contact Time

The effect of contact time on removal of fluoride by MA-CM and MA-USM for an initial fluoride concentration of 10 mg/L is shown in figure 4-39. It was observed that fluoride removal gradually increased as the contact time increased and equilibrium was achieved in 180 min with the adsorption capacity of 1.544 mg/g and percentage removal of 77.2% for MA-CM. Whereas, for MA-USM equilibrium was attained in 90 min with the defluoridation capacity of 1.826 mg/g and percentage removal of 91.3% which was higher as compared to MA-CM adsorbent. After 90 min, there was no significant fluoride removal was observed when MA-USM was used as an adsorbent and hence, it was considered as the optimum time for defluoridation studies. It was again observed that MA-USM exhibited better efficiency in terms of lower equilibrium time (90 min) as well as higher defluoridation capacity (1.826 mg/g, for dosage of 5 g/L and initial F^- concentration of 10 mg/L) than MA-CM.

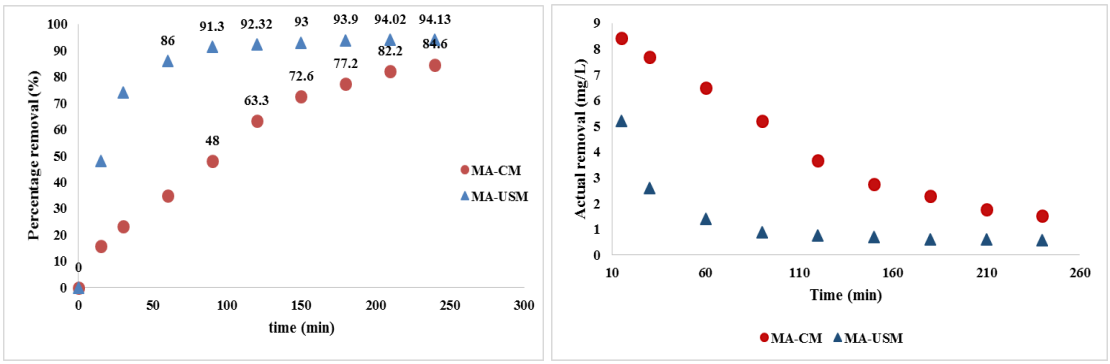

Figure 4-39. Effect of contact time on percentage removal (%) and actual removal (mg/L), (F^- concentration: 10 mg/L, contact time: 15-240 min, dose: 5 g/L, pH 7, temperature: 30 ± 0.5ºC).

4.22.3. EFFECT OF INITIAL FLUORIDE CONCENTRATION

Different initial fluoride concentrations varying from 0-45 mg/L were used to study its effect on MA-CM and MA-USM by keeping other parameters such as dosage (5 g/L) and contact time (90 min) constant as presented in figure 4-40. It was observed that adsorption capacity increased with increase in initial fluoride concentration. This is attributed to the fact that higher F^- concentrations create higher concentration gradients in the aqueous medium and hence the driving force for adsorption was higher. The saturation was reached at concentrations above 30 mg/L, when the adsorbent was exhausted as there were no active sites left on the surface of adsorbent. Similar results were noted by (Mondal and George, 2015b). It was observed that the defluoridation capacity of MA-USM was higher compared to MA-CM, therefor further studies on effect of pH, co-ions in aqueous medium, adsorption isotherms, rate kinetics and thermodynamic studies were limited to with adsorbent MA-USM only.

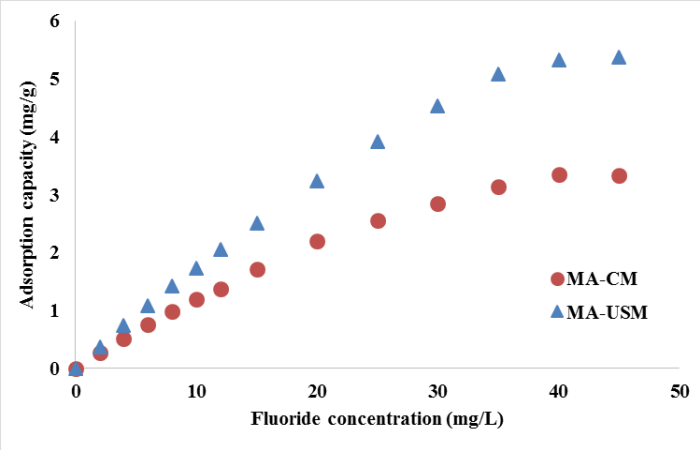

Figure 4-40. Effect of initial fluoride concentration on adsorption capacity (mg/g) (F^- concentration: 0-45 mg/L, contact time: 90 min, dose: 5 g/L, pH 7, temperature: 30 ± 0.5ºC).

4.22.4. Effect of pH

pH of the medium plays a significant role as it can influence the defluoridation capacity of the adsorbent. Experiments were conducted to quantify the effect of pH on fluoride adsorption by marble apatite, MA-CM and MA-USM and results are shown in figure 4-41. It was seen that for MA-CM, adsorption of fluoride was maximum at pH 6 whereas, the capacity was slightly reduced at pH ≤ 5 and pH ≥ 8. This can be due to the fact that at higher pH, OH-ions compete to acquire active sites with fluoride ions present in the solution and at lower pH weakly ionized hydrofluoric (HF) acid is formed. For MA-USM, defluoridation capacity was unaffected for conditions of pH in the range 5 ≤ pH ≤ 8, i.e. the drinking water pH range and maximum removal for MA-CM was observed at pH 7 at 91.35%. The surface zero charge (pH_{PZC}) of MA-CM and MA-USM was found to be 8.5. pH_{PZC} of an adsorbent defines the pH at which net surface charge is neutral. Therefore, at pH < pH_{PZC} (8.5) adsorbent will be positively charged and will attract the negative fluoride ions, hence higher fluoride adsorption capacity was observed at pH < 8.5. The fluoride removal capacity of both adsorbents MA-CM and MA-USM were mostly unaffected by pH which is an added advantage for its application for drinking water treatment.

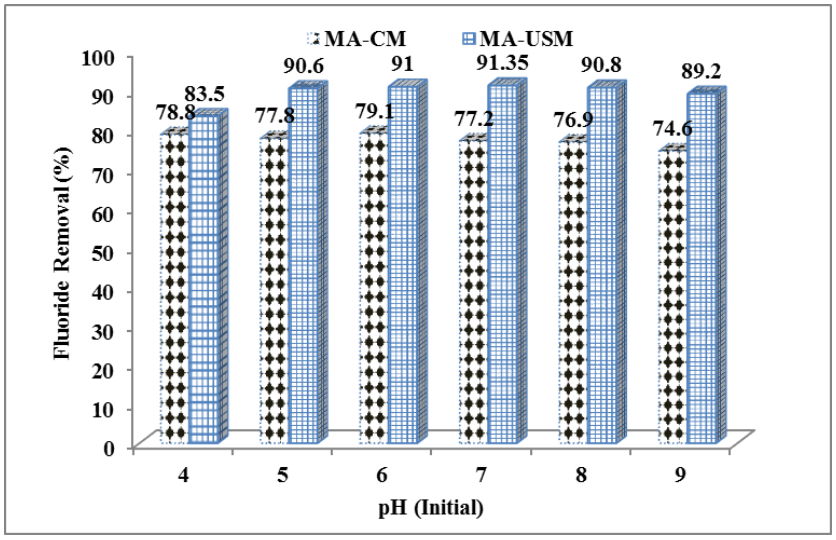

Figure 4-41. Effect of pH on fluoride removal (%), (F^- concentration: 10 mg/L, contact time: 90 min, dose: 5 g/L, pH 4-9, temperature: 30 ± 0.5ºC).

4.22.5. EFFECT OF CO-IONS

Groundwater usually contains several other co-existing anions that may compete with fluoride ion for adsorption sites during defluoridation. Hence, it is necessary to study the effect on defluoridation capacity of MA-USM in the presence of other ions like Cl^-, NO_3^-, SO_4^{2-}, HCO_3^- and PO_4^{3-} , in the common groundwater concentration range of these ions mostly varying from 100 to 300 mg/L and keeping 10 mg/L as initial fluoride concentration. Figure 4-42 shows the influence of co-ions in the defluoridation capacity of MA-USM. The results indicated that most of the ions did not have any effect on fluoride removal capacity of MA-USM. Defluoridation capacity slightly decreased in the presence of HCO_3^- ions which was due to the competition of bicarbonates ions with fluoride ions in the adsorption process. However, the interference by phosphate is not a serious concern because the phosphate content in groundwater is usually much less.

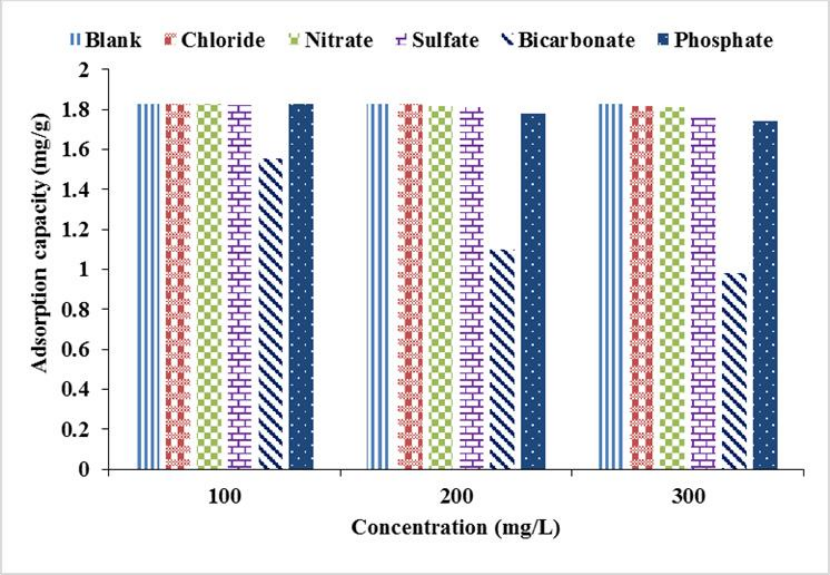

Figure 4-42. Effect of co-existing ions on adsorption capacity (mg/g) (F^- concentration: 10 mg/L, contact time: 90 min, dose: 5 g/L, temperature: 30 ± 0.5ºC).

4.22.6. ADSORPTION ISOTHERMS

In order to gain better understanding of fluoride adsorption mechanism, different adsorption isotherms were studied, i.e. Langmuir, Freundlich, Temkin and Dubinin-Raduschkevich and the best fit adsorption isotherm identified.

The estimated isotherm parameters from the model fits are given in Table 4.13. The experimental data fitted comparatively well with Langmuir isotherm model, which is evident from smaller χ^2 value and R^2 value close to unity, which represent homogeneous distribution of active sites on the adsorbents surface and monolayer adsorption. The predicted q_{max}, i.e. the maximum adsorption capacity is 6.406 mg/g.

Table 4.13 Adsorption isotherm for defluoridation using MA-USM.

Isotherms	Parameters	Values
Langmuir	q_{exp}	1.826 mg/g
	q_{max} (mg/g)	6.406
	k(L g^{-1})	0.318
	R^2	0.9908
	χ^2	0.21

Freundlich	1/n	0.5828
	n	1.715
	k_F (mg/g)	1.406
	R^2	0.988
	χ^2	0.15
Temkin	A_T (L/mg)	3.608
	B_T	0.6579
	R^2	0.9653
	χ^2	0.34
Dubibin-Raduschkevich	q_d (mg/g)	0.6928
	B	-7E-08
	R^2	0.927
	χ^2	0.267

4.22.7. ADSORPTION KINETICS

Rate of adsorption is an important factor in any adsorption process. In this study, batch fluoride adsorption kinetic studies were conducted using MA-CM and MA-USM. MA-USM has successfully removed fluoride within a short period i.e. most of the fluoride removal took place in the first 60 min of contact time and the equilibrium was reached in 90 min. To describe the kinetics of fluoride adsorption in a better manner, adsorption kinetics was analyzed using two mass transfer models (pseudo-first and pseudo-second order) and one intraparticle diffusion model. The kinetic parameters such as correlation coefficient (R^2), rate constant, and SSE values obtained from these model fits are summarized in Table 4.14.

Table 4.14 Kinetic parameters for MA-USM adsorbent.

q_{exp} mg/g	**Pseudo-first-order Kinetics**				**Pseudo-second-order-Kinetics**				**Intraparticle diffusion**		
	K_1	q_e(mg/g)	R^2	SSE	K_2	q_e(mg/g)	R^2	SSE	R^2	K_i	SSE
1.826	0.0476	1.716	0.9912	0.522	0.720	1.985	0.999	0.22	0.9378	0.4725	0.38

From Table 4.14 , it is evident that the kinetic data fit well with the pseudo second-order equation. Higher correlation coefficient values and lower SSE values depict a better fit of the kinetic model. It is clear that R^2 value for the pseudo-second order was

highest (0.999) with lowest corresponding SSE value (0.22). Also, the calculated equilibrium capacity (q_e) from the pseudo-second order is closer to experimental values (q_{exp}). Therefore, it can be concluded that adsorption of fluoride on marble apatite synthesized using USM method (MA-USM) follows pseudo-second order adsorption kinetics.

4.22.8. THERMODYNAMIC STUDY

Thermodynamic studies were conducted at different temperatures (303K, 313K and 323K) for MA-USM adsorbent. The studies showed that percentage removal of fluoride was increased from 91.35% to 98% with the increase in temperature, indicating the endothermic behavior of adsorption (figure 4-43). To estimate the feasibility and spontaneity of the adsorption process, the thermodynamic parameters including Gibbs free energy change (ΔG^o), enthalpy change (ΔH^o), and entropy change (ΔS^o) were assessed. These parameters were calculated using the following equations:

$$\Delta G^{\circ} = -RT ln\, Ke \tag{30}$$

$$\Delta G^{\circ} = \Delta H^{\circ} - T\Delta S^{\circ} \tag{31}$$

This equation can be written as;

$$lnKe = \Delta S^{\circ} R - \Delta HRT \tag{32}$$

where R is the universal gas constant (8.314 J mol−1 K−1), T is the temperature (K), and Ke is the distribution coefficient. The Ke value was calculated using following equation;

$$Ke = \frac{Cx}{Cy} \tag{33}$$

where Cx and Cy are the equilibrium concentration of fluoride ions on adsorbent and in the solution, respectively.

The values of ΔH° and ΔS° can be obtained from the slope and intercept of the plot of ln K_e versus 1/T. The values of Gibbs free energy at 303, 313, and 323 K were found to be -3.78, -3.71 and -3.64 kJ/mol, respectively. The negative values of ΔG° confirm the spontaneous nature of adsorption of the fluoride ion by the adsorbent, while

the positive value of ΔH˚ (5.89 kJ/mol) shows that the process is endothermic in nature. The endothermic nature can also predicted from figure 4-43 where increase in fluoride adsorption capacity of MA-USM is evident with the increase in temperature. The value of entropy was found to be (0.007 kJ/mol/K). The positive value of ΔSº indicates the possibility of randomness at the solid/liquid interface during fluoride adsorption on MA-USM adsorbent.

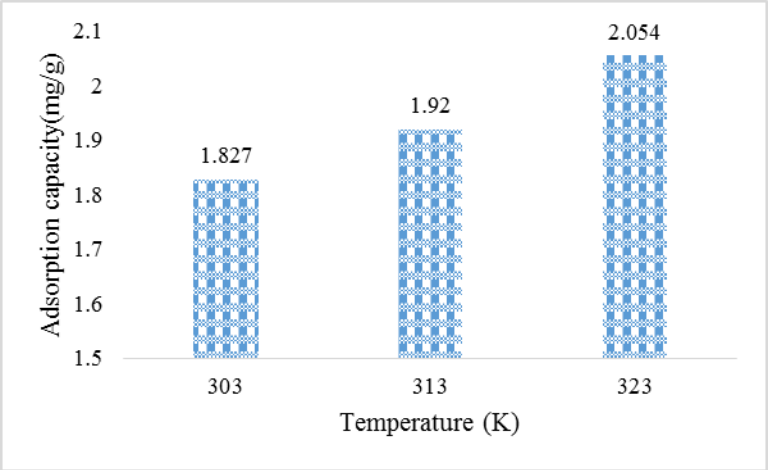

Figure 4-43. Adsorption capacity of MA-USM with increase in temperature.

Table 4.15 Thermodynamic parameters of fluoride adsorption on MA-USM adsorbent.

ΔGº (kJ/mol)			ΔHº (kJ/mol)	ΔSº (kJ/mol/K)
303K	**313K**	**323K**		
-3.78	**-3.71**	**-3.64**	**5.86**	**0.007**

4.23. WATER QUALITY PARAMETERS

The quality of water treated with MA-USM adsorbent (dose: 5 g/L, contact time: 90 min) was studied for various parameters as it determines the suitability of the adsorbent for practical applications. The value of various parameters studied before and after adsorption are given in Table 4.16 along with the permissible limits determined by WHO and BIS. Alkalinity and hardness of water in the treated sample was 371 and 417 mg/L respectively. pH of water after adsorption was 6.90 and the TDS was found to be 404 mg/L. Calcium content leached into treated water was 70.34 mg/L while the phosphorous concentration was below detection limit. Results showed that the

synthesized adsorbent, MA-USM can be used for treatment of fluoride in drinking water and all the parameters are within permissible limit.

Table 4.16 Treated water quality parameter analysis.

	Before adsorption	**After adsorption**	**Permissible limit (BIS)**
pH	7.47	6.90	6.5-8.5
TDS (mg/L)	33	404	500
Alkalinity ($CaCO_3$ eqv; mg/L)	0	371	600
Total Hardness ($CaCO_3$ eqv; mg/L)	0	417	500
Calcium (mg/L)	0	70.34	200
Phosphate (mg/L)	0	Below detection limit	Not mentioned
Fluoride (mg/L)	10	0.865	1.5
Turbidity (NTU)	<0.3	<0.3	10

4.24. NOVELTY OF THE WORK

- The current work reports an innovative attempt to prepare apatites using marble waste powder which is otherwise an environmental concern.
- To the best of our knowledge, the synthesis of apatite (primarily consisting of hydroxyapatite) derived from marble waste via conventional (CM) and sonochemical method (USM) and its application for water defluoridation has not yet been reported.
- The material synthesized using CM and USM assisted method has been compared using various characterization techniques and further batch defluoridation studies were carried out with varying process parameters (pH, dose, contact time, fluoride concentration).
- The adsorption isotherm were tested on different isotherm models, and kinetic studies were conducted to estimated rate of reaction and its feasibility to be used as an adsorbent for defluoridation was tested.
- Utilizing marble waste will not only reduce the cost of the product, but also it will be an economic advantage in developing cheaper defluoridation process besides bringing environmental benefit through reducing the quantity of waste accumulated.

4.25. SUMMARY OF THE CHAPTER

- Marble apatite primarily composed of hydroxyapatite was synthesized using marble waste via conventional (CM) and ultrasonication method (USM) method for the purpose of defluoridation of drinking water. The XRD analysis revealed that when ultrasonication was used for synthesis, product obtained was more crystalline with lesser intermediate phases. Whereas, SEM and TEM studies depict that with sonication effect well defined spherical morphology is obtained with crystalline nature whereas sword like agglomerated structure was observed when conventional method was used for synthesis.
- Yield of marble apatite was improved from 67.5% to 78.4% when USM method was used for synthesis.
- The adsorption capacity of marble apatite was higher (1.826 mg/g) when ultrasonication was used as compared to (1.544 mg/g) when conventional method was used for synthesis.
- The experimental data fitted very well with Langmuir isotherm and the kinetics of the process fitted best in pseudo-second order model. Analysis of water quality parameters clearly proved that the treated water is fit for drinking purposes as per WHO and Indian drinking water standards.

The limitation observed while working with this method is the purity of hydroxyapatite. Along with Hap few of the intermediates in the form of calcium phosphate and magnesium calcium silicates were present. Therefore, further examination was required to improvise the methodology to synthesize the pure form of hydroxyapatite using marble waste powder.

The next chapter deals with the improved methodology for synthesizing pure Hap from marble waste powder.

PART IV.

MARBLE HYDROXYAPATITE AS AN ADSORBENT

Part IV details about the improved method for the synthesis of hydroxyapatite utilizing marble waste powder. Conventional precipitation method and ultrasonication method was used for the synthesis. Material obtained using both the methods were characterized and used as an adsorbent for water defluoridation.

PART IV.
MA-HAP AS AN ADSORBENT

4.26. INTRODUCTION

In the previous chapter, attempts were made to synthesize hydroxyapatite using marble waste powder, but XRD studies revealed that intermediates in the form of calcium phosphates and calcium magnesium silicates along with hydroxyapatite was obtained. In order to remove the impurities, previous method was modified and Marble hydroxyapatite was synthesized (MA-Hap) using conventional (MA-Hap CM) and ultrasonication method (MA-Hap USM). In this chapter MA-Hap synthesized was characterized using FTIR, XRD, SEM, TEM/EDS, TGA/DTA and BET surface area techniques. Defluoridation studies were also conducted in batch mode and quality of treated water after adsorption studies were also checked.

4.27. SYNTHESIS OF MARBLE-HYDROXYAPATITE (MA-HAP)

The Marble-hydroxyapatite was synthesized using both conventional precipitation method and ultrasonication method. The details methodology for the synthesis is given in following sections.

4.27.1. MATERIALS

The materials used for the synthesis of marble hydroxyapatite were same as explained in section 4.20.1. The main difference between the synthesis of marble apatite and marble hydroxyapatite is the preparation method of calcium nitrate from marble waste powder which is explained in the following section.

4.27.2. PREPARATION OF CALCIUM NITRATE USING MWP

The marble waste powder (MWP) comprised of $CaMgCO_3$ and SiO_2 and on calcination at 650ºC and 850ºC, it will dissociate thermally and forms calcium carbonate, magnesium oxide and calcium oxide respectively as reported in section 4.12.2 and section 4.12.5. So with this approach, MWP obtained was washed using deionized water followed by calcination at 650ºC and 850ºC in a muffle furnace for 2 h and the temperature was increased slowly during calcination at the rate of 20ºC/min. The calcination of MWP at 650ºC and 850ºC will result into the formation of calcium carbonate ($Ca(CO)_3$) and calcium oxide (CaO) respectively.

The reaction which will be followed is shown in eq.(30) and eq.(31).

$$CaMg(CO)_3 \xrightarrow{\Delta 650^{o}C} Ca(CO)_3 + MgO + CO_2 \quad (34)$$

$$CaMg(CO)_3 \xrightarrow{\Delta 850^{o}C} CaO + MgO + 2CO_2 \quad (35)$$

Calcined MWP was added slowly with regular stirring into the preheated solution of dilute nitric acid (0.64M) in order to convert ($CaCO_3$) and (CaO) to calcium nitrate ($Ca(NO_3)_2$) and the reaction which followed is as shown in eq.(32) and eq.(33) respectively:

$$CaCO_3 + 2HNO_3 \rightarrow Ca(NO_3)_2 + CO_2 + H_2O \quad (36)$$

$$CaO + 2HNO_3 \rightarrow Ca(NO_3)_2 + H_2O \quad (37)$$

The MWP was added to nitric acid solution heated at 50ºC till the completion of reaction with regular stirring. The solution was kept for cooling and filtered using Whatman No. 42 filter paper. The unreacted waste settled down which was later filtered and characterized using XRD to confirm the separation of impurities from the waste. The two solutions of $Ca(NO_3)_2$ obtained after reaction with $CaCO_3$ and CaO was later used for the synthesis of hydroxyapatite (Hap) separately and named as MA-Hap 650 and MA-Hap 850 respectively according to the calcination temperature.

4.27.3. SYNTHESIS OF MA-HAP USING CONVENTIONAL METHOD (CM)

The conventional precipitation method was used for the synthesis of hydroxyapatite using marble waste powder and the schematic diagram is shown in figure 4-44. The solution of 0.32 M calcium nitrate obtained was used as a source of calcium nitrate. The solution of 0.19 M KH_2PO_4 was then added drop wise to the $Ca(NO_3)_2$ solution under constant stirring using magnetic stirrer (Model: 5MLH, Remi, India) with a controlled flow rate of 5 ml/min as shown in figure 4-44. All further steps were similar to that explained in previous chapter **Error! Reference source not found.** The adsorbent as further characterized using FTIR, XRD, SEM, TEM/EDS and TGA/DTA and comparative analysis of both the materials were accomplished.

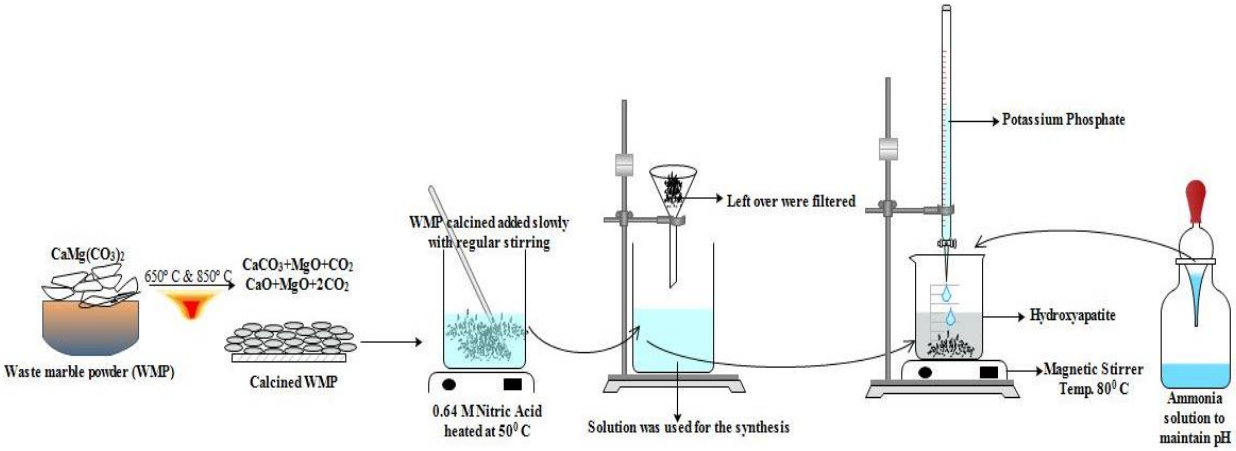

Figure 4-44. Schematic representation of synthesis of marble hydroxyapatite (MA-Hap) using CM method.

4.27.4. SYNTHESIS OF MA -HAP USING ULTRASONICATION METHOD (USM)

The solution of 0.32 M of 40 ml $Ca(NO_3)_2$ was subjected to sonication using an ultrasonic horn (Make: Sonics, USA, operating frequency; 20 kHz and rated output power 750 W) at 40% amplitude for 30 min with a 30 s pulse and 5 s relaxation cycle with drop-wise addition of 0.19 M of 60 ml KH_2PO_4 solution as shown in figure 4-45.

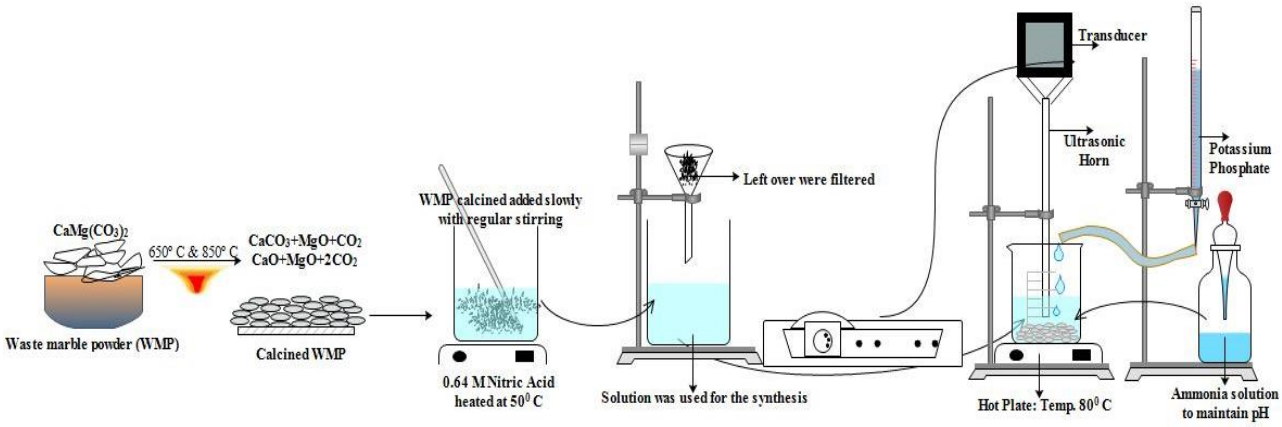

Figure 4-45. Schematic representation of synthesis of marble hydroxyapatite (MA-Hap) using USM method.

After complete addition of KH_2PO_4, the solution was again exposed to acoustic cavitation (by using ultrasonic horn) for further 15 min, 30 min and 45 min by keeping all sonication parameters constant (same as that was used during mixing), to observe the effect of time required to carry out the complete reaction of calcium nitrate with potassium dihydrogen phosphate to form hydroxyapatite. After optimization of time which was 60 min; the temperature of the reaction was maintained at $80^{°C}$ using hot plate during the synthesis in ultrasonication process. The rest of the procedure was same as described before in Section 4.20.3.

4.27.5. Reaction Scheme

The reaction scheme for the synthesis of Hap using calcium nitrate $(Ca(NO_3)_2$ obtained from WMP and potassium phosphate (KH_2PO_4) with ammonia solution (NH_4OH) as a base to maintain the pH is as follows:

$$10Ca(NO_3)_2 + 6KH_2PO_4 + 20NH_4OH \rightarrow Ca_{10}(PO_4)_6(OH)_2 + 6KOH + 20NH_4NO_3 + 12H_2O \quad (38)$$

4.27.6. Reaction Time and % Yield

The process time for synthesis of the conventionally synthesized (CM) MA-Hap 650 and MA-Hap 850 was 240 min while process time for synthesis of MA-Hap 650 using ultrasonication method (USM) method was 60 min (Table 4.17). The influence of acoustic cavitation was apparent reason for the reduction in the synthesis time because of rapid

micromixing and faster reaction. The percentage yield was estimated on the basis of theoretical and the actual weight of the product obtained after complete drying and considering the initial weight of the reagents. The product yield with the use of ultrasonication method was 89.06% which is consistently higher compared to conventional method with 81.90% yield for the synthesis of MA-Hap.

Table 4.17 Reaction time and % yield of the conventionally and ultrasonochemically synthesized marble hydroxyapatite.

Method	Material	Reaction time (min)	Yield (%)
Conventional	MA-Hap 650 CM	240	78.90%
Ultrasonication	MA-Hap 650 USM	60	89.06%

4.28. CHARACTERIZATION OF MA-HYDROXYAPATITE (MA-HAP)

The adsorbent synthesized using CM and USM method were characterized as follows using FTIR, XRD (X'Pert Powder Panalytical, CuKα radiations), TGA and DTA, SEM, TEM/EDS, TGA/DTA and BET surface area.

4.28.1. XRD OF UNREACTED MARBLE WASTE POWDER

During the addition of calcined marble waste powder into preheated nitric acid solution, calcium present in marble waste reacted to form calcium nitrate but rest of the impurities were settled down and later filtered out in order to obtain pure calcium nitrate solution. The unreacted marble waste was characterized using XRD analysis as shown in figure 4-46 to confirm the separation of impurities. Major peaks of magnesium oxide and calcium magnesium silicate indicate that these compounds have remained unreacted and separated out from the solution. Magnesium silicate were also present in the left out powder which was present in case of marble apatite as an impurity along with hydroxyapatite as observed in section 4.21.2. These observations make a clear picture that most of the impurities present in the marble waste powder remained unreacted and

pure solution of calcium nitrate was obtained which was used for the synthesis of hydroxyapatite using both conventional and ultrasonication method.

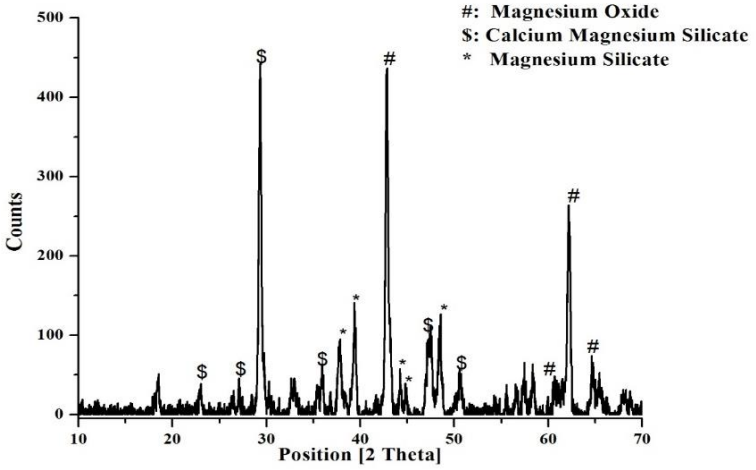

Figure 4-46. XRD spectra of unreacted marble waste powder.

4.28.2. FTIR OF MA-HAP

FTIR spectra of MA-Hap synthesized by conventional and ultrasonication method is shown in figure 4-47. The formation of Hap was denoted by the phosphate band centered from about 1000 to 1100 cm^{-1}. Sharp narrow peaks in the range of 600 cm^{-1} and 3500 cm^{-1} refer to structural OH- groups. Under the influence of thermal treatment, absorption band of physically adsorbed water becomes narrower as seen in figure 4-47a and figure 4-47b. In conventional method, temperature was maintained at 80 ºC and hence the bands were narrower as compared to MA-Hap synthesized using ultrasonication method (figure 4-47c). The pH during the synthesis of hydroxyapatite was maintained using ammonia solution, hence characteristic peak at 1400 cm^{-1} corresponds to NH_4^- group. Similar characterisitic peaks were observed in MA-Hap 650 CM, MA-Hap 850 CM and MA-Hap 650 USM. The presence of PO_4^{3-} and O-H group in FTIR spectra of MA-Hap synthesized using conventional method and ultrasonication method confirmed that Hap was being formed and further validation was done using XRD analysis.

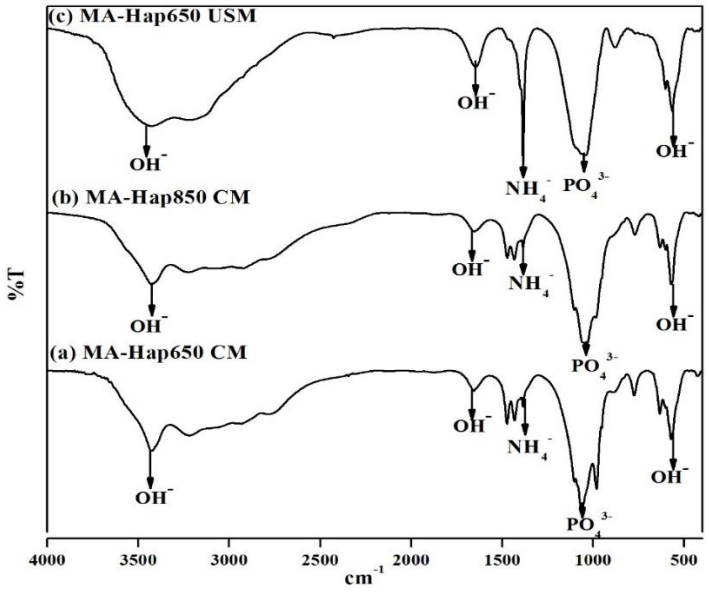

Figure 4-47. FTIR spectra of marble hydroxyapatite synthesized using (a&b) CM method (c) USM method.

4.28.3. XRD OF MA-HAP CM

X-ray powder diffraction (XRD) was primarily used for phase identification and average bulk composition of a material. The XRD patterns for the synthesis of MA-Hap 650 and MA-Hap 850 CM are shown in figure 4-48. The purity of hydroxyapatite synthesized by utilizing calcium nitrate which was prepared from marble waste powder calcined at 650º C and 850ºC was analyzed. It was observed that, major peak in both the spectra were of hydroxyapatite and phase identification of synthesized MA-Hap 650 CM and MA-Hap 850 CM exactly matched with the diffraction patterns with JCPDS card no. 00-001-1008. figure 4-48b depicts that MA-Hap 850 synthesized through conventional method (CM) contain few intermediate phases of calcium phosphate hydrate (JCPDS card no. 00-015-0204) but the major peaks were of hydroxyapatite. Whereas, in XRD spectra of MA-Hap 650 CM all the peaks were of hydroxyapatite with no impurities and no intermediates were observed as seen in figure 4-48a. It was attributed from the results that calcium nitrate prepared from MWP calcined at 650 ºC and its utilization will result in pure hydroxyapatite, and hence there is no further need of calcination. There was no major difference between the two product i.e. MA-Hap 650 CM and MA-Hap 850 CM

other than the few intermediates, due to this MA-Hap 650 CM was taken into consideration for further studies.

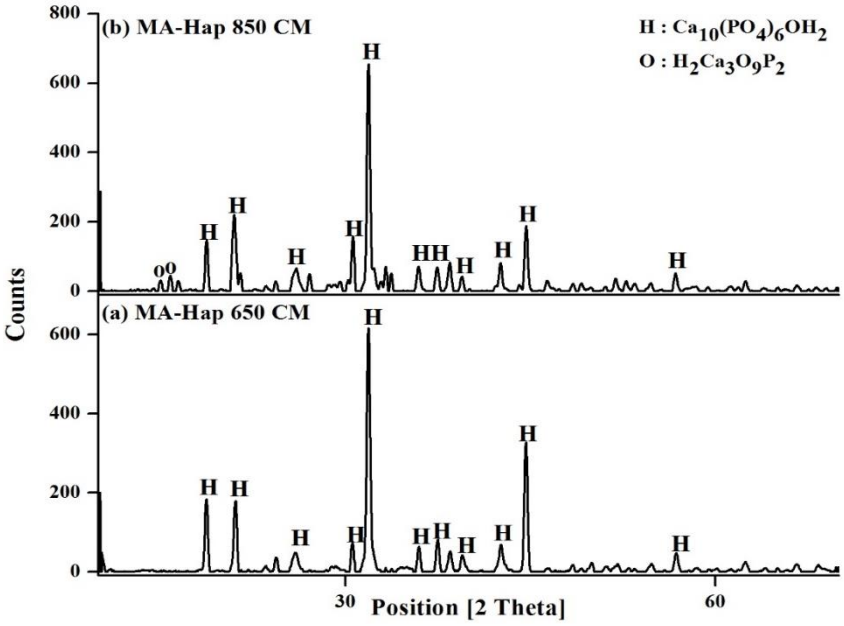

Figure 4-48. XRD spectra of marble hydroxyapatite synthesized using CM method when (a) MW calcined at 650ºC (b) MW calcined at 850ºC

4.28.4. XRD OF MA-HAP 650 USM

The XRD patterns of MA-hydroxyapatite samples prepared by ultrasonication method (USM) are shown in figure 4-49. Ultrasonication method was used for the synthesis of hydroxyapatite and effect of sonication time on the synthesis of MA-Hap was analyzed. It was observed from the figure 4-49a that during the sonication for 45 min major peak was of hydroxyapatite but few of the intermediates were also formed which can be attributed to the fact that due to insufficient sonication time the reaction was not completed and hence intermediates were observed. As the sonication time was increased to 60 min, a comprehensive phase transformation occurred as all the peaks matched with the diffraction patterns with JCPDS card no. 00-001-1008 and pure Hap was obtained as shown in figure 4-49b. It can be attributed to the influence of ultrasonication in the process, as increase in sonication time, the impact of sonication was increased which ensured efficient micromixing of the reactants in the reaction system. Acoustic cavitation

also causes an increase in the effective surface area, resulting in intensification of the chemical reaction due to improved mass transfer at the molecular level. It was observed from figure 4-49 c that, beyond 60 min of sonication, few peaks of calcium phosphate hydrate was observed which implies that excess sonication causes the breakdown of the material, and hence intermediates were formed.

During sonication the temperature of the material was gradually increased to 72 ºC. In case of conventional precipitation method, temperature was maintained at 80 ºC for the synthesis of hydroxyapatite. In order to check the effect of temperature in ultrasonication method, temperature was maintained at 80 ºC during the synthesis of MA-Hap 650 USM. It was observed from the figure 4-49d that with the major peak of hydroxyapatite, few intermediates were formed which was attributed to the fact that at higher temperature the magnitude of the cavity collapse would be high that would lead to the breakdown of the material. As per the results obtained from the XRD spectra, 60 min sonication time was optimized for the synthesis of MA-Hap using USM method as pure form of hydroxyapatite was obtained.

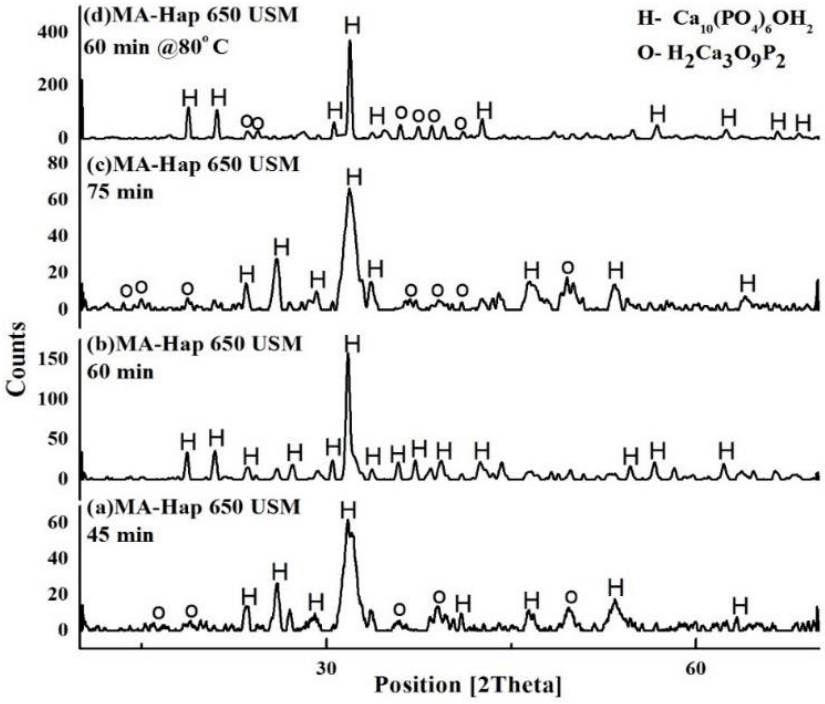

Figure 4-49. XRD spectra of marble hydroxyapatite synthesized using USM method at (a) 45 min (b) 60 min (c) 75 min (d) 60 min @ 80ºC.

4.28.5. COMPARATIVE XRD ANALYSIS OF MA-HAP 650 CM AND MA-HAP 650 USM

The comparative XRD analysis of MA-Hap 650 synthesized using conventional and ultrasonication method is shown in figure 4-50. XRD pattern of synthesized MA-Hap for both CM and USM process exactly matched with the diffraction pattern of Hap. It was also observed that there is difference in the type of crystalline phase in the two products as peaks at different crystal planes matches exactly with each other. But due to ultrasonication, crystallinity of the product ranged substantially. It was found that CM synthesized MA-Hap showed more crystallinity than USM synthesized MA-Hap. This may be because of ultrasonication which facilitate faster reaction, and do not allow the nucleation and crystal growth to occur fully as well as ultrasonication prevents agglomeration of particles during the synthesis and maintained effective size distribution of Hap particles. The increase in randomness of the Brownian motion of MA-Hap molecules due to high energy dissipation rate caused by cavitation, did not allow regular crystal formation which reduced the ability of the molecules to remain stable in its lattice plan leading to the lowering of crystallinity. The peaks intensity of CM synthesized MA-Hap is more than the peaks intensity of USM synthesized MA-Hap which can be seen from figure 4-50a and figure 4-50b clearly indicating the presence of larger crystals for CM synthesized MA-Hap. Peak broadening in case of USM synthesized MA-Hap, clearly indicated that small nanocrystals are present in the samples.

The mean crystallite size of MA-Hap synthesized using different methods was also estimated using Debye-Scherer formula as shown in equation (3) and values are given in Table 4.18.

It was found that the average crystallite size of the USM synthesized MA-Hap was 21.93 nm which was considerably lower than the MA-Hap (73.1 nm) synthesized conventionally (CM). This may be because of fact that as the crystallinity reduces, its crystallite size is also reduced.

Table 4.18 Mean crystallite size of marble hydroxyapatite synthesized using conventional method (CM) and ultrasonication method (USM).

Adsorbent	Wavelength (Å)	Peak Width (Degree)	Peak Position (Degree)	Crystallite Size (nm)
MA-Hap 650 CM	1.54056	0.1181º	31.8685	73.1 nm
MA-Hap 650 USM	1.54056	0.3936º	31.7376	21.93 nm

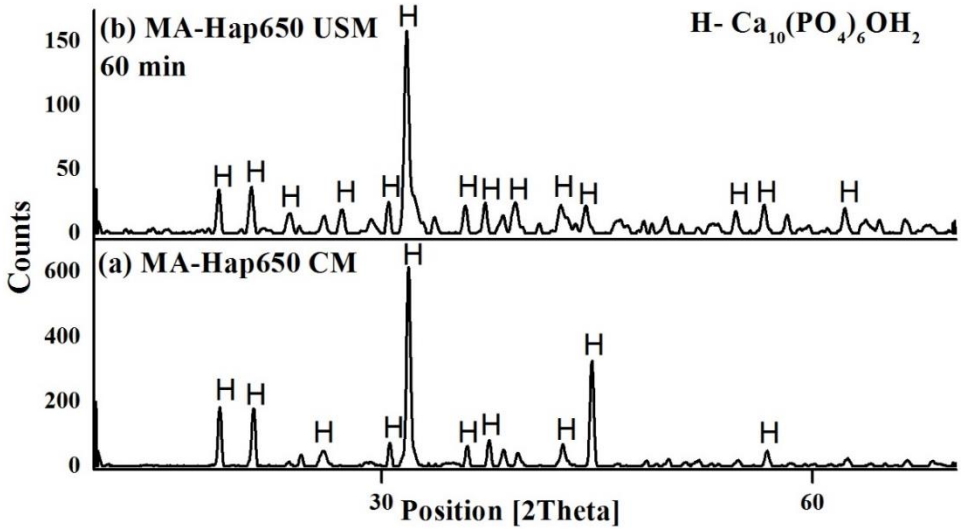

Figure 4-50. Comparative analysis of marble hydroxyapatite synthesized from MW calcined at 650ºC using (a) CM method (b) USM method

4.28.6. SEM ANALYSIS

The morphology, surface characteristics as well as crystallographic information of MA-Hap synthesized using conventional and ultrasonication method was analyzed from the results of SEM. From the SEM micrographs of conventionally synthesized MA-Hap 650 and MA-Hap 850 shown in figure 4-51a and figure 4-51 b. It was observed that there was no major difference in the surface morphology of both products which was when compared with same magnification at 200,000 X. This observation also supported the results obtained from XRD analysis. In both MA-Hap 650 CM and MA-Hap 850 CM, the particles were spherical in shape which was uniformly distributed throughout the surface. In order to make more clear observation, samples were analyzed upto their maximum magnification i.e. the spectra for MA-Hap 650 CM was analyzed upto 300,000 X whereas MA-Hap 850 CM was analyzed upto 400,000 X

magnification which is depicted in figure 4-51c and figure 4-51d respectively. On higher magnification too, no difference between the surface morphology of both materials was observed.

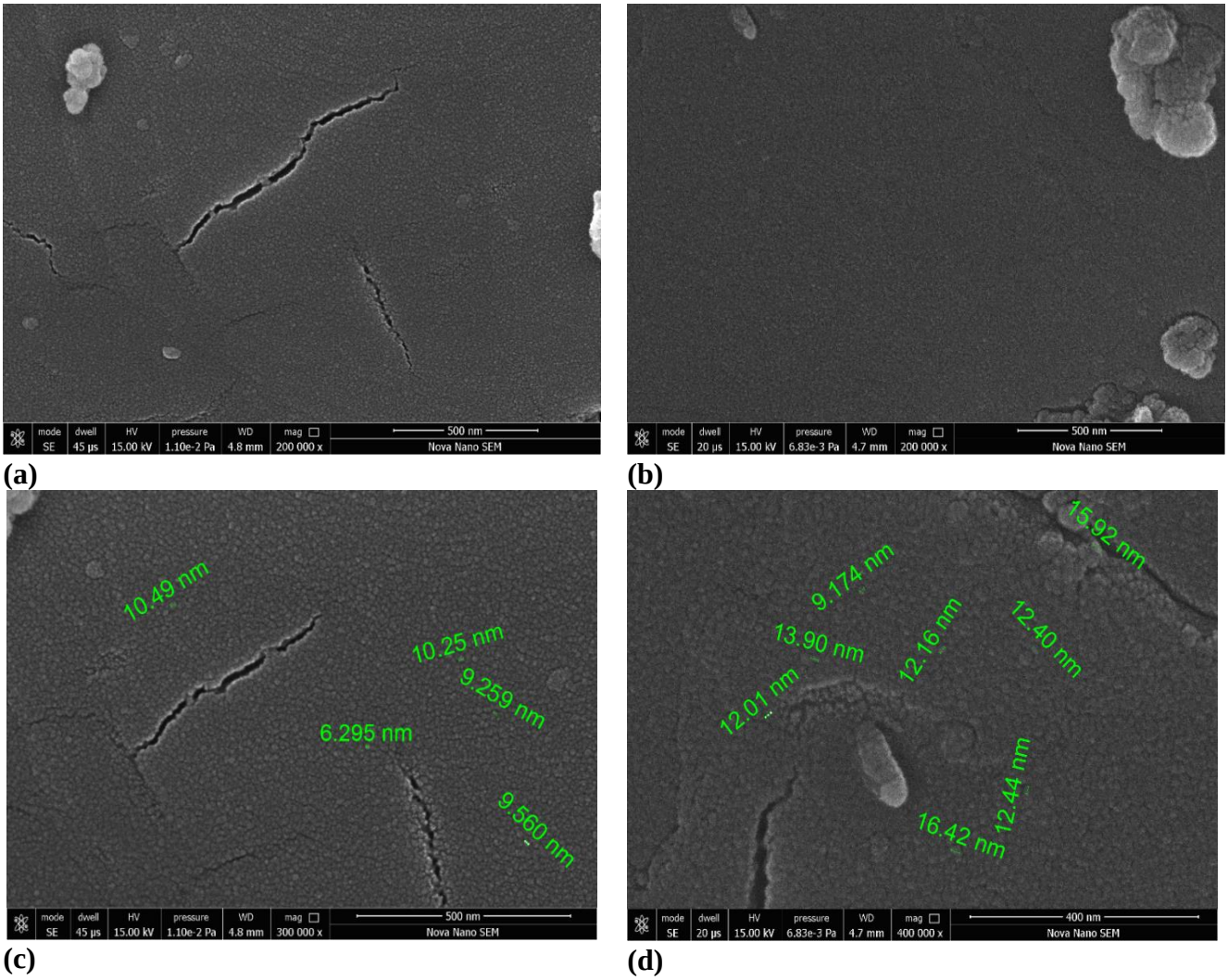

Figure 4-51. SEM micrograph at 200000 X magnification (a) MA-Hap 650 CM (b) MA-Hap 850 CM (c) MA-Hap 650 CM 300,000 X magnification (d) MA-Hap 850 CM 400,000 X magnification

The SEM spectra of MA-Hap synthesized using ultrasonication method (USM) was also compared with MA-Hap 650 CM synthesized conventionally at the same magnification of 100,000 X (figure 4-52a and figure 4-52 b). The USM synthesized MA-Hap showed not only comparatively smaller particle sizes as per the scale of SEM spectra but also considerably prominent spherical shaped morphology. From the low and high-magnification SEM images of MA-Hap 650 USM (figure 4-52b and figure 4-53b) we can

observe that evenly dispersed and uniform nano-spherical shaped particles were prepared by using ultrasonication approach. The influence of ultrasonication in reducing the particle size not only helped in improving material properties by increasing the effective surface area but also helped in formation of different types of crystal. More detailed analysis was done using TEM analysis for both the products.

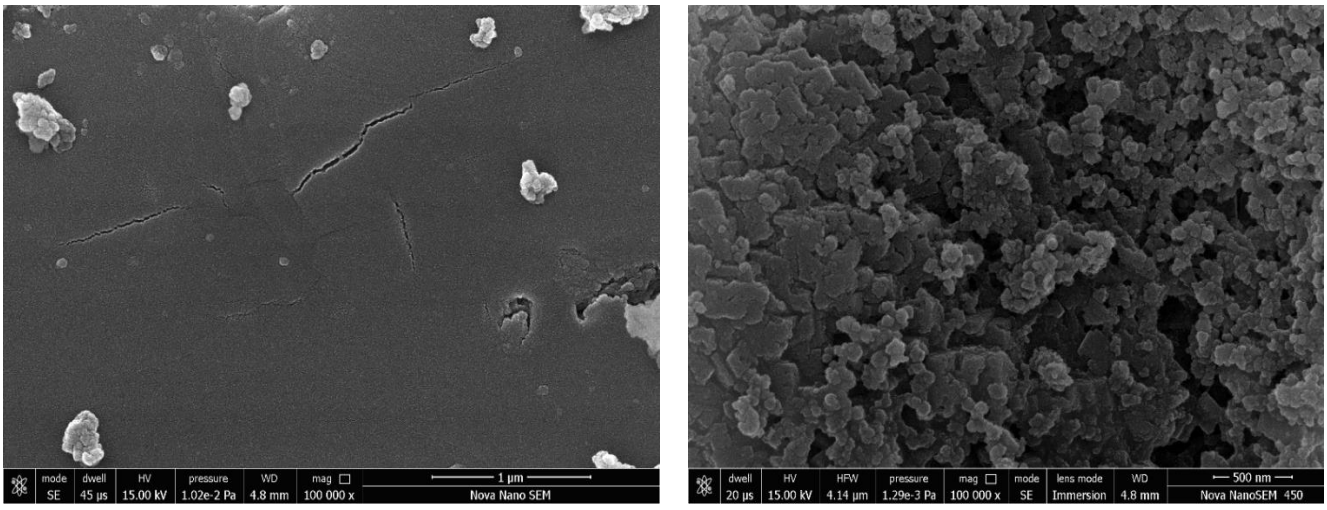

(a) **(b)**

Figure 4-52 SEM micrograph at 100000 X magnification (a) MA-Hap 650 CM (b) MA-Hap 650 USM.

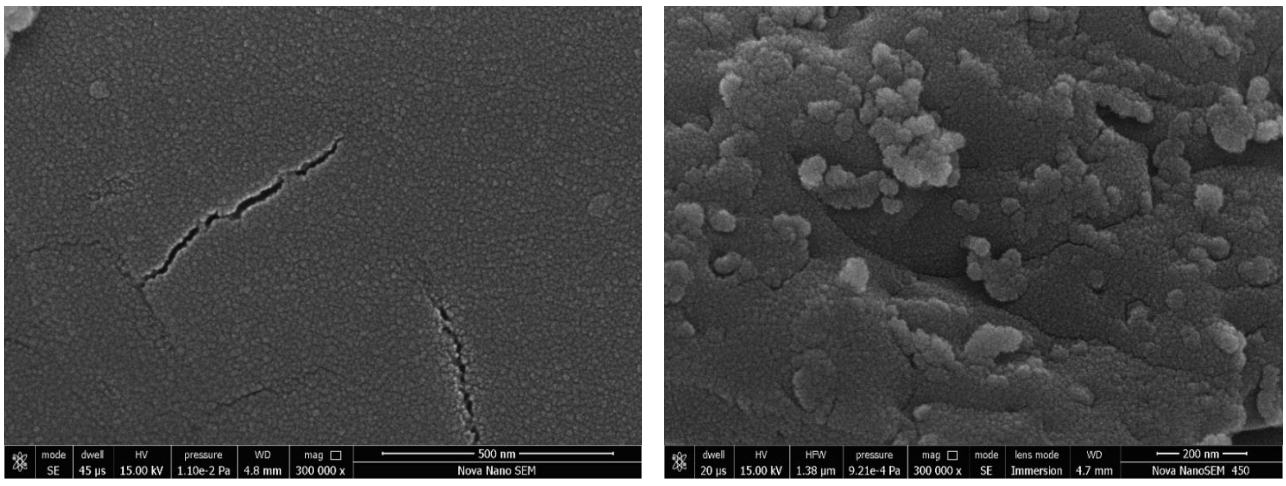

(a) **(b)**

Figure 4-53. SEM micrograph at 300000 X magnification (a) MA-Hap 650 CM (b) MA-Hap 650 USM.

4.28.7. TEM/EDS ANALYSIS

TEM images of MA-Hap synthesized by conventional and ultrasonication method is reported in figure 4-54. It was observed from the TEM micrographs that needle

like morphology of MA-Hap was obtained when synthesized using conventional and ultrasonication method. The average length of the needles has been observed to be around 6 nm (figure 4-54a). The obtained TEM results are consistent with that of marble apatite synthesized using conventional method in the previous chapter part III. There is significant reduction in size of the particles of MA-Hap 650 USM as shown in figure 4-54b when ultrasonication method was used. Moreover, significant reduction in agglomeration was observed, which is due to the effect of ultrasonic irradiation. Further, the particle size was controlled by providing smaller induction period and better control of the growth rate of crystal because of the presence of cavitation during chemical precipitation method.

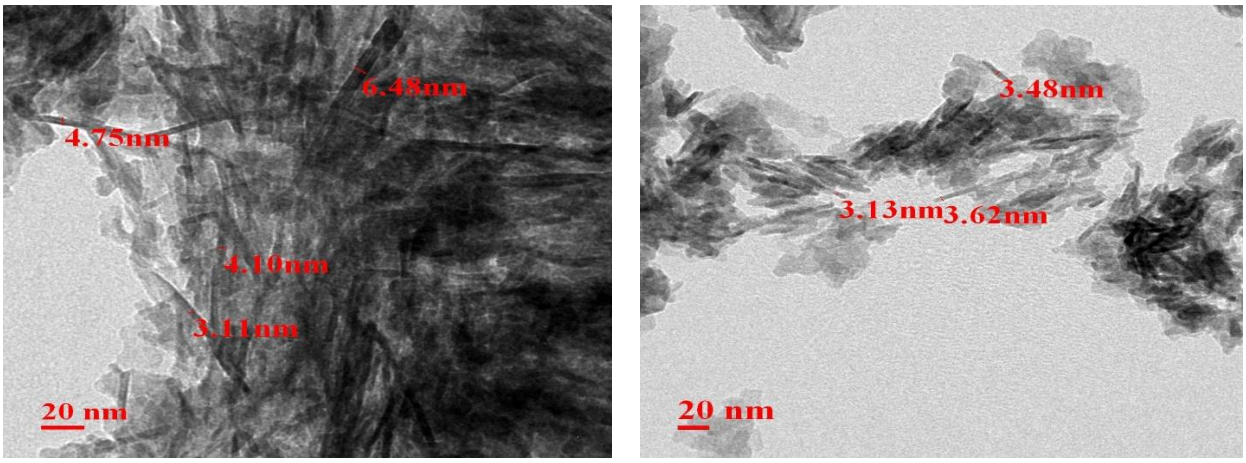

(a) **(b)**

Figure 4-54. TEM analysis (a) MA-Hap 650 CM, (b) MA-Hap 650 USM 60 min

The EDS spectra of MA-Hap 650 CM and MA-Hap 650 USM 60 min is shown in figure 4-55 respectively to analyze the elemental composition of the material synthesized. It was observed that other than calcium and phosphorous which are the primary reagents used for synthesis, no other impurities were present as were observed in case of marble apatite in previous chapter. Other than this no impurities were present in case of MA-Hap 650 CM and MA-Hap 650 USM 60 min, hence pure hydroxyapatite was obtained using marble waste powder from conventional and ultrasonication method.

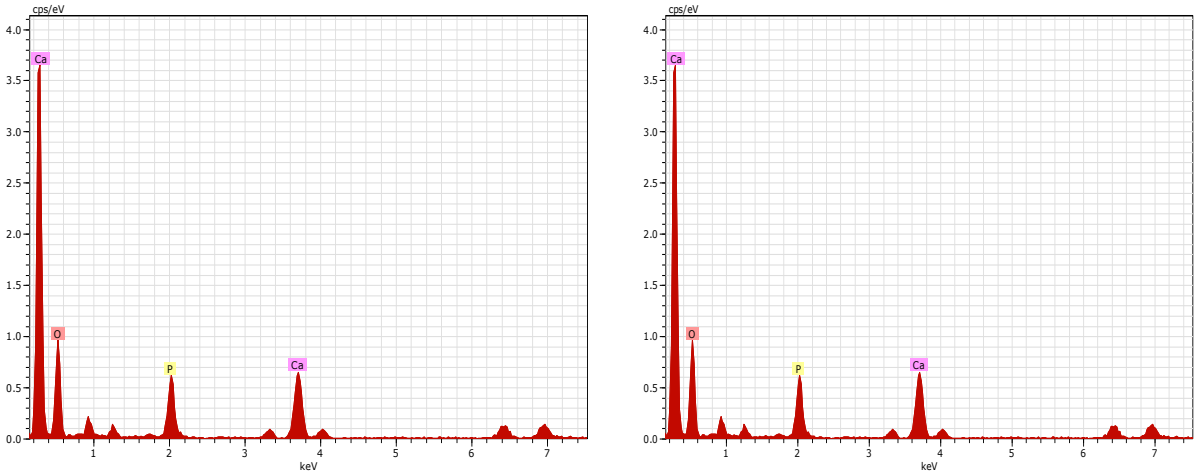

(a) **(b)**

Figure 4-55. EDS spectra of (a) MA-Hap 650 CM, (b) MA-Hap 650 USM 60.

4.28.8. TGA/DTA

The TGA-DTA curves as shown in figure 4-56 demonstrates three main weight losses in the temperature range from 35 ºC to 102.59 ºC, 160.50 ºC to 309.32 ºC and 613.59 ºC to 689.85 ºC which corresponds to endothermic peak at 102.59ºC (weight loss 2.66%) due to loss of surface water, 239.4 ºC (weight loss 8.12%) attributed to the conversion of hydrogen phosphates into pyrophosphates and 642.09 ºC (weight loss 7.47%) respectively in the DTA curve. At temperature above 500 °C, the structure of hydroxyapatite had lost OH ions and converted to β−tricalcium phosphate. The results of TGA/DTA were comparable to that of pure Hap.

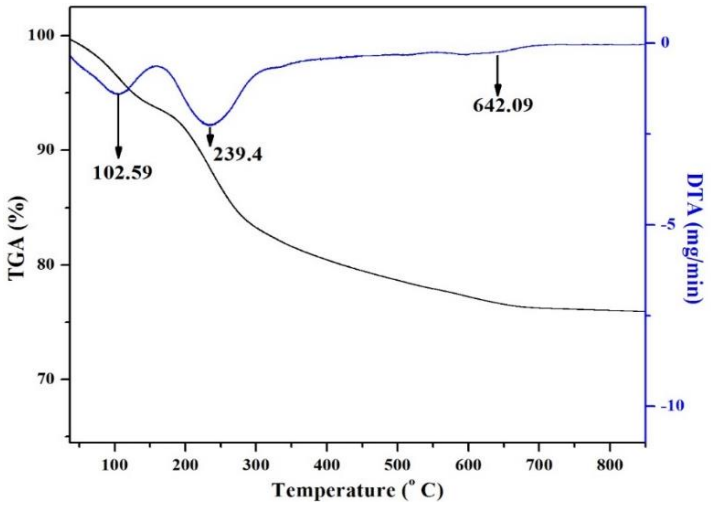

Figure 4-56. TGA-DTA plot of marble hydroxyapatite.

4.28.9. BET SURFACE AREA

The BET surface area of MA-Hap 650 CM and MA-Hap 650 USM were 31.19 and 44.92 m^2/g. The increase in surface area of MA-Hap 650 USM was because of decrease in particle size after ultrasonication process.

4.29. BATCH DEFLUORIDATION STUDIES

Batch defluoridation studies were carried out using adsorbents MA-Hap 650 CM, MA-Hap 850 CM and MA-Hap 650 USM 60 min in order to check the removal efficiency of fluoride.

4.29.1. EFFECT OF SORBENT DOSE

To fix the optimum dosage for fluoride removal using MA-Hap, experiments were carried out with dosage ranging from 0.5 g/L-12 g/L for treating initial fluoride concentration of 10 mg/L and the results are as shown in figure 4-57. It was observed that with increase in adsorbent dosage, percentage removal was increased. In case of MA-Hap 650 CM and MA-Hap 850 CM dose was optimized to 7 g/L whereas dose was optimized to 5 g/L for MA-Hap 650 USM.

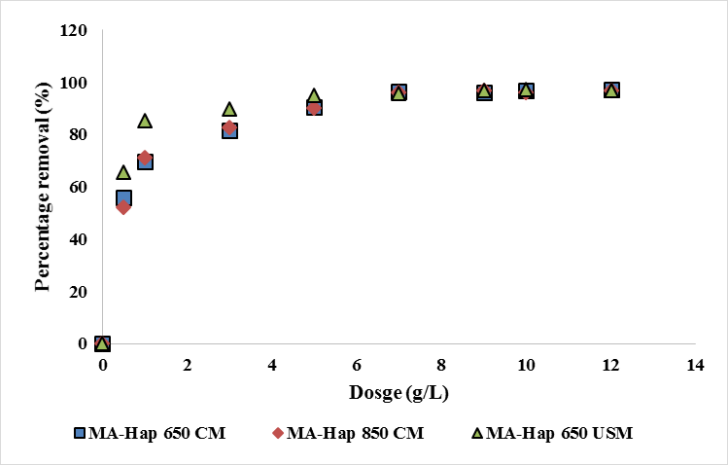

Figure 4-57. Effect of adsorbent dose on percentage removal (%) (F^- concentration: 10 mg/L, dose: 0.5-12 g/L, pH 7, temperature: 30 ± 0.5ºC).

The percentage removal was higher in case of MA-Hap 650 USM i.e. 95% of fluoride was removed with the capacity of 1.824 mg/g whereas adsorption capacity decreased in case of MA-Hap 650 CM and MA-Hap 850 CM to 1.331 mg/g as adsorbent dose was

increased from 2 to 14 g/L. The increase in capacity is due to effect of ultrasonication in reduction of particle size of the adsorbent which eventually increased the surface area and hence adsorption capacity was increased.

4.29.2. EFFECT OF CONTACT TIME

The effect of contact time on removal of fluoride by MA-Hap 650 CM, MA-Hap 850 CM and MA-Hap 650 USM for an initial fluoride concentration of 10 mg/L is shown in figure 4-58. With increase in contact time from 0 to 250 min, fluoride removal gradually increased. It was observed that saturation was reached in 20 min, and equilibrium was attained at 30 min for MA-Hap 650 CM and MA-Hap 850 USM whereas saturation was reached in 30 min, and equilibrium was attained at 60 min for MA-Hap 850 CM which was significantly less when marble apatite was used as an adsorbent as seen in pervious chapter. After 30 min there was no substantial increase in fluoride removal and hence it was considered as the optimum time for further studies.

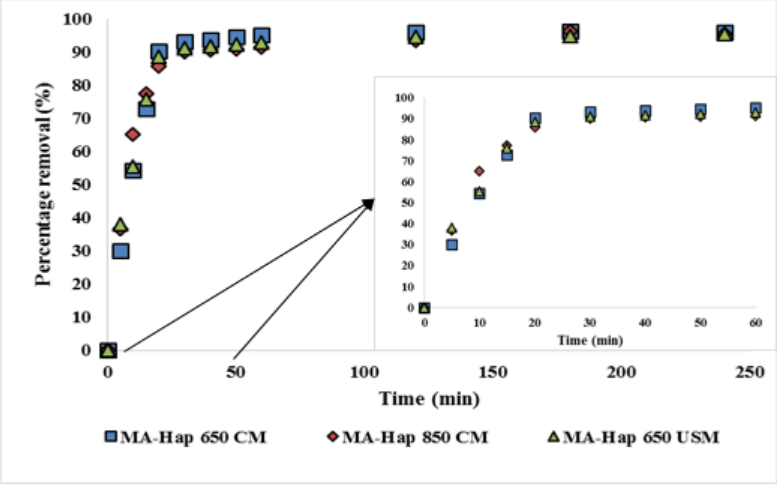

Figure 4-58. Effect of contact time on percentage removal (%), (F^- concentration: 10 mg/L, contact time: 15-240 min, dose: 7 g/L (MA-Hap CM) and 5 g/L (MA-Hap USM), pH 7, temperature: 30 ± 0.5ºC).

4.29.3. EFFECT OF pH

The effect of pH on fluoride adsorption by marble hydroxyapatite synthesized using CM and USM methods are shown in figure 4-59. Adsorption of fluoride was examined at various pH ranging from 3 to 11. Maximum removal was observed at pH 7 for all three adsorbents. In acidic range (< 5pH), fluoride removal was decreased, due to

the formation of weakly ionized hydrofluoric acid. As the pH was increased beyond 7 fluoride removal was decreased due to competition between F^- and OH^- ions for the active sites. This can also be explained by surface zero charge (pH_{PZC}) value for MA-Hap, which was found to be 8. pH_{PZC} of an adsorbent defines the pH at which net surface charge is neutral. Therefore, when pH <pH_{PZC} (8) MA-Hap will be positively charged and will attract the negative fluoride ions.

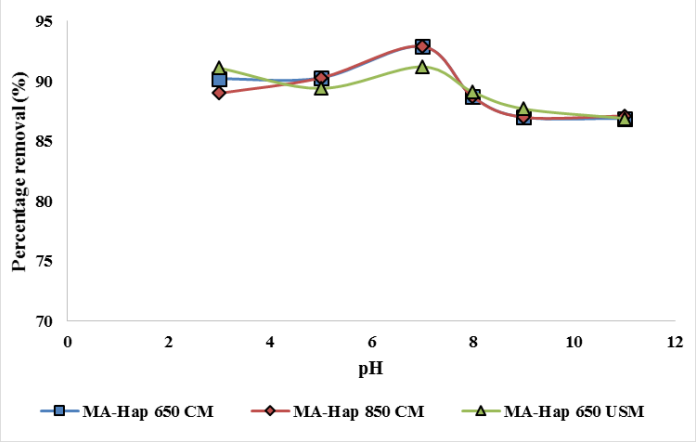

Figure 4-59. Effect of pH on fluoride removal (%), (F- concentration: 10 mg/L, contact time: 60 min (MA-Hap CM) & 30 min (MA-Hap USM), dose: 7g/L (MA-Hap CM) and 5 g/L (MA-Hap USM), pH 4-9, temperature: 30 ± 0.5°C).

4.29.4. EFFECT OF CO-IONS

The Defluoridation capacity of MA-Hap 650, MA-Hap 850CM and MA-Hap 650 USM in the presence of competing ions like chloride, nitrate, phosphate sulphate and bicarbonate was experimentally verified. Concentration of anions was 100 mg/L with 10 mg/L as initial fluoride. From the figure 4-60 no significant influence on defluoridation capacity of the material in the presence of different anions was observed. It was observed that MA-Hap has been a selective adsorbent for fluoride and interference from other anions did not affect its adsorption capacity comprehensively, which is an added advantage compared to all other adsorbents evaluated so far.

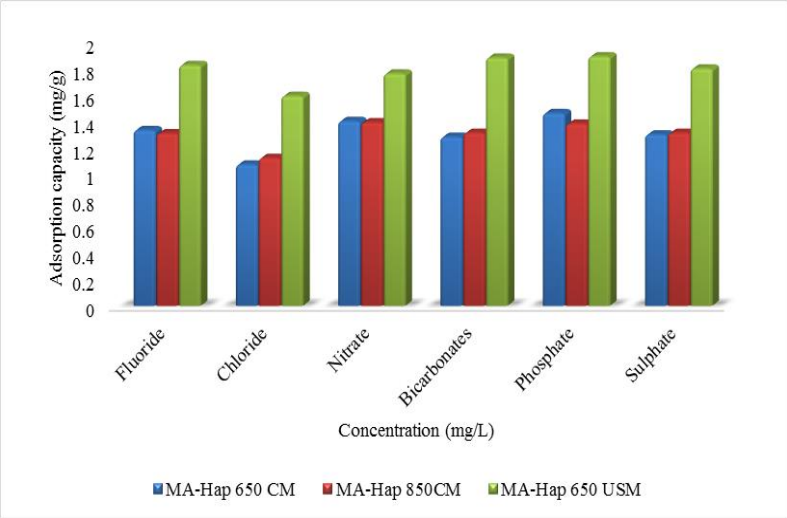

Figure 4-60. Effect of co-existing ions on adsorption capacity (mg/g).

4.29.5. ADSORPTION ISOTHERMS

Adsorption isotherms studies were done by fitting Langmuir, Freundlich, Temkin and Dubinin-Raduschkevich models to describe the relationship of adsorbed fluoride on the surface of adsorbent and the equilibrium concentration of fluoride in the medium. The isotherm constants were calculated and are summarized in Table 4.19. The R^2 and χ^2 values for both the adsorbents were determined and they fitted best with the Langmuir isotherm model indicating a monolayer adsorption. The Langmuir adsorption capacity for MA-Hap 650 CM and MA-Hap 650 USM was 3.137 mg/g and 4.557 mg/g respectively.

The experimental data fitted comparatively well with Langmuir isotherm model for both the adsorbents, which is evident from smaller χ^2 value and R^2 value close to unity, which represent homogeneous distribution of active sites on the adsorbents surface and monolayer adsorption.

Table 4.19 Adsorption isotherm for defluoridation using MA-Hap 650 CM and MA-Hap 650 USM.

Isotherms	**Parameters**	**MA-Hap 650 CM**	**MA-Hap 650 USM**
	q_{exp} (mg/g)	1.331 mg/g	1.824 mg/g

Langmuir	q_{max} (mg/g)	3.137	4.559
	k(L g^{-1})	0.877	1.462
	R^2	0.996	0.9907
	χ^2	0.27	0.025
Freundlich	1/n	0.4315	0.4602
	n	2.317	2.172
	k_F (mg/g)	1.28	1.7061
	R^2	0.9014	0.9199
	χ^2	0.011	0.003
Temkin	A_T (L/mg)	4.423	8.019
	B_T	1.5552	1.1109
	R^2	0.9773	0.9773
	χ^2	0.62	0.2
Dubinin-Raduschkevich	q_d (mg/g)	0.6404	0.5908
	B	-7E-08	-6E-08
	R^2	0.9361	0.8663
	χ^2	0.82	0.43

4.29.6. ADSORPTION KINETICS

Kinetics of fluoride adsorption on the surface of MA-Hap 650 CM and MA-Hap 650 USM were studied following three different kinetic models: pseudo-first order, pseudo-second order and intraparticle diffusion. Rate constant, R^2 and SSE values for pseudo first-order, pseudo second order and intraparticle diffusion are shown in Table 4.20.

Table 4.20 Kinetic parameters for MA-Hap 650 CM & MA-Hap 650 USM adsorbent

q_{exp} mg/g	**Pseudo-first-order Kinetics**				**Pseudo-second-order-Kinetics**			**Intraparticle diffusion**			
	K_1	q_e (mg/g)	R^2	SSE	K_2	q_e (mg/g)	R^2	SSE	R^2	K_i	**SSE**
MA-Hap 650 CM **(1.331 mg/g)**	0.472	19.63	0.7583	0.54	0.424	1.428	0.9976	2E-3	0.965	3.6193	**0.18**
MA-Hap-650 USM (1.824 mg/g)	0.167	2.4808	0.9065	0.12	1.949	1.9436	0.9992	1.34E-03	0.9213	2.6156	**0.15**

As mentioned before, higher correlation coefficient (R^2) values and lower SSE values depict a better fit of the kinetic model. The R^2 value for the pseudo-second order was

highest for both MA-Hap 650 CM (0.9976) and MA-Hap 650 USM (0.999) with lowest corresponding SSE value. Also, the calculated equilibrium capacity from the pseudo-second order is closer to experimental values. Therefore, it can be concluded that adsorption of fluoride on marble waste powder follows pseudo-second order adsorption kinetics. It implied that chemisorption process had taken place during the adsorption process.

4.30. WATER QUALITY PARAMETERS

The quality of water treated with MA-Hap 650 CM, MA-Hap 850 CM and MA-Hap 650 USM was analyzed in order to determine the feasibility of the adsorbents for practical applications. The values of various parameters such as total hardness, calcium, alkalinity, TDS, before and after treatment were studied with the permissible limit as given in figure 4-61. pH of the water after treating with MA-Hap 650 CM, MA-Hap 850 CM and MA-Hap 650 USM adsorbents were 7.12, 6.9 and 7.06 respectively. The conductivity of MA-Hap 650 CM, MA-Hap 850 CM and MA-Hap 650 USM were 785 , 935 712 µS/cm respectively while the permissible limit is 2000 µS/cm.

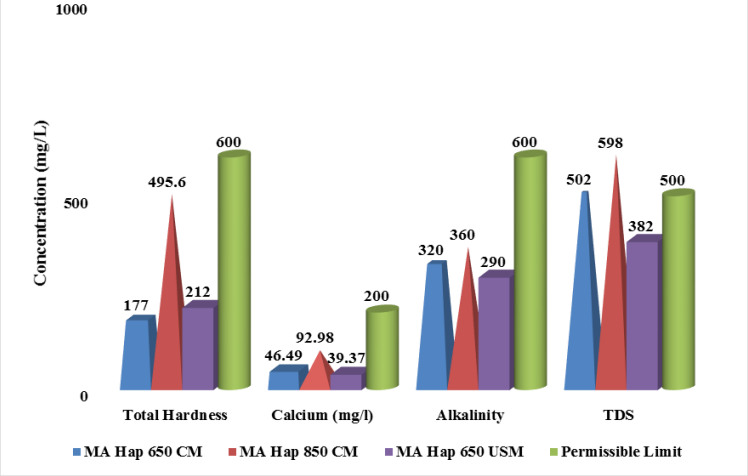

Figure 4-61. Treated water quality parameter analysis.

It was observed that hardness in case of MA-Hap 850 CM was 495.6 mg/L which was higher than other adsorbents but under the permissible limit (600 mg/L). Results showed that synthesized adsorbent can be used for treating fluoridated water as all the parameters were in permissible limit.

4.31. ENERGY EFFICACY

The energy efficacy for two synthesis methods i.e. conventional precipitation (CM) and ultrasonication (USM) method for obtaining MA-Hap has been estimated and the calculations are reported in Appendix A. The energy utilized for the synthesis of MA-Hap is the total energy supplied (kJ) per unit weight of the material processed/ obtained (g). The reaction time in conventional method was 4 h and for ultrasonication method was 60 min. Total energy required per unit weight of the material obtained to synthesize MA-Hap CM and MA-Hap USM method were 79.18 kJ/g and 774 J/g respectively. Thus, among the two methods, USM synthesis method proved to be an energy efficient method as compared to conventional method.

4.32. NOVELTY OF THE WORK

In previous chapter marble waste powder was utilized for the preparation of marble apatite which was primarily composed of hydroxyapatite. The limitation of the reported method was the presence of intermediates in the form of calcium phosphate and magnesium calcium silicate along with hydroxyapatite. So in order to prepare pure form of hydroxyapatite using marble waste powder another studies were required by using different approach.

- The present work reports an innovative method to prepare pure Hap using marble waste powder which is otherwise a huge problem for the environment.
- The problem of impurities in the form of intermediates is resolved and a novel method is developed to synthesis pure hydroxyapatite.
- To the best of our knowledge synthesis of pure marble hydroxyapatite (MA-Hap) utilizing marble waste from conventional precipitation method (CM) and ultrasonication method (USM) for its application in water defluoridation has not yet been reported.
- Different characterization techniques were used to compare the MA-Hap synthesized using CM and USM.
- The study also presents batch defluoridation experiments which were carried out by varying process parameters such as dose, contact time, pH and fluoride

concentration. The mechanism of adsorption was studied through different isotherm models, and kinetic studies were also discussed.

4.33. SUMMARY OF THE CHAPTER

- A method was successfully developed to synthesize pure hydroxyapatite from marble waste powder using conventional and ultrasonication method. The synthesis time for synthesis was decreased from 240 min to 60 min and yield was increased from 81.90% to 89.06% using USM approach. From the XRD analysis of MA-Hap CM, the best results were obtained when MWP was calcined at 650ºC and used for the preparation of calcium nitrate which was then used as calcium source for synthesis of MA-Hap. Alternatively, when ultrasonication was applied for 60 min pure MA-Hap 650 was obtained with the crystallite size of 21.93 nm which lower than that of MA-Hap 650 CM (73.1 nm). The SEM morphology of both the adsorbents possess spherical shaped particles whereas, TEM analysis depicted needle shaped morphology with the average size of 6 nm to 10 nm. The BET surface area of MA-Hap 650 USM was 44.92 m^2/g which was comparatively higher than (31.19 m^2/g) MA-Hap 650 CM. The higher surface area resulted in higher defluoridation capacity of MA-Hap 650 USM than that of MA-Hap 650 CM i.e. 1.824 mg/g and 1.331 mg/g respectively. The adsorption isotherm and kinetics for both MA-Hap 650 CM and MA-Hap 650 USM followed Langmuir model and Pseudo-second order kinetics respectively. Water quality parameters studied were in the permissible range making MA-Hap 650 CM and MA-Hap 650 USM a potent adsorbent for drinking water application.

  Hence, this study represents a simple but effective technique to synthesize marble hydroxyapatite from marble waste primarily composed of hydroxyapatite using ultrasonication method and utilize it for defluoridation of drinking water. Marble apatite can be a good alternative for defluoridation as it can be synthesized from marble waste which will lead to effective reuse of tons of marble waste generated, making it very cost effective and thus reducing the environmental threat of waste disposal.

CHAPTER 5

SYNTHESIS OF MA-HAP IN LAB REACTOR (MA-HAP LR)

Pilot scale synthesis of marble hydroxyapatite in a lab reactor and the characterization of material obtained is discussed in this chapter.

CHAPTER 5
SYNTHESIS OF MA-HAP IN LAB REACTOR (MA-HAP LR)

Synthesis of Hap nanoparticles in large scale is a challenging task due to agglomeration of particles which resulted in uncontrolled morphology. Various methods have been developed such as conventional chemical precipitation method, sol-gel method, hydrothermal method and ultrasonication method to synthesize Hap particles with controlled structures like nanorods, nanoparticles, plate-like, spherical etc. as explained in chapter 2. Also, the mechanical properties of biomaterials could be enhanced by the formation of single dimensional structure such as Hap nano-rods, nanotubes and nanofibres. Synthesis of Hap by conventional precipitation method has been extensively used because of the simplicity of the process, low cost and applicability in industrial production. The morphology of the Hap particles can also be controlled by controlling reaction parameters during the synthesis in the conventional precipitation method.

The aim of this work was to scale up the laboratory synthesis of marble hydroxyapatite to a pilot scale using a pilot scale lab reactor and to check the influence of main technological parameters such as temperature on the properties of the material synthesized. The advantages of semi-batch reactor includes flexible and simple operations such as addition of reagent, precipitation reaction and separation by settling of material in a single reaction tank. It has been observed from the results of previous chapter that MA-Hap 650 CM resulted in pure hydroxyapatite than MA-Hap 850 CM. Therefore, in this chapter studies focused only on synthesis of MA-Hap 650 in a lab reactor.

5.1. SYNTHESIS OF MA-HAP IN LAB REACTOR (MA-HAP LR)

A pilot scale lab reactor was used with the capacity of 100 Liters to scale up the synthesis process of marble hydroxyapatite. All the materials were similar which was used in the previous chapter as discussed in section 4.27.1. A fully controlled setup was fabricated which comprised of magnetic drive pump, peristaltic pump, mechanical stirrers, temperature controller with indicator, pH controller with dossing pump and manual top discharge centrifuge with the capacity of 20 L. The schematic representation of Lab reactor is also shown in figure 5-1.

Acid tank (20 L) which was fitted with mechanical stirrer and heating rod (1 kW) and calcium nitrate was prepared. Marble waste powder calcined at 650 ºC was added into the preheated (50 ºC) nitric acid solution with regular stirring. After the reaction was completed, the solution of calcium nitrate formed was allowed to cool at room temperature and unreacted marble powder was settled down. The calcium nitrate solution formed was then transferred to reactor tank using magnetic driven pump. After addition of calcium nitrate, potassium dihydrogen phosphate was added into a reactor tank with the controlled flow rate of 99 ml/min using peristaltic pump. The pH and temperature during the reaction was monitored and controlled by automatic pH controller with dossing pump and temperature controller respectively. The pH throughout the reaction was maintained at 9 whereas, effect of temperature on the properties of material was studied by synthesizing marble hydroxyapatite at 62 ºC, 72 ºC and 82 ºC and named MA-Hap LR 62, MA-Hap LR 72 and MA-Hap LR 82 respectively according to the synthesis temperature. As the reaction was proceeded, white colored suspension solution was formed which was left overnight and later transferred to manual top discharge centrifuge. The solution was centrifuged at 2000 rpm for 10 min and the precipitates obtained was washed with deionized water, dried at 110 ºC for 10-12 h in an hot air oven and was grounded to powdered form for further studies. The effect of temperature and properties of material synthesized was characterized using FTIR, XRD, SEM, TEM/EDS and BET surface area analyzer.

Synthesis of MA-Hap in Lab Reactor (MA-Hap LR)

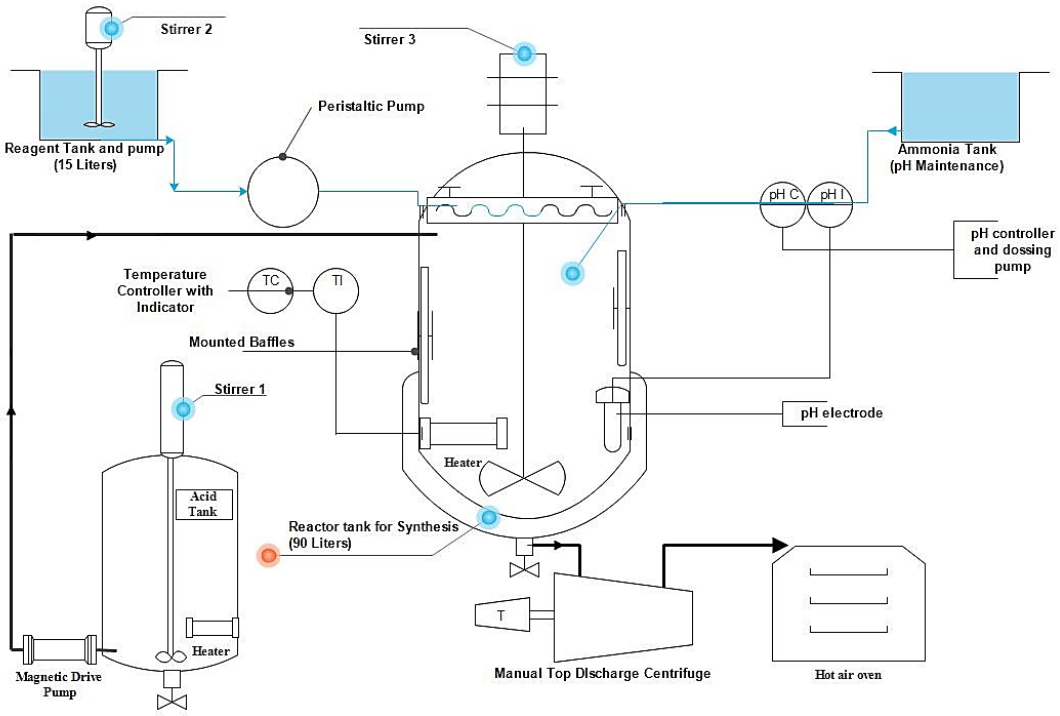

Figure 5-1. Schematic representation of Lab Reactor for the synthesis of MA-Hap LR.

5.2. CHARACTERIZATION OF MA-HAP LR

The effect of temperature and properties of marble hydroxyapatite synthesized in lab reactor was characterized using the Fourier transform infrared (FTIR), X-ray Diffraction analysis (XRD) (X'Pert Powder Panalytical, CuKα radiations), Scanning Electron Microscope (SEM), Transmission electron microscopy (TEM) and BET surface area.

5.2.1. FTIR OF MA-HAP LR

FTIR spectra of MA-Hap LR synthesized at different temperature is shown in figure 5-2. It was observed that all the peaks were similar in MA-Hap LR 62, MA-Hap LR 72 and MA-Hap LR 82. The sharp narrow peak in the range of 3400 cm^{-1} is of OH^- group whereas peaks in the range of 1000 cm^{-1} and 560 cm^{-1} refer to bending mode of PO_4^{3-} vibrations. Characteristic peak at 1400 cm^{-1} corresponds to NH_4^- group as it was used to maintain the pH during the synthesis of marble hydroxyapatite. The presence of PO_4^{3-} and O-H group in FTIR spectra of MA-Hap LR 62, 72 & 82 confirms that Hap was

being formed and further validation was done using XRD analysis. Similar peaks were observed when MA-Hap was synthesized at lab scale using conventional precipitation method as discused in section 4.28.2. The basic difference in the spectra of MA-Hap 650 CM is in the peaks in the range of 3400 cm^{-1}. This may be due to the higher temperatures which leads to broadening of OH^- bond as observed in Hap LR 72.

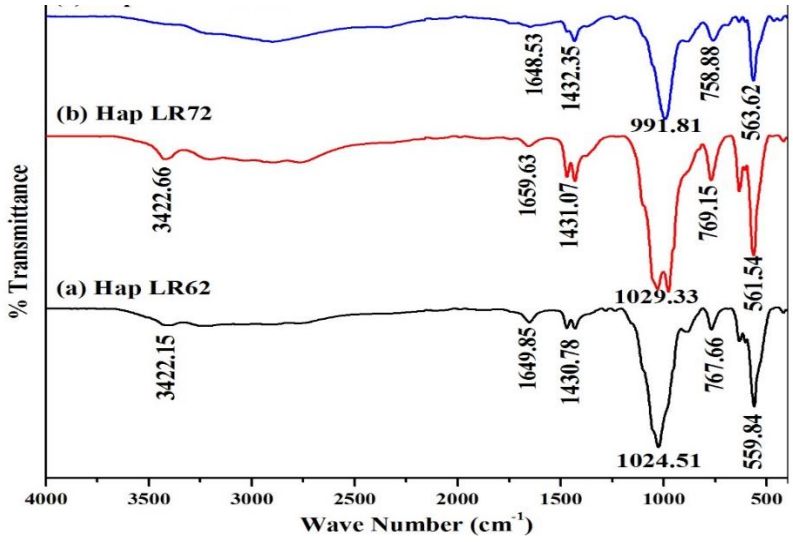

Figure 5-2. FTIR spectra of (a) MA-Hap LR 62, (b) MA-Hap LR 72 & (c)MA-Hap LR 82.

5.2.2. XRD OF MA-HAP LR

The crystallinity and effect of synthesis temperature of MA-Hap LR was analyzed by XRD technique. Diffraction patterns of all MA-Hap LR samples synthesized at different temperature, are shown in figure 5-3. It was observed that there was no major difference between the XRD spectra of MA-Hap LR 62, MA-Hap LR 72 and MA-Hap LR 82. The XRD patterns of synthesized samples was compared with the standard JCPDS data and the characteristic peaks of Hap were identified. There were few intermediate peaks corresponding to calcium phosphate phases when temperature during the synthesis of MA-Hap LR was 62 ºC (figure 5-3a). As the temperature was increased to 72 ºC, peaks corresponding to intermediate phases decreased significantly giving the pure hydroxyapatite phases. This can be attributed that on increasing the temperature, Brownian motion of the molecules increases which results in increase in chance of their

colliding with each other and hence completing the reaction with more efficiency. The average crystallite size was calculated from the XRD pattern using the Scherrer formula given in eq (3). The mean crystallite size (Table 5.1) of MA-Hap LR 62, MA-Hap LR 72 & MA-Hap LR 82 were 48.7 nm, 43.87 nm and 41.59 nm respectively.

Table 5.1 Mean crystallite size of MA-Hap LR 62, 72, 82 and pure hap synthesized in lab reactor

Adsorbent	Wavelength (Å)	Crystallite Size (nm)
MA-Hap LR 62	1.54056	48.76 nm
MA-Hap LR 72	1.54056	43.87 nm
MA-Hap LR 82	1.54056	41.59 nm
Pure Hap	1.54056	54.83

However with increase in temperature, the crystallite size was decreased which can due to nucleation of the particles. The results also indicates that the synthesized material is crystalline in nature as the intensity of the peaks increased with increase in synthesis temperature and maximum phases of hydroxyapatite was obtained.

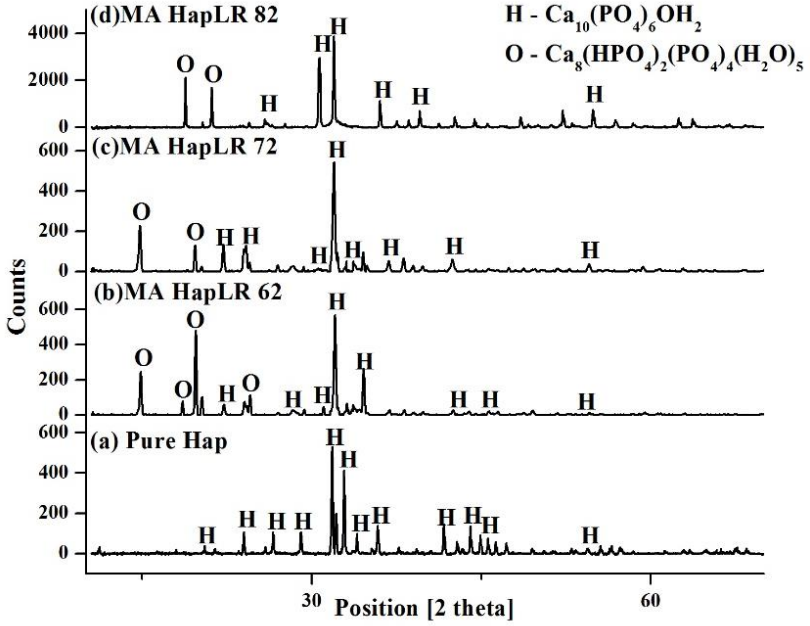

Figure 5-3. XRD spectra of (a) Pure Hap (b) MA-Hap LR 62, (c) MA-Hap LE 72 & (d) MA-Hap LR 82.

In case of batch scale synthesis process of MA-Hap CM, pure hydroxyapatite with no intermediates was obtained with the crystallite size of 24.36 nm whereas in the lab scale during the formation of MA-Hap LR 72 few intermediates such calcium hydrogen orthophohates were formed along with Hap and the crystallite size was 43.87 nm. There is no major difference between the XRD spectra of the two products. During laboratory scale synthesis, all the process parameters such pH, synthesis temperature and stirring speed were controlled whereas, in case of synthesis in the lab reactor, process parameters had a variations within ±20% and there were heat loses which could be the reason for the formation of intermediates.

5.2.3. SEM

The effect of reaction temperature is an important factor that can affect the morphology and the crystallinity of the synthesized material. The SEM micrographs of MA-Hap LR prepared at different temperature were compared with the same magnification of 100,000 X with the immersion mode as shown in figure 5-4(a-c). It has been observed that the synthesized MA-Hap LR 62 (figure 5-4a) were in the form of countless bundles of nanorod/needle like structure. According to the reports published, it was observed that at low temperature the particles are thin and longer in size with agglomerations due to Ostwald ripening process. Similar results have reported about the needle like morphology at low synthesis temperature which was confirmed by SEM results. As the synthesis temperature was increased to 72ºC and 82ºC (figure 5-4 b-c) distinguished changes in morphology of the material was observed. The size of the nanorods decreases as the temperature was increased which can be attributed to the fact that, increase in temperature overspent the Ostwald ripening and capillary force and induced nucleation which results in the formation of smaller and regular nano-rods. The increase in synthesis temperature leads to more regular and smaller Hap particles which can be clearly seen from figure 5-5(a-b) at a magnification of 200,000 X.

In case of MA-Hap synthesized via bench scale using conventional precipitation method, the particles were spherical in shape, distributed uniformly throughout the surface as discussed in section 4.28.6, whereas nano-rods type morphology was observed in case of MA-Hap synthesized via lab reactor. Change in morphology may be due to scale up of

the process and variation in synthesis parameters such as temperature and pH during the reaction. The possible cause for the variation in morphology due to temperature and pH may be due to the difference in the effective interaction of molecules with the surface of the crystals present in the reaction mixture.

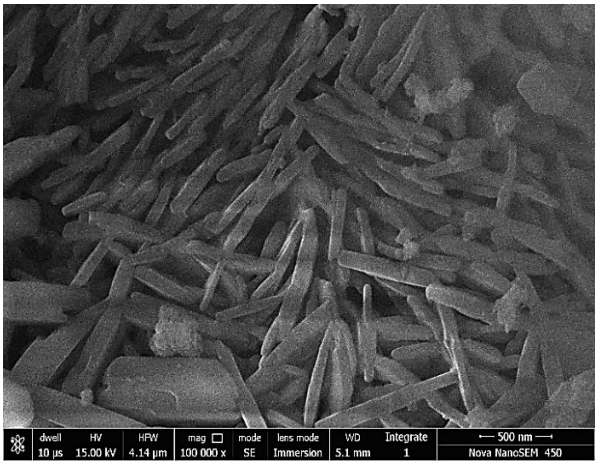

(a) MA-Hap LR 62

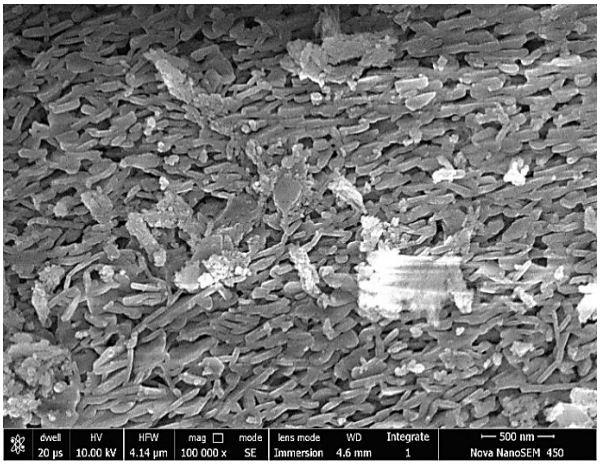

(b) MA-Hap LR 72

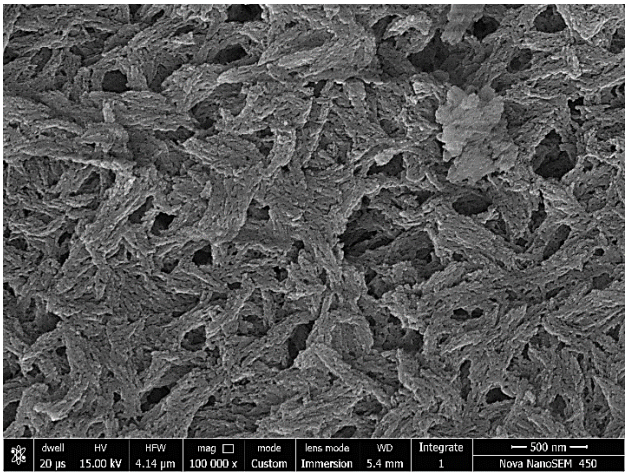

(c) MA-Hap LR 82

Figure 5-4. SEM micrographs at 100,000 X; (a) MA-Hap LR 62 (b) MA-Hap LR 72 (c) MA-Hap LR 82.

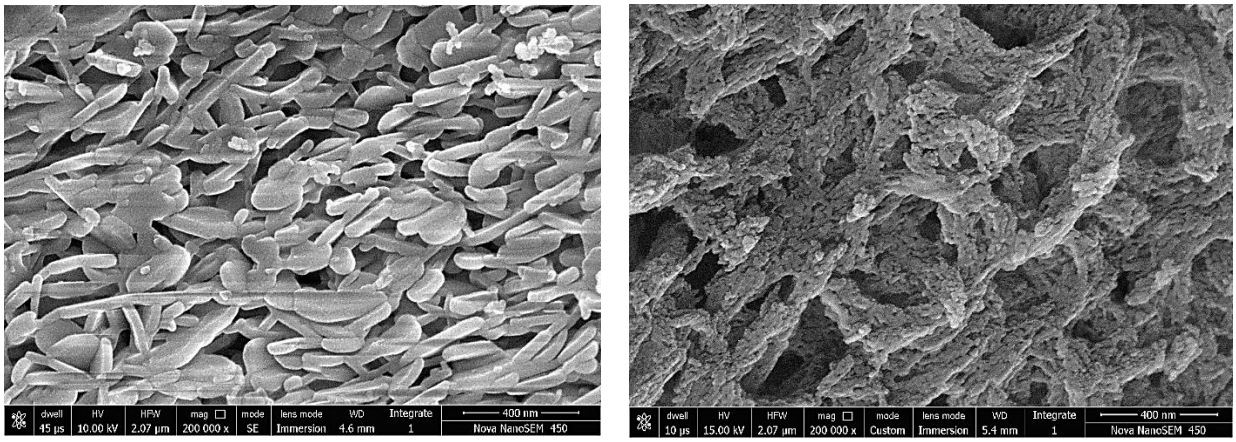

(a) MA-Hap LR 72 **(b) MA-Hap LR 82**

Figure 5-5. SEM micrographs at 200,000 X; (a) MA-Hap LR 72 (b) MA-Hap LR 82.

5.2.4. TEM

TEM study was performed to evaluate the difference in particle size and morphology of the material synthesized at different temperatures as shown in figure 5-6 (a-c). It has been observed from the TEM micrographs that, MA-Hap LR particles were randomly oriented with aggregated needle like morphology. TEM micrographs indicated, MA-Hap LR particles and MA-Hap were randomly oriented with aggregated needle like morphology. Similar results were obtained for both bench scale and Lab scale synthesis process as described in section 4.28.7. With increase in synthesis temperature, agglomeration between the particles were decreased with more prominent nano-needle shape (figure 5-6b & figure 5-6c). This can be attributed to nucleation and growth of the particles due to relative specific surface energies which regulate the OH^- quantity, associated with the different surfaces of hydroxyapatite crystal. It has been reported that on increasing the temperature morphology of particles changes in uniaxial direction. However, this phenomenon is not yet clear, further theoretical studies can be done to understand the complexity of growth mechanism of the particles. The average particle size of MA-Hap LR particles obtained from TEM was ~35 nm in length and 3 nm in width.

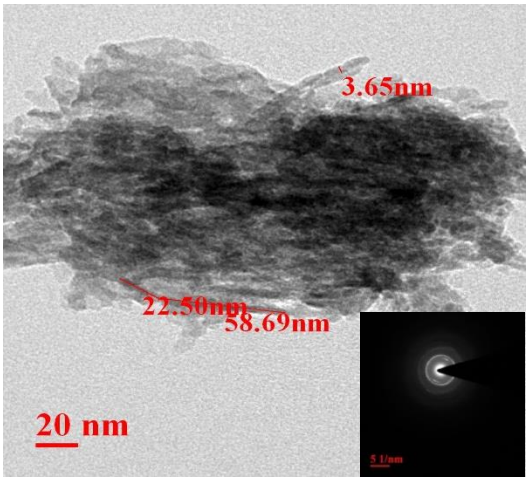

(a) MA-Hap LR 62

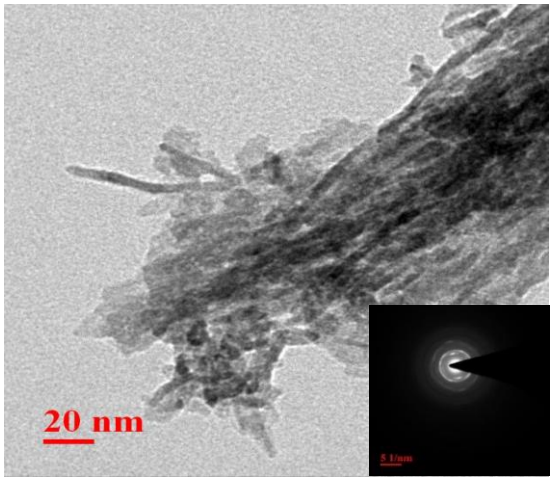

(b) MA-Hap LR 72

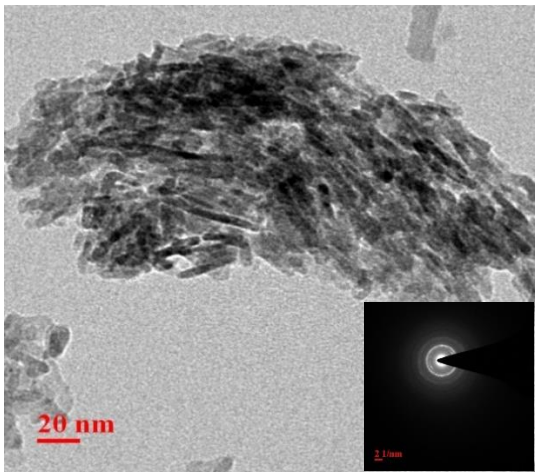

(c) MA-Hap LR 82

Figure 5-6. TEM Micrographs (a) MA-Hap LR 62, (b) MA-Hap LR 72 & (c) MA-Hap LR 82.

5.3. SUMMARY OF THE CHAPTER

Marble hydroxyapatite was successfully scaled up and synthesized in pilot scale lab reactor with the capacity of 60 Liters as shown in figure 5-7. MA-Hap LR was synthesized at different temperatures and 72ºC was optimized based on purity which was analyzed using FTIR and XRD analysis. The rod like morphology of MA- Hap LR 72 was obtained which was similar to pure Hap attributing that this methodology can be used for the preparation of rod-like hydroxyapatite. The synthesized MA-Hap LR 72 was pelletized can used for column studies.

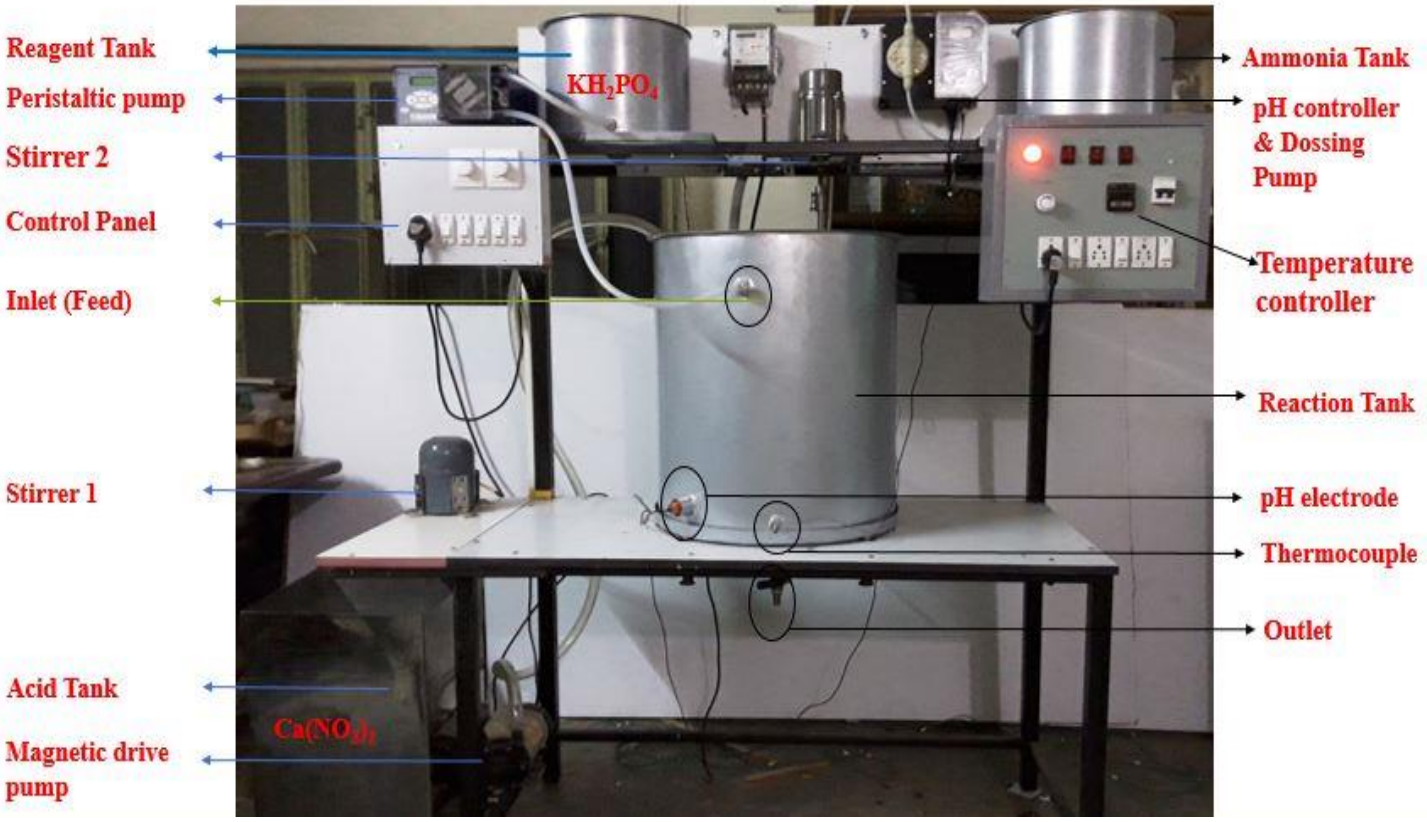

Figure 5-7. Pilot scale lab reactor for synthesis of MA-Hap LR

CHAPTER 6

PELLETS PREPARATION AND COLUMN STUDIES

The MA-Hap LR 72 synthesized using Lab reactor was pelletized using PVA as a binder for column defluoridation studies.

CHAPTER 6
PELLETS PREPARATION AND COLUMN STUDIES

In the previous chapter we have discussed the synthesis of MA-Hap in lab reactor for the preparation of pellets which can be used in column studies. This chapter focuses on the preparation of pellets which was also explained in section 3.5.1. Moreover, the practical feasibility of MA-Hap LR 72 pellets was checked by using them for column defluoridation studies for studying various parameters. Three kinetic models (Hutchins BDST model, Thomas model, and Yoon-Nelson model) were used to fit the adsorption data. In addition, the pellets which were prepared using extrusion-spheronization technique were analyzed in comparison with exhausted and regenerated MA-Hap LR 72 pellets and also characterized using FTIR, XRD and SEM studies. The eluent concentration required for the purpose of regeneration of exhausted pellets was also optimized based on characterization studies.

6.1. PELLETS PREPARATION

The MA-Hap synthesized in lab reactor was pelletized using Extrusion-Spheronization technique as explained in section 3.5.1 and the steps which are followed for the preparation are also elaborated in figure 3-2. The pellets formed were of different sizes which were segregated with respect to their size i.e. 2 mm to 2.5 mm and 2.5 mm to 3 mm which was later used for the column studies. The pellets formed, exhausted pellets and regenerated pellets were compared and characterized using FTIR, XRD and SEM analysis which is detailed in section 6.6.

6.2. COLUMN STUDIES

The continuous column experimental studies were done to evaluate the column performance for the removal of fluoride using MA-Hap LR 72 pellets prepared by using Extrusion- Spheronization technique. The column was operated in a continuous mode until the fluoride concentration overshoot 1.0 mg/L, which is maximum permitted limit in India. The effect of various parameters such as particle size, bed height, flow rate and initial fluoride concentration on the column performance was tested and presented in the form of breakthrough curves.

6.2.1. EFFECT OF PARTICLE SIZE

Column studies were conducted for two different particle sizes viz. 2 mm to 2.5 mm and 2.5 mm to 3 mm by keeping other operational parameters such as flow rate (1 LPH or 16 mL/min), bed height (25 cm) and inlet fluoride concentration (10 mg/L) constant. The breakthrough curves obtained for different particle sizes are shown in figure 6-1.

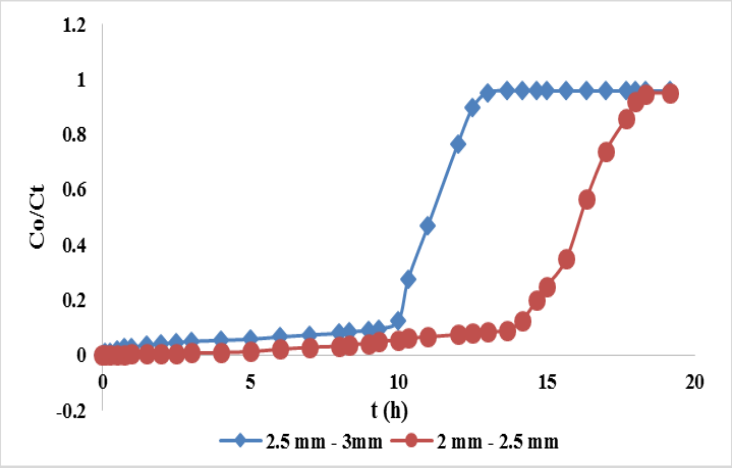

Figure 6-1. Breakthrough curve for fluoride adsorption onto MA-Hap LR 72 pellets of different particle size (flow rate= 1 LPH, bed height = 25 cm and initial fluoride concentration = 10 mg/L).

From the figure it was observed that with increase in particle size from 2.0 mm-2.5 mm to 2.5 mm -3 mm breakthrough time decreases considerably from 14 h to 10 h and breakthrough adsorption capacity decreases from 1.21 mg/g to 0.865 mg/g. this can

be attributed that smaller particle size have higher interfacial surface and therefore higher adsorption capacity. Whereas in large particle sizes, some of the interior pores are not accessible for adsorption resulting in lower capacity and faster breakthrough point. From the observation made, pellets of 2 mm-2.5 mm particle size were chosen for further experiments.

6.2.2. EFFECT OF BED HEIGHT

The effect of bed height on the breakthrough curve was determined by passing 10 mg/L of fluoride solution with the flow rate of 1LPH through the column by varying bed height. The breakthrough curve obtained for fluoride adsorption onto MA-Hap LR 72 pellets at different bed height i.e. 5 cm, 15 cm and 25 cm are shown in figure 6-2.

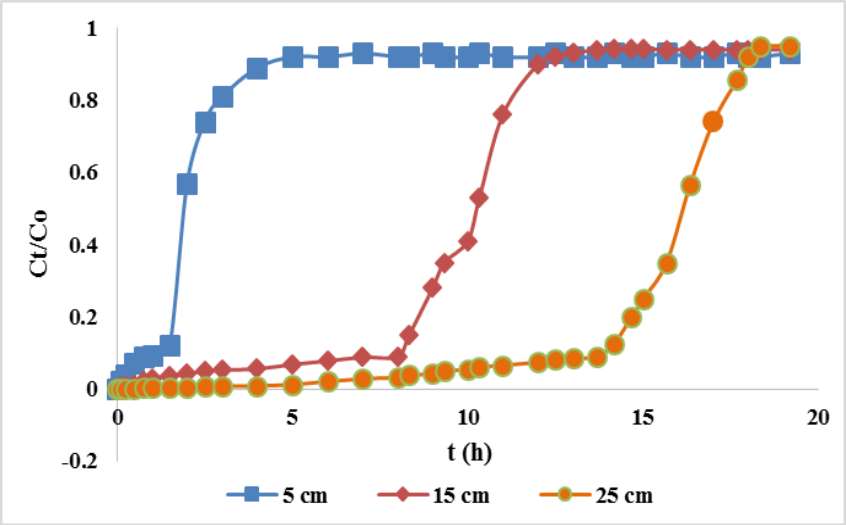

Figure 6-2. Breakthrough curve for fluoride adsorption onto MA-Hap LR 72 pellets at different bed height (flow rate= 1 LPH, initial fluoride concentration = 10 mg/L).

It was observed that breakthrough time increased from 1.5 h to 14 h with increase in bed height from 5 cm to 25 cm. With the increase in bed height, the residence time of fluoridated solution inside the column increased as the mass transfer zone moved slowly down the column, allowing the higher contact time and higher fluoride removal efficiency. The bed height is proportional to the mass of the adsorbent packed in the column which had increased number of adsorption sites with increase in bed height leading to higher adsorption capacity. Also, with increase in bed height surface area of

the adsorbent is increased, which provide more binding sites for the adsorption. The volume of solution treated upto breakthrough point is 1.5 L, 8 L and 14 L for 5 cm, 15 cm and 25 cm bed heights respectively while their corresponding breakthrough capacities are 0.64 mg/g, 1.1 mg/g and 1.21 mg/g. Hence, the bed height of 25 cm has higher adsorption capacity compared to other bed heights.

6.2.3. EFFECT OF FLOW RATE

The performance of the column in continuous mode study is significantly affected by flow rate as it is an important parameter for evaluating the adsorption process performance for a continuous treatment process on the pilot or industrial scale (Saha et al., 2012). Therefore, the effect of flow rate on adsorption of fluoride by MA-Hap LR 72 pellets was examined by varying by varying feed flow rate at 1, 1.5 and 2 LPH i.e. 16, 25 and 33 mL/min with a constant bed height of 25 cm and inlet fluoride concentration of 10 mg/L as shown by BTC in figure 6-3. It was found that, with increase in flow rate, breakthrough time and adsorption capacity decreases. The breakthrough time for the flow rate of 1 LPH was 15 h, 1.5 LPH was 7 h and 2 LPH was 4 h. This can be attributed to the fact that as the flow rate increased, the mass transfer zone quickly moved out of the column and residence time of fluoride ions in the column decreased so there will be a less contact time with the adsorbent and adsorbate left the column before equilibrium occurs. But, when the flow rates were low, adsorbate had more contact time with the MA-Hap LR 72 pellets, resulting in a narrow adsorption zone as well as higher adsorption capacity. The volume treated upto breakpoint was 14 L, 10.5 L and 8 L for 1 LPH, 1.5 LPH and 2 LPH respectively. The various breakthrough curve parameters are also presented in Table 6.1.

Empty bed contact time is a critical parameter that determines the residence time between the adsorbent and adsorbate being treated. The flow rate represents the EBCT in the column, which affects the breakthrough volume and the shape of the breakthrough curve (Hadi et al., 2011). The empty bed contact time (EBCT) for the flow rate of 1 LPH, 1.5 LPH and 2 LPH were observed to be 29.4 min, 19.6 min and 14.7 min respectively. It was worth observing that decrease in flow rate results into increase in EBCT which means that the throughput volume is also increased. Hence fluoride ions had more time

to contact with the adsorbent resulting in higher removal of fluoride ions in the adsorption column.

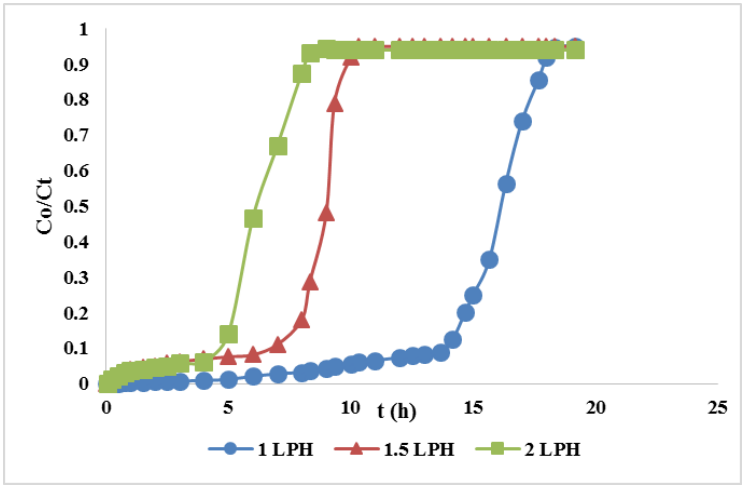

Figure 6-3. Breakthrough curve for fluoride adsorption onto MA-Hap LR 72 pellets at different flow rate (bed height= 25 cm, initial fluoride concentration = 10 mg/L).

6.2.4. Effect of initial fluoride concentration

The initial fluoride concentration of the effluent is important parameter, since a given mass of adsorbent can only adsorb a fixed amount of adsorbate. Therefore, as the concentration of effluent increase, volume of effluent treated by a fixed mass of adsorbent decreases. To study the effect of initial fluoride concentration on the performance of MA-Hap LR 72 pellets, column experiments were done by varying fluoride concentration from 5 mg/L to 15 mg/L. During these experiments, other parameters such as bed height (25 cm) and flow rate (1 LPH or 16 mL/min) were kept constant. The BTCs obtained for adsorbate concentrations of 5, 10 and 15 mg/L are illustrated by figure 6-4.

From the figure it can be observed that, as the initial fluoride concentration increased from 5 to 15 mg/L, the breakthrough and exhaustion time decreased considerably. The breakthrough time for the 5 mg/L, 10 mg/L and 15 mg/L was 16 h, 14 h and 12 h respectively, whereas the exhaustion time for 5 mg/L, 10 mg/L and 15 mg/L was 21 h, 18 h and 15 h respectively. The volume of treated water upto breakthrough point was 16 L, 14 L and 12 L for initial fluoride concentrations of 5 mg/L, 10 mg/L and 15 mg/L respectively. This can be attributed to the fact that with the increase in fluoride

concentration, there is swift saturation i.e. more sorption sites of the adsorbent are being covered that leads to the earlier breakthrough and exhaustion time. At lower fluoride concentration, the breakthrough was flatter, indicating a relatively wide mass transfer zone (MTZ). Whereas, the breakthrough curve of higher fluoride concentration is sharp, inferring a comparatively smaller MTZ. Similar results have been reported by other researchers (Baral et al., 2009).

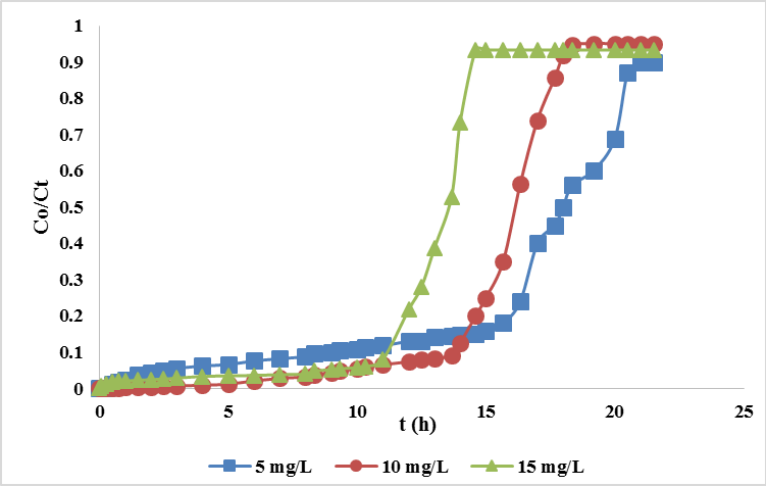

Figure 6-4. Breakthrough curve for fluoride adsorption onto MA-Hap LR 72 pellets at different fluoride concentration (bed height= 25 cm, flow rate =1 LPH or 16 ml/min).

The delayed BTCs for lower fluoride concentration (5 mg/L) depicts that the volume treated will be higher, since the lower concentration gradient caused slower transport due to decreased diffusion coefficient. Whereas increase in the feed fluoride concentration, decreases the treated volume as shown in Table 6.1. At the higher fluoride concentration (15 mg/L), the binding sites of the bed saturated more quickly, leading to earlier breakthrough and exhaustion time. It means lower the feed fluoride concentrations, latter will be exhaustion of the adsorbent pellets. Also, the length of adsorption zone (δ) decrease with increase in fluoride concentration as it increases the driving force for mass transfer.

The adsorption capacity of MA-Hap LR 72 pellets at breakpoint and at exhaustion point were observed to increase from 0.692 to 1.615 mg/g and 0.78 to 2.01 mg/g respectively, with increase in fluoride concentration from 5 to 15 mg/L. The increase in adsorption capacity at higher fluoride concentration may because of higher driving forces

for the transfer process to overcome mass transfer resistance. Whereas at lower fluoride concentration, all the fluoride molecules present in the solution adsorb on the binding sites of the adsorbent resulting in higher adsorption which become saturated at a certain concentration.

Table 6.1 Process conditions of column experiments for adsorption of fluoride using MA-Hap LR 72 pellets

Parameters	q_b(mg/g)	q_{EX}(mg/g)	t_b (h)	t_{EX} (h)	V_b (L)	V_{EX} (L)
Particle size (mm)						
2-2.5	1.21	1.55	14	18	14	18
2.5-3	0.865	1.04	10	12	10	12
Bed height (cm)						
5	0.64	1.71	1.5	4	1.5	4
15	1.1	1.6	8	11	8	11
25	1.21	1.55	14	18	14	18
Flow rate (LPH)						
1	1.21	1.55	14	18	14	18
1.5	1.038	1.29	7	10	10.5	15
2	0.692	1.03	4	6	8	12
Initial Fluoride (mg/L)						
5	0.692	0.78	16	21	16	21
10	1.21	1.55	14	18	14	18
15	1.615	2.01	12	15	12	15

It can be concluded for the above studies that for efficient column performance, smaller particle size, greater bed height and slow flow rate is required. With increase in feed concentration, the adsorption capacity was increased but the column saturation was faster and the breakthrough time was decreased. From the breakthrough curves obtained and experimental column adsorption data for different process parameters (Table 6.1); it was clear that maximum bed height i.e. 25 cm with the flow rate of 1 LPH and feed concentration 10 mg/L were optimum for efficient column performance.

6.3. ESTIMATION OF DESIGN PARAMETERS

In section 6.3, breakthrough curves were obtained for observing effect of various parameters such as particle size, bed height, flow rate and initial fluoride concentration on the column performance. Estimation of column design parameters such as t_x (time to

establish primary adsorption zone), t_f (time for formation of primary adsorption zone), t_z (time for movement of primary adsorption zone down the column), δ (length of primary adsorption zone), f (fractional capacity of MA-Hap LR 72 pellets in adsorption zone) zone), % S (percentage saturation in the column), and H_{UNB} (unused bed height) was carried out using the breakthrough curves. Primary adsorption zone (PAZ) is the part of the adsorbent bed present between exhaustion concentration (C_{EX}) and the concentration for breakthrough (C_b).

Time to establish primary adsorption zone (t_x) can be defined as the time needed for the primary adsorption zone to establish and move out of the adsorption column. It can be mathematically expressed using the following eq (39):

$$t_x = \frac{V_{EX}}{F} \tag{39}$$

Time required for movement of PAZ down the column (t_z) is the time needed for the movement of the adsorption zone down its own length in the column and is calculated from the following eq (40):

$$t_z = \frac{V_{EX} - V_b}{F} \tag{40}$$

Considering a bed depth 'Z' for MA-Hap LR 72 pellets, the depth and time ratios can be computed as follows (41)(Kundu and Gupta 2005; Ghosh et al. 2015):

$$\frac{\delta}{Z} = \frac{t_z}{t_x - t_f} \tag{41}$$

The time for the formation of PAZ (t_f) was assessed by the following expression (42):

$$t_f = (1 - f)\delta \tag{42}$$

The fractional capacity of the MA-Hap LR 72 pellets (f) in the adsorption zone was calculated as follows (43):

$$f = \frac{\int_{V_b}^{V_{EX}} (C_0 - C_t)dv}{C_0(V_{EX} - V_B)} \tag{43}$$

Percentage saturation of the adsorption column (%S) was estimated by the using the following expression (44):

$$\%S = \left[1 + \frac{\delta(f-1)}{Z}\right] X\ 100 \quad (44)$$

Height of unused bed (H_{UNB}) in the adsorption column was evaluated from the following equation (45):

$$H_{UNB} = \frac{Z}{t_{EX}}\ (t_{EX} - t_b) \quad (45)$$

Design parameters for the adsorption column were calculated using equation 1 to 5 and the values thus obtained the listed in Table 6.2. It can be observed from Table 6.2 that the time required for the formation of the primary adsorption zone reduced with decrease in adsorbent bed height, rise in flow rate of fluoridated water and initial fluoride concentration. That means the more the bed height, the greater time it will take to form the PAZ. Likewise, with reduction in flow rate, the contact time required for formation of the adsorption zone also decreases.

The length of the column adsorption zone was noticed to increase as the bed height and flow rate were increased. On the other hand, the percentage saturation for the adsorption column increased with increase in bed height and decreased as the flow rate increased. However, the fractional capacity of column at breakthrough point declined with increase in flow rate, initial fluoride concentration and increasing adsorbent bed height. The fractional capacity of MA-Hap LR 72 pellets in adsorption zone decreased attributing to less number of F- ions available per active site with increase in bed height of the adsorbent.

When the flow rate was increased, the length of the adsorption zone also increased while the percentage saturation decreased as the adsorption zone travelled quicker. Additionally, due to the greater degree of freedom of the F^- ions over the MA-Hap LR 72 adsorbent pellet surface, the adsorption zone was found to reduce with increase in initial fluoride concentration of the feed water. From Table 6.2, it is evident that when higher bed height of adsorbent was used, the adsorbent bed remained unused. Similarly, when the flow rate was more, the height of unused adsorbent bed was also observed to be high.

Table 6.2. Design parameters for column

	Z (cm)			F (L/h)			C_0 (mg/L)		
Parameters	5	15	25	1	1.5	2	5	10	15
t_x(h)	4	11	18	18	10	6	21	18	15
t_z(h)	2.5	3	4	4	3	2	5	4	3
t_f(h)	1.37	1.65	2.13	2.13	1.8	1.25	2.5	2.13	1.74
δ(cm)	4.77	4.81	6.3	6.3	9.14	10.52	6.75	6.3	5.65
f	0.45	0.45	0.466	0.466	0.4	0.375	0.5	0.466	0.42
%S	47.53	82.3	86.5	86.5	78	73.5	86.5	86.5	86.8
H_{UNB}	3.12	4.1	5.48	5.48	7.4	8.2	5.87	5.48	4.91

6.4. APPLICATION OF THE BREAKTHROUGH CURVE

To study the adsorption behavior of fluoride ions in the column packed with MA-Hap LR 72 pellets, three mathematical models were applied viz. Hutchins Bed depth service time model (BDST model), the Thomas model and Yoon-Nelson model.

6.4.1. APPLICATION OF BED DEPTH SERVICE TIME (BDST) MODEL

The adsorption capacities and kinetic constants were determined by fitting the experimental results obtained from fluoride adsorption in a column by MA-Hap LR 72 pellets. The service time, i.e., the exhaustion time of the column were studied corresponding to different flow rate at constant feed concentration and different feed concentration at constant flow rate as shown in figure 6-5.

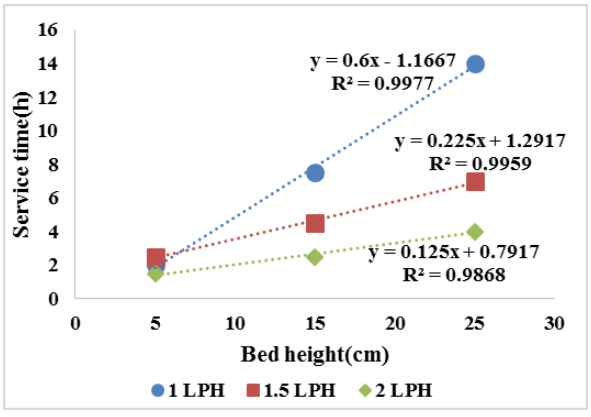

(a) BDST plot for varying flow rates

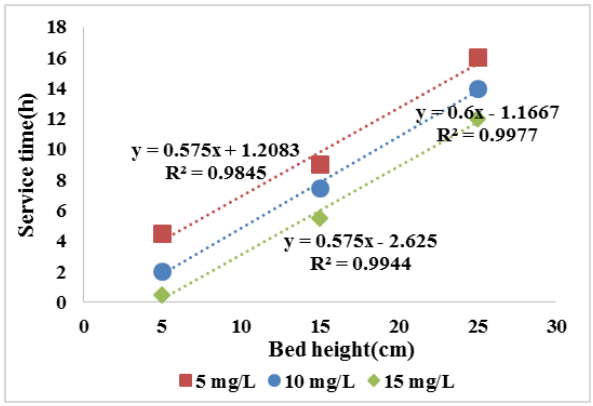

(b) BDST plot for varying feed fluoride concentration

Figure 6-5. Bed depth service time plot for fluoride adsorption onto MA-Hap LR 72 pellets.

From the slope and intercept of these BDST plot, the BDST parameters viz. adsorption rate constant (K_a), BDST adsorption potential (N_0), and critical bed depth (Z_0) were calculated and are listed in Table 6.3.

Table 6.3 Bed depth service time (BDST) model parameters

Parameter	**F(L/h)**			**C_0 (mg/L)**		
	1	1.5	2	5	10	15
N_0 (mg/L)	357.14	172.19	127.55	146.68	357.14	440.04
K_a (L/mgh)	0.082	0.169	0.276	0.228	0.082	0.055
R^2	0.998	0.995	0.986	0.984	0.998	0.994
Z_0 (cm)	3.81	5.75	6.34	2.1	3.81	4.62

High values of correlation coefficient (R^2) showed that the variation of the service time with the flow rate and feed concentration is highly linear for all the systems, thus, indicating the validity of the BDST model when applied to the continuous column studies. The values of the rate constant, (K_a), as shown in Table 6.3 were 0.082, 0.169, and 0.276 at flow rates of 1, 1.5, and 2 LPH, respectively which depicts that with increase in flow rate, the value of the rate constants also increase. This can be attributed by the fact that the overall system kinetics in the column studies were dominated by external mass transfer in the initial part of the adsorption.

The BDST adsorption potential represented by N_O increased when the fluoride concentration was increased from 5 to 15 mg/L and the N_O was observed to decrease gradually from 357.14 mg/L to 127.55 mg/L when the flow rate increased 1 L/h to 2 L/h. The high value of N_0 along with high correlation coefficient (R^2) suggests the high efficiency of MA-Hap LR 72 pellets and ensures the validity of Hutchins BDST model for the column adsorption system.

The values of critical bed depth Z_0 are also listed in Table 6.3 which was calculated from Eq. (21). The value of critical bed depth increases with increase in flow rates and fed concentration. This can be explained on the basis that as the contact time between adsorbate and pellets decrease and more adsorbent will be required to prevent the effluent concentration to be less than C_b. Similarly, the critical bed depth in case of

high fluoride concentration needs to be higher as more number of fluoride ions are available to be adsorbed on the surface of MA-Hap LR 72 pellets.

6.4.2. APPLICATION OF THOMAS MODEL

Thomas model was applied to the adsorption kinetic data at three different bed height, flow rates, feed concentration and particle size. The Thomas rate constant (K_{th}) and the Thomas adsorption capacity (q_0) were calculated from the slope and intercept of the plot between ln (C_0/C_e-1) versus t (h) as shown in figure 6-6. The calculated values of K_{th} and q_0 along with the regression coefficients (R^2) are presented in Table 6.4.

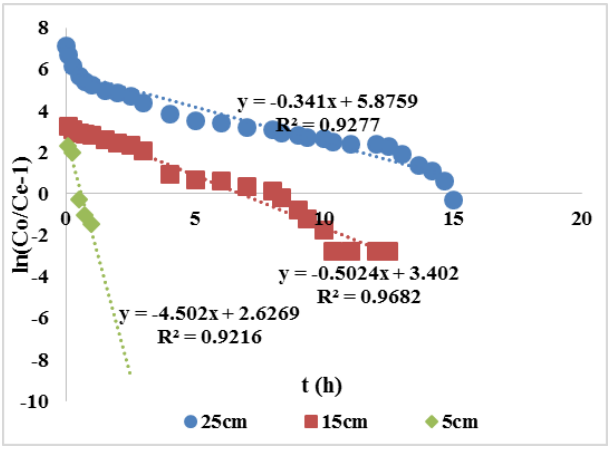

(a) Thomas model plot for varying bed height

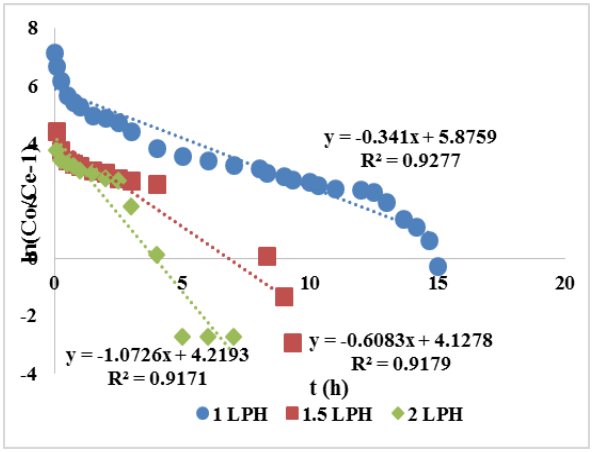

(b) Thomas model plot for varying flow rates

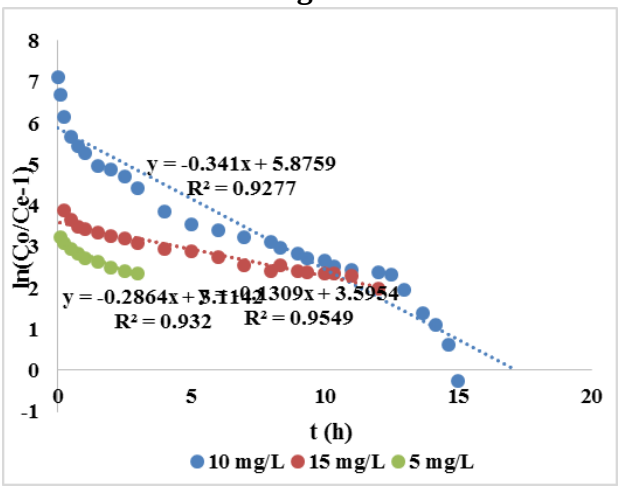

(c) Thomas model plot for varying feed fluoride concentration

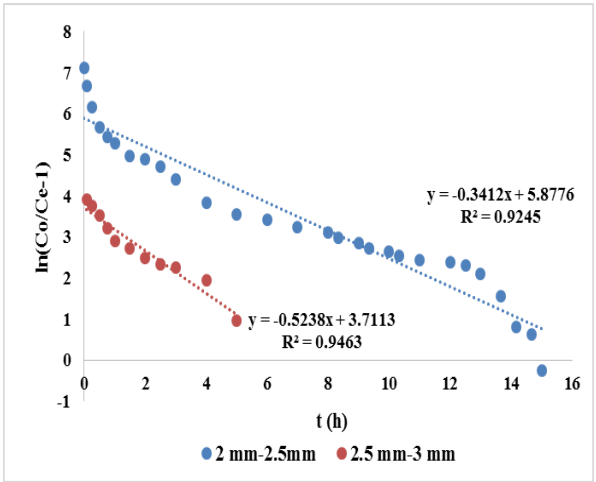

(d) Thomas model plot for varying particle size

Figure 6-6. Thomas model plot for fluoride adsorption onto MA-Hap LR 72 pellets.

The comparatively higher value of R^2 at all the operating conditions suggested that the Thomas model was suitable for describing the column adsorption data of fluoride by MA-Hap LR 72. It was observed from Table 6.4 that the value of 'K_{th}' decreased with increase in bed depth, flow rate, initial fluoride and particle size. This can be due to increased mass transport resistance as it is proportional to axial dispersion and thickness of the liquid film on particle surface (Malkoc et al., 2006). Also with increase in bed height the value of q_0 was also increased because of higher contact time of fluoride ions with MA-Hap LR 72 pellets. With increase in flow rate the value of K_{TH} was increased whereas, the value of q_0 was decreased because of faster exhaustion of adsorbent and lesser mass transport resistance. Similar observations were made in case of initial fluoride concentration. The value of q_0 was higher i.e. 4.2 mg/L at higher fluoride concentration as more number of fluoride ions were loaded per unit active site of adsorbent (MA-Hap LR 72 pellets) which causes faster saturation and lower throughput volume.

In case of particle size the value of q_0 decreased from 1.66 to 0.686 mg/g while the value of K_{th} increases. This can be due to the fact that adsorbent with lower particle size have large surface area for adsorption and hence Thomas adsorption capacity was high.

Table 6.4 Kinetics parameters for Thomas model

	Bed height (cm)			**Flow rate (LPH)**			**Initial F (mg/L)**			**Particle size (mm)**	
Parameters	25	15	5	1	1.5	2	5	10	15	2-2.5	2.5-3
K_{th} (L/mg h)	0.034	0.050	0.45	0.034	0.060	0.1	0.057	0.034	0.008	0.034	0.052
q_0 (mg/g)	1.66	1.07	0.277	1.66	0.99	0.8	0.525	1.66	4.2	1.66	0.686
R^2	0.927	0.968	0.921	0.927	0.917	0.917	0.932	0.927	0.955	0.927	0.946

6.4.3. APPLICATION OF YOON-NELSON MODEL

Yoon-Nelson model was also applied to the column experimental data obtained from fluoride adsorption by MA-Hap LR 72 pellets. The values of k_Y (Yoon-Nelson rate constant) and τ (time required for 50% adsorbate breakthrough) were determined from the graph between $\ln(C_e/C_0-C_e)$ vs. 't' at varying flow rates, bed heights, particle sizes and feed fluoride concentrations as shown in figure 6-7.

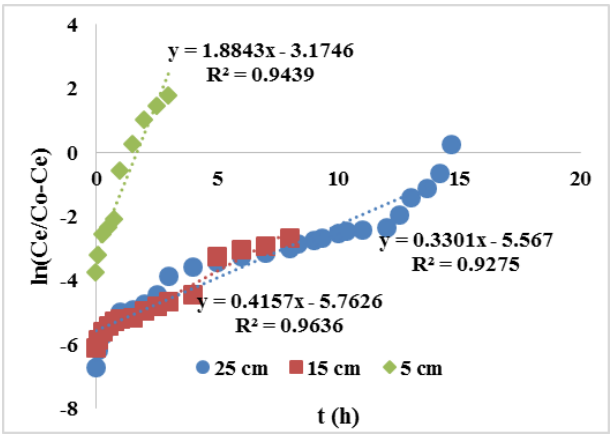

(a) Yoon-Nelson model plot for varying bed height

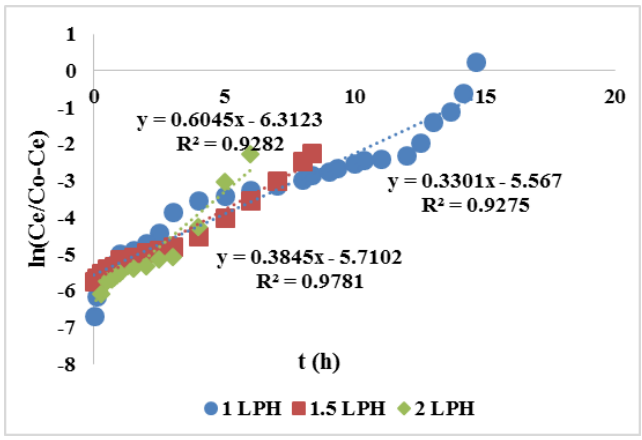

(b) Yoon-Nelson model plot for varying flow rates

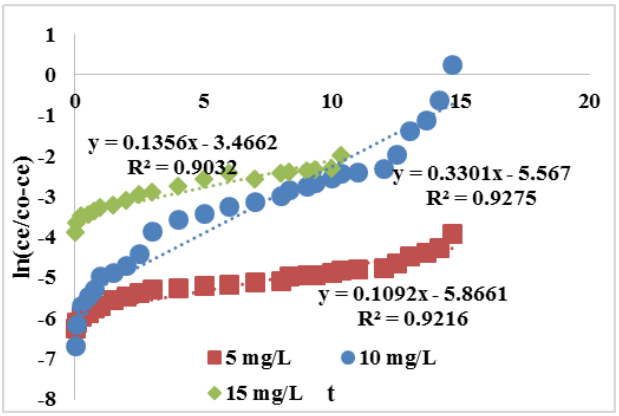

(c) Yoon-Nelson model plot for varying feed fluoride concentration

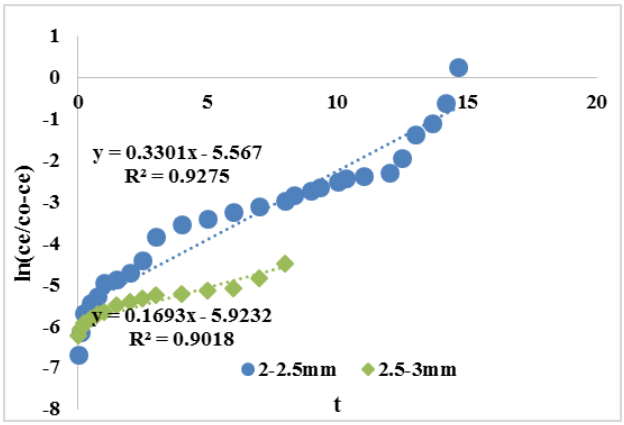

(d) Yoon-Nelson model plot for varying particle size

Figure 6-7. Yoon-Nelson model plots.

The values of different Yoon-Nelson parameters are also depicted in Table 6.5. It was observed that the values of 'τ' increases with increase in bed height whereas it decreases with increase in flow rate, fluoride concentration and particle size. Moreover, the value of correlation coefficient (R^2) was less than 0.96 in all the parameters showing a poor fitting compared to other models explained in previous sections.

Table 6.5 Kinetic parameters for Yoon-Nelson model

Parameter	**Z(cm)**			**F(L/h)**			**C_0 (mg/L)**			**Particle size (mm)**	
	5	15	25	1	1.5	2	5	10	15	2-2.5	2.5-3
k_Y (h^{-1})	1.88	0.415	0.331	0.331	0.384	0.604	0.109	0.331	0.169	0.331	0.169
τ (h)	1.688	13.88	16.81	16.81	14.85	10.45	53.81	16.81	3.49	16.81	0.349
R^2	0.943	0.963	0.927	0.927	0.973	0.928	0.921	0.927	0.901	0.927	0.901

6.5. COLUMN PERFORMANCE INDICATORS

To estimate the performance of column systems the number of bed volumes (BV) treated before the breakthrough point and the adsorbent exhaustion rate (AER) are used as indicators. The number of bed volumes (BV) can be evaluated from the following expression (46).

$$BV = \frac{Treated\ water\ volume\ at\ breakthrough\ (L)}{Adsorbent\ bed\ volume(L)} \quad (46)$$

The greater the number of bed volumes before the breakthrough point, the better is the performance of the adsorption column system.

Mass of adsorbent used per volume of solution treated at breakpoint can be called as adsorption exhaustion rate (AER). AER also indicates the performance efficiency of the column system. The AER value of represents the goodness of the adsorbent bed performance.

AER can be calculated from the following eq (47).

$$AER(g/L) = \frac{Mass\ of\ MA - Hap\ LR\ 72\ (g)}{Volume\ of\ water\ treated\ (L)} \quad (47)$$

Table 6.6. Column performance indicators at various operating conditions

Parameter	**Z(cm)**			**F(L/h)**			**C_0 (mg/L)**			**Particle size (mm)**	
	5	15	25	1	1.5	2	5	10	15	2-2.5	2.5-3
BVs Processed	15.29	27.1	28.5	28.5	14.28	8.16	32.65	28.5	24.4	28.5	20.4
AER (g/L)	14	7.8	7.4	7.4	14.8	26	6.5	7.4	8.6	7.4	10.4

The values of Bed volumes processed and Adsorbent exhaustion rate are presented are given in Table 6.6. It was clearly observed that the number of processed BVs prior to the breakthrough increased with increase in the bed height while it decreased with increase in flow rate, initial fluoride concentration and particle size. Alternatively, the AER was found to be faster at elevated flow rates, lower bed heights, higher particle

sizes and higher fluoride concentration as predicted. The same trend of BV and AER has been reported by many other researchers (Baral et al., 2009; Ghosh et al., 2015; Malkoc et al., 2006).

6.6. REGENERATION STUDIES

Regeneration and reuse of the spent or exhausted adsorbent is an important procedure as it can reduce the running cost of the adsorbent process which will be an economical solution for rural population. The optimal concentration of regenerant/eluent solution is also crucial for consideration as it can have adverse effects upon adsorbent characteristics. Fluoride saturated pellets of MA-Hap LR 72 was washed with deionized water and 2% desorption was observed which can be due to removal of loosely adhered F^- ions from the surface. Later pellets were subjected for regeneration using different concentration of eluent (NaOH) ranging from 0.1M to 1.5 M. The upflow mode with a flow rate of 1 LPH was used due to better contact between the exhausted bed and eluent for faster regeneration. After regeneration, the column was reestablished and the pellets were washed with deionized water for approximately 4 h with the same flow rate until pH of the outlet was neutral (7.0 ± 0.2). The reactivated MA-Hap LR 72 pellets were again ready for the next defluoridation cycle. The process was repeated and the performance of MA-Hap LR 72 pellets were studied for upto four cycle of adsorption-regeneration process as depicted in figure 6-8.

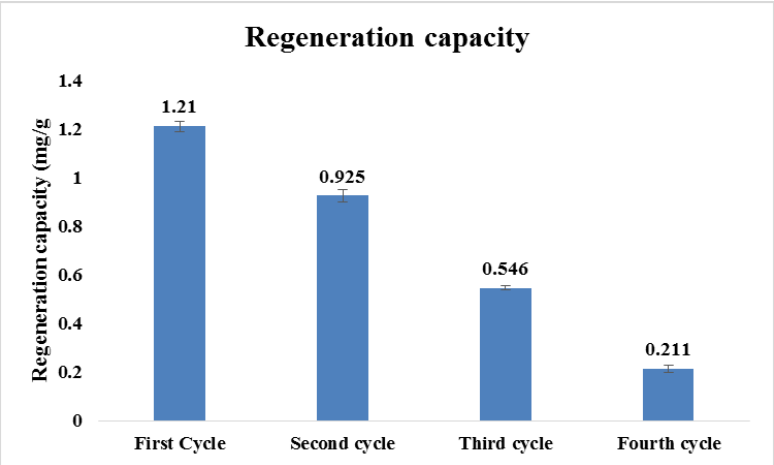

Figure 6-8. Adsorption regeneration process.

The saturated, exhausted and regenerated pellets were characterized and detailed in following section.

6.6.1. CHARACTERIZATION OF MA-HAP LR 72 PELLETS

6.6.1.1. FTIR

The FTIR spectra of unsaturated, exhausted and regenerated MA-Hap LR 72 pellets is shown in figure 6-9. Similar bonding patterns of MA-Hap LR 72 pellets and MA-Hap LR 72 Re were observed as shown in figure 6-9a and figure 6-9c respectively. The results indicate that pelletization does not cause interference with the bonding of the material synthesized. The characteristic bonding patterns of ammonia was observed at 1400 cm^{-1} whereas P-O bond centred from about 1000 to 1100 cm^{-1}. Also peaks in the range of 600 cm^{-1} and 3500 cm^{-1} were of OH- group. Additional peak of OH-F was observed in figure 6-9b i.e. for exhausted adsorbent which corresponds that hydroxyl ions in the MA-Hap LR 72 are replaced by fluoride ions during the adsorption process.

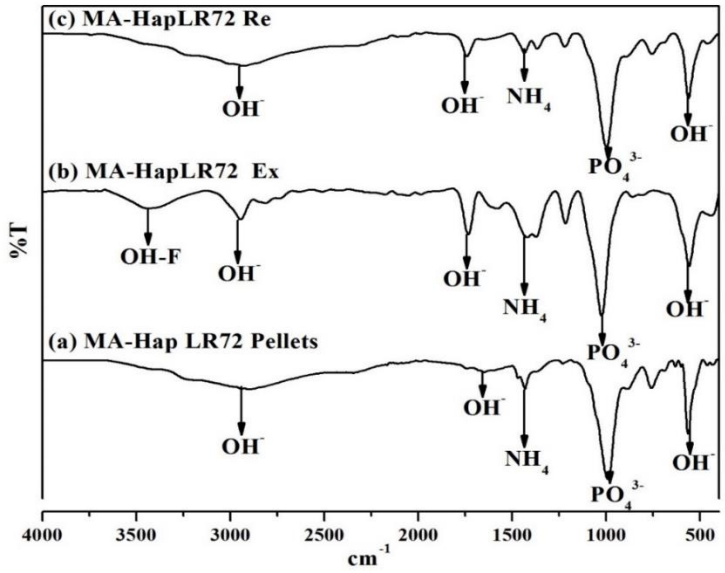

Figure 6-9. FTIR spectra of MA-Hap LR 72 pellets (a) Unsaturated (b) exhausted and (c) regenerated.

6.6.1.2. XRD

The XRD spectra of MA-Hap LR 72 unsaturated, exhausted and regenerated pellets at different concentration is depicted in figure 6-10. There was no major difference

between the XRD spectra of MA-Hap LR 72 and MA-Hap LR 72 pellets was observed which confirms that after addition of binder no compositional changes were made. Spectra obtained of exhausted MA-Hap LR 72 pellets depicts the formation of fluorapatite and the peaks were matched with the JCPDS card no. 01-083-0557. This can be attributed to the fact that OH^- ions present in the hydroxyapatite was replaced by fluoride producing fluorapatite as shown in figure 6-10b. Regeneration of saturated pellets were done with different concentration of NaOH varying from 0.1 M to 1.5 M and optimum concentration was fixed with respect to MA-Hap LR 72 adsorbent. From figure 6-10 c-f it was observed that with Increase in concentration of eluent regeneration increase. Pure Hap was obtained using 1.0 M and 1.5 M NaOH concentration as seen from figure 6-10 e and f. there was no major difference between the XRD spectra of 1.0 M NaOH concentration and 1.5 M NaOH concentration therefor 1.0 M NaOH was optimized for the regeneration of MA-Hap LR 72 pellets.

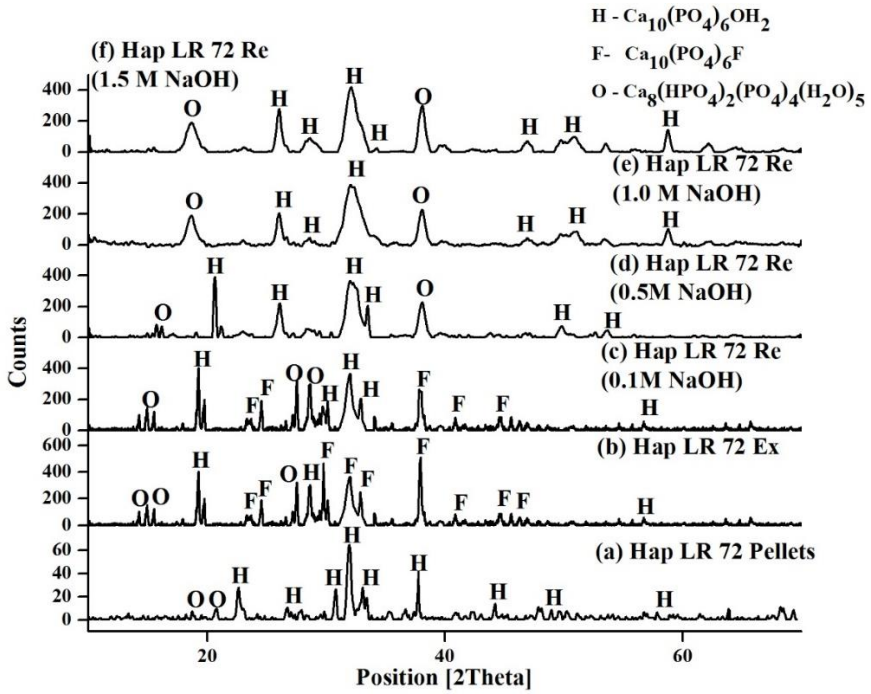

Figure 6-10. XRD spectra MA-Hap LR 72 pellets (a) Unsaturated (b) Exhausted (c) Regenerated at 0.1 M (d) Regenerated at 0.5 M (e) Regenerated at 1.0 M (f) Regenerated at 1.5 M.

6.6.1.3. SEM

Scanning electron micrograph of unsaturated, exhausted and regenerated MA-Hap LR 72 pellets are shown in figure 6-11. The micrograph of unsaturated MA-Hap LR

72 pellets at lower and higher magnification is depicted in figure 6-11a. It was observed that even after pelletization of MA-Hap LR 72, the rod like morphology as observed in figure 5-4 were present on the surface of pellets indicating that no pellets will facilitate adsorption figure 6-11b shows the fluoride distribution along the Hap LR 72 pellets after the column test. The lower magnification (104 X) and higher magnification (5000 X) of Hap LR 72 pellets clearly depicts agglomerated morphology with the surface covered with fluoride ions. However, after regeneration of MA-Hap LR 72 pellets, rod like morphology reappeared as shown in figure 6-11c with magnification of 200,000 X. Also, the superficial SEM spectra of regenerated pellets showed a porous morphology confirming the removal of fluoride from the surface of adsorbent.

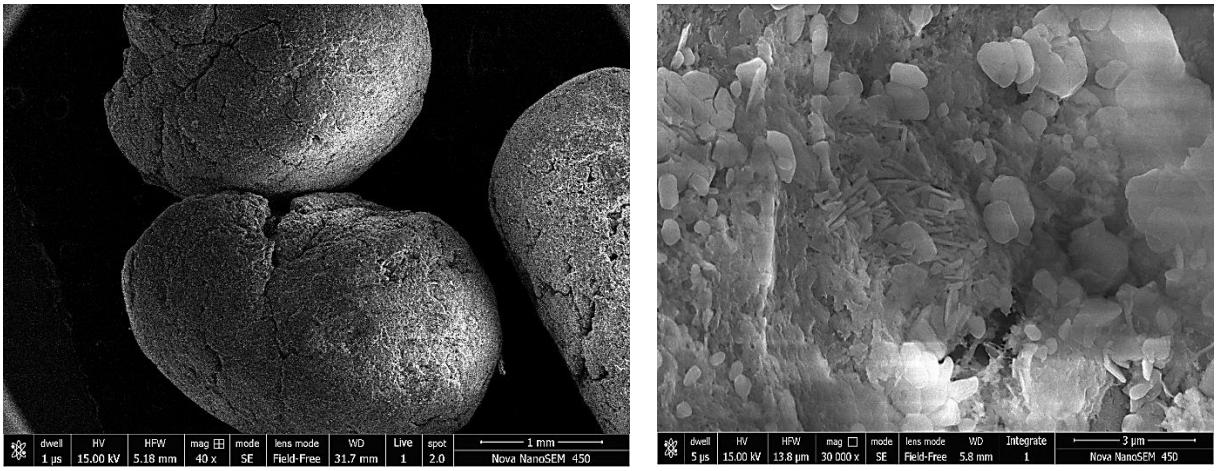

(a) MA-Hap LR 72 Pellets

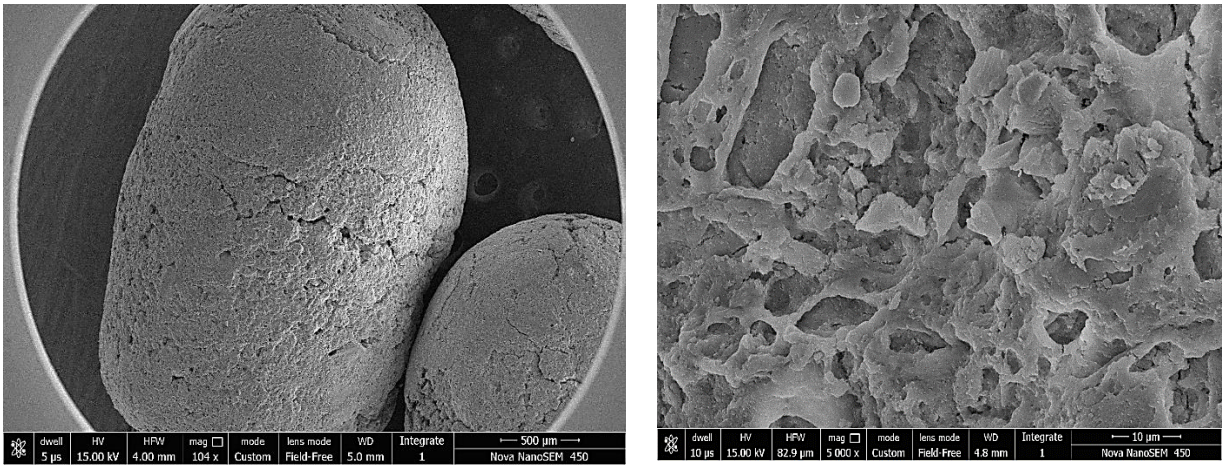

(b) MA-Hap LR 72 Pellets Exhausted

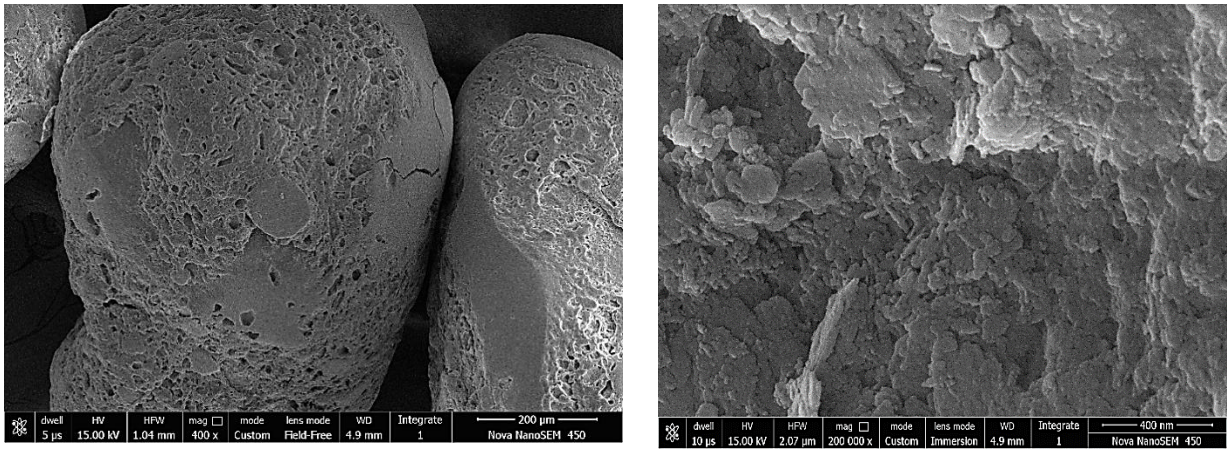

(c) MA-Hap LR 72 Pellets Regenerated

Figure 6-11. SEM micrograph of MA-Hap LR 72 pellets (a) Unsaturated (b) Exhausted (c) Regenerated.

6.6.2. WATER QUALITY PARAMETERS

The quality of water treated with MA-Hap LR 72 pellets determine its feasibility for practical applications. The different parameters studied such as hardness, calcium, magnesium, alkalinity and TDS is shown in figure 6-12. The hardness of treated water was 175 mg/L whereas, calcium and magnesium was 20 mg/L and 15 mg/L respectively. The pH of the treated water was found to be 7.43. The value of alkalinity and TDS was also under the permissible limit making the treated water suitable for drinking.

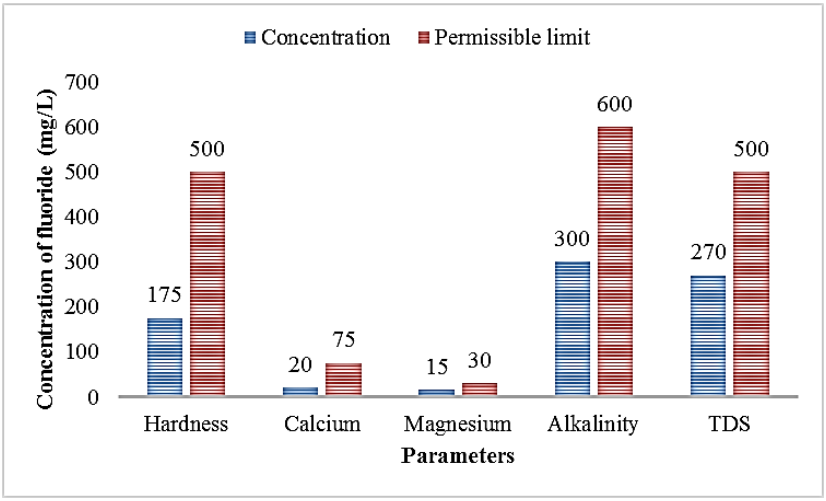

Figure 6-12. Water quality of treated water using MA-Hap LR 72 pellets.

6.7. SUMMARY OF THE CHAPTER

The adsorbent MA-Hap was converted into pellets via the extrusion-spheronization technique. The pellets thus synthesized were observed to be good defluoridating agent in column studies. Various column operational parameters like flow rate, initial fluoride concentration, particle size, and bed height were studied. The column adsorption capacity was found to be 1.21 mg/g at initial fluoride concentration of 10 mg/L, 1 LPH flow rate and bed height of 25 cm. It was noticed that for 25 cm bed height, 28.5 bed volumes can be processed and the AER for the same was 7.4 g/L. The data obtained experimentally were fitted to Hutchins BDST model, Thomas model and Yoon-Nelson model so that the characteristic parameters from each of the model can be obtained. Thomas and Hutchins Bed depth service time model fitted well with the data with very high correlation coefficient value. Adsorption capacity as estimated from Thomas model was very close to the experimental adsorption capacity at all operation conditions. Column regeneration studies were carried out and the results showed that MA-Hap LR 72 pellets can be reused upto four cycles. Assessment of treated water quality for pH, alkalinity, hardness and TDS suggested that it is acceptable according to WHO and BIS regulations. The adsorption capacities of the column system (1.21 mg/g) and batch studies (1.33 mg/g) were comparable for the same initial fluoride concentration (10 mg/L).

The characterization of MA-Hap LR 72 pellets helped in getting clear picture of the defluoridation process and regeneration. The FTIR results obtained after adsorption of fluoride confirmed that hydroxyl ions in the adsorbent are replaced by fluoride ions. The XRD spectra of MA-Hap LR 72 unsaturated, exhausted and regenerated pellets at different concentration confirmed no compositional changes formation of fluoroapatite and regeneration from 1.0 M NaOH concentration. SEM micrograph depicted rod-like morphology for fresh adsorbent which was covered with the layer of fluoride after exhaustion. Post regeneration, the surface of the pellets again displayed a rod-like structure signifying the removal of fluoride from pores attributing that MA-Hap LR 72 pellets can again be used for defluoridation experiments.

CHAPTER 7

SUMMARY OF THE ADSORBENTS SYNTHESIZED

The different forms of hydroxyapatite synthesized are compared using characterization techniques and adsorption capacities of studied adsorbents are summarized in this chapter.

CHAPTER 7
SUMMARY OF ADSORBENTS SYNTHESIZED

This chapter summarizes the different form of hydroxyapatite synthesized and compared with pure hydroxyapatite. FTIR, XRD and SEM of the optimized hydroxyapatite adsorbents are compared in order to check the major difference. The BET surface area and adsorption capacities of the adsorbents studied are also briefed.

7.1. CHARACTERIZATION

The main emphasis were given in the study on the synthesis of pure hydroxyapatite and hydroxyapatite using marble waste powder from two methods i.e. conventional precipitation method and ultrasonication method. It was observed from the previous chapters that optimization of different adsorbents were done based on the purity of hydroxyapatite obtained. The comparative analysis of optimized hydroxyapatite is depicted for the better understanding of the product obtained. Marble apatite and marble hydroxyapatite was compared with pure hydroxyapatite in order to check the similarity based on the characterization.

7.1.1. FTIR

The FTIR spectra of pure hydroxyapatite and various forms of hydroxyapatite synthesized using marble waste powder was compared and depicted in figure 7-1. Characteristic peaks of –OH, PO_4^{3-} and NH_4 were observed in all the adsorbents, clearly indicating the formation of hydroxyapatite. No significant differences were observed from the FTIR spectra of hydroxyapatite synthesized using marble waste powder when compared with pure hydroxyapatite. However, a shift in hydroxyl group from 3500 cm-1 to 3000 cm-1 in MA-Hap LR 72 pellets was noticed which may be due to pelletization

of the adsorbent. For further understanding of crystallographic information and purity of the material synthesized, comparative XRD analysis is discussed in section 7.1.2.

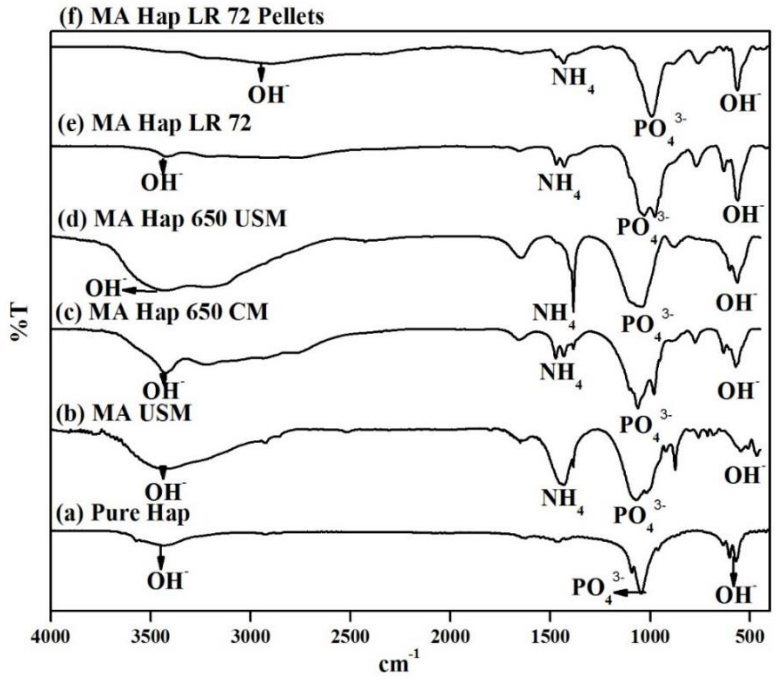

Figure 7-1. Comparative FTIR spectra of different hydroxyapatite synthesized.

7.1.2. XRD

The XRD spectra of pure hydroxyapatite was compared with different forms of Hap synthesized using marble waste powder for better understanding of the purity and similarity of the hydroxyapatite obtained as depicted in figure 7-2. Marble apatite synthesized using ultrasonication method produced Hap with lesser impurities as compared to marble apatite synthesized using conventional method (discussed in section 4.21.2). When MA USM was compared with pure Hap (figure 7-2a), major peak of hydroxyapatite in both the materials matched exactly with pure Hap. Few impurities in the form of calcium hydrogen phosphate and calcium magnesium silicates were present in marble apatite indicating further requirement of purification in order to obtain Hap with better purity. Working in this direction, the method for synthesis of MA was modified and hydroxyapatite was synthesized using conventional and ultrasonication method. The best spectra obtained as discussed in section 4.27 is compared with pure Hap (figure 7-2b).

It was observed that both the methods produced hydroxyapatite with no intermediates and no major differences in the spectra of pure Hap were observed. The results obtained indicates that both the methods can be used for the preparation of pure Hap using marble waste powder.

This synthesis method was then used to scale up the process and the product obtained was named MA-Hap LR. Different synthesis temperatures were used for the optimization of synthesis temperature as explained in section 5.2.2. The best results obtained is compared with pure Hap (figure 7-2 c) and no significant difference between the two spectra was observed. Intermediates in the form of calcium hydrogen oxygen phosphate were present when MA-Hap LR was synthesized at large scale.

For performing column studies, MA-Hap LR 72 was pelletized using PVA based binder and to check the purity of material after pelletization, MA-Hap LR 72 pellets were characterized and compared with pure hydroxyapatite (figure 7-2 d). MA- Hap LR 72 was amorphous in nature due to addition of polymer however no significant change in purity and was noticed.

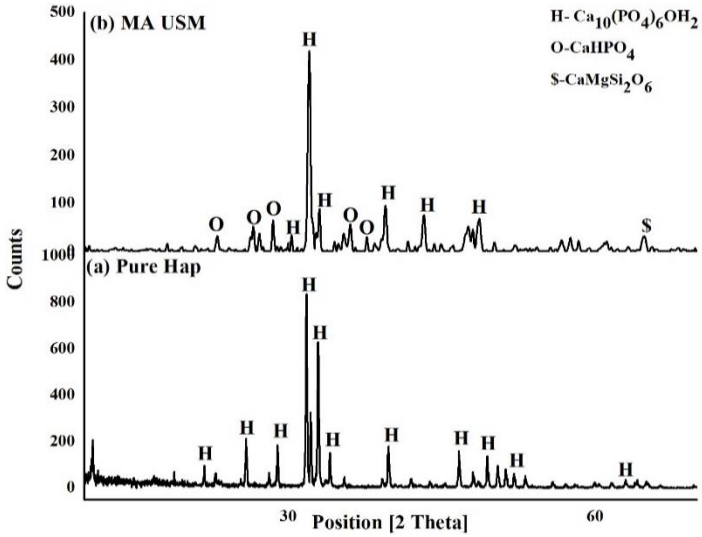

(a)

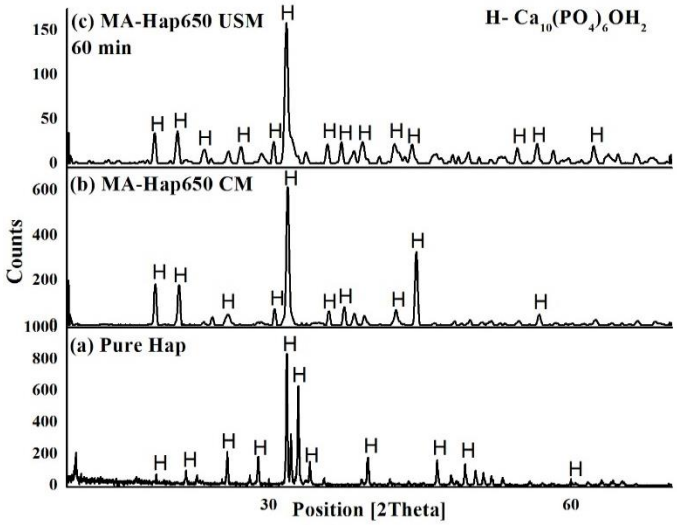

(b)

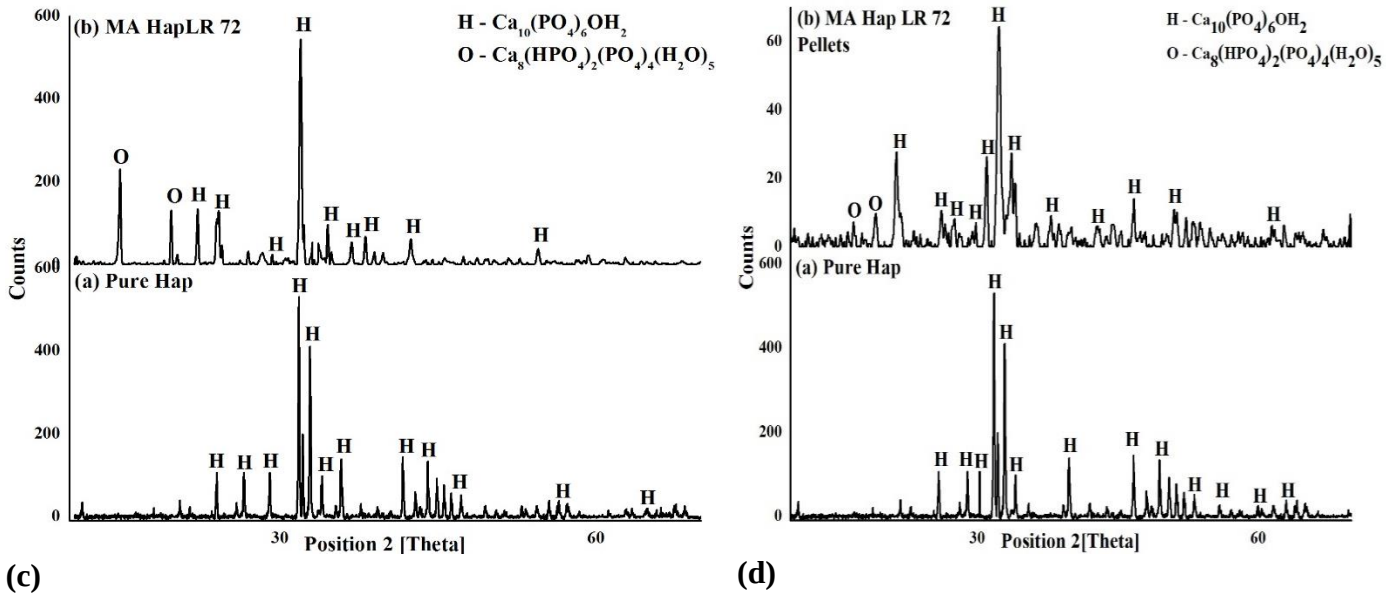

Figure 7-2. Comparative XRD spectra of different hydroxyapatite synthesized.

7.1.3. SEM

The morphology of different forms of hydroxyapatite synthesized in this research work is summarized and shown in figure 7-3. As discussed in Chapter 2 (Literature Review) different morphology of hydroxyapatite can be obtained. In most of the cases, morphology of Hap synthesized with conventional method was rod-like whereas, ultrasonication method produced spherical shaped nano-particles.

Similar observations were made in our studies when Hap was synthesized using conventional method, Hap was obtained in the form of nano-rods as shown in figure 7-3a and figure 7-3e. Ultrasonication is known to produce nano-particles which can be seen from the SEM micrograph. Marble apatite and marble hydroxyapatite synthesized using ultrasonication method produced spherical shaped hydroxyapatite with particle size in the range of 10-15 nm. As explained in section 4.28.5, ultrasonication do not allow the nucleation and crystal growth to occur fully as well as ultrasonication prevents agglomeration of particles during the synthesis and maintain effective size distribution of Hap particles. No major difference in the morphology of MA-Hap CM (figure 7-3c) and MA-Hap USM (figure 7-3d) was observed. After pelletization of MA-Hap LR 72 (figure 7-3f), the rod-like structure can be seen on the surface of pellets which will facilitate adsorption.

It is interesting to note that pure Hap and Hap synthesized using marble waste powder in lab reactor (MA-Hap LR 72) showed similar rod-shaped morphology of the particles.

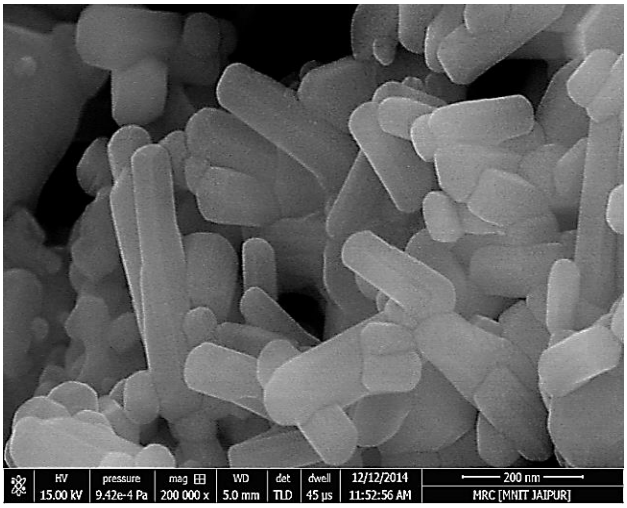

(a) Pure Hap

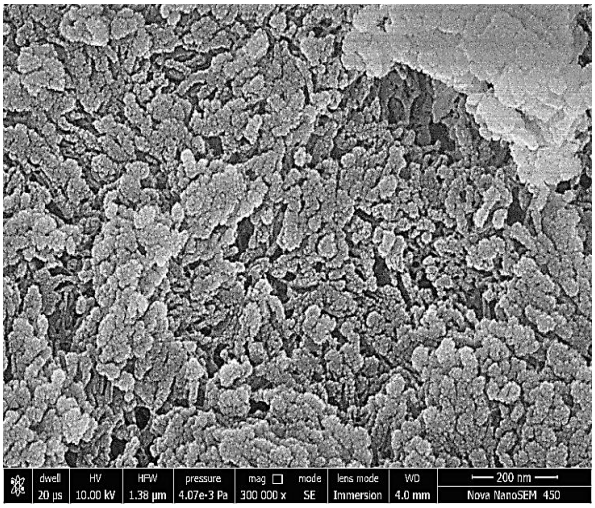

(b) MA USM

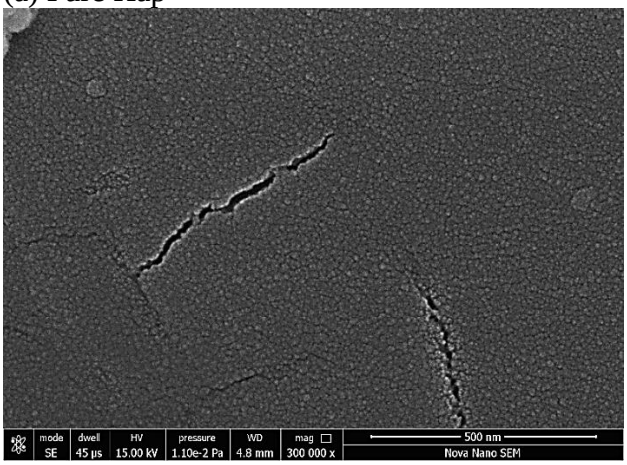

(c) MA Hap 650 CM

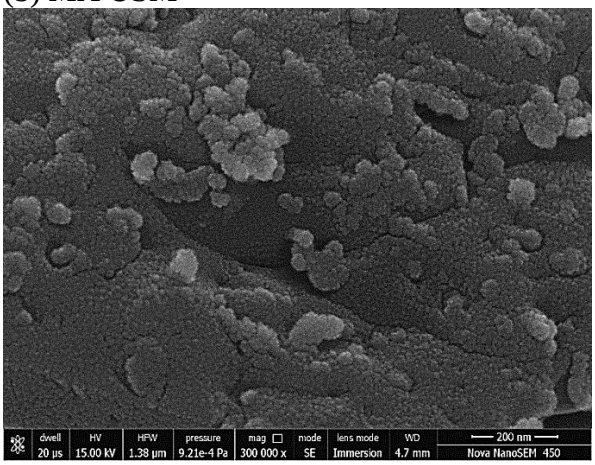

(d) MA Hap 650 USM

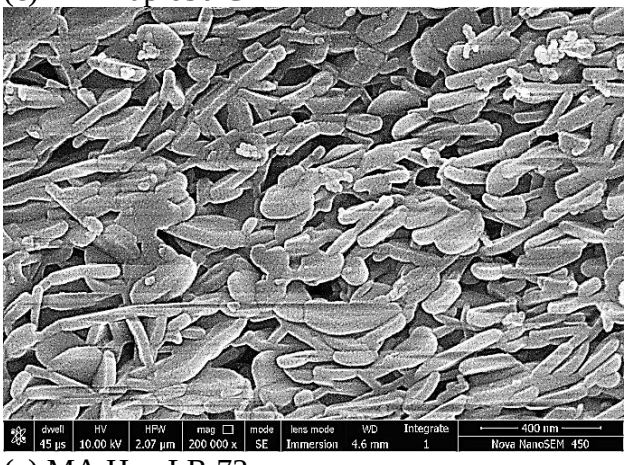

(e) MA Hap LR 72

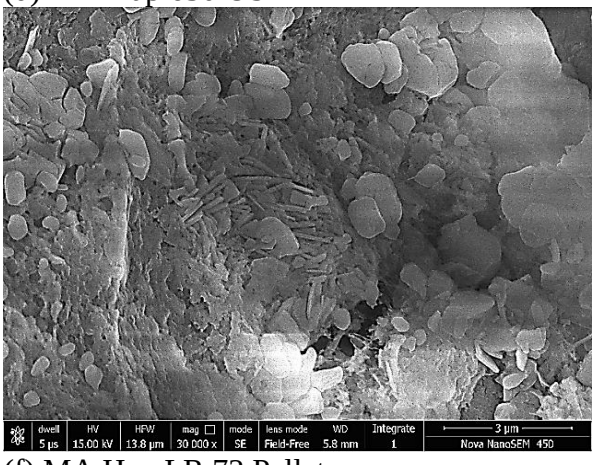

(f) MA Hap LR 72 Pellets

Figure 7-3. Comparative SEM micrographs of different Hydroxyapatite synthesized.

7.2. COMPARATIVE BET SURFACE AREA FOR THE ADSORBENTS USED

The surface area of adsorbent play an important role for the determination of its adsorption capacity. As evident from Table 7.1 the BET surface area of MA-Hap 650 USM and MA USM was higher i.e. 44.92 m^2/g and 39.47 m^2/g as compared to other adsorbents. The higher surface area is responsible for better adsorption capacity.

Table 7.1. Comparative BET Surface area analysis of different adsorbents

S.No.	Adsorbents	BET Surface Area (m^2/g)
1	Marble waste Powder (MWP)	7.18
2	Pure Hydroxyapatite (Hap) USPM	21.25
3	MA-CM	8.41
	MA-USM	39.47
4	MA- Hap 650 CM	31.19
	MA-Hap 650 USM	44.92
5	MA-Hap LR- 72	27.73
6	MA-Hap LR- 72 Pellets	24.66

7.3. COMPARATIVE ADSORPTION CAPACITY

The comparative adsorption capacity of marble waste powder (MWP), pure hydroxyapatite (Hap), marble apatite (MA) and marble hydroxyapatite (MA) synthesized using conventional and ultrasonication method is shown in figure 7-4 and detailed in Table 7.3. As depicted from the figure, material synthesized via ultrasonication resulted into higher adsorption capacities as compared to conventionally synthesized materials. This can be attributed to the fact that acoustic cavitation causes an increase in the effective surface area, resulting in intensification of the chemical reaction due to improved mass transfer at the molecular level. The increased surface area which can also be seen from Table 7.1 facilitates better adsorption capacity. Both MA-Hap and MA displayed comparable adsorption capacities of 1.824 and 1.826 mg/g respectively when ultrasonication was the method for synthesis. On the other hand MA-Hap and MA synthesized using conventional method showed 1.331 mg/g and 0.96 mg/g adsorption capacity respectively. The equilibrium was reached in 30 min for MA-Hap 650 USM

whereas for MA-USM equilibrium time was 90 min. All these factors make MA-Hap 650 USM the most suitable adsorbent for removal of fluoride from drinking water.

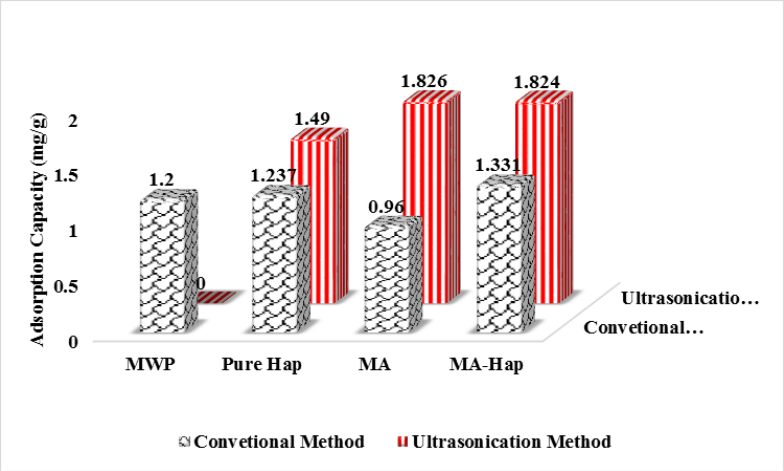

Figure 7-4. Comparative Adsorption capacity of different adsorbents.

7.4. COMPARATIVE COST ANALYSIS OF DIFFERENT ADSORBENT

The cost analysis of different adsorbents estimated on a laboratory scale basis has been listed in Table 7.2 and the detailed cost estimations are attached in appendix I.

Table 7.2 Cost analysis of different adsorbents

Adsorbent	Adsorption capacity (mg/g)	Mode of operation	Cost in Rs. For treating 1 liter of Fluoride water (Conc:10 mg/L)
MWP (Powder)	1.20	Batch	399.84
Hap-900 USPM (Powder)	1.49	Batch	410.45
MA-CM (Powder)	0.96	Batch	626.57
MA-USM (Powder)	1.826	Batch	288.15
MA-Hap CM (Powder)	1.331	Batch	385.78
MA-Hap USM (Powder)	1.824	Batch	253.45
MA-Hap LR 72 (Pellets)	1.21	Column *	18.14

*Breakthrough time for treating 14 liters of 10 mg/L of fluoride solution was 14 h at flow rate of 1LPH, Adsorbent used for 25 cm column bed height was 104 gms.

It was found that MA-Hap USM had the least synthesis cost @ of Rs. 46.25/- per gram compared to Pure Hap @ Rs. 61.17/- per gram. The conventional method was more costlier than ultrasonication method. the cost of treating 1 liter of 10 mg/L of fluoride water for each adsorbent was estimated with respect to its adsorption capacity and the least cost was for MA-Hap USM @ Rs. 253.45/-.

MA-Hap LR derived from the conventional lab scale reactor was pelletized and the cost of the pellets are @ Rs. 2.37/- per gram. The pellets were used in the column studies and the breakthrough time for treating 14 liters of 10 mg/L of fluoride solution was 14 h at flow rate of 1LPH, adsorbent used for 25 cm column bed height was 104 gms, therefore for treating 1 liter of 10 mg/L fluoride water is @ Rs. 18.14/-.

Table 7.3. Summary of adsorbents synthesized along with different parameters studied.

S.No	Material Used	Method for synthesis	Material Named	Compound obtained	Adsorbent in Batch studies	F^- uptake capacity	Contact time	pH after adsorption	Crystallite Size	Particle Size (SEM)
1	Marble Waste Powder	Calcination at 650ºC, 850ºC and 1000ºC	1.1. MWP, **1.2. MWP 650**, 1.3. MWP850 & 1.4. MWP1000	$CaMgCO_3$; $CaCO_3$ MgO, CaO, MgO	MWP 650	1.20 mg/g	3 h	9	Not calculated	---
2	$Ca(NO_3)_2$ and KH_2PO_4 (Analytical Grades)	Conventional precipitation (Reaction time: 4 hrs)	2.1 Hap-(CM) 900,	Pure Hap, agglomerated Nano-rods					70.37 nm Hap-(CM) 900	200 nm
		Ultrasonication with precipitation (Reaction time: 90 min)	2.2.Hap-(USPM), 2.3.Hap 500 (USPM), 2.4.Hap 700 (USPM)& 2.5.**Hap 900**(USPM)	Prominent elongated nano-rods obtained	Hap 900 (USPM)	1.49 mg/g	3 h	7.23	54.83 nm Hap 900 (USPM)	110 nm
3	$Ca(NO_3)_2$ precipitates obtained from Marble waste and KH_2PO_4	Conventional (Reaction time: 4 hrs)	3.1. MA-CM	Hap, intermediate and impurities		0.96 mg/g	90 min		87.45 nm MA 850-CM	900 nm
		Ultrasonication (Reaction time: 45 min)	**3.2. MA-USM**	Hap and intermediate	MA 850-USM	1.826 mg/g	90 min	6.90	58.46 nm MA850-USM	10 nm
4	$Ca(NO_3)_2$ solution obtained from Marble waste and KH_2PO_4	Conventional (Reaction time: 4 hrs)	**4.1.MA-Hap 650 CM** & 4.2.MA-Hap 850 CM	Pure Hap	MA-Hap 650 CM MA-Hap 850 2CM	1.331 mg/g 1.303 mg/g	30 min 90 min	7.12	24.36 nm WM-Hap 650 CM	10 nm
		Ultrasonication (Reaction time: 60 min)	4.3.MA-Hap 650 USM 4.3.1. 45 min, **60 min** 75 min, 60 min @80ºC	Pure Hap	MA-Hap 650 USM, 60 min	1.824 mg/g	30 min	7.24	9.14 nm WM-Hap 650 USM	7 nm
5	$Ca(NO_3)_2$solution obtained from Marble waste and KH_2PO_4	Lab Reactor (Reaction time: 6-7 hrs)	5.1.MA-Hap LR 62	Hap with intermediates	Hap LR-72	Column Studies: 1.21 mg/g			48.76 nm Hap LR 62	600 nm
			5.2.MA-Hap LR72, LR82 & 5.3.MA-Hap LR pellets	Pure Hap					43.87 nm Hap LR 72	200 nm

CONCLUSION

This chapter recapitulates the work done in this thesis. The major findings and significant contribution to the existing knowledge are also mentioned.

CONCLUSION

Scarcity of potable water is causing serious concern all over the globe. Increase in fluoride concentration in groundwater above permitted limit has also contributed to this unfortunate issue. An effective and low-cost adsorbent is need of the era as an efficient treatment technology for treating fluoride in drinking water.

Marble waste powder was converted into a value added product Hydroxyapatite which has good capacity for fluoride removal and was effectively used for treating drinking water from groundwater resources. The basic goal of this study was to develop an economic method through laboratory scale and pilot scale studies for processing of pure Hydroxyapatite from raw marble waste as the raw material. In the present work, experiments were carried out to synthesize pure Hap and Hap from marble waste powder and then utilizing it in defluoridation studies. Both batch and continuous column experiments were performed. The synthesized MA- Hap powder was further made into pellets for column studies. Isotherm models, kinetic studies and possibility of regeneration was also explored in the study.

The following conclusions may be drawn from different adsorbent studied in this research:

Pure Hydroxyapatite: Adsorbent synthesis and batch defluoridation studies.

- Pure Hap was successfully synthesized by both conventional precipitation (CM) and ultrasonication with precipitation (USPM) method. The XRD studies revealed that as calcination temperature was increased from ambient to 900ºC, intermediate phases disappeared and pure Hap nanorods of crystalline structure was obtained when synthesized using USPM process. SEM and TEM studies confirmed the formation of nanorod-like crystalline structures in the micrographs. The yield of the Hap nanorods improved from 83.24% to 90.2% when ultrasonication was incorporated in the Hap synthesis as in the USPM process. Defluoridation studies was focused only on Hap synthesized from ultrasonication method using RSM

approach with Central Composite Design for optimization of process variables viz; pH, adsorbent dose and contact time to estimate fluoride removal efficiency. A quadratic model representing defluoridation efficiency was developed as a function of these three variables, and statistical analysis (ANOVA) evaluated the effects of individual variables as well as their combined effects on the removal process. Numerical optimization helped in determining the optimum process variables estimated at contact time of 3 h, adsorbent dose of 7 g/L and pH of 7 for treating an initial fluoride concentration of 10 mg/L. The percentage fluoride removal was numerically predicted to be at 93.64%, while the experimentally observed value was at 92.86%, which were in good agreement with $R^2 = 0.9950$. Study of adsorption isotherms indicated that fluoride adsorption on Hap 900 (USPM) followed Freundlich isotherm behavior with multi-layered adsorption with an estimated adsorption capacity of 1.49 mg/g. The process followed a pseudo-second order reaction and 3 h of equilibrium time was required to achieve 93% fluoride removal. Analysis of water quality parameters clearly indicate that the treated water is fit for drinking purposes as per World Health Organization (WHO) and Indian drinking water standards.

This study presented a simple, effective technique to synthesize Hap nanorods using ultrasonication with precipitation method for its utilization in defluoridation of drinking water. Production of crystalline hydroxyapatite and its study may also open new dimensions to a better understanding of biomaterials and their efficacy for biomedical applications in bone and dental implants due to its structural similarity to natural bone and teeth material. But the limitation encountered while using Pure Hap was its low adsorption capacity and the higher production cost.

Marble waste powder: Adsorbent synthesis and batch defluoridation studies.

- During synthesis, the calcination temperature influenced the properties of marble waste powder in a significant manner by activating the calcium component present in the powder that further affected the defluoridation capacity. Batch experiments showed that MWP650 had higher removal capacity i.e.1.20 mg/g than MWP, MWP850, and MWP1000. The adsorption was multilayered in nature

since the experimental data fitted very well with Freundlich isotherm and the kinetics of the process fitted best in pseudo-second order model. The mechanism of fluoride mitigation was found to be via both adsorption and precipitation process.

The limitations of using marble waste powder as a defluoridating agent was higher pH, alkalinity and hardness of treated water as per WHO and BIS norms. Therefore, further improvement was required for proper utilization of marble waste powder by using different approach.

Marble apatite: Adsorbent synthesis and batch defluoridation studies.

- Marble apatite primarily composed of hydroxyapatite was synthesized using marble waste by conventional (CM) and ultrasonication method (USM) method for defluoridation of drinking water. The XRD analysis revealed that when ultrasonication was used for synthesis, product obtained was more crystalline with lesser intermediate phases. SEM and TEM studies depicted that with sonication effect well defined spherical morphology was obtained of crystalline nature whereas sword like agglomerated structure was observed when conventional method was used for synthesis. Yield of marble apatite also improved from 67.5% to 78.4% when USM method was employed for synthesis. The adsorbent prepared is more of practical relevance since the maximum fluoride removal was achieved at neutral pH within a contact time of 90 min and a dose of 5.0 g/L. Moreover, no major effect of interfering ions except bicarbonates was observed. The adsorption capacity of marble apatite was higher (1.826 mg/g) when ultrasonication was used as compared to (1.544 mg/g) when conventional method was used for synthesis. The adsorption was homogeneous in nature since the experimental data fitted well with Langmuir isotherm and the kinetics of the process fitted best in pseudo-second order model. Analysis of water quality parameters clearly proved that the treated water is fit for drinking purposes as per WHO and Indian drinking water standards.

  The limitation observed while working with this method is the purity of hydroxyapatite. Along with Hap few of the intermediates in the form of calcium

phosphate and magnesium calcium silicates were present. Therefore, further examination was required to improvise the methodology to synthesize the pure form of hydroxyapatite using marble waste powder.

Marble Hydroxyapatite: Adsorbent synthesis and batch defluoridation studies.

- A method was successfully developed to synthesize pure hydroxyapatite from marble waste powder using conventional and ultrasonication method. The synthesis time for synthesis was decreased from 240 min to 60 min and yield was increased from 81.90% to 89.06% using USM approach. From the XRD analysis of MA-Hap CM, the best results were obtained when MWP was calcined at 650ºC and used for the preparation of calcium nitrate which was then used as calcium source for synthesis of MA-Hap. Alternatively, when ultrasonication was applied for 60 min pure MA-Hap 650 was obtained with the crystallite size of 21.93 nm which lower than that of MA-Hap 650 CM (73.1 nm). The SEM morphology of both the adsorbents possess spherical shaped particles whereas, TEM analysis depicted needle shaped morphology with the average size of 6 nm to 10 nm. The BET surface area of MA-Hap 650 USM was 44.92 m^2/g which was comparatively higher than (31.19 m^2/g) MA-Hap 650 CM. The higher surface area resulted in higher defluoridation capacity of MA-Hap 650 USM than that of MA-Hap 650 CM i.e. 1.824 mg/g and 1.331 mg/g respectively. The adsorption isotherm and kinetics for both MA-Hap 650 CM and MA-Hap 650 USM followed Langmuir model and Pseudo-second order kinetics respectively. Water quality parameters studied were in the permissible range making MA-Hap 650 CM and MA-Hap 650 USM a potent adsorbent for drinking water application.

  Marble hydroxyapatite can be a good alternative for defluoridation as it can be synthesized from marble waste which will lead to effective reuse of tons of marble waste generated, making it very cost effective and thus reducing the environmental threat of waste disposal.

Synthesis of MA-Hap in Lab Reactor (MA-Hap LR):

- Marble hydroxyapatite was successfully scaled up and synthesized in pilot scale lab reactor with the capacity of 60 Liters. MA-Hap LR was synthesized at different temperatures and 72ºC was considered the optimum temperature based on the purity analyzed using FTIR and XRD analysis. The rod like morphology of MA- Hap LR 72 was obtained which was similar to pure Hap attributing that this methodology can be used for the preparation of rod-like hydroxyapatite. The synthesized MA-Hap LR 72 was pelletized was then used for column studies.

MA-Hap LR 72: Pelletization and Column Studies:

- The adsorbent MA-Hap was converted into pellets via the extrusion-spheronization technique. The pellets thus synthesized were observed to be good defluoridating agent in column studies. Various column operational parameters like flow rate, initial fluoride concentration, particle size, and bed height were studied. The column adsorption capacity was found to be 1.21 mg/g at initial fluoride concentration of 10 mg/L, 1 LPH flow rate and bed height of 25 cm. It was noticed that for 25 cm bed height, 28.5 bed volumes can be processed and the AER for the same was 7.4 g/L. The data obtained experimentally were fitted to Hutchins BDST model, Thomas model and Yoon-Nelson model so that the characteristic parameters from each of the model can be obtained. Thomas and Hutchins Bed depth service time model fitted well with the data with very high correlation coefficient value. Adsorption capacity as estimated from Thomas model was very close to the experimental adsorption capacity at all operation conditions. Column regeneration studies were carried out and the results showed that MA-Hap LR 72 pellets can be reused upto four cycles. Assessment of treated water quality for pH, alkalinity, hardness and TDS suggested that it is acceptable according to WHO and BIS regulations.

Significant contributions to the scientific community

- An effective process technology for conversion of the marble waste powder into hydroxyapatite (Hap) that was used efficiently for defluoridation to bring down

fluoride concentrations in drinking water within permissible range. These calcium based material obtained will be only in the form of residual calcium which will be an addition of nutrition into the treated water. Moreover it helps in the conversion of an abundantly generated marble waste powder into a value added product Hap which has a high market value.

- Synthesis of hydroxyapatite nanorods via the conventional method and ultrasonication with precipitation method and its application for water defluoridation has not yet been reported.
- Marble waste powder has never been used for fluoride removal studies making it a novel adsorbent. Further, the importance of utilizing marble waste lies in the economic advantage for developing defluoridation cheaper defluoridation systems besides bringing environmental benefit through reducing the quantity of waste accumulated.
- A semi-batch lab reactor was fabricated to scale up the synthesis process of MA-Hap and adsorption column studies indicated towards the practical viability of the MA-Hap LR 72 pellets in defluoridation of drinking water.
- Furthermore, the MA-Hap LR 72 adsorbent may be regenerated with 0.1 M NaOH eluent for its reusage upto four cycles which is essential for its long term feasibility. The physico-chemical parameters of treated water point that the all the water quality as per the BIS and WHO guidelines.

  Thus, usage of marble waste powder for defluoridation serves a two-way path by mitigating excess fluoride as well as reducing the marble waste produced.

RECOMMENDATIONS FOR FUTURE WORK

The possibility to explore further has always fascinated the researchers and this is what drives the research community. Some recommendations about scope for future work which may be done in this particular area are suggested as follows:

- Different forms of "Marble Hydroxyapatite" may be synthesized using other method such as sol-gel, hydrothermal, or electrodeposition method. This might improve the properties of the materials.

- The adsorbent MA-Hap may also be utilized for water contaminated with several heavy metals ions.

- Biomedical applications of MA-Hap can be investigated and in-vivo studies may open the field to study the biodegradability and biocompatibility of material synthesized.

- Column studies may be conducted with lower flow rates for attaining higher adsorption capacity. Studies can be conducted using fluidized bed column system to achieve even better column performance.

- Some mathematical algorithms and models may be developed for fluoride adsorption studies.

- Regeneration routes other than chemical method may be explored. This may increase the effectiveness of the material.

- The process may be scaled up at commercial level however, before that vigilant analysis of all governing factors is essential.

REFERENCES

REFERENCES

Agrawal, K., Gaharwar, P.S., 2013. A Study on Trend of Export of Natural Stones from India to Various Countries. Int. J. Adv. Res. Technol. 2, 360–379.

Aimutis, W.R., 2012. Lactose cariogenicity with an emphasis on childhood dental caries. Int. Dairy J. 22, 152–158. doi:10.1016/j.idairyj.2011.10.007

Akbulut, H., Gürer, C., 2007. Use of aggregates produced from marble quarry waste in asphalt pavements. Build. Environ. 42, 1921–1930. doi:10.1016/j.buildenv.2006.03.012

Al-Zboon, K., Al-Zou'by, J., 2015. Recycling of stone cutting slurry in concrete mixes. J. Mater. Cycles Waste Manag. 17, 324–335. doi:10.1007/s10163-014-0246-x

Al-Zboon, K., Tahat, M., Abu-Hamatteh, Z.S.H., Al-Harahsheh, M.S., 2010. Recycling of stone cutting sludge in formulations of bricks and terrazzo tiles. Waste Manag. Res. 28, 568–574. doi:10.1177/0734242X09350246

Alberius-Henning, P., Adolfsson, E., Grins, J., Fitch, A., 2001. Triclinic oxy-hydroxyapatite. J. Mater. Sci. 36, 663–668. doi:10.1023/A:1004876622105

Aliabdo, A.A., Abd Elmoaty, A.E.M., Auda, E.M., 2014. Re-use of waste marble dust in the production of cement and concrete. Constr. Build. Mater. 50, 28–41. doi:10.1016/j.conbuildmat.2013.09.005

Aminian, A., Solati-Hashjin, M., Samadikuchaksaraei, A., Bakhshi, F., Gorjipour, F., Farzadi, A., Moztarzadeh, F., Schm??cker, M., 2011. Synthesis of silicon-substituted hydroxyapatite by a hydrothermal method with two different phosphorous sources. Ceram. Int. 37, 1219–1229. doi:10.1016/j.ceramint.2010.11.044

Amit, V., Singh, R.R., 2013. Soil Properties and Protect Environment. J. Environ. Res. Dev. 7, 1479–1483.

Anee Kuriakose, T., Kalkura, S.N., Palanichamy, M., Arivuoli, D., Dierks, K., Bocelli, G., Betzel, C., 2004. Synthesis of stoichiometric nano crystalline hydroxyapatite by ethanol-based sol-gel technique at low temperature. J. Cryst. Growth 263, 517–523.

doi:10.1016/j.jcrysgro.2003.11.057

Anwar, R., Kamarun, H.R., Vermol, V. V., Hassan, O.H., 2011. Marble dust incorporate in standard local ceramic body as enhancement in sanitary ware products. 2011 IEEE Colloq. Humanit. Sci. Eng. CHUSER 2011 355–357. doi:10.1109/CHUSER.2011.6163750

APHA/AWWA/WEF, 2012. Standard Methods for the Examination of Water and Wastewater. Stand. Methods 541. doi:ISBN 9780875532356

Arce, H., Montero, M.L., Sáenz, A., Castaño, V.M., 2004. Effect of pH and temperature on the formation of hydroxyapatite at low temperatures by decomposition of a Ca-EDTA complex. Polyhedron 23, 1897–1901. doi:10.1016/j.poly.2004.04.021

Arey, J.S., Seaman, J.C., Bertsch, P.M., 1999. Immobilization of uranium in contaminated sediments by hydroxyapatite addition. Environ. Sci. Technol. 33, 337–342. doi:10.1021/es980425+

Arora, M., Maheshwari, R.C., Jain, S.K., Gupta, A., 2004. Use of membrane technology for potable water production. Desalination 170, 105–112. doi:10.1016/j.desal.2004.02.096

Aruntaş, H.Y., Gürü, M., Dayi, M., Tekin, I., 2010. Utilization of waste marble dust as an additive in cement production. Mater. Des. 31, 4039–4042. doi:10.1016/j.matdes.2010.03.036

Badillo-Almaraz, V.E., Armando Flores, J., Arriola, H., López, F.A., Ruiz-Ramirez, L., 2007. Elimination of fluoride ions in water for human consumption using hydroxyapatite as an adsorbent. J. Radioanal. Nucl. Chem. 271, 741–744. doi:10.1007/s10967-007-0335-6

Barakat, N.A.M., Khil, M.S., Omran, A.M., Sheikh, F.A., Kim, H.Y., 2009. Extraction of pure natural hydroxyapatite from the bovine bones bio waste by three different methods. J. Mater. Process. Technol. 209, 3408–3415. doi:10.1016/j.jmatprotec.2008.07.040

Baral, S.S., Das, N., Ramulu, T.S., Sahoo, S.K., Das, S.N., Chaudhury, G.R., 2009. Removal of Cr(VI) by thermally activated weed Salvinia cucullata in a fixed-bed column. J. Hazard. Mater. 161, 1427–1435. doi:10.1016/j.jhazmat.2008.04.127

References

Behbahani, M., Moghaddam, M.R.A., Arami, M., 2011. Techno-economical evaluation of fluoride removal by electrocoagulation process: Optimization through response surface methodology. Desalination 271, 209–218. doi:10.1016/j.desal.2010.12.033

Bhanvase, B.A., Kutbuddin, Y., Borse, R.N., Selokar, N.R., Pinjari, D. V., Gogate, P.R., Sonawane, S.H., Pandit, A.B., 2013. Ultrasound assisted synthesis of calcium zinc phosphate pigment and its application in nanocontainer for active anticorrosion coatings. Chem. Eng. J. 231, 345–354. doi:10.1016/j.cej.2013.07.030

Bhargava, S., 2014. Batch studies of water fishbone defluoridation charcoal 63, 848–858.

Bhaumik, R., Mondal, N.K., Das, B., Roy, P., Pal, K.C., Das, C., Banerjee, A., Datta, J.K., 2012. Eggshell powder as an adsorbent for removal of fluoride from aqueous solution: Equilibrium, kinetic and thermodynamic studies. E-Journal Chem. 9, 1457–1480. doi:10.1155/2012/790401

Bhaumik, R., Mondal, N.K., Das, B., Roy, P., Pal, K.C., Das, C., Banerjee, a., Datta, J.K., 2012. Eggshell powder as an adsorbent for removal of fluoride from aqueous solution: Equilibrium, kinetic and thermodynamic studies. E-Journal Chem. 9, 1457–1480. doi:10.1155/2012/790401

Boonyang, U., Chaopanich, P., Wongchaisuwat, A., Senthongkaew, P., Siripaisarnpipat, S., 2010. Effect of Phosphate Precursor on the Production of Hydroxyapatite from Crocodile Eggshells. J. Biomim. Biomater. Tissue Eng. 5, 31–37. doi:10.4028/www.scientific.net/JBBTE.5.31

Brendel, T., Engel, A., Rüssel, C., 1992. Hydroxyapatite coatings by a polymeric route. J. Mater. Sci. Mater. Med. 3, 175–179. doi:10.1007/BF00713445

Brunson, L.R., Sabatini, D.A., 2009. An Evaluation of Fish Bone Char as an Appropriate Arsenic and Fluoride Removal Technology for Emerging Regions. Environ. Eng. Sci. 26, 1777–1784. doi:10.1089/ees.2009.0222

Tas, A., 2000. Synthesis of biomimetic Ca-hydroxyapatite powders at 37ºC in synthetic body fluids. Biomaterials 21, 1429–1438. doi:10.1016/S0142-9612(00)000193

References

C.A, A.R. and and N.R.E.., 2015. Ground Water Levels of Nitrate and Fluoride in Tiruchirappalli East and West Taluka in Tamilnadu India. Res. J. Chem. Sci. 5, 42–48.

Cao, H., Zhang, L., Zheng, H., Wang, Z., 2010. Hydroxyapatite nanocrystals for biomedical applications. J. Phys. Chem. C 114, 18352–18357. doi:10.1021/jp106078b

Cao, L.Y., Zhang, C.B., Huang, J.F., 2005. Synthesis of hydroxyapatite nanoparticles in ultrasonic precipitation. Ceram. Int. 31, 1041–1044. doi:10.1016/j.ceramint.2004.11.002

Catros, S., Guillemot, F., Lebraud, E., Chanseau, C., Perez, S., Bareille, R., Amédée, J., Fricain, J.C., 2010. Physico-chemical and biological properties of a nano-hydroxyapatite powder synthesized at room temperature. Irbm 31, 226–233. doi:10.1016/j.irbm.2010.04.002

Chaudhuri, B., Mondal, B., Modak, D.K., Pramanik, K., Chaudhuri, B.K., 2013. Preparation and characterization of nanocrystalline hydroxyapatite from egg shell and K2HPO4 solution. Mater. Lett. 97, 148–150. doi:10.1016/j.matlet.2013.01.082

Chen, D.Z., Tang, C.Y., Chan, K.C., Tsui, C.P., Yu, P.H.F., Leung, M.C.P., Uskokovic, P.S., 2007. Dynamic mechanical properties and in vitro bioactivity of PHBHV/HA nanocomposite. Compos. Sci. Technol. 67, 1617–1626. doi:10.1016/j.compscitech.2006.07.034

Chen, F., Wang, Z.C., Lin, C.J., 2002. Preparation and characterization of nano-sized hydroxyapatite particles and hydroxyapatite/chitosan nano-composite for use in biomedical materials. Mater. Lett. 57, 858–861. doi:10.1016/S0167-577X(02)00885-6

Chen, H., Clarkson, B.H., Sun, K., Mansfield, J.F., 2005. Self-assembly of synthetic hydroxyapatite nanorods into an enamel prism-like structure. J. Colloid Interface Sci. 288, 97–103. doi:10.1016/j.jcis.2005.02.064

Chen, J., Wang, Y., Chen, X., Ren, L., Lai, C., He, W., Zhang, Q., 2011. A simple sol-gel technique for synthesis of nanostructured hydroxyapatite, tricalcium phosphate and biphasic powders. Mater. Lett. 65, 1923–1926. doi:10.1016/j.matlet.2011.03.076

Chen, L., Mccrate, J.M., Lee, J.C.-M., Li, H., 2011. The role of surface charge on the uptake

and biocompatibility of hydroxyapatite nanoparticles with osteoblast cells. Nanotechnology 22, 105708. doi:10.1088/0957-4484/22/10/105708

Chen, L., Zhang, K.S., He, J.Y., Xu, W.H., Huang, X.J., Liu, J.H., 2016. Enhanced fluoride removal from water by sulfate-doped hydroxyapatite hierarchical hollow microspheres. Chem. Eng. J. 285, 616–624. doi:10.1016/j.cej.2015.10.036

Choi, H.D., Jung, W.S., Cho, J.M., Ryu, B.G., Yang, J.S., Baek, K., 2009. Adsorption of Cr(VI) onto cationic surfactant-modified activated carbon. J. Hazard. Mater. 166, 642–646. doi:10.1016/j.jhazmat.2008.11.076

Choubisa, S.L., Choubisa, L., Choubisa, D.K., 2001. Endemic fluorosis in Rajasthan. Indian J. Environ. Health 43, 177–189.

Conca, J.L., Wright, J., 2006. An apatite II permeable reactive barrier to remediate ground water containing Zn, Pb and Cd. Appl. Geochemistry 21, 1288–1300. doi:10.1016/j.apgeochem.2006.06.008

Cury, J.A., Tenuta, L.M.A., 2009. Enamel remineralization: controlling the caries disease or treating early caries lesions? Braz. Oral Res. 23, 23–30. doi:10.1590/S1806-83242009000500005

Demirel, B., 2010. The effect of the using waste marble dust as fine sand on the mechanical properties of the concrete. Int. J. Phys. Sci. 5, 1372–1380. doi:10.1016/j.envint.2006.11.003

Deydier, E., Guilet, R., Sarda, S., Sharrock, P., 2005a. Physical and chemical characterisation of crude meat and bone meal combustion residue: “Waste or raw material?” J. Hazard. Mater. 121, 141–148. doi:10.1016/j.jhazmat.2005.02.003

Deydier, E., Guilet, R., Sarda, S., Sharrock, P., 2005b. Physical and chemical characterisation of crude meat and bone meal combustion residue: “Waste or raw material?” J. Hazard. Mater. 121, 141–148. doi:10.1016/j.jhazmat.2005.02.003

Dhanapandian, S., Gnanavel, B., 2009. An investigation on the effect of incorporation of granite and marble wastes in the production of bricks. Arpn J. Eng. Appl. Sci. 4.

References

Dollase, W.A., 1986. Correction of Intensities of Preferred Orientation in Powder Diffractometry: Application of the March Model. J. Appl. Crystallogr. 19, 267–272. doi:10.1107/S0021889886089458

Durmaz, F., Kara, H., Cengeloglu, Y., Ersoz, M., 2005. Fluoride removal by donnan dialysis with anion exchange membranes. Desalination 177, 51–57. doi:10.1016/j.desal.2004.11.016

Earl, J.S., Wood, D.J., Milne, S.J., 2006. Hydrothermal synthesis of hydroxyapatite. J. Phys. Conf. Ser. 26, 268–271. doi:10.1088/1742-6596/26/1/064

Eliche-Quesada, D., Corpas-Iglesias, F.A., Pérez-Villarejo, L., Iglesias-Godino, F.J., 2012. Recycling of sawdust, spent earth from oil filtration, compost and marble residues for brick manufacturing. Constr. Build. Mater. 34, 275–284. doi:10.1016/j.conbuildmat.2012.02.079

Eshtiagh-Hosseini, H., Housaindokht, M.R., Chahkandi, M., 2007. Effects of parameters of sol-gel process on the phase evolution of sol-gel-derived hydroxyapatite. Mater. Chem. Phys. 106, 310–316. doi:10.1016/j.matchemphys.2007.06.002

Fan, X., Parker, D.J., Smith, M.D., 2003. Adsorption kinetics of fluoride on low cost materials. Water Res. 37, 4929–4937. doi:10.1016/j.watres.2003.08.014

Fan, X., Parker, D.J., Smith, M.D., 2003. Adsorption kinetics of fluoride on low cost materials. Water Res. 37, 4929–37. doi:10.1016/j.watres.2003.08.014

Fathi, M.H., Hanifi, A., Mortazavi, V., 2008. Preparation and bioactivity evaluation of bone-like hydroxyapatite nanopowder. J. Mater. Process. Technol. 202, 536–542. doi:10.1016/j.jmatprotec.2007.10.004

Felipe-Sesé, M., Eliche-Quesada, D., Corpas-Iglesias, F.A., 2011. The use of solid residues derived from different industrial activities to obtain calcium silicates for use as insulating construction materials. Ceram. Int. 37, 3019–3028. doi:10.1016/j.ceramint.2011.05.003

Ferraz, M.P., Monteiro, F.J., Manuel, C.M., 2004. Hydroxyapatite nanoparticles : A review of. J. Appl. Biomater. 2, 74–80. doi:1722-6899/074-07$15.00/0

Frengstad, B., Banks, D., Siewers, U., 2001. The chemistry of Norwegian groundwaters: IV. The pH-dependence of element concentrations in crystalline bedrock groundwaters. Sci. Total Environ. 277, 101–117. doi:10.1016/S0048-9697(00)00867-6

Gao, S., Cui, J., Wei, Z., 2009a. Study on the fluoride adsorption of various apatite materials in aqueous solution. J. Fluor. Chem. 130, 1035–1041. doi:10.1016/j.jfluchem.2009.09.004

Gao, S., Sun, R., Wei, Z., Zhao, H., Li, H., Hu, F., 2009b. Size-dependent defluoridation properties of synthetic hydroxyapatite. J. Fluor. Chem. 130, 550–556. doi:10.1016/j.jfluchem.2009.03.007

Gao, S., Sun, R., Wei, Z., Zhao, H., Li, H., Hu, F., 2009c. Size-dependent defluoridation properties of synthetic hydroxyapatite. J. Fluor. Chem. 130, 550–556. doi:10.1016/j.jfluchem.2009.03.007

George, S., Pandit, P., Gupta, A.B., 2010. Residual aluminium in water defluoridated using activated alumina adsorption - Modeling and simulation studies. Water Res. 44, 3055–3064. doi:10.1016/j.watres.2010.02.028

Gergely, G., Wéber, F., Lukács, I., Tóth, A.L., Horváth, Z.E., Mihály, J., Balázsi, C., 2010. Preparation and characterization of hydroxyapatite from eggshell. Ceram. Int. 36, 803–806. doi:10.1016/j.ceramint.2009.09.020

Ghahremani, D., Mobasherpour, I., Salahi, E., Ebrahimi, M., Manafi, S., Keramatpour, L., 2017. Potential of nano crystalline calcium hydroxyapatite for Tin(II) removal from aqueous solutions: Equilibria and kinetic processes. Arab. J. Chem. 10, S461–S471. doi:10.1016/j.arabjc.2012.10.006

Ghorai, S., Pant, K.K., 2005. Equilibrium, kinetics and breakthrough studies for adsorption of fluoride on activated alumina. Sep. Purif. Technol. 42, 265–271. doi:10.1016/j.seppur.2004.09.001

Ghosh, A., Chakrabarti, S., Biswas, K., Ghosh, U.C., 2015. Column performances on fluoride removal by agglomerated Ce(IV)-Zr(IV) mixed oxide nanoparticles packed fixed-beds.

J. Environ. Chem. Eng. 3, 653–661. doi:10.1016/j.jece.2015.02.001

Giardina, M.A., Fanovich, M.A., 2010. Synthesis of nanocrystalline hydroxyapatite from Ca(OH)2 and H3PO4 assisted by ultrasonic irradiation. Ceram. Int. 36, 1961–1969. doi:10.1016/j.ceramint.2010.05.008

Goloshchapov, D.L., Kashkarov, V.M., Rumyantseva, N.A., Seredin, P. V., Lenshin, A.S., Agapov, B.L., Domashevskaya, E.P., 2013. Synthesis of nanocrystalline hydroxyapatite by precipitation using hen's eggshell. Ceram. Int. 39, 4539–4549. doi:10.1016/j.ceramint.2012.11.050

Gonzalez-Davila, M., Santana-Casiano, J.M., Millero, F.J., 1990. The adsorption of Cd(II) and Pb(II) to chitin in seawater. J. Colloid Interface Sci. 137, 102–110. doi:10.1016/0021-9797(90)90046-Q

Gopal, V., Elango, K.P., 2007. Equilibrium, kinetic and thermodynamic studies of adsorption of fluoride onto plaster of Paris. J. Hazard. Mater. 141, 98–105. doi:10.1016/j.jhazmat.2006.06.099

Gopi, D., Indira, J., Kavitha, L., Sekar, M., Mudali, U.K., 2012. Synthesis of hydroxyapatite nanoparticles by a novel ultrasonic assisted with mixed hollow sphere template method. Spectrochim. Acta - Part A Mol. Biomol. Spectrosc. 93, 131–134. doi:10.1016/j.saa.2012.02.033

Gorchev, H.G., Ozolins, G., 2011. WHO guidelines for drinking-water quality. WHO Chron. doi:10.1016/S1462-0758(00)00006-6

Gu, Y.W., Khor, K.A., Cheang, P., 2004. Bone-like apatite layer formation on hydroxyapatite prepared by spark plasma sintering (SPS). Biomaterials 25, 4127–4134. doi:10.1016/j.biomaterials.2003.11.030

Habraken, W.J.E.M., Wolke, J.G.C., Jansen, J.A., 2007. Ceramic composites as matrices and scaffolds for drug delivery in tissue engineering. Adv. Drug Deliv. Rev. 59, 234–248. doi:10.1016/j.addr.2007.03.011

Hadi, M., Samarghandi, M.R., McKay, G., 2011. Simplified fixed bed design models for the

adsorption of acid dyes on novel pine cone derived activated carbon. Water. Air. Soil Pollut. 218, 197–212. doi:10.1007/s11270-010-0635-2

Hameed, B.H., Tan, I.A.W., Ahmad, A.L., 2008. Optimization of basic dye removal by oil palm fibre-based activated carbon using response surface methodology. J. Hazard. Mater. 158, 324–332. doi:10.1016/j.jhazmat.2008.01.088

Hamza, R. a., El-Haggar, S., Khedr, S., 2011. Marble and Granite Waste: Characterization and Utilization in Concrete Bricks. Int. J. Biosci. Biochem. Bioinforma. 21, 115–119. doi:10.7763/IJBBB.2011.V1.54

Han, Y., Li, S., Wang, X., Chen, X., 2004. Synthesis and sintering of nanocrystalline hydroxyapatite powders by citric acid sol-gel combustion method. Mater. Res. Bull. 39, 25–32. doi:10.1016/j.materresbull.2003.09.022

Handa, B.K., 1975. Geochemistry and genesis of fluoride containing groundwaters in India. Ground Water.

Hashimoto, Y., Taki, T., Sato, T., 2009. Sorption of dissolved lead from shooting range soils using hydroxyapatite amendments synthesized from industrial byproducts as affected by varying pH conditions. J. Environ. Manage. 90, 1782–1789. doi:10.1016/j.jenvman.2008.11.004

Heaney, R.P., Weaver, C.M., 2003. Calcium and vitamin D, Endocrinology and Metabolism Clinics of North America. doi:10.17226/13050

Herliansyah, M.K., Hamdi, M., Ide-Ektessabi, A., Wildan, M.W., Toque, J.A., 2009. The influence of sintering temperature on the properties of compacted bovine hydroxyapatite. Mater. Sci. Eng. C 29, 1674–1680. doi:10.1016/j.msec.2009.01.007

Hsieh, M.F., Perng, L.H., Chin, T.S., Perng, H.G., 2001. Phase purity of sol-gel-derived hydroxyapatite ceramic. Biomaterials 22, 2601–2607. doi:10.1016/S0142-9612(00)00448-8

Hu, J., Agrawal, D.K., Fang, Y., Roy, R., 1993. Synthesis of hydroxyapatite using phosphate-rich glasses in the system CaO-P2O5-H2O and acoustic waves. J. Mater. Sci. 28, 5297–

5300. doi:10.1007/BF00570080

Huang, Y.C., Hsiao, P.C., Chai, H.J., 2011. Hydroxyapatite extracted from fish scale: Effects on MG63 osteoblast-like cells. Ceram. Int. 37, 1825–1831. doi:10.1016/j.ceramint.2011.01.018

Hwang, K., Lim, Y., 1999. Chemical and structural changes of hydroxyapatite films by using a sol-gel method. Surf. Coatings Technol. 115, 172–175. doi:10.1016/S0257-8972(99)00174-7

Institute, M.-D., Govt. of India, Ministry of Micro, S.& M.E., 2009. Status report on commercial utilization of marble slurry in rajasthan.

Ioiţescu, A., Vlase, G., Vlase, T., Ilia, G., Doca, N., 2009. Synthesis and characterization of hydroxyapatite obtained from different organic precursors by sol-gel method. J. Therm. Anal. Calorim. 96, 937–942. doi:10.1007/s10973-009-0044-1

Isiklan, N., Sanli, O., 2005. Separation characteristics of acetic acid-water mixtures by pervaporation using poly(vinyl alcohol) membranes modified with malic acid. Chem. Eng. Process. Process Intensif. 44, 1019–1027. doi:10.1016/j.cep.2005.01.005

Islam, M., Mishra, P.C., Patel, R., 2011. Arsenate removal from aqueous solution by cellulose-carbonated hydroxyapatite nanocomposites. J. Hazard. Mater. 189, 755–763. doi:10.1016/j.jhazmat.2011.03.051

Itokazu, M., Yang, W., Aoki, T., Ohara, A., Kato, N., 1998. Synthesis of antibiotic-loaded interporous hydroxyapatite blocks by vacuum method and in vitro drug release testing. Biomaterials 19, 817–819. doi:10.1016/S0142-9612(97)00237-8

Jagtap, S., Yenkie, M.K., Labhsetwar, N., Rayalu, S., 2012. Fluoride in drinking water and defluoridation of water. Chem. Rev. 112, 2454–2466. doi:10.1021/cr2002855

Jarag, K.J., Pinjari, D. V., Pandit, A.B., Shankarling, G.S., 2011. Synthesis of chalcone (3-(4-fluorophenyl)-1-(4-methoxyphenyl)prop-2-en-1-one): Advantage of sonochemical method over conventional method. Ultrason. Sonochem. 18, 617–623. doi:10.1016/j.ultsonch.2010.09.010

Jia, Y., Zhu, B.S., Zhang, K.S., Jin, Z., Sun, B., Luo, T., Yu, X.Y., Kong, L.T., Liu, J.H., 2015. Porous 2-line ferrihydrite/bayerite composites (LFBC): Fluoride removal performance and mechanism. Chem. Eng. J. 268, 325–336. doi:10.1016/j.cej.2015.01.080

Jiang, D., Li, D., Xie, J., Zhu, J., Chen, M., Lü, X., Dang, S., 2010. Shape-controlled synthesis of F-substituted hydroxyapatite microcrystals in the presence of Na2EDTA and citric acid. J. Colloid Interface Sci. 350, 30–38. doi:10.1016/j.jcis.2010.06.034

Jiménez-Reyes, M., Solache-Ríos, M., 2010. Sorption behavior of fluoride ions from aqueous solutions by hydroxyapatite. J. Hazard. Mater. 180, 297–302. doi:10.1016/j.jhazmat.2010.04.030

Jinawath, S., Polchai, D., Yoshimura, M., 2002. Low-temperature, hydrothermal transformation of aragonite to hydroxyapatite. Mater. Sci. Eng. C 22, 35–39. doi:10.1016/S0928-4931(02)00110-8

Jokić, B., Mitrić, M., Radmilović, V., Drmanić, S., Petrović, R., Janaćković, D., 2011. Synthesis and characterization of monetite and hydroxyapatite whiskers obtained by a hydrothermal method. Ceram. Int. 37, 167–173. doi:10.1016/j.ceramint.2010.08.032

Jungbauer, A., Hahn, R., Deinhofer, K., Luo, P., 2004. Performance and characterization of a nanophased porous hydroxyapatite for protein chromatography. Biotechnol. Bioeng. 87, 364–375. doi:10.1002/bit.20121

Kim, S.R., Riu, D.H., Lee, Y.J., Kim, Y.H., 2002. Synthesis and characterization of silicon substituted hydroxyapatite. Bioceram. 14 218–2, 85–88. doi:10.4028/www.scientific.net/KEM.218-220.85

Kim, W., Saito, F., 2001. Sonochemical synthesis of hydroxyapatite from H3PO4 solution with Ca(OH)2. Ultrason. Sonochem. 8, 85–88. doi:10.1016/S1350-4177(00)00034-1

Kokubo, T., Takadama, H., 2006. How useful is SBF in predicting in vivo bone bioactivity? Biomaterials 27, 2907–2915. doi:10.1016/j.biomaterials.2006.01.017

Kumar, D., Gittings, J.P., Turner, I.G., Bowen, C.R., Bastida-Hidalgo, A., Cartmell, S.H.,

2010. Polarization of hydroxyapatite: Influence on osteoblast cell proliferation. Acta Biomater. 6, 1549–1554. doi:10.1016/j.actbio.2009.11.008

Kumar, G.S., Girija, E.K., 2013. Flower-like hydroxyapatite nanostructure obtained from eggshell: A candidate for biomedical applications. Ceram. Int. 39, 8293–8299. doi:10.1016/j.ceramint.2013.03.099

Kumar, G.S., Thamizhavel, A., Girija, E.K., 2012. Microwave conversion of eggshells into flower-like hydroxyapatite nanostructure for biomedical applications. Mater. Lett. 76, 198–200. doi:10.1016/j.matlet.2012.02.106

Lak, A., Mazloumi, M., Mohajerani, M., Kajbafvala, A., Zanganeh, S., Arami, H., Sadrnezhaad, S.K., 2008. Self-assembly of dandelion-like hydroxyapatite nanostructures via hydrothermal method. J. Am. Ceram. Soc. 91, 3292–3297. doi:10.1111/j.1551-2916.2008.02600.x

Lapworth, D.J., Baran, N., Stuart, M.E., Ward, R.S., 2012. Emerging organic contaminants in groundwater: A review of sources, fate and occurrence. Environ. Pollut. 163, 287–303. doi:10.1016/j.envpol.2011.12.034

Larsen, M.J., Pearce, E.I., Jensen, S.J., 1993. Defluoridation of water at high pH with use of brushite, calcium hydroxide, and bone char. J. Dent. Res. 72, 1519–1525. doi:10.1177/00220345930720111001

Lee, J.H., Lee, K.S., Chang, J.S., Cho, W.S., Kim, Y.H., Kim, S.R., Kim, Y.T., 2004. Biocompatibility of Si-Substituted Hydroxyapatite. Key Eng. Mater. 254–256, 135–138. doi:10.4028/www.scientific.net/KEM.254-256.135

Lemos, A.F., Rocha, J.H.G., Quaresma, S.S.F., Kannan, S., Oktar, F.N., Agathopoulos, S., Ferreira, J.M.F., 2006. Hydroxyapatite nano-powders produced hydrothermally from nacreous material. J. Eur. Ceram. Soc. 26, 3639–3646. doi:10.1016/j.jeurceramsoc.2005.12.011

Li, J., Yin, Y., Yao, F., Zhang, L., Yao, K., 2008. Effect of nano- and micro-hydroxyapatite/chitosan-gelatin network film on human gastric cancer cells. Mater. Lett.

62, 3220–3223. doi:10.1016/j.matlet.2008.02.072

Li, Y., Tjandra, W., Tam, K.C., 2008. Synthesis and characterization of nanoporous hydroxyapatite using cationic surfactants as templates. Mater. Res. Bull. 43, 2318–2326. doi:10.1016/j.materresbull.2007.08.008

Liang, W., Rahaman, M.N., Day, D.E., Marion, N.W., Riley, G.C., Mao, J.J., 2008. Bioactive borate glass scaffold for bone tissue engineering. J. Non. Cryst. Solids 354, 1690–1696. doi:10.1016/j.jnoncrysol.2007.10.003

Liang, W., Zhan, L., Piao, L., Rssel, C., 2011. Fluoride removal performance of glass derived hydroxyapatite. Mater. Res. Bull. 46, 205–209. doi:10.1016/j.materresbull.2010.11.015

Lin, K., Pan, J., Chen, Y., Cheng, R., Xu, X., 2009. Study the adsorption of phenol from aqueous solution on hydroxyapatite nanopowders. J. Hazard. Mater. 161, 231–240. doi:10.1016/j.jhazmat.2008.03.076

Lin, S.Y., Chen, W.F., Cheng, M.T., Li, Q., 2013. Investigation of factors that affect cationic surfactant loading on activated carbon and perchlorate adsorption. Colloids Surfaces A Physicochem. Eng. Asp. 434, 236–242. doi:10.1016/j.colsurfa.2013.05.048

Liu, D.M., Troczynski, T., Tseng, W.J., 2001. Water-based sol-gel synthesis of hydroxyapatite: Process development. Biomaterials 22, 1721–1730. doi:10.1016/S0142-9612(00)00332-X

Liu, D.M., Yang, Q., Troczynski, T., Tseng, W.J., 2002. Structural evolution of sol-gel-derived hydroxyapatite. Biomaterials 23, 1679–1687. doi:10.1016/S0142-9612(01)00295-2

Liu, J., Ye, X., Wang, H., Zhu, M., Wang, B., Yan, H., 2003. The influence of pH and temperature on the morphology of hydroxyapatite synthesized by hydrothermal method. Ceram. Int. 29, 629–633. doi:10.1016/S0272-8842(02)00210-9

Liu, Q., Huang, S., Matinlinna, J.P., Chen, Z., Pan, H., 2013. Insight into biological apatite: Physiochemical properties and preparation approaches. Biomed Res. Int. 2013. doi:10.1155/2013/929748

References

Liu, W.T., Zhang, Y., Li, G.Y., Miao, Y.Q., Wu, X.H., 2008. Structure and composition of teleost scales from snakehead Channa argus (Cantor) (Perciformes: Channidae). J. Fish Biol. 72, 1055–1067. doi:10.1111/j.1095-8649.2007.01790.x

Liu, Y., Hou, D., Wang, G., 2004. A simple wet chemical synthesis and characterization of hydroxyapatite nanorods. Mater. Chem. Phys. 86, 69–73. doi:10.1016/j.matchemphys.2004.02.009

Lunge, S., Thakre, D., Kamble, S., Labhsetwar, N., Rayalu, S., 2012. Alumina supported carbon composite material with exceptionally high defluoridation property from eggshell waste. J. Hazard. Mater. 237–238, 161–169. doi:10.1016/j.jhazmat.2012.08.023

Ma, Q.Y., Traina, S.J., Logan, T.J., Ryan, J.A., 1994. Effects of Aqueous Al, Cd, Cu, Fe(Ii), Ni, and Zn On Pb Immobilization By Hydroxyapatite. Environ. Sci. Technol. 28, 1219–1228. doi:10.1021/es00056a007

Maliyekkal, S.M., Sharma, A.K., Philip, L., 2006. Manganese-oxide-coated alumina: A promising sorbent for defluoridation of water. Water Res. 40, 3497–3506. doi:10.1016/j.watres.2006.08.007

Maliyekkal, S.M., Shukla, S., Philip, L., Nambi, I.M., 2008. Enhanced fluoride removal from drinking water by magnesia-amended activated alumina granules. Chem. Eng. J. 140, 183–192. doi:10.1016/j.cej.2007.09.049

Malkoc, E., Nuhoglu, Y., Abali, Y., 2006. Cr(VI) adsorption by waste acorn of Quercus ithaburensis in fixed beds: Prediction of breakthrough curves. Chem. Eng. J. 119, 61–68. doi:10.1016/j.cej.2006.01.019

Malmberg, P., Nygren, H., 2008. Methods for the analysis of the composition of bone tissue, with a focus on imaging mass spectrometry (TOF-SIMS). Proteomics 8, 3755–3762. doi:10.1002/pmic.200800198

Materials, F., 2015. Nanoceramics in Clinical Use. doi:10.1039/9781782622550

McCann, H.G., 1952. Reactions of fluoride ion with hydroxyapatite. J. Biol. Chem. 201, 247–259.

Medellin-Castillo, N.A., Leyva-Ramos, R., Ocampo-Perez, R., Garcia de la Cruz, R.F., Aragon-Piña, A., Martinez-Rosales, J.M., Guerrero-Coronado, R.M., Fuentes-Rubio, L., 2007. Adsorption of Fluoride from Water Solution on Bone Char. Ind. Eng. Chem. Res. 46, 9205–9212. doi:10.1021/ie070023n

Mehta, D., George, S., Mondal, P., 2014. Synthesis of Hydroxyapatite by Chemical Precipitation Technique and Study of Its Biodegradability. Int. J. Res. Advent Technol. 2, 159–161.

Mehta, D., Mondal, P., George, S., 2016. Utilization of marble waste powder as a novel adsorbent for removal of fluoride ions from aqueous solution. J. Environ. Chem. Eng. 4, 932–942. doi:10.1016/j.jece.2015.12.040

Mehta, D., Mondal, P., Saharan, V.K., George, S., 2017. Synthesis of hydroxyapatite nanorods for application in water defluoridation and optimization of process variables: Advantage of ultrasonication with precipitation method over conventional method. Ultrason. Sonochem. 37, 56–70. doi:10.1016/j.ultsonch.2016.12.035

Metz, J.R., de Vrieze, E., Lock, E.J., Schulten, I.E., Flik, G., 2012. Elasmoid scales of fishes as model in biomedical bone research. J. Appl. Ichthyol. 28, 382–387. doi:10.1111/j.1439-0426.2012.01990.x

Misra, A.K., Mathur, R., Rao, Y. V, Singh, A.P., Goel, P., 2010. A new technology of marble slurry waste utilisation in roads. J. Sci. Ind. Res. (India). 69, 67–72.

Mizutani, Y., Hattori, M., Okuyama, M., Kasuga, T., Nogami, M., 2005. Large-sized hydroxyapatite whiskers derived from calcium tripolyphosphate gel. J. Eur. Ceram. Soc. 25, 3181–3185. doi:10.1016/j.jeurceramsoc.2004.07.028

Mlilo, T.B., Brunson, L.R., Sabatini, D. a., 2010. Arsenic and Fluoride Removal Using Simple Materials. J. Environ. Eng. 136, 391–398. doi:10.1061/(ASCE)EE.1943-7870.0000154

Mobasherpour, I., Salahi, E., Pazouki, M., 2012. Comparative of the removal of Pb 2+, Cd 2+ and Ni 2+ by nano crystallite hydroxyapatite from aqueous solutions: Adsorption isotherm study. Arab. J. Chem. 5, 439–446. doi:10.1016/j.arabjc.2010.12.022

References

Moholkar, V.S., Sable, S.P., Pandit, A.B., 2000. Mapping the cavitation intensity in an ultrasonic bath using the acoustic emission. AIChE J. 46, 684–694. doi:10.1002/aic.690460404

Molli, G., Conti, P., Giorgetti, G., Meccheri, M., Oesterling, N., 2000. Microfabric study on the deformational and thermal history of the Alpi Apuane marbles (Carrara marbles), Italy. J. Struct. Geol. 22, 1809–1825. doi:10.1016/S0191-8141(00)00086-9

Mondal, P., George, S., 2015a. Removal of Fluoride from Drinking Water Using Novel Adsorbent Magnesia-Hydroxyapatite. Water, Air, Soil Pollut. 226, 241. doi:10.1007/s11270-015-2515-2

Mondal, P., George, S., 2015b. Removal of Fluoride from Drinking Water Using Novel Adsorbent Magnesia-Hydroxyapatite. Water. Air. Soil Pollut. 226. doi:10.1007/s11270-015-2515-2

Mondal, P., George, S., 2014. A review on adsorbents used for defluoridation of drinking water. Rev. Environ. Sci. Biotechnol. doi:10.1007/s11157-014-9356-0

Mondal, P., George, S., Mehta, D., 2014. Use of Calcite for Defluoridation of Drinking Water in Acidic medium. Res. J. Chem. Sci. Res. J. Chem. Sci 4, 2231–606.

Mondal, P., Mehta, D., George, S., 2016. Defluoridation studies with synthesized magnesium-incorporated hydroxyapatite and parameter optimization using response surface methodology. Desalin. Water Treat. 3994, 1–20. doi:10.1080/19443994.2016.1167628

Montero, M.L., Saenz, A., Castano, V.M., 2009. Synthesis of nano-hydroxyapatite from silica suspensions through chemical compensation. J. Exp. Nanosci. 4, 193–202. doi:Pii 911663752\rDoi 10.1080/17458080902774663

Mourabet, M., El Rhilassi, A., El Boujaady, H., Bennani-Ziatni, M., El Hamri, R., Taitai, A., 2015. Removal of fluoride from aqueous solution by adsorption on hydroxyapatite (HAp) using response surface methodology. J. Saudi Chem. Soc. 19, 603–615. doi:10.1016/j.jscs.2012.03.003

Murugan, R., Kumar, T.S.S., Rao, K.P., 2002. Fluorinated bovine hydroxyapatite: Preparation

and characterization. Mater. Lett. 57, 429–433. doi:10.1016/S0167-577X(02)00805-4

Muthu Prabhu, S., Meenakshi, S., 2014. Synthesis of surface coated hydroxyapatite powders for fluoride removal from aqueous solution. Powder Technol. 268, 306–315. doi:10.1016/j.powtec.2014.08.041

Mwaniki, D.L., 1992. Fluoride sorption characteristics of different grades of bone charcoal, based on batch tests. J. Dent. Res. 71, 1310–1315. doi:10.1177/00220345920710060801

Nakahira, A., Okajima, T., Honma, T., Yoshioka, S., Tanaka, I., 2006. Arsenic Removal by Hydroxyapatite-based Ceramics. Chem. Lett. 35, 856–857. doi:10.1246/cl.2006.856

Nakamura, A., 1998. Banner Advertisement selecting method. US Pat. 7058628. doi:10.1016/j.(73)

Nath, S.K., Dutta, R.K., 2010. Fluoride removal from water using crushed limestone. Indian J. Chem. Technol. 17, 120–125.

Nayak, A.K., 2010. Hydroxyapatite synthesis methodologies: An overview. Int. J. ChemTech Res. 2, 903–907.

Nayar, S., Guha, A., 2009. Waste utilization for the controlled synthesis of nanosized hydroxyapatite. Mater. Sci. Eng. C 29, 1326–1329. doi:10.1016/j.msec.2008.10.002

Neira, I.S., Guiti??n, F., Taniguchi, T., Watanabe, T., Yoshimura, M., 2008. Hydrothermal synthesis of hydroxyapatite whiskers with sharp faceted hexagonal morphology. J. Mater. Sci. 43, 2171–2178. doi:10.1007/s10853-007-2032-9

Ngoc, U.N., Schnitzer, H., 2009. Sustainable solutions for solid waste management in Southeast Asian countries. Waste Manag. 29, 1982–95. doi:10.1016/j.wasman.2008.08.031

Nie, Y., Hu, C., Kong, C., 2012. Enhanced fluoride adsorption using Al (III) modified calcium hydroxyapatite. J. Hazard. Mater. 233–234, 194–199. doi:10.1016/j.jhazmat.2012.07.020

O'Hare, P., Meenan, B.J., Burke, G.A., Byrne, G., Dowling, D., Hunt, J.A., 2010. Biological

responses to hydroxyapatite surfaces deposited via a co-incident microblasting technique. Biomaterials 31, 515–522. doi:10.1016/j.biomaterials.2009.09.067

Oliveira, M., Mansur, H.S., 2007. Synthetic tooth enamel: SEM characterization of a fluoride hydroxyapatite coating for dentistry applications. Mater. Res. 10, 115–118. doi:10.1590/S1516-14392007000200004

Omelon, S.J., Grynpas, M.D., 2008. Relationships between polyphosphate chemistry, biochemistry and apatite biomineralization. Chem. Rev. 108, 4694–4715. doi:10.1021/cr0782527

Orlovskii, V.P., Komlev, V.S., Barinov, S.M., 2002. Hydroxyapatite and hydroxyapatite-based ceramics. Inorg. Mater. 38, 973–984. doi:10.1023/A:1020585800572

Ozawa, M., Suzuki, S., 2002. Microstructural Development of Natural Hydroxyapatite Originated from Fish-Bone Waste through Heat Treatment. J. Argent. Chem. Soc. 17, 2000–2002. doi:10.1111/j.1151-2916.2002.tb00268.x

Padmanabhan, S.K., Balakrishnan, A., Chu, M.C., Lee, Y.J., Kim, T.N., Cho, S.J., 2009. Sol-gel synthesis and characterization of hydroxyapatite nanorods. Particuology 7, 466–470. doi:10.1016/j.partic.2009.06.008

Pandi, K., Viswanathan, N., 2016. In Situ Fabrication of Magnetic Iron Oxide over Nano-hydroxyapatite Gelatin Eco-polymeric Composite for Defluoridation Studies. J. Chem. Eng. Data 61, 571–578. doi:10.1021/acs.jced.5b00727

Pandi, K., Viswanathan, N., 2015. Synthesis and applications of eco-magnetic nano-hydroxyapatite chitosan composite for enhanced fluoride sorption. Carbohydr. Polym. 134, 732–739. doi:10.1016/j.carbpol.2015.08.003

Pandi, K., Viswanathan, N., 2014. Synthesis of alginate bioencapsulated nano-hydroxyapatite composite for selective fluoride sorption. Carbohydr. Polym. 112, 662–667. doi:10.1016/j.carbpol.2014.06.029

Pappu, A., Saxena, M., Asolekar, S.R., 2007. Solid wastes generation in India and their recycling potential in building materials. Build. Environ. 42, 2311–2320.

doi:10.1016/j.buildenv.2006.04.015

Patel, N., Follon, E.L., Gibson, I.R., Best, S.M., Bonfield, W., 2003. Comparison of Sintering and Mechanical Properties of Hydroxyapatite and Silicon-Substituted Hydroxyapatite. Key Eng. Mater. 240–242, 919–922. doi:10.4028/www.scientific.net/KEM.240-242.919

Pei, L.-Z., Yin, W.-Y., Wang, J.-F., Chen, J., Fan, C.-G., Zhang, Q.-F., 2010. Low temperature synthesis of magnesium oxide and spinel powders by a sol-gel process. Mater. Res. 13, 339–343. doi:10.1590/S1516-14392010000300010

Percival, M., 1999. Bone health & osteoporosis. Appl. Nutr. Sci. Reports 5, 1–6.

Poinern, G.E.J., Brundavanam, R.K., Thi Le, X., Nicholls, P.K., Cake, M.A., Fawcett, D., 2014. The synthesis, characterisation and in vivo study of a bioceramic for potential tissue regeneration applications. Sci. Rep. 4, 6235. doi:10.1038/srep06235

Poinern, G.E.J., Ghosh, M.K., Ng, Y.J., Issa, T.B., Anand, S., Singh, P., 2011. Defluoridation behavior of nanostructured hydroxyapatite synthesized through an ultrasonic and microwave combined technique. J. Hazard. Mater. 185, 29–37. doi:10.1016/j.jhazmat.2010.08.087

Pradesh, A., Pradesh, M., Pradesh, A., 1957. 56 Marble.

Prasad, K., Pinjari, D. V., Pandit, A.B., Mhaske, S.T., 2010. Phase transformation of nanostructured titanium dioxide from anatase-to-rutile via combined ultrasound assisted sol-gel technique. Ultrason. Sonochem. 17, 409–415. doi:10.1016/j.ultsonch.2009.09.003

Prentice, A., 2004. Diet, nutrition and the prevention of osteoporosis. Public Health Nutr. 7, 227–243. doi:10.1079/PHN2003590

Rabiei, A., Blalock, T., Thomas, B., Cuomo, J., Yang, Y., Ong, J., 2007. Microstructure, mechanical properties, and biological response to functionally graded HA coatings. Mater. Sci. Eng. C 27, 529–533. doi:10.1016/j.msec.2006.05.036

Rafique, T., Naseem, S., Bhanger, M.I., Usmani, T.H., 2008. Fluoride ion contamination in

the groundwater of Mithi sub-district, the Thar Desert, Pakistan. Environ. Geol. 56, 317–326. doi:10.1007/s00254-007-1167-y

Ramanan, S.R., Venkatesh, R., 2004. A study of hydroxyapatite fibers prepared via sol-gel route. Mater. Lett. 58, 3320–3323. doi:10.1016/j.matlet.2004.06.030

Ramasamy, V., Ponnusamy, V., Sabari, S., Anishia, S.R., Gomathi, S.S., 2009. Effect of grinding on the crystal structure of recently excavated dolomite. Indian J. Pure Appl. Phys. 47, 586–591.

Rao, T.R., 1996. Kinetics of calcium carbonate decomposition. Chem. Eng. Technol. 19, 373–377. doi:10.1002/ceat.270190411

Rassin, A.G., 2012. A Comprehensive Study of Marble Industry.

Reig, F.B., Adelantado, J.V.G., Moya Moreno, M.C.M., 2002. FTIR quantitative analysis of calcium carbonate (calcite) and silica (quartz) mixtures using the constant ratio method. Application to geological samples. Talanta 58, 811–821. doi:10.1016/S0039-9140(02)00372-7

Rey, C., Combes, C., Drouet1, C., Glimcher, M., 2010. Bone mineral: update on chemical composition and structure. Osteoporos. Int. 20, 1013–1021. doi:10.1007/s00198-009-0860-y.Bone

Rojas-Mayorga, C.K., Bonilla-Petriciolet, A., Aguayo-Villarreal, I.A., Hernández-Montoya, V., Moreno-Virgen, M.R., Tovar-Gómez, R., Montes-Morán, M.A., 2013. Optimization of pyrolysis conditions and adsorption properties of bone char for fluoride removal from water. J. Anal. Appl. Pyrolysis 104, 10–18. doi:10.1016/j.jaap.2013.09.018

Rojas, J., Bedoya, M., Ciro, Y., 2015. World â€TM s largest Science , Technology & Medicine Open Access book publisher Current Trends in the Production of Cellulose Nanoparticles and Nanocomposites for Biomedical Applications, in: Cellulose-Fundamental Aspects and Current Trends. pp. 193–228.

Rondeau, V., Jacqmin-Gadda, H., Commenges, D., Helmer, C., Dartigues, J.F., 2009. Aluminum and silica in drinking water and the risk of Alzheimer's disease or cognitive

decline: Findings from 15-year follow-up of the PAQUID cohort. Am. J. Epidemiol. 169, 489–496. doi:10.1093/aje/kwn348

Rouhani, P., Taghavinia, N., Rouhani, S., 2010. Rapid growth of hydroxyapatite nanoparticles using ultrasonic irradiation. Ultrason. Sonochem. 17, 853–856. doi:10.1016/j.ultsonch.2010.01.010

RT_2000, Rhee, S., 2000. Effect of Chondroitin Sulfate on the Crystal Growth of Hydroxyapatite. Society 102, 2100–2102.

Ruban Kumar, A., Kalainathan, S., 2010. Sol-gel synthesis of nanostructured hydroxyapatite powder in presence of polyethylene glycol. Phys. B Condens. Matter 405, 2799–2802. doi:10.1016/j.physb.2010.03.067

Saboya, F., Xavier, G.C., Alexandre, J., 2007. The use of the powder marble by-product to enhance the properties of brick ceramic. Constr. Build. Mater. 21, 1950–1960. doi:10.1016/j.conbuildmat.2006.05.029

Sadat-Shojai, M., Khorasani, M.T., Dinpanah-Khoshdargi, E., Jamshidi, A., 2013. Synthesis methods for nanosized hydroxyapatite with diverse structures. Acta Biomater. 9, 7591–7621. doi:10.1016/j.actbio.2013.04.012

Saha, P. Das, Chowdhury, S., Mondal, M., Sinha, K., 2012. Biosorption of Direct Red 28 (Congo Red) from Aqueous Solutions by Eggshells: Batch and Column Studies. Sep. Sci. Technol. 47, 112–123. doi:10.1080/01496395.2011.610397

Sairam Sundaram, C., Viswanathan, N., Meenakshi, S., 2009a. Defluoridation of water using magnesia/chitosan composite. J. Hazard. Mater. 163, 618–624. doi:10.1016/j.jhazmat.2008.07.009

Sairam Sundaram, C., Viswanathan, N., Meenakshi, S., 2009b. Fluoride sorption by nano-hydroxyapatite/chitin composite. J. Hazard. Mater. 172, 147–151. doi:10.1016/j.jhazmat.2009.06.152

Sairam Sundaram, C., Viswanathan, N., Meenakshi, S., 2008. Uptake of fluoride by nano-hydroxyapatite/chitosan, a bioinorganic composite. Bioresour. Technol. 99, 8226–8230.

doi:10.1016/j.biortech.2008.03.012

Sanderson, R.T., 1988. Principles of electronegativity. J. Chem. Educ. 65, 227–231. doi:10.1021/ed065p112

Santos, M.H., Oliveira, M. De, Souza, L.P.D.F., Mansur, H.S., Vasconcelos, W.L., 2004. Synthesis control and characterization of hydroxyapatite prepared by wet precipitation process. Mater. Res. 7, 625–630. doi:10.1590/S1516-14392004000400017

Sarkar, M., Banerjee, A., Pramanick, P.P., Sarkar, A.R., 2006. Use of laterite for the removal of fluoride from contaminated drinking water. J. Colloid Interface Sci. 302, 432–41. doi:10.1016/j.jcis.2006.07.001

Segadães, A.M., Carvalho, M.A., Acchar, W., 2005. Using marble and granite rejects to enhance the processing of clay products. Appl. Clay Sci. 30, 42–52. doi:10.1016/j.clay.2005.03.004

Seol, Y.J., Kim, J.Y., Park, E.K., Kim, S.Y., Cho, D.W., 2009. Fabrication of a hydroxyapatite scaffold for bone tissue regeneration using microstereolithography and molding technology. Microelectron. Eng. 86, 1443–1446. doi:10.1016/j.mee.2009.01.053

Shahraki, B.K., Mehrabi, B., Dabiri, R., 2009. Thermal behavior of Zefreh dolomite mine (Central Iran). J. Min. Metall. Sect. B Metall. 45, 35–44. doi:10.2298/JMMB0901035S

Singh, A., 2012. Hydroxyapatite, a biomaterial: Its chemical synthesis, characterization and study of biocompatibility prepared from shell of garden snail, Helix aspersa. Bull. Mater. Sci. 35, 1031–1038. doi:10.1007/s12034-012-0384-5

Singh, J., Singh, P., Singh, A., 2016. Fluoride ions vs removal technologies: A study. Arab. J. Chem. 9, 815–824. doi:10.1016/j.arabjc.2014.06.005

SL Shanthi, P.M., Ashok, M., Balasubramanian, T., Riyasdeen, A., Akbarsha, M.A., 2009. Synthesis and characterization of nano-hydroxyapatite at ambient temperature using cationic surfactant. Mater. Lett. 63, 2123–2125. doi:10.1016/j.matlet.2009.07.008

Sobczak, A., Kida, A., Kowalski, Z., Wzorek, Z., 2009a. Evaluation of the biomedical

properties of hydroxyapatite obtained from bone waste. Polish J. Chem. Technol. 11, 37–43. doi:10.2478/v10026-009-0010-5

Sobczak, A., Kowalski, Z., Wzorek, Z., 2009b. Preparation of hydroxyapatite from animal bones. Acta Bioeng. Biomech. 11, 23–28.

Standard, I., 2012. Indian Standards Drinking Water Specifications IS 10500:2012.

Sternitzke, V., Kaegi, R., Audinot, J.N., Lewin, E., Hering, J.G., Johnson, C.A., 2012. Uptake of fluoride from aqueous solution on nano-sized hydroxyapatite: Examination of a fluoridated surface layer. Environ. Sci. Technol. 46, 802–809. doi:10.1021/es202750t

Strietzel, F.P., Reichart, P.A., Graf, H.L., 2007. Lateral alveolar ridge augmentation using a synthetic nano-crystalline hydroxyapatite bone substitution material (Ostim®). Preliminary clinical and histological results. Clin. Oral Implants Res. 18, 743–751. doi:10.1111/j.1600-0501.2007.01416.x

Suchanek, W.L., Shuk, P., Byrappa, K., Riman, R.E., TenHuisen, K.S., Janas, V.F., 2002. Mechanochemical-hydrothermal synthesis of carbonated apatite powders at room temperature. Biomaterials 23, 699–710. doi:10.1016/S0142-9612(01)00158-2

Sujana, M., Mohanty, S., 2011. Characterization and fluoride uptake studies of nano-scale iron oxide-hydroxide synthesized by microemulsion method. Int. J. Eng. Sci. Technol. 2, 1–12. doi:10.4314/ijest.v2i8.63775

Sujana, M.G., Anand, S., 2010. Iron and aluminium based mixed hydroxides: A novel sorbent for fluoride removal from aqueous solutions. Appl. Surf. Sci. 256, 6956–6962. doi:10.1016/j.apsusc.2010.05.006

Sun, L., Zhao, Q., Xiang, J., Shi, J., Wang, L., Hu, S., Su, S., 2009. Adsorption of NO and NH3 over CuO/γ-Al2O3 catalyst by DRIFTS. Huagong Xuebao/CIESC J. 60, 444–449. doi:10.1007/s11771

Sundaram, C.S., Viswanathan, N., Meenakshi, S., 2008. Defluoridation chemistry of synthetic hydroxyapatite at nano scale: Equilibrium and kinetic studies. J. Hazard. Mater. 155, 206–215. doi:10.1016/j.jhazmat.2007.11.048

Sung, Y.-M., Shin, Y.-K., Ryu, J.-J., 2007. Preparation of hydroxyapatite/zirconia bioceramic nanocomposites for orthopaedic and dental prosthesis applications. Nanotechnology 18, 65602. doi:10.1088/0957-4484/18/6/065602

Sunyecz, J., 2008. The use of calcium and vitamin D in the management of osteoporosis. Ther. Clin. Risk Manag. 4, 827–836. doi:10.1016/j.bone.2007.10.005

Suslick, K.S., 1998. Sonochemistry. Kirk-Othmer Encycl. Chem. Tecnol.

Tang, X.L., Xiao, X.F., Liu, R.F., 2005. Structural characterization of silicon-substituted hydroxyapatite synthesized by a hydrothermal method. Mater. Lett. 59, 3841–3846. doi:10.1016/j.matlet.2005.06.060

Tang, Y., Guan, X., Su, T., Gao, N., Wang, J., 2009. Fluoride adsorption onto activated alumina: Modeling the effects of pH and some competing ions. Colloids Surfaces A Physicochem. Eng. Asp. 337, 33–38. doi:10.1016/j.colsurfa.2008.11.027

Thakre, D., Rayalu, S., Kawade, R., Meshram, S., Subrt, J., Labhsetwar, N., 2010. Magnesium incorporated bentonite clay for defluoridation of drinking water. J. Hazard. Mater. 180, 122–30. doi:10.1016/j.jhazmat.2010.04.001

Thomson, B.M., Smith, C.L., Busch, R.D., Siegel, M.D., Baldwin, C., 2003. Removal of Metals and Radionuclides Using Apatite and Other Natural Sorbents. J. Environ. Eng. 129, 492–499. doi:10.1061/(ASCE)0733-9372(2003)129:6(492)

Tomar, G., Thareja, A., Sarkar, S., 2015. Enhanced fluoride removal by hydroxyapatite-modified activated alumina. Int. J. Environ. Sci. Technol. 12, 2809–2818. doi:10.1007/s13762-014-0653-5

Tozsin, G., Arol, A.I., Oztas, T., Kalkan, E., 2014. Using marble wastes as a soil amendment for acidic soil neutralization. J. Environ. Manage. 133, 374–7. doi:10.1016/j.jenvman.2013.12.022

Trautz, 0 R, Zapanta, R.R., 1961. Experiments With Calcium Carbonate Phosphates and the Effect of Topical Application of Sodium Fluoride. Arch. oral Bid. Spec. Suppl. 4, 122–133. doi:10.1016/0003-9969(61)90090-5

Tsiourvas, D., Tsetsekou, A., Kammenou, M.I., Boukos, N., 2011. Controlling the formation of hydroxyapatite nanorods with dendrimers. J. Am. Ceram. Soc. 94, 2023–2029. doi:10.1111/j.1551-2916.2010.04342.x

Vagenas, N., 2003. Quantitative analysis of synthetic calcium carbonate polymorphs using FT-IR spectroscopy. Talanta 59, 831–836. doi:10.1016/S0039-9140(02)00638-0

Vagenas, N. V., Gatsouli, A., Kontoyannis, C.G., 2003. Quantitative analysis of synthetic calcium carbonate polymorphs using FT-IR spectroscopy. Talanta 59, 831–836. doi:10.1016/S0039-9140(02)00638-0

Vijayalakshmi Natarajan, U., Rajeswari, S., 2008. Influence of calcium precursors on the morphology and crystallinity of sol-gel-derived hydroxyapatite nanoparticles. J. Cryst. Growth 310, 4601–4611. doi:10.1016/j.jcrysgro.2008.07.118

Villaescusa, I., Fiol, N., Martínez, M., Miralles, N., Poch, J., Serarols, J., 2004. Removal of copper and nickel ions from aqueous solutions by grape stalks wastes. Water Res. 38, 992–1002. doi:10.1016/j.watres.2003.10.040

Viswanathan, N., Meenakshi, S., 2010. Enriched fluoride sorption using alumina/chitosan composite. J. Hazard. Mater. 178, 226–232. doi:10.1016/j.jhazmat.2010.01.067

Walker, G.M., Hansen, L., Hanna, J.-A., Allen, S.J., 2003. Kinetics of a reactive dye adsorption onto dolomitic sorbents. Water Res. 37, 2081–9. doi:10.1016/S0043-1354(02)00540-7

Walsh, P.J., Buchanan, F.J., Dring, M., Maggs, C., Bell, S., Walker, G.M., 2008. Low-pressure synthesis and characterisation of hydroxyapatite derived from mineralise red algae. Chem. Eng. J. 137, 173–179. doi:10.1016/j.cej.2007.10.016

Wang, A., Yin, H., Liu, D., Wu, H., Ren, M., Jiang, T., Cheng, X., Xu, Y., 2007. Size-controlled synthesis of hydroxyapatite nanorods in the presence of organic modifiers. Mater. Lett. 61, 2084–2088. doi:10.1016/j.matlet.2006.08.019

Wang, J., Shaw, L.L., 2007. Morphology-enhanced low-temperature sintering of nanocrystalline hydroxyapatite. Adv. Mater. 19, 2364–2369.

doi:10.1002/adma.200602333

Wang, P., Li, C., Gong, H., Jiang, X., Wang, H., Li, K., 2010. Effects of synthesis conditions on the morphology of hydroxyapatite nanoparticles produced by wet chemical process. Powder Technol. 203, 315–321. doi:10.1016/j.powtec.2010.05.023

Wenk, H.R., Heidelbach, F., 1999. Crystal alignment of carbonated apatite in bone and calcified tendon: Results from quantitative texture analysis. Bone 24, 361–369. doi:10.1016/S8756-3282(98)00192-6

WHO/UNICEF, 2015. 2015 Update and MDG Assessment. World Heal. Organ. 90. doi:10.1007/s13398-014-0173-7.2

Williams, P.T., 2005. Waste treatment and disposal services, Metal Finishing. doi:10.1016/0026-0576(95)90333-X

Wu, S.C., Hsu, H.C., Wu, Y.N., Ho, W.F., 2011. Hydroxyapatite synthesized from oyster shell powders by ball milling and heat treatment. Mater. Charact. 62, 1180–1187. doi:10.1016/j.matchar.2011.09.009

Wu, Y., Bose, S., 2005. Nanocrystalline hydroxyapatite: Micelle templated synthesis and characterization. Langmuir 21, 3232–3234. doi:10.1021/la046754z

Xiang, Q., Liang, Y., Chen, L., Wang, C., Chen, B., Chen, X., Zhou, M., 2003. Effect of fluoride in drinking water on children's intelligence. Fluoride 36, 84–94.

Yan, L., Li, Y., Deng, Z.X., Zhuang, J., Sun, X., 2001. Surfactant-assisted hydrothermal synthesis of hydroxyapatite nanorods. Int. J. Inorg. Mater. 3, 633–637. doi:10.1016/S1466-6049(01)00164-7

Yao, J., Tjandra, W., Chen, Y.Z., Tam, K.C., Ma, J., Soh, B., 2003. Hydroxyapatite nanostructure material derived using cationic surfactant as a template. J. Mater. Chem. 13, 3053. doi:10.1039/b308801d

Ye, Q., Ohsaki, K., Li, K., Li, D.J., Zhu, C.S., Ogawa, T., Tenshin, S., Takano-Yamamoto, T., 2001. Histological reaction to hydroxyapatite in the middle ear of rats. Auris Nasus

Larynx 28, 131–136. doi:10.1016/S0385-8146(00)00079-1

Yoganand, C.P., Selvarajan, V., Goudouri, O.M., Paraskevopoulos, K.M., Wu, J., Xue, D., 2011. Preparation of bovine hydroxyapatite by transferred arc plasma. Curr. Appl. Phys. 11, 702–709. doi:10.1016/j.cap.2010.11.035

Yoon, Y.H., Nelson, J.H., 1984. Application of Gas Adsorption Kinetics I. A Theoretical Model for Respirator Cartridge Service Life. Am. Ind. Hyg. Assoc. J. 45, 509–516. doi:10.1080/15298668491400197

Yu, X., Tong, S., Ge, M., Zuo, J., 2013. Removal of fluoride from drinking water by cellulose@hydroxyapatite nanocomposites. Carbohydr. Polym. 92, 269–275. doi:10.1016/j.carbpol.2012.09.045

Zanotto, A., Saladino, M.L., Martino, D.C., Caponetti, E., 2012. Influence of Temperature on Calcium Hydroxyapatite Nanopowders. Adv. Nanoparticles 1, 21–28. doi:10.4236/anp.2012.13004

Zhan, X., Li, J., Wang, M., Xu, Z., 2006. Effects of fluoride on growth and thyroid function in young pigs 39, 95–100.

Zhan, Y., Lin, J., Zhu, Z., 2011. Removal of nitrate from aqueous solution using cetylpyridinium bromide (CPB) modified zeolite as adsorbent. J. Hazard. Mater. 186, 1972–1978. doi:10.1016/j.jhazmat.2010.12.090

Zhang, D., Luo, H., Zheng, L., Wang, K., Li, H., Wang, Y., Feng, H., 2012. Utilization of waste phosphogypsum to prepare hydroxyapatite nanoparticles and its application towards removal of fluoride from aqueous solution. J. Hazard. Mater. 241–242, 418–426. doi:10.1016/j.jhazmat.2012.09.066

Zhang, H., Darvell, B.W., 2011. Formation of hydroxyapatite whiskers by hydrothermal homogeneous precipitation using acetamide. J. Am. Ceram. Soc. 94, 2007–2013. doi:10.1111/j.1551-2916.2010.04338.x

Zhang, H., Yan, Y., Wang, Y., Li, S., 2002. Thermal stability of hydroxyapatite whiskers prepared by homogenous precipitation. Adv. Eng. Mater. 4, 916–919.

doi:10.1002/adem.200290003

Zhang, H.G., Zhu, Q., 2005. Surfactant-assisted preparation of fluoride-substituted hydroxyapatite nanorods. Mater. Lett. 59, 3054–3058. doi:10.1016/j.matlet.2005.05.019

Zhang, Y., Liu, Y., Ji, X., Banks, C.E., Song, J., 2011. Flower-like agglomerates of hydroxyapatite crystals formed on an egg-shell membrane. Colloids Surfaces B Biointerfaces 82, 490–496. doi:10.1016/j.colsurfb.2010.10.006

Zhang, Z., Li, M., Chen, W., Zhu, S., Liu, N., Zhu, L., 2010. Immobilization of lead and cadmium from aqueous solution and contaminated sediment using nano-hydroxyapatite. Environ. Pollut. 158, 514–519. doi:10.1016/j.envpol.2009.08.024

Zhao, B., Zhang, Y., Dou, X., Wu, X., Yang, M., 2012. Granulation of Fe-Al-Ce trimetal hydroxide as a fluoride adsorbent using the extrusion method. Chem. Eng. J. 185–186, 211–218. doi:10.1016/j.cej.2012.01.085

Zhao, H., He, W., Wang, Y., Zhang, X., Li, Z., Yan, S., Zhou, W., Wang, G., 2008. Biomineralization of large hydroxyapatite particles using ovalbumin as biosurfactant. Mater. Lett. 62, 3603–3605. doi:10.1016/j.matlet.2008.04.007

Zhou, Z.H., Zhou, P. Le, Yang, S.P., Yu, X. Bin, Yang, L.Z., 2007. Controllable synthesis of hydroxyapatite nanocrystals via a dendrimer-assisted hydrothermal process. Mater. Res. Bull. 42, 1611–1618. doi:10.1016/j.materresbull.2006.11.041

Zhu, B.S., Jia, Y., Jin, Z., Sun, B., Luo, T., Yu, X.Y., Kong, L.T., Huang, X.J., Liu, J.H., 2015. Controlled synthesis of natroalunite microtubes and spheres with excellent fluoride removal performance. Chem. Eng. J. 271, 240–251. doi:10.1016/j.cej.2015.03.011

Zhu, R., Yu, R., Yao, J., Wang, D., Ke, J., 2008. Morphology control of hydroxyapatite through hydrothermal process. J. Alloys Compd. 457, 555–559. doi:10.1016/j.jallcom.2007.03.081

Zuo, Q., Chen, X., Li, W., Chen, G., 2008. Combined electrocoagulation and electroflotation for removal of fluoride from drinking water. J. Hazard. Mater. 159, 452–7. doi:10.1016/j.jhazmat.2008.02.039

APPENDIX

A1. Energy calculations for pure Hydroxyapatite:

i. Energy delivered during sonication with precipitation (USPM) method

- Efficiency of sonication bath = 16.19% (estimated using calorimetric studies).
- Actual energy dissipated in sonication bath= Sonication power × efficiency × processing time.
  = 100 W × 30 min×60 sec × 0.1619
  = 29142.96 J = 29.142 kJ
- Amount of solution processed in sonication bath
  = 15.11 g $(CaNO_3)_2$ + 7.755 g (KH_2PO_4) + 498 g (H_2O)
  = 520.86 g
- Energy utilized per unit mass of material processed in sonication bath = Actual energy dissipated in sonication bath / gram of solution processed
  = 29.142/520.86 = 0.056 kJ/g
- Energy delivered during magnetic stirrer for 1 h prior to 30 min of sonication
- Power supplied= 230 V × 2.5 A = 575 W
- Energy utilized in magnetic stirrer
  = 575 (J/s) × 1 (h) × 3600 (sec) = 2070 kJ
- Energy utilized per unit mass of material processed during initial stirring of 1 h
  = 2070/520.86 = 3.974 kJ/g
- Total energy utilized in USPM method = (Energy utilized during sonication + Energy utilized during magnetic stirring) **= 4.03 kJ/g**

ii. Energy delivered during conventional precipitation (CM) method

- Voltage input in magnetic stirrer (Model 5MLH, Remi, India) = 230 V.
- Amps= 2.5 A
- Power supplied= 575 W
- Amount of energy utilized in 4 h of synthesis:
  = 575 (J/s) × 4 (h) × 3600 (sec) = 8280 kJ
- Total energy utilized per unit mass of material processed in CM method= 8280 kJ/520.86 g **= 15.86 kJ/g**

iii. Energy saved

- Net energy saved = (Total energy utilized in CM method - Total energy utilized in USPM method) = 15.86 (kJ/g) – 4.03 (kJ/g) = **11.83 (kJ/g).**

A2. Energy calculations for Marble Hydroxyapatite (MA-Hap):

i. Energy delivered during sonication (USM) method

- Efficiency of sonication horn = 3% (estimated using calorimetric studies).
- Actual energy dissipated in sonication horn= Power of horn × efficiency × processing time.
  = 750(J/s) × (60×60) sec × 0.03
  = 81kJ
- Amount of solution processed in sonication horn
  = 104.57 g
- Energy utilized per unit mass of material processed in sonication horn = Actual energy dissipated in sonication bath / gram of solution processed
  = 81/104.57 = 0.774 kJ/g

ii. Energy delivered by conventional precipitation method (CM)

- Voltage input in magnetic stirrer (Model 5MLH, Remi, India) = 230 V.
- Power supplied= 230 V × 2.5 A = 575 W
- Energy utilized in magnetic stirrer
  = 575 (J/s) × (4 × 3600) (sec) = 8280 kJ
- Energy utilized per unit mass of material processed during initial stirring of 1 h
  = 8280/104.57 = 79.18 kJ/g

iii. Energy saved

Net energy saved = (Total energy utilized in CM method - Total energy utilized in USPM method) = (79.18– 0.774) kJ/g = 78.406 kJ/g

A3. Calculation for cost analysis of different adsorbent

1. Pure Hap

Yield of Hap 900 CM-1.54 gms

1.1. Conventional Method

Chemical Cost: *Analytical Grade, cost in Rs. for 500 gms* ,KH_2PO_4: Rs. 345/-, $Ca(NO_3)_2$: Rs. 220/-, NH_4OH: Rs. 150/-)

For preparation 100 ml Hap

KH_2PO_4: 1.5514 gms- Cost – Rs. 1/-

$Ca(NO_3)_2$: 3.0227 gms- Cost- Rs. 1.32/-

NH_4OH: 3 ML- Cost- Rs. 1/-

Total Chemical Cost- Rs. 3.32/-

Operating Cost:

Magnetic Stirrer: Use- 1 h, 0.5 kW×1h×6 Rs./unit = Rs. 3/-

Hot air oven: Use- 3h, 1.2 kW×3h×6Rs./Unit= Rs. 21.6/-

Muffle Furnance: Use- 3h, 4 kW×3h×6 Rs./Unit= Rs.72/-

Total Operating cost= Rs. 96.6/-

Total synthesis Cost per unit gram of Hap 900 CM

= Operating cost + Chemicals cost

= 99.92/1.54= Rs. 64.88/- per gram.

1.2. Ultrasonication Method-

Yield of Hap 900 USM- 1.67 gms

Operating cost

Ultrasonic Bath: 30 min, 0.75 kW× 0.5h ×6 Rs./Unit = Rs. 2.25/-

Magnetic Stirrer= Rs. 3/-

Hot air oven: Use- 3h, 1.2 kW×3h×6Rs./Unit= Rs. 21.6/-

Muffle Furnance: Use- 3h, 4 kW×3h×6 Rs./Unit= Rs.72/-

Total Operating cost= Rs. 98.85/-

- **Total synthesis Cost per gram of Hap 900 USPM**

= 98.85+3.32= 102.17/1.67= Rs. 61.17/- per gram.

Required dosage of Hap 900 USPM (Capacity: 1.49 mg/g) for treating 10 mg/L of 1 Liter of Fluoride water ***= 6.71 g***

- **Cost for treating 1 L of 10 mg/L Fluoride solution = Rs. 410.45/-**

2. Marble waste Powder

Operating Cost:

Muffle Furnace: 2h= Rs. 48/-

Required dosage of MWP (Capacity: 1.20 mg/g) for treating 10 mg/L of 1 Liter of Fluoride water: 8.33 g/L

- **Cost for treating/L of Fluoride= Rs. 399.84/-**

3. Marble Apatite

MA-CM- 1.246 gms

Operating cost:

Calcination- 2 h- Rs. 48/-

Drying- Rs. 21.6/-

Magnetic Stirrer- Rs. 3/-

Total operating cost = Rs. 72.6/-

Chemicals:

KH_2PO_4- Rs. 1/-

Nitric Acid: Cost- 125- 500 mL, Used- 1.631 mL Cost- Rs. 0.4/-

Ammonia- Rs. 1/-

Total cost of chemicals used: Rs. 2.4/-

3.1. Conventional Method

Total Cost for MA-Hap CM= Operating cost +Chemical= 72.6+2.4= Rs. 75/-

Total synthesis cost per g for MA-Hap CM= 75/1.246= Rs. 60.19/-

Required dosage of MA-CM (Capacity: 0.96 mg/g) for treating 10 mg/L of 1 Liter of Fluoride water **= 10.41 g/L**

- **Cost for treating/L of Fluoride = Rs. 626.57/-**

3.2. Ultrasonication method

Yield of MA-USM-1.452 gms

Operating Cost

Calcination- 2 h- Rs. 48/-

Drying- Rs. 21.6/-

Sonication Horn- Rs. 4.5/-

Total operating cost= Rs.74.1/-

Total cost for MA-Hap USM= 74.1+2.4 = Rs.76.5/-

Total synthesis cost per g for MA-Hap USM= Rs.52.68 /-

Required dosage of MA-CM (Capacity: 1.826 mg/g) for treating 10 mg/L of 1 Liter of Fluoride water = 5.47 g/L

- **Cost for treating/L of Fluoride= Rs.288.15/-**

4. Marble Hydroxyapatite

Yield of MA-Hap 650 CM- 1.46 gms

Operating cost:

Calcination- 2 h- Rs.48/-

Drying- Rs.21.6/-

Magnetic Stirrer- Rs. 3/-

Total operating cost = Rs.72.6/-

Chemicals:

KH_2PO_4- Rs.1/-

Nitric Acid: Cost- 125- 500 mL, Used- 1.631 mL Cost- Rs.0.4/-

Ammonia- Rs.1/-

Total cost of chemicals used = Rs.2.4/-

Total Cost for MA-Hap CM= Operating cost +Chemical= 72.6+2.4=Rs.75/-

4.1. Conventional Method

Total synthesis cost per g for MA-Hap CM= 75/1.46= Rs.51.36/-

Required dosage of MA-Hap CM (Capacity: 1.331 mg/g) for treating 10 mg/L of 1 Liter of Fluoride water **= 7.51 g/L**

- **Cost for treating/L of Fluoride = Rs.385.78/-**

4.2. Ultrasonication Method

Yield of MA-Hap 650 USM- 1.654 gms

Calcination- 2 h- Rs.48/-

Drying- Rs.21.6/-

Sonication Horn- Rs.4.5/-

Total operating cost:

Total cost for MA-Hap USM= 74.1+2.4=Rs.76.5/-

Total synthesis cost per g for MA-Hap USM= 76.5/1.654= Rs.46.25/-

Required dosage of MA-Hap USM (Capacity: 1.824 mg/g) for treating 10 mg/L of 1 Liter of Fluoride water = 5.48 g/L

- **Cost for treating/L of Fluoride= Rs.253.45/-**

5. Marble Hydroxyapatite Lab reactor (MA-Hap LR) = 470 gms

Operating Cost:

Units Consumed= 8X6= Rs.48/-

Centrifuge= 0.745 kW×0.5h ×6= Rs.2.23/-

Drying= 1.2 kW×6h× 6= Rs.43.2/-

Muffle Furnace= Rs.48/-

Cost for preparation of pellets: 3 kW × 0.25h × 6= Rs.4.5/-

Total operating cost= Rs.145.93/-

Chemicals:

KH_2PO_4=930.6 gms= Rs.517/-

Nitric Acid= 490 ml= Rs.122.5/-

NH_4OH= 1000 mL= Rs.320/-

PVA and Malonic acid: 10 gms+1.05 gms= Rs.11.05/-

Total cost of chemical used= Rs.970.55/-

Total cost for the synthesis of MA-Hap LR= 970.55+145.93= Rs.1115.93/-

Total cost for the synthesis of per gram of MA-Hap LR= Rs.2.37/-

Cost of treatment/L of fluoride containing water:

Breakthrough time for treating 14 liters of 10 mg/L of fluoride solution = 14 h at flow rate of 1LPH, Adsorbent used for 25 cm column bed height = 104 gms

Total cost of adsorbent= 104 g × Rs.2.37/-= **Rs.246.48/-**

Running cost of the column= 0.09 kW × 14h × 6= Rs.7.56/-

Volume of 10 mg/L of fluoride treated= 14 Liters

Total cost for treating 14 Liters of 10 mg/L fluoride solution = Rs.254.04/-

Total cost for treating 1 Liters of 10 mg/L fluoride solution = Rs.18.14 /-

BRIEF BIODATA

Mr. Dhiraj Mehta is a Research scholar in Department of Chemical Engineering, Malaviya National Institute of Technology (MNIT), Jaipur. He has received his B.Tech and M.Tech degree in Biotechnology from Department of Biotechnology, Lovely Professional University, Punjab, India in 2013. He had joined Ph.D. in 2013 under the supervision of Dr. Suja George, Department of Chemical Engineering, MNIT, Jaipur. He has been awarded MHRD scholarship from Government of India.

His research interests are mainly in the areas Water treatment & Analysis, Waste minimization, Material characterization and Biomaterials synthesis. During his research work he has published seven research papers in International Journals. He has also attended various National and International Conferences & Workshops.

Contact no.: +91-7734966806

Email id: dhiraj.mbiotech@gmail.com